

State of Washington Water Research Center Annual Technical Report FY 2015

Introduction

Like most Western States today, The State of Washington faces substantial water resource challenges. Last summer the state had one of the worst droughts of the century, exacerbated by a warm winter and low snowpack throughout the Cascades. The Columbia River Treaty of 1964 between the U.S. and Canada is being considered for renegotiation, and legal and surface-groundwater interactions and conjunctive use are center stage in legal and policy developments regarding instream flows, Native American Treaty rights, and residential and municipal groundwater development. Proposals for more surface and aquifer storage and recovery continue to be introduced, while water market infrastructure continues to develop across the state to facilitate water transfers. Water quality issues relating to stormwater runoff into the Puget Sound and concentrated livestock production east of the Cascade are holding the attention of both the courts and the State Legislature. All of these issues and decisions require and can benefit from science-based research and outreach from water research and management professionals across the state. The State of Washington Water Research Center is working to position itself to be a critical provider and coordinator of these science-based research and information needs.

The State of Washington Water Research Center continues to engage the scientific community, the public sector, and water resource stakeholders at large to address these challenges and improve water resource management throughout the state and region.

In the spirit of the WRRRA of 1964, the mission of the State of Washington Water Research Center (WRC) has three components: 1. To conduct and facilitate applied water-related research. 2. To foster education and training of future water professionals. 3. To serve as a nexus between the academic community, water resource managers and water stakeholders. These three elements of the WRC mission are the fundamental goals supporting the WRC vision, objectives, strategies, and assessment metrics described in this Strategic Plan.

The current WRC administration envisions strengthen WRC impact through the following activities: 1) Actively engaging water research professionals at other academic institutions to encourage their participation in the administration and activities of the WRC, 2) Developing broader collaborations among water researchers within WSU and between WSU and other water-focused organizations. 3) Increasing programmatic and extramural funding to support the WRC and its activities. 4) Developing more focused and integrated water resource education programs at WSU. 5) Creating a wider network for outreach, and contribute more broadly to information dissemination for water stakeholders and policymakers.

The mission and vision of the WRC will be guided according to the following guiding principles:

1) WRC will focus on and facilitate integrative research and education throughout all core water-related programs. At the heart of modern integrative water research is a need for interdisciplinary collaboration. 2) WRC will endeavor to complement rather than duplicate the efforts and missions of other water-focused centers both within WSU and across other state and regional organizations. 3) WRC will continue and strengthen its direct involvement in water-related research, but will also strengthen its indirect contributions to impactful water research by increasing the level of support and incentives provided to prospective researchers in the form of administrative support, information provision, focus and guidance, and direct facilitation of and collaboration in research and academic pursuits. 4) WRC will maintain and strengthen its reputation as an independent and neutral provider of reputable science and policy research.

The administrative activities of the WRC include grant management and planning, collaboration-building across the State of Washington, and technical administration of other WRC activities.

In addition to the USGS WRIA 104(b) grant program, the WRC is administering two extramural grants and has been both following through with past grant research and pursuing other opportunities through grant proposal submission and planning. The 2016 Columbia River Basin Long-Term Water Supply and Demand Forecast (\$1.8 million) is the most substantial research project and is engaging about 15 researchers through the WRC. Associate Director Adam is the Lead Investigator and Director Yoder is the Project Director for this research effort.

In the quest of building a more collaborative atmosphere the SWWRC has relocated to WSU's new PACCAR Environmental Technology building. The PACCAR building was constructed using renewable materials and technologies developed at WSU. It incorporates features such as water capture and re-use, heat recovery, individual control of air quality factors, maximized daylighting and optimal siting, making it a technological showcase for minimizing the carbon footprint of the built environment. Besides the WRC, the new building houses four other of WSU's longstanding research centers dedicated to tackling multifaceted environmental issues through interdisciplinary collaboration. Areas of focus include water quality, sustainable design and construction and atmospheric sciences.

In collaboration with two other Centers at WSU, the WRC received a National Science Foundation workshop grant and hosted a Food-Energy-Water Nexus workshop in Seattle, WA. In addition, the WRC submitted a proposal with the Washington Stormwater Center to host a EPA Environmental Finance Center (\$4.8 million, unsuccessful), submitted two separate NSF proposals with researchers involved in the Freshwater Initiative at the University of Washington, and have a pending proposal with the Palouse Basin Aquifer Committee. We have been strengthening our ties to the the USGS Water Science Center, the Washington Stormwater Center, the Idaho Water Resources Research Institute, and other organizations for collaboration, and the Water Resources program at the Washington Department of Ecology. We have also initiated communication with the WSU Office of State and Office of Federal Relations to build prospective funding opportunities through them. Several other possibilities are in incubation stage.

Collaboration continues with the Center for Environmental Research, Education, and Outreach (CEREO), with which we share our administrative staff. CEREO's mission is broader than that of the WRC, but still encompasses water as an important issue. CEREO and WRC are developing a working relationship that arises from our shared mission of facilitating multidisciplinary research, focusing on complementarities and synergies between the two Centers and making use of our shared personnel resources.

We are collaborating with other Centers at WSU as well. The WRC and CEREO administrators jointly submitted a USDA AFRI CAP proposal in 2015 through the Center for Sustaining Agriculture and Natural Resources (CSANR). We are also working to build operational connections with the Washington Stormwater Center, which has a strong WSU presence and a home in Western Washington. This Center has expertise and a focus that is both historically and currently different but complementary to the focus and expertise of the WRC, and there are some promising opportunities for collaboration. The Ruckelshaus Center is a joint effort between WSU and UW that focuses on conflict resolution. They relatively frequently are asked to become involved in water-related conflicts, and we are working with them to assure that we utilize our complementary positions in science and policy activities to help resolve water-related conflicts.

Locally, the WRC is working with the Palouse Basin Aquifer Committee (PBAC) to provide the two cities and the two universities in the basin the science to help address the problem of declining aquifers and increasing water demand. WRC is also building ties to the USGS Water Science Center (WSC) in Tacoma, Washington. These two centers have a common USGS connection, but in recent years there has been little collaboration between the two Centers. The USGS is introducing new programs for 2015 that provides additional incentives and opportunities for USGS Science Centers and NIWR Centers to collaborate, and we are exploring opportunities to take advantage of these new resources. The WRC staff visited the USGS WSC in early 2015 to kick start seminar exchanges and collaborative research efforts.

The WRC currently has two primary connections to State government: the Washington State Department of Ecology, and the State Legislature. The Department of Ecology has been the source of a substantial share of WRC extramural funding in recent years to support WRC research to provide long-run water supply and demand forecasts for the State of Washington, which the Ecology Office of Columbia River oversees on a five year cycle. The WRC is also currently building stronger ties to the Ecology Water Resource Program, which oversees a broader array of water resource and regulatory issues. The State legislature has over the last several years identified the WRC as a source of independent research on water-related issues. The Yakima Basin Integrated Plan Benefit-Cost analysis was a legislatively funded mandate, and we have been charged also to review certain U.S. Bureau of Reclamation Benefit-Cost analyses as they are produced, relating to large Yakima Basin infrastructure projects. We are now also beginning a new legislatively mandated project examining mitigation options for exempt ground wells in Skagit Basin in response to a court-ordered moratorium.

The WRC administration intends to continue fostering its role as an independent source of quality research to help address the State of Washington's needs. The WRC administration is in communication with the WSU office of State relations to begin to explore ways of securing additional state base funding to support personnel for actively, permanent outreach and research programs.

Research Program Introduction

WRC's research program is active along several dimensions. First, the WRC manages a seed grant program funded by the Water Resources Research Act (WRRRA) 104(b) funds. Second, it is currently managing three extramural grants to support research and the administration is involved in an additional grant with water-related dimensions. Third, it has submitted and has begun preparing several proposals this past year for additional funding. Finally, it is pursuing a broad strategy for developing and strengthening research funding opportunities and collaborative opportunities within and outside of WSU and the State of Washington.

The WRC funded three small water-related grants (\$27,500/grant) under the WRRRA 104(b) FY2015 grant program. These projects are currently under way:

> "Climate Change Effects on Water Supply: Linkages Between Wildfire and Accelerated Snowmelt." Kaspari, Susan and Gazis, Carey Alice, Assistant Professors, Washington State University. Project 2015WA394B.

> "Development and Update of Rainfall and Runoff Intensity-Duration-Frequency Curves for Washington State Counties in Response to Observed and Anticipated Extreme Rainfall and Snow Events." Demissie, Yonas and Hossain, Akram of Washington State University Tricity, and Adam, Jennifer, Associate Director, Washington State University. Project 2015WA402B.

> "Bedload dynamics at the confluence of large rivers." Petrie, John Eric Assistant Professor, Washington State University and Muhunthan, Balasingam, Professor, Washington State University. Project #2015WA404B.

The extramural grants that the WRC is managing (or managed and completed) this year include:

> 2016 Columbia River Basin Long-Term Water Supply and Demand Forecast. Funded by the Washington State Department of Ecology Office of Columbia River. Jennifer Adam (PI), Michael Brady, Michael Barber (U. Utah), Chad Kruger, Mingliang Liu, Dan Haller (Aspect Consulting), Claudio Stockle, and Jonathan Yoder. Three-year project initiated in 2014. (\$1.8 million).

> NSF Food-Energy-Water workshop. The WRC along with two other centers acquired National Science Foundation funding to carry out a workshop focusing on the Food-Energy-Water nexus. The workshop was held in Seattle, WA on October 7-9, 2015. 50 participants from across the country attended. A white paper was submitted to NSF and a journal article is in preparation (\$45,000).

> Skagit Exempt Well Mitigation Study. This study is funded by the Washington State Department of Ecology to identify and assess mitigation options to allow development in the Skagit River Basin. Due to recent court action, there is a moratorium on building in the Skagit without mitigation. This is a short-term study, March-December 2016 (\$72,000).

In addition, the Director and Associate Director are involved in another grant in relation to the hydrology and economic elements of wildfire:

> FireEarth: Advancing Resilience to Compounding Disasters: An Integrated Natural-Human Systems Assessment of Wildfire Vulnerability. National Science Foundation; University of Idaho with subaward to WSU. WRC Associate Director Adam and Director Yoder are both Co-PIs on the grant (WSU, \$948,517 of a total of \$2,775,000).

Research Program Introduction

The Administrative team continues to pursuing further extramural support in line with the WRC strategic plan. It was a major contributor to a proposal submission to the USDA AFRI CAP Water for Agriculture program, with a request for joint effort between WRC, CEREO, CSANR, and the School of the Environment (\$10 million) submitted through CSANR. In addition, members of the WRC administration were involved in a total of four NSF INFEWS proposals this year, another proposal to host an EPA Environmental Finance Center (\$5,000,000), as well as two project proposals in collaboration with the University of Washington (NSF Coastal SEES, in addition to an NSF INFEWS proposal, part of the four listed above). More generally, the WRC has been positioning itself for future research funding and collaborative opportunities. Some of these activities are described above.

Specific grant proposals administered through the WRC or participated in by WRC staff related to water science and management include:

- > Padowski, Julie, Jonathan Yoder, Jennifer Adam, Stephanie Hampton, and Chad Kruger. August 2015. Addressing the Food-Energy-Water System Trilemma: Balancing Reliance on Technological and Institutional Solutions. National Science Foundation SEES workshop proposal: Interactions of Food Systems with Water and Energy Systems. \$44,953. Funded and completed.
- > Coastal SEES Collaborative Research: Shaping sustainable trajectories for coastal watersheds: The role of model predictions, uncertainty and risk. \$469,594. Pending. In collaboration with University of Washington.
- > Big Data Spoke for Drought Mitigation led by New Mexico State University. NSF Big Data Regional Innovation Hubs (BD Hubs) program. <http://www.nsf.gov/pubs/2016/nsf16510/nsf16510.htm>. Pending.
- > NSF Innovations at the Nexus of Food, Energy and Water Systems (INFEWS), Track 1: “Increasing regional to global-scale resilience in FEW systems through coordinated management of storage in concert with innovations in technology and institutions.” In preparation. With other WSU faculty in collaboration with PNNL (Ian Kraukunas, PNNL Lead). \$3,000,000 budget limit. Pending. > NSF Innovations at the Nexus of Food, Energy and Water Systems (INFEWS), Track 1: “Food-Energy-Water Systems in Mountainous Coastal Watersheds: Examining historical trajectories and the influence of human decisions”. In preparation. In collaboration with University of Washington. \$3,000,000 budget limit. Pending.
- > Yoder, Jonathan, Tanyalee Erwin, and John Stark. Proposal to House the U.S. Environmental Protection Agency Pacific NW Environmental Finance Center (PNWEFC). \$4.8Million. Not funded.
- > Katz, Stephen, et al. 2015. Maximizing the utility and adaptability of agricultural water-use science in supporting management for the Columbia River Basin’s next 30 years. Submitted to the USDA Water For Agriculture program. \$9,997,942. Not funded.
- > Padowski, Julie. Co-PI on USDA Water CAP proposal: Maximizing the utility and adaptability of agricultural water use science in supporting management for the Columbia River Basin’s next 30 years. Not funded.
- > Padowski, Julie. Co-PI on Palouse Basin Aquifer Committee proposal -- Active Management Option for Slowing or Halting the Decline of Grand Ronde Water Levels in the Moscow-Pullman Corridor. Not funded.

Student support: The extramural grant funding being managed through the WRC this fiscal year has supported 4 PhD students and one undergraduate student (for the summer of 2015).

Climate Change Effects on Water Supply: Linkages Between Wildfire and Accelerated Snowmelt

Basic Information

Title:	Climate Change Effects on Water Supply: Linkages Between Wildfire and Accelerated Snowmelt
Project Number:	2015WA394B
Start Date:	3/1/2015
End Date:	2/28/2016
Funding Source:	104B
Congressional District:	Washington 8
Research Category:	Climate and Hydrologic Processes
Focus Category:	Water Quantity, Climatological Processes, Geochemical Processes
Descriptors:	None
Principal Investigators:	Susan Kaspari, Carey Alice Gazis

Publications

There are no publications.

CLIMATE CHANGE EFFECTS ON WATER SUPPLY: LINKAGES BETWEEN WILDFIRE AND ACCELERATED SNOWMELT

Dr. Susan Kaspari, Associate Professor

Ted Uecker, MS student

Department of Geological Sciences, Central Washington University

Problem and Research Objectives

In Washington State the majority of runoff comes from the melting snowpack (Mote et al., 2005). In recent decades reductions in the seasonal snowpack have affected runoff timing and magnitude, and the availability of water resources. A consequence of the earlier snowmelt is an increase in wildfire activity (Westerling et al., 2006), which in turn affects snowmelt because decreased forest canopy in the post-fire environment causes an increase in snowpack net radiation, increasing the rate and advancing the timing of snowmelt (Burles and Boon, 2011; Harpold et al., 2014; Winkler, 2011). Recent research has demonstrated that snowmelt is further accelerated by the deposition of burned woody debris from charred snags (dead trees) on the snowpack that reduces snow albedo (i.e., reflectivity) and further accelerates melt (Gleason et al., 2013). However, it is not known how this effect attenuates over time, how it varies with burn severity, nor how black carbon from the charred snags contributes to the snow albedo reductions. We are working to quantify the duration and magnitude of earlier snowmelt in the post-wildfire environment by measuring: black carbon, charcoal and burned woody debris deposition; snow albedo; and snowmelt timing in forest plots of varying burn age and burn severity.

Methodology and Principal Findings

Note: Funding for this project became available in March 2015. 2015 was an anomalously low snowpack year in Washington State, and we were limited in our ability to conduct the required fieldwork to test our hypotheses. We conducted extensive fieldwork in 2016, and are currently conducting laboratory analyses.

To measure how BC deposition in the post-wildfire environment changes with time, three sites in the Cascades with varying burn age but similar burn severity and forest composition were sampled during the period of peak snowpack recorded by Snow Telemetry (SNOTEL) sensors (wcc.nrcs.usda.gov/snow). The sample sites include the 2006 Tripod Complex fire in northern Washington, the 2012 Table Mountain fire and the 2015 Chelan Complex fire, both in central Washington (Figure 1). Variations in BC deposition with burn severity was addressed by sampling in areas of low, moderate and high burn severity as classified using Monitoring Trends in Burn Severity maps (mtbs.gov). Hemispheric digital photographs of the forest canopy were taken at each sample location using a leveled fish-eye lens. These images will be evaluated using Gap Light Analyzer 2.0 (Frazer et al., 1999) to quantify canopy closure and determine forest density.

Transects were sampled at each study site. At each transect location, the entire snow column was sampled using a two-meter coring device, so each core sample represents BC deposition over the entire snow accumulation period. Surface snow samples were collected from the upper 2 cm of the snowpack where impurities most strongly affect snow albedo, and snow albedo was measured using a Spectral Evolution portable ultraviolet-visible near-infrared (UV-VIS-NIR) spectroradiometer. Additional measurements taken in the field included snow density and depth for calculating snow water equivalent, as well as classification of the surrounding forest structure and composition.

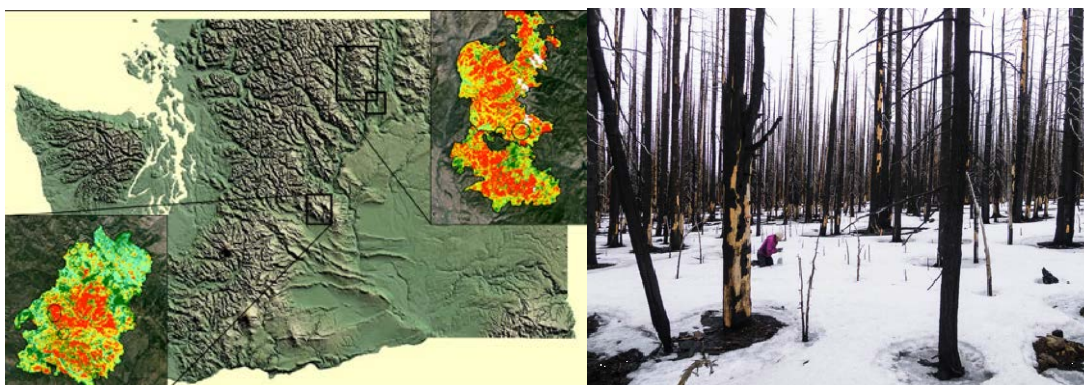


Figure 1. Left: Study areas in the Cascade Range including the 2006 Tripod Complex fire (upper right), and the 2012 Table Mountain fire (lower left). Burn severity is represented in by dark green (unburned), light green (light burn), yellow (moderate burn), and red (severely burned). Black circles represent sample sites (modified from MTBS.gov). Right: Collecting snow samples in a severely burned portion of the 2012 Table Mountain fire.

All snow samples are kept frozen until just prior to analysis. The snow samples will be melted, and BC concentrations will be measured using a Single Particle Soot Photometer (SP2) (Wendl et al., 2014). Select samples will be measured using a Sunset Lab Organic Carbon-Elemental Carbon (OC-EC) Aerosol Analyzer (Zhang et al., 2012). SP2 measures individual BC particles (80-1000 nm diameter), whereas the Sunset OC-EC differentiates between organic and elemental carbon and is used to measure carbon particles larger than those detected by the SP2. Bulk samples will be filtered to measure total impurity load. These data will help establish how BC deposition varies with respect to time since burn, distance from burn, burn severity, and forest density. Comparing BC concentrations with measurements of surface albedo, snow depth, and snow water equivalent throughout the spring will help us characterize post-fire BC deposition and its contribution to accelerated snowmelt.

Preliminary results indicate that charred material from trees post wildfire can substantially reduce snow reflectivity (related to albedo) (Figure 2), and that the reduction in reflectivity is affected by forest density. If analysis of our 2016 data supports this result, this would suggest that the effect of BC and woody debris deposition is fairly localized (i.e., isn't transported long distances). This is counter to our earlier findings that suggested that BC from charred forests can be transported long distances (Delaney et al., 2015). We have considerable laboratory work and interpretation of the resultant data to address our hypotheses.

Significance

Spatial analysis conducted by Gleason et al. [2013] indicated that between 2000-2012, over 80% of forest fires in the western U.S. burned in the seasonal snow zone (Figure 3), and forest fires in the snow zone were 4.4 times larger than those outside the seasonal snow zone. Furthermore, in the Western United States 48% of all forest fires in the seasonal snow zone occurred within the Columbia River Basin, suggesting that runoff and water resources in the Pacific Northwest are particularly affected by the post-wildfire effect. Climate change models project that due to warming temperatures, the April 1 snowpack will decrease by approximately 38-46% by the 2040s relative to the 1917-2006 mean (Elsner et al., 2010). These projected changes will result in earlier snowmelt runoff, reduced summer flows, and a reduction in water supplies. Additionally, the area burned by fire regionally is projected to double by the 2040s and triple by the 2080's (Littell et al., 2009). In light of the observed and projected changes to the snowpack and wildfire

activity, an improved understanding of the linkage between wildfire activity and snowmelt is necessary to understand climate change effects on water resources.

References

- Burles, K., Boon, S., 2011. Snowmelt energy balance in a burned forest plot, Crowsnest Pass, Alberta, Canada. *Hydrological Processes* 25, 3012-3029.
- Delaney, I., Kaspari, S., Jenkins, M., 2015. Black carbon concentrations in snow at Tronsen Meadow in Central Washington from 2012 to 2013: Temporal and spatial variations and the role of local forest fire activity. *Journal of Geophysical Research* 120, 9160–9172.
- Elsner, M.M., Cuo, L., Voisin, N., Deems, J.S., Hamlet, A.F., Vano, J.A., Mickelson, K.E.B., Lee, S.Y., Lettenmaier, D.P., 2010. Implications of 21st century climate change for the hydrology of Washington State. *Climatic Change* 102, 225-260.
- Gleason, K.E., Nolin, A.W., Roth, T.R., 2013. Charred forests increase snowmelt: Effects of burned woody debris and incoming solar radiation on snow ablation. *Geophysical Research Letters* 40, 4654-4661.
- Harpold, A.A., Biederman, J.A., Condon, K., Merino, M., Korgaonkar, Y., Nan, T., Sloat, L.L., Ross, M., Brooks, P.D., 2014. Changes in snow accumulation and ablation following the Las Conchas Forest Fire, New Mexico, USA. *Ecohydrology* 7, 440-452.
- Littell, J.S., Mcguire Elsner, M., Whitely Binder, L.C., Snover, A.K., 2009. The Washington Climate Change Impacts Assessment: Evaluating Washington's Future in a Changing Climate - Executive Summary. University of Washington, Seattle, Washington.
- Mote, P.W., Hamlet, A.F., Clark, M.P., Lettenmaier, D.P., 2005. Declining mountain snowpack in western north America. *Bulletin of the American Meteorological Society* 86, 39-+.
- Wendl, I., Menking, J.A., Farber, Gysel, M., Kaspari, S., Laborde, Schwikowski, M., 2014. Optimized method for black carbon analysis in ice and snow using the Single Particle Soot Photometer. *Atmospheric Measurement Techniques* 7.
- Westerling, A.L., Hidalgo, H.G., Cayan, D.R., Swetnam, T.W., 2006. Warming and earlier spring increase western US forest wildfire activity. *Science* 313, 940-943.
- Winkler, R.D., 2011. Changes in snow accumulation and ablation after a fire in south-central British Columbia. *Streamline Watershed Management Bulletin* 14, 1-7.
- Zhang, Y.L., Perron, N., Ciobanu, V.G., Zotter, P., Minguillón, M.C., Wacker, L., Prévôt, A.S.H., Baltensperger, U., Szidat, S., 2012. On the isolation of OC and EC and the optimal strategy of radiocarbon-based source apportionment of carbonaceous aerosols. *Atmos. Chem. Phys.* 12, 10841-10856.

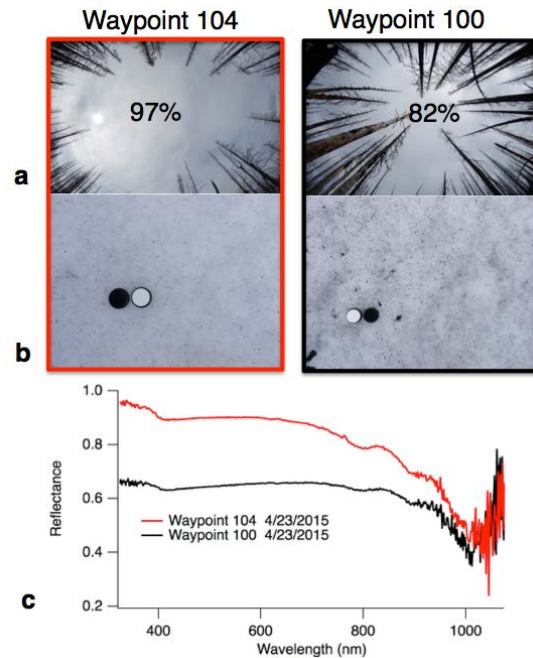


Figure 2. a) Hemispheric photos taken at Waypoints 104 (left) and 100 (right) at Table Mountain on 4/23/2015 showing percent canopy exposure, which is used to measure the amount of material available for deposition. b) Photos showing deposition of burned material on the snowpack; the black and white circles are reflectance standards. c) Snow reflectance data for Waypoints 104 and 100. Reflectance (related to albedo) is lower at Waypoint 100 than 104, which is consistent with higher tree density and greater impurity deposition as shown in b.

Development and Update of Rainfall and Runoff Intensity-Duration-Frequency Curves for Washington State Counties in Response to Observed and Anticipated Extreme Rainfall and Snow Events

Basic Information

Title:	Development and Update of Rainfall and Runoff Intensity-Duration-Frequency Curves for Washington State Counties in Response to Observed and Anticipated Extreme Rainfall and Snow Events
Project Number:	2015WA402B
Start Date:	3/1/2015
End Date:	2/28/2016
Funding Source:	104B
Congressional District:	4
Research Category:	Climate and Hydrologic Processes
Focus Category:	Hydrology, Floods, Climatological Processes
Descriptors:	None
Principal Investigators:	yonas Demissie, Jennifer Adam

Publications

1. Moges, E., Y. Demissie, H. Li, 2016, Hierarchical mixture of experts and diagnostic modeling approach to reduce hydrologic model structural uncertainty, Water Resources Research, 52, 2551-2570.
2. Mortuza, R., 2015, Regional frequency analysis and copula multivariate statistics for characterizing extreme precipitation and drought, MS Dissertation, Civil and Environmental Engineering, Washington State University, Richland, WA, p. 77.



6/28/2016

Development and Update of Rainfall and Runoff Intensity- Duration-Frequency Curves for Washington State Counties in Response to Observed and Anticipated Extreme Rainfall and Snow Events

[Document subtitle]

Yonas Demissie and Md Rubayet Mortuza

Department of Civil and Environmental Engineering
Washington State University

Submitted to: State of Washington Water Research Center

June 28, 2016

I. EXECUTIVE SUMMARY

I.1. Background

The observed and anticipated increasing trends in extreme storm magnitude and frequency, as well as the associated flooding risk in the Pacific Northwest highlighted the need for revising and updating the local intensity-duration-frequency (IDF) curves, which are commonly used for designing critical water infrastructure. In Washington State, much of the drainage system installed in the last several decades use IDF curves that are outdated by as much as half a century, making the system inadequate and vulnerable for flooding as seen more frequently in recent years. In this study, we have developed new and forward looking rainfall and runoff IDF curves for each county in Washington State using recently observed and projected precipitation and watershed data. Regional frequency analysis coupled with Bayesian uncertainty quantification and model averaging methods were used to develop and update the rainfall IDF curves, which were then used in hydrologic model to develop the runoff IDF curves that explicitly account for effects of snow and drainage characteristic into the IDF curves and related designs. The resulted rainfall and runoff IDF curves provide more reliable, forward looking, and spatially resolved characteristics of storm events in Washington State that can assist local decision makers and engineers to thoroughly review and/or update the current design standards for urban and rural stormwater management infrastructure.

I.2. Objectives

The overall objective of this study is to revise the rainfall IDF curves for Washington State using recent and future precipitation data, develop the associated Runoff IDF curves, and quantify the uncertainty related to model and parameters. Specifically, the study: 1) gather and screen the most up-to-date gaged rainfall data from various sources, 2) conduct trend and seasonality analyses on historical extreme precipitation, 3) delineate climatologically homogeneous regions for each rainfall durations considered, 4) identify multiple appropriate probability distributions for each region and apply Bayesian Averaging Method to combine them, 5) estimate the distribution parameters and associated uncertainty, 6) generate rainfall IDF curves for each regions with rainfall durations from 1-hour to 10-day and return periods from 2 years to 100 years, 7) spatially interpolate the resulted IDF curve values using a site-specific scale factor to account for regional variability, 8) interpolate the IDF curves to county level using the overlapped areas of the regions and counties as scaling factor, 9) incorporate climate projections in the estimated IDF values, 10) generate the runoff IDF curves for selected watersheds, and 11) present revised IDF estimates in tabular and graphical forms. The report provides precipitation and runoff frequency estimates for durations of 15-minutes through 10-days at average recurrence intervals of 1-year through 100-year for the WA state with associated 90% confidence intervals and supplementary information on temporal and spatial distributions of heavy precipitation and runoff, analysis of seasonality and trends in precipitation annual maxima, etc. It includes pertinent information on development methodologies and intermediate results. The detail results will also publish through our interactive webserver.

I.3. Data Used

The study uses rainfall and snow data obtained from 645 daily and 116 sub-daily (hourly and 15-minute) rainfall and snow recording stations throughout Washington and part of Idaho, Oregon and Canada. The daily data covers from 1891 to 2014, while the sub-daily data covers from – to --. These datasets went through rigorous screening, quality checking and filling of the missing values. For daily data, stations with record length greater than 30 years and data coverage of more than 90% were selected from National Climatic Data Center's Global Historical Climatology Network (GHCND), Global Summary of the Day (GSOD) and Natural Resources Conservation Service's SNOTEL databases. For sub-daily data, stations having at-least 15 years of data with 80% coverage were selected from National Climatic Data Center's Cooperative Observer Network (COOP) and Washington State University Irrigated Agriculture Research and Extension Center's AgWeatherNet datasets. Discordancy analysis was conducted based on the entire stations records to identify stations with possible outlier records. Discordant stations were further investigated to examine the source of the outliers and decide whether to keep or remove the stations.

I.4. Methodologies

Regional frequency analysis, Bayesian methodology and hydrologic model were respectively used to update the current IDF curves, quantify the associated uncertainty and generate the runoff IDF curves. The regional frequency analysis based on L-moment statistics of the precipitation annual maxima was used to identify climatologically homogeneous regions, chose appropriate frequency distributions, estimate the parameters of the distributions, and compute quantile estimates. Unlike to site-specific frequency analysis which relies on data from a given station, the regional frequency analysis allows polling data from stations within

climatologically homogeneous region in order to improve the overall accuracy of the quantile estimates. We have introduced Fuzzy clustering approach to delineate the climatological homogenous regions based on physical characteristics of rainfall stations and to automate adjustment of regions during the homogeneity analysis. Assuming that the extreme precipitation spatial patterns and coverages change with their durations, the regional frequency analysis was conducted independently for each rainfall duration considered in this study. This is a departure from most other similar studies which considered similar regions for various rainfall durations. In addition, instead of selecting a single best-fitted probability distribution for each region, this study selects multiple probability distributions that reasonably fit the observed extreme precipitation data and apply Bayesian Model Averaging technique to combine their quantile estimates. The HEC-HMS hydrologic model was used for selected watershed in Washington State to estimate the peak flows associated with design storms and to develop the runoff IDF curves.

I.5. Results

Stationarity of the extreme precipitation data is a required condition for reliable estimate of their quantiles and for developing the IDf curves. In this study trend, correlation, and heteroscedasticity analyses were conducted for precipitation annual maxima with durations from 15 minutes to 10 days. Overall, more stations (up to 33%) show statistically significant decreasing trends for short durations precipitation annual maxima, while up to 8% of the stations showed increasing trends for longer durations (daily and longer) precipitation annual maxima. No noticeable correlations were observed in precipitation annual maxima for all the durations considered in this study, while some stations consistently show increasing variance for all the durations. Similar trend, correlation, and heteroscedasticity analyses were conducted at regional

level using precipitation annual maxima polled from stations within homogenous regions. No noticeable trend, correlation and heteroscedasticity were observed at regional level, allowing for direct application of regional frequency analysis to develop the IDF curves without the need for further data filtering. There are also distinct variations on the seasonality of the extreme storms in Washington State, with majority of the storms occur during winter (DJF) in Western Washington and during spring (AMJ) in Eastern Washington.

The homogeneity analysis using Fuzzy clustering and L-moment statistics identify: 1) 5 regions with average 17 stations per regions for 15 and 30 minutes storms, 2) 6 regions with average 18 stations per regions for 1, 2, 3, 6, 12 hours storms, and 3) 26 regions with average 22 stations for 1 to 10 days storms. Earlier study by Wallis et al. (2007), divided WA into 12 regions to estimate the 2 hour and 24 hour precipitations frequencies. Unlike to the traditional regional frequency analysis which select a single probability distribution for each region that best-fit the precipitation annual maxima, in this study multiple probability distributions that reasonable fit the data were selected and combined using Bayesian Model Averaging method. For the 15-minute storms, the Generalized Normal (GNO) and Pearson Type III (PE3) distributions are found to be suitable for 40% of the regions, while the Generalized Logistic (GLO), Generalized Extreme Value (GEV) and GNO distributions are suitable for 20% of the regions, and only GNO is suitable for the remaining 40% of the region. For the 30-minute storms, the GLO, GEV, and GNO are suitable for 60% of the regions, while GNO and PE3 are suitable for 40% of the regions. For 1-hour storms, the GLO, GEV, and GNO are suitable for 50% the regions, while the rest of the regions use either GLO and GEV or GNO and GEV. Different combinations of these distributions and other distributions such as Generalized Pareto (GPA) and Kappa are found to be suitable for the remaining durations and associated regions.

Rainfall IDF curves with associated 95% uncertainty ranges were generated for each homogenous region, which were then interpolated to gridded map and county level IDF curves using, respectively, the mean annual maximum precipitation and the overlapped areas of counties and homogenous regions as scaling or weighting factors. The resulted IDF curve values were compared to currently available IDF values in Washington, which are obtained from the Washington State Department of Transportation (WSDOT), NOAA Atlas 2 and Wallis et al. (2007) spatial maps for 2-hour and 24-hour durations extreme precipitations. The results from the first two comparisons (i.e., WSDOT and NOAA Atlas 2) are presented in this report, while the comparison with the Wallis et al. (2007) results showed large differences along the mountains that need further examination and thus are not included in this report. Overall, except for Walla Walla, the WSDOT estimates larger amount of precipitations for 2-year storms compared to this study and that of NOAA, while for the 100-year storms, this study estimated relatively large amount of precipitation in the southeast (Yakima, Walla Walla, and to some extent Kennewick) compared to the one estimated by WSDOT and NOAA. Based on these preliminary observations, the current drainage systems designed based on WSDOT's estimate of precipitations are expected to be adequate for draining design storm with shorter return periods in most parts of the state. However, for design storm with larger return periods, depending on locations, retrofitting of the drainage system might be required.

To investigate the effect of future climate on extreme precipitation and associated IDF values, the study considered data from two climate models (BCC-CSM1.1 and CanESM2) and two scenarios (RCP 4.5 and RCP 8.5). However the resulted extreme precipitation estimates were found to be smaller than the historical values, suggesting for further studies by including more

climate models, addressing their uncertainty and limitations in projecting extreme storm events as most of the climate models are primarily designed to capture mean patterns.

Finally, the runoff IDF curves generated the study for selected watershed in Washington provide a direct link between anticipated severe storms, which can be obtained from the rainfall IDF curves, and runoff peaks and flood risk, which in return can be used to better design and manage drainage systems. In addition, the runoff estimate allows to incorporate effect of snowmelt and drainage changes in the IDF analysis and assessment of effectiveness of drainage and flood control structures and managements.

Acknowledgments

This project was financially supported by State of Washington Water Research Center under grant G11AP20113.

Contents

I. Executive Summary.....	I
I.1. Background.....	I
I.2. Objectives.....	II
I.3. Data Used.....	III
I.4. Methodologies.....	III
I.5. Results.....	IV
Acknowledgements.....	VIII
Contents.....	IX
List of Tables.....	XI
List of Figures.....	XII
1. Introduction.....	1
1.1. Objectives.....	3
2. Data and Study Regions.....	4
2.1. Study Regions.....	4
2.2. Data.....	6
2.2.1. Filtering Measurement Errors.....	8
2.2.2. Trend, Correlation and Change in Variance.....	11
2.2.3. Seasonality of Extreme Precipitation.....	14
3. Methodologies.....	16
3.1. Regional Frequency Analysis (RFA)	17
3.1.1. Trend and Randomness Test.....	17
3.1.2. Discordancy Measures.....	18

3.1.3. Initial Regions.....	19
3.1.4. Final Homogenous Regions.....	20
3.1.5. Identifying Appropriate Distributions.....	21
3.2. Uncertainty Analysis using Bayesian Approaches.....	22
3.2.1. Parameter Uncertainty.....	22
3.2.2. Model Uncertainty.....	24
3.3. Hydrologic Modeling.....	25
3.3.1. HEC-HMS modeling.....	26
3.3.2. Yakima River Basin (YKB)	30
3.3.3. Snohomish River Basin (SRB)	32
3.3.4. Puyallup River Basin (PRB)	35
3.3.5. Green-Duwamish River Basin (GRB)	37
4. Results.....	40
4.1. Identifying Homogenous Regions.....	40
4.2. Choosing Frequency Distribution.....	44
4.3. County Level IDF Curves.....	46
4.4. Spatial Maps of Extreme Precipitation.....	48
4.5. Comparison with Currently Available IDF values.....	49
4.6. Climate Projections.....	52
4.7. Runoff IDF Curves.....	54
References.....	59
Appendix A: Maps of homogenous regions for various durations.....	78
Appendix B: County level IDF curves.....	82
Appendix C: Tables for county level IDF values and their 95% CI.....	100
Appendix D: Spatial maps of the extreme precipitation.....	123

List of Tables

Table 1. Datasets used for the study and their sources.....	7
Table 2. Trend, correlation and change variance for storms with durations ranging from 15-minute to 10-day.	13
Table 3. Melt-rate as a function of antecedent temperature index (ATI).	30
Table 4. Average number of stations within each region.....	43.
Table 5. L-CV and mean annual maximum precipitation for 15-min to 1-day storms.....	44

List of Figures

Figure 1. Spatial distribution of mean annual precipitation in Washington.....	5
Figure 2. Spatial variation of average daily maximum precipitation in Washington.....	6
Figure 3. Spatial variation of average hourly maximum precipitation.....	6
Figure 4. Locations of stations with 15-minute precipitation records, record length greater 20 years and data coverage greater than 70%.....	7
Figure 5. Locations of stations with daily precipitation records, record length greater 30 years and data coverage greater than 90%.....	8
Figure 6. Results from discordancy testing, showing discordant stations ($D \geq 3$) in triangles.....	9
Figure 7. AM time series for stations which are considered to be discordant ($D \geq 3$). The time series for most of the stations indicate the presence of potential measurement errors.....	10
Figure 8. Time series for annual maximum precipitation (left) and daily precipitation (right) showing the impact of missed records on annual maximum data.....	11
Figure 9. Locations of stations with significant decreasing trends in storms with 15-minute, 1-hour, 6-hour and 24-hour durations.....	14
Figure 10. Seasonality of extreme precipitations occurrence across Washington State.....	16
Figure 11. Work flow for regionalization and uncertainty methodologies.....	16
Figure 12. Yakima River Basin and distribution of mean annual precipitation.....	31
Figure 13. Yakima River stage near the basin outlet following the January 9, 2009 storm.....	32
Figure 14. Snohomish River Basin and distribution of mean annual precipitation.....	33

Figure 15. Snohomish River stage near the basin outlet following the January 7, 2009 storm.....	34
Figure 16. Snohomish River stage near the basin outlet following the December 08, 2015 storm.....	34
Figure 17. Puyallup River Basin and distribution of mean annual precipitation.....	36
Figure 19. Puyallup River stage near the basin outlet following the December 08, 2015 storm.....	37
Figure 20. Green-Duwamish River Basin and distribution of mean annual precipitation.....	38
Figure 21. Green-Duwamish River stage near the basin outlet following the January 7, 2009 storm.	39
Figure 22. Green-Duwamish River stage near the basin outlet following the December 08, 2015 storm.	42
Figure 23. Initial and final regions, as well as corresponding H statistics for 1-day extreme precipitation in Washington.....	42
Figure 24. Climatologically homogenous regions for 1-hour extreme precipitation in Washington.	43
Figure 25. Selected frequency distributions for each duration and region. The numbers on the charts are the percentage of regions, which use the given combination of distributions...	45
Figure 26. County-level IDF curves for selected counties in eastern and western Washington.	47
Figure 27. Distribution of 25-year extreme precipitations which have 30-minute and 24-hour durations.....	49

Figure 28. Comparisons of IDF curves from this study with that of WSDOT and NOAA-Atlas 2 for selected cities.....	52
Figure 29. Extreme precipitation based on projected and historical data.....	54
Figure 30. Calibration (left) and validation (right) results for the four watersheds considered....	56
Figure 31. Runoff IDF curves for Yakima, Snohomish, Puyallup and Green-Duwamish watershed outlets.....	58

1. Introduction

Stormwater and flood management infrastructures are commonly designed to handle specific design storms derived from historical rainfall intensity-duration-frequency (IDF) curves based on the assumptions that these rainfall characteristics will remain unchanged throughout the design lifetimes of the infrastructures. However, the historical and projected increase in frequency and intensity of extreme rainfall (Kunkel et al. 2013, Groisman et al. 2012) may violate this assumption, making the infrastructures inadequate and vulnerable for flooding as seen more frequently in recent years. In Washington State, for example, majority of the drainages and flood control structures were designed based on IDF curves information obtained from: (1) Arkell and Richards (1986) for shorter duration (or less than one hour) rainfall; (2) NOAA Atlas 2, Volume 9 (Miller et al. 1973) for 1-24 hour rainfall; (3) Technical Paper 49 (Miller 1964) for 2-10 day rainfall. The Washington State Department of Transportation (WSDOT) updated the 2-hour and 24-hour rainfall frequencies and spatial maps using precipitation records up to 2000 for Western Washington (Schaefer et al. 2002) and up to 2003 for Eastern Washington (Schaefer et al. 2006). Due to the use of these outdated data, much of the drainage installed in Washington State in the last several decades might be too small to handle current and future storms. This could lead to inadequate drainage systems that potentially lead to higher flood risk, as seen in recent years.

Several studies (e.g., Janssen et al. 2014, Kunkel et al. 2013, Mass et al. 2011) have evaluated historical trends of extremes precipitation of various durations, and have found a dramatic increase in extreme storm events across the Pacific Northwest and other parts of U.S. during the past half century. For instance, the third National Climate Assessment (Melillo et al. 2014) showed that the frequency of heavy precipitation (defined as top one percent of

precipitation) has increased by almost 20% on average in the U.S. and by about 12% in the Pacific Northwest since 1958. In a similar study, Madsen and Figdor (2007) analyzed the historical trends of extreme precipitation from 1948 to 2006 for the entire Washington State and Puget Sound region, and found 30% and 45% increase in the frequency of extreme precipitation, respectively. Rosenberg et al (2010) evaluated the changes in annual precipitation maxima between 1956–1980 and 1981–2005 for storm duration ranging from 1-hour to 10-day in Seattle-Tacoma, Portland, and Spokane areas. Their results showed that the annual maximum precipitations have increased for all durations in Seattle-Tacoma, with the 24-hour storms showing the maximum increase of about 25%. The probability of occurrence of a 50-year storm in any given year has increased from 2% to 12% during these periods, and is thus about six times as likely to occur. For Portland and Spokane, the changes depend on the storm durations and range from -4% for 1-hour storms to 10% for 10-day storms in Portland and from -10% for the 5-day storm to 15% for 12-hour storms in Spokane. In addition to the increased frequency, the recent U.S. Environmental Protection Agency report (USEPA 2014) also showed increasing trend in the spatial coverage of 1-day extreme precipitation in the U.S. during 1910-2013.

The increasing trends in heavy precipitation are expected to continue in the future, with likely intensification in most part of U.S. (NRC 2013, Groisman et al. 2012, Westra et al. 2013). Particularly, the atmospheric rivers, which is the primary weather phenomena for causing extreme precipitation and flooding in the Western U.S. (Neiman et al 2011, Ralph et al. 2006), are projected to transport 26-30% more water vapor in the future (Warner et al. 2012), potentially leading to increased severe storm and flood events in the region (Dettinger 2011). In the Seattle-Tacoma area alone, the magnitude of a 24-hour storm is projected to increase 14-28% during the next 50 years. Snover et al. (2013) also found the number of days of a given extreme precipitation rate in the

Pacific Northwest increases by the 2050s relative to 1970 to 1999. Salathé et al. (2010) showed increasing trend in future extreme precipitation intensity (annual total precipitation divided by the number of wet days) over the northwestern portion of the state, while the rest of the regions do not show significant trends.

The observed and expected increase in extreme precipitation events illustrate the vulnerabilities of the storm drainage and flood control structures in Washington State, particularly where stormwater detention and conveyance facilities were designed under assumptions of stationary storm events that may no longer be valid. The heavy precipitation combined with aging and inadequate drainage infrastructure has resulted in substantial changes in flood risks over much of the western Washington (Rosenberge et al. 2010, Hamlet and Lettenmaier 2007). For instance, since 1990, the King County has experienced 12 federally declared flood disasters, and Interstate 5 has closed four times due to flooding. The overall cost of flood damage in the state has also increased over the years. The recent major flood and landslide events in Washington State, including the December 2007 and January 2009 floods of the Chehalis River, the January 2009 floods in Seattle, and the March 2014 mudslide in Oso show the vulnerabilities of the current drainage and flood control structures in the state to the change in extreme precipitation and resulted flood. As the climate warms, the flood frequency is projected to increase in the future, with the largest increases predicted in Puget Sound, southwest Washington, and east side of the Cascades (Mantua et al. 2010).

1.1. Objectives

To address the non-stationarity of storms and associated flood risk, this study updated the current IDF curves in Washington State using recently observed and projected precipitation data.

Runoff IDF curves based on peak flow simulations results were generated for selected watersheds in Washington State in order to directly take into account the effects of drainage and snowpack/melt into IDF curves and associated flood risk. Specifically, the results include: (1) new and updated rainfall and runoff IDF curves with 90% confidence intervals for rainfall durations from 1-hour to 10-day and return periods from 2 years to 500 years for every county in Washington State, (2) extreme precipitation maps for all the durations and return periods we have considered, (3) assessment of risk posed by climate change and variability on existing storm drainage in Benton County which is the most downstream county for the Yakima River drainage, and (4) tabulated and geo-referenced data and use manual describing the data and the methodologies that can easily be downloaded from our research webpage. The updated IDF curves will provide up-to-date and local design standards and guidelines for storm drainage and flood control structures.

2. Data and Study Region

2.1. Study Region

The study area covers the State of Washington, which has significant and complex spatial variability in climate and vegetation ranging from temperate coastal rain forests to glaciated mountain ranges to arid scrublands (Salathé et al. 2010). The average yearly precipitation ranges from more than 250 inches near to the coast and on the Cascade Mountain to less than 10 inches in the southeast area (Figure 1). The Cascade Mountain, which extends from north to south splits the state into west and east sides, create a rain-shadow effect that increase the rainfall amount on west side of the mountain but block the penetration of moisture into east side. The precipitation in the state also varies significantly from year-to-year because of the El Niño–Southern Oscillation and its modulation by the Pacific Decadal Oscillation (Salathé et al. 2010). The extreme

precipitation events are particularly very different spatially, even with minor physiographic differences (Mikkelsen et al. 2005). Figures 1, 2 and 3 show the spatial variations of average annual precipitation, average daily maximum precipitation and average hourly maximum precipitation, respectively. Shorter durations maximum precipitations show more spatial variations compared to longer durations maximum precipitations, verifying the need to delineate homogenous regions for each storm durations we have consider.

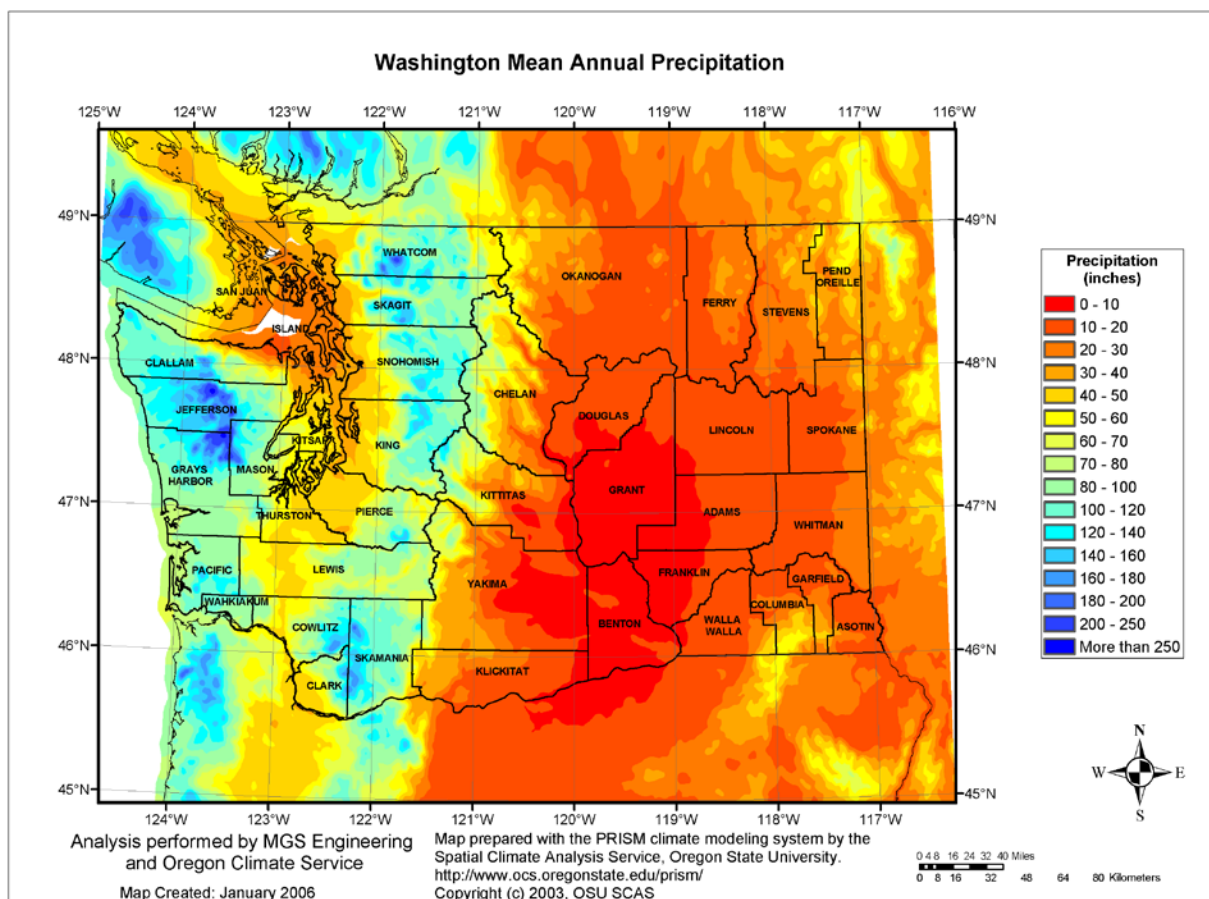


Figure 1. Spatial distribution of mean annual precipitation in Washington (Source: MGS Engineering Consultants)

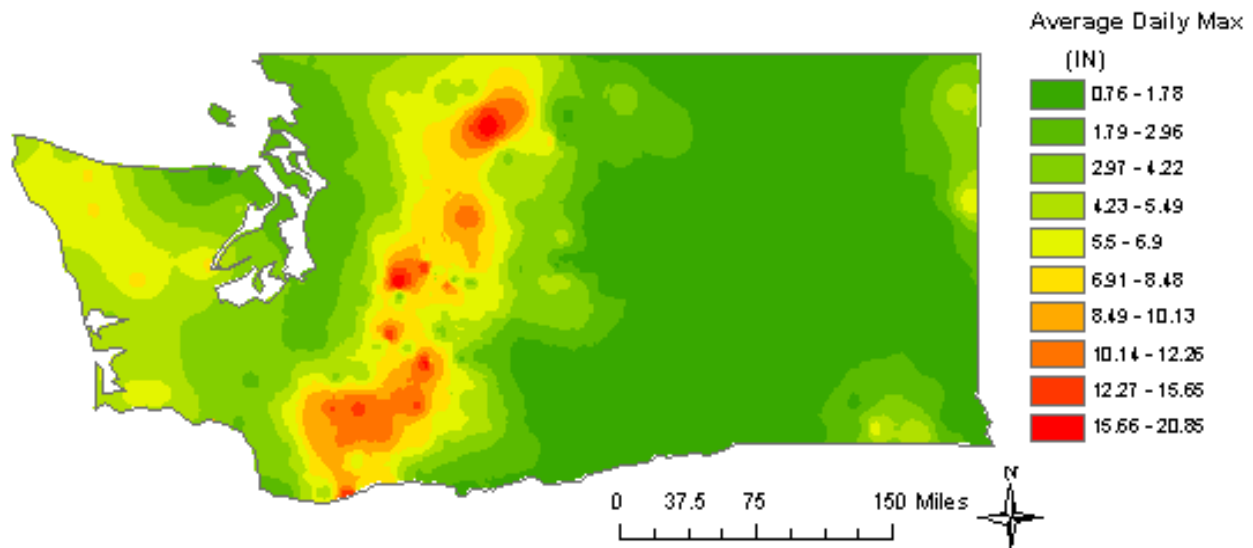


Figure 2. Spatial variation of average daily maximum precipitation in Washington.

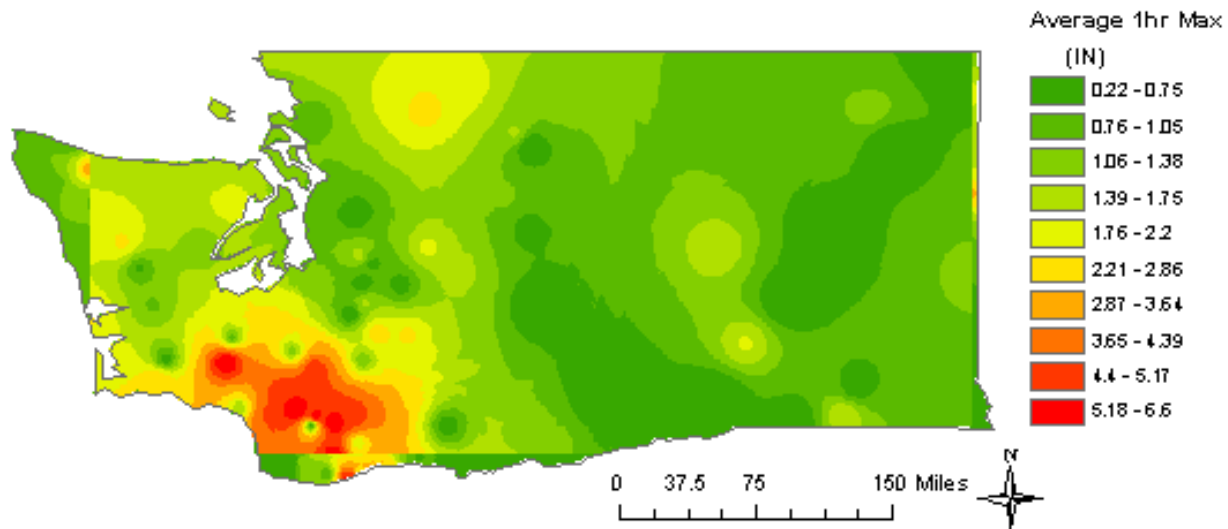


Figure 3. Spatial variation of average hourly maximum precipitation

2.2. Data

The study utilized 15-minute, hourly, and daily rainfall data obtained from various sources (Table 1) for latitude range from **40°00'00"N** to **50°00'00"N** and longitude range **116°00'00"W** to **125°00'00"W**. The daily data for most of the sites were obtained from the National Climatic Data Center's Global Historical Climatology Network (GHCN) and Global Summary of the Day (GSOD) databases, and from the Natural Resources Conservation Service's

SNOTEL database. The hourly data were obtained from U.S. Hourly Precipitation Data (DSI-3240) and Integrated Surface Global Hourly Data (DSI-3505) archived at the NCDC. The 15-minute data were obtained from the U.S. 15 Minute Precipitation Data (DSI-3260) archived at the NCDC and the Washington State University Irrigated Agriculture Research and Extension Center's AgWeatherNet database. Figure 4 and 5 show the locations of stations with 15-min and daily records after screening for data coverages.

Table 1. Datasets used for the study and their sources

Recording Intervals	Data Source	Number of Stations Before Filtered	Number of Stations After Filtered
15-minute	DSI-3260	98	56
	AgWeatherNet	170	44
1-hour	DSI-3420	183	57
	DSI-3505	283	59
1-day	GHCN	2478	616
	GSOD	282	28
	SNOTEL	98	58

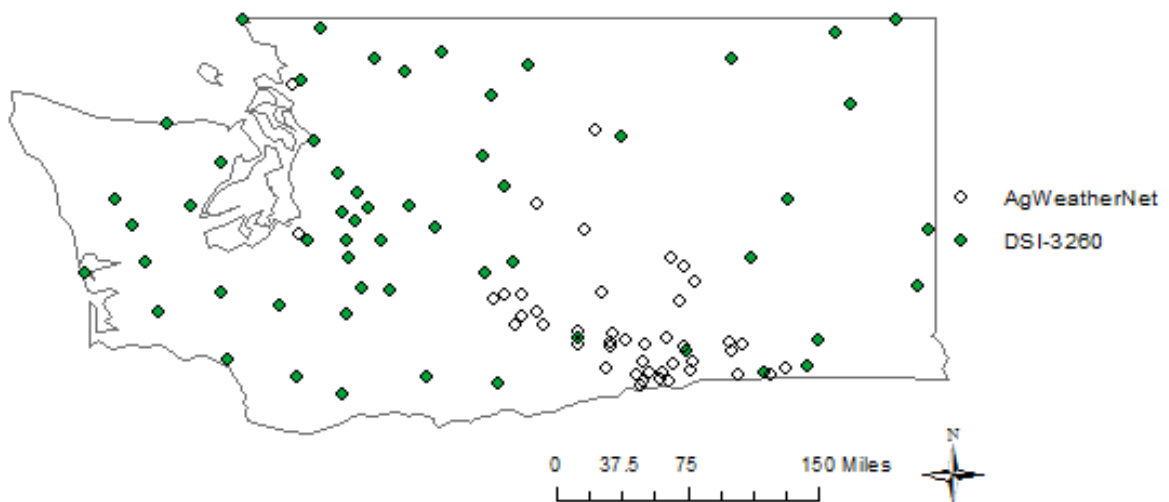


Figure 4. Locations of stations with 15-minute precipitation records, record length greater 20 years and data coverage greater than 70%.

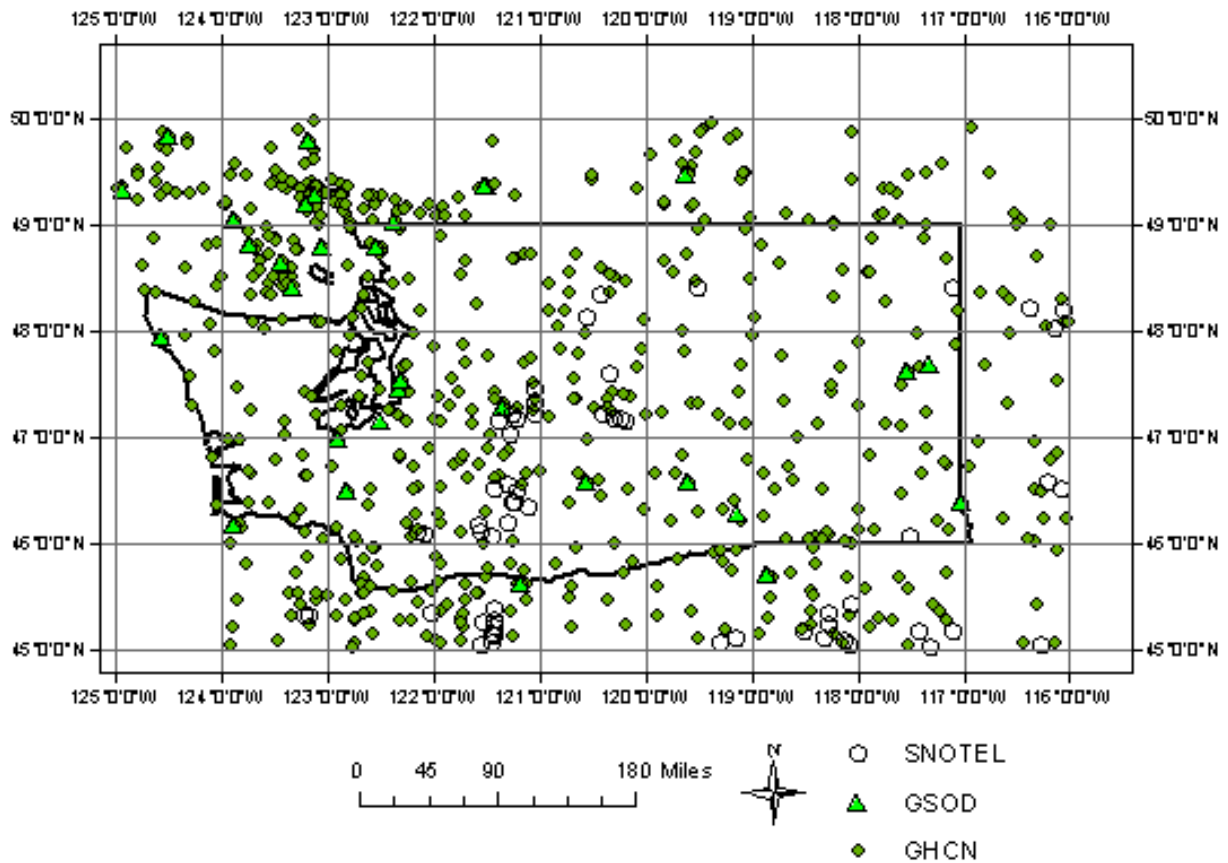


Figure 5. Locations of stations with daily precipitation records, record length greater 30 years and data coverage greater than 90%.

2.2.1. Filtering Measurement Errors

In order to screen the data for potential measurement errors and outliers, we have conducted the discordancy test (Hosking and Wallis 1997) for all the AM series at each site. The L-moments and their ratios were estimated for all the AM series at each site after normalizing them by the at-site mean. The L-moment ratios were then used to estimate the discordancy measure (D) which identifies statistically unrelated site within the study area. By comparing the L-moment ratios of a station with those of a region as a whole, the discordancy measure identifies sites having different

L-moment ratios relative to other stations in a region. Station having a high value of the discordancy measure within the study area can be identified as discordant. Hosking and Wallis (1997) suggested critical value of D to be 3 for a station within a region having more than 15 member stations. Figure 6 shows discordant stations for 1-day AM series, while Figure 7 shows the 1-day AM series for those discordant stations. As shown in Figure 7, some of the discordances are resulted from possible measurement errors, which were removed from the daily data and the associated AM series were regenerated. In addition to assisting in locating abnormalities in a data set, the discordancy measure can aid in identifying homogeneous regions. If a site is discordant in a particular region, it could be moved to another region, which may have relatively similar L-moment ratios. This is discussed further in section 3.1.4.

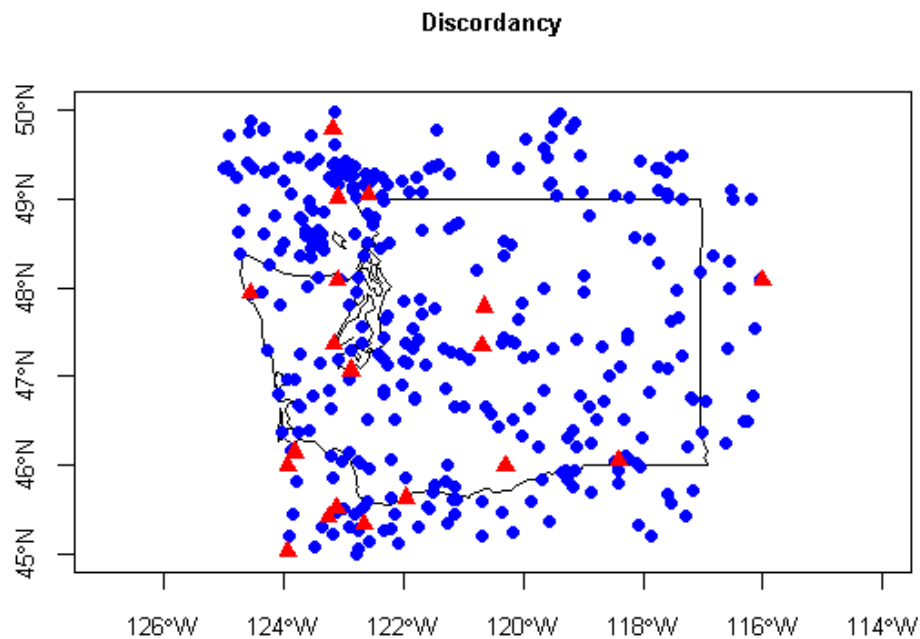


Figure 6. Results from discordancy testing, showing discordant stations ($D \geq 3$) in triangles.

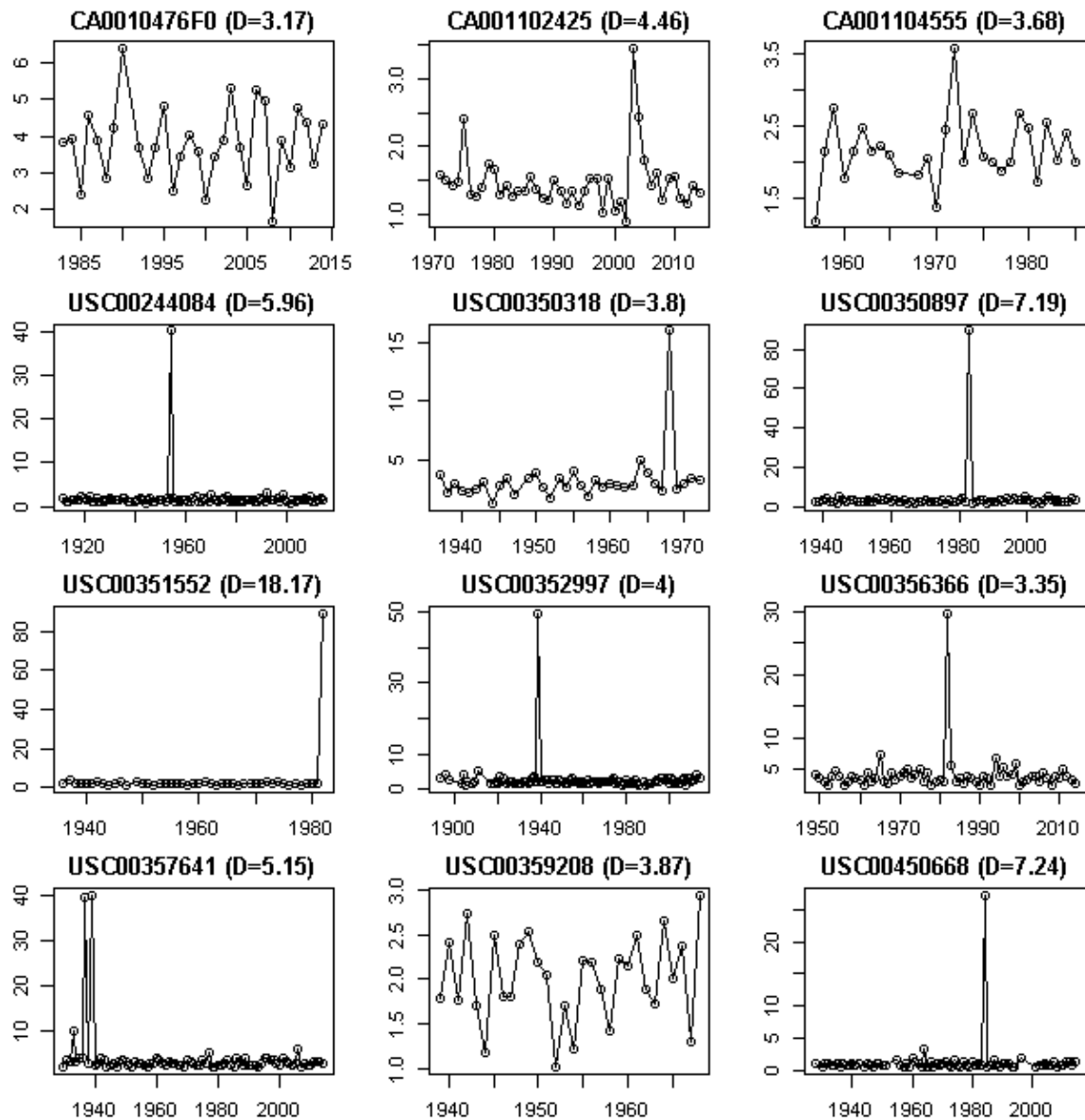


Figure 7. AM time series for stations which are considered to be discordant ($D \geq 3$). The time series for most of the stations indicate the presence of potential measurement errors.

In order to avoid underestimating the precipitation annual maximum for a given year, the record for a particular year was removed when the record coverage for the same year was less than 90% for daily or less than 70% for hourly and 15-minute data. This is illustrated in Figure 8, which

shows the missed records in year 1908 resulting to relatively small precipitation annual maximum for 1908. Such record years were removed from our analysis.

Finally, The 1, 2 and 5 day durations annual maximum precipitation (AM1, AM2 and AM5) at each station were extracted and rescaled by dividing them with their respective average values.

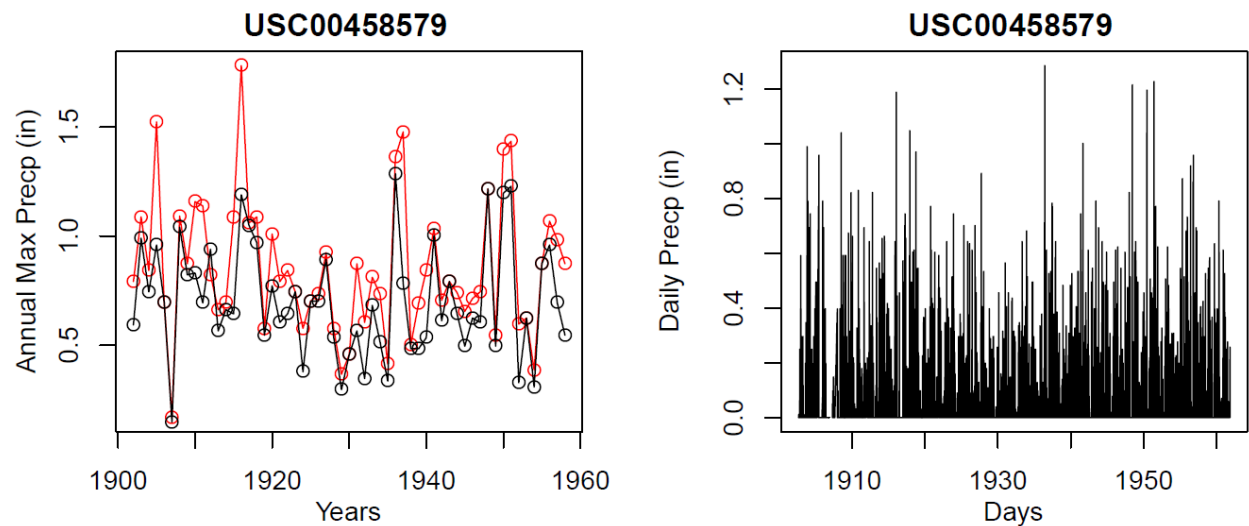


Figure 8. Time series for annual maximum precipitation (left) and daily precipitation (right) showing the impact of missed records on annual maximum data.

2.2.2. Trend, Correlation and Change in Variance

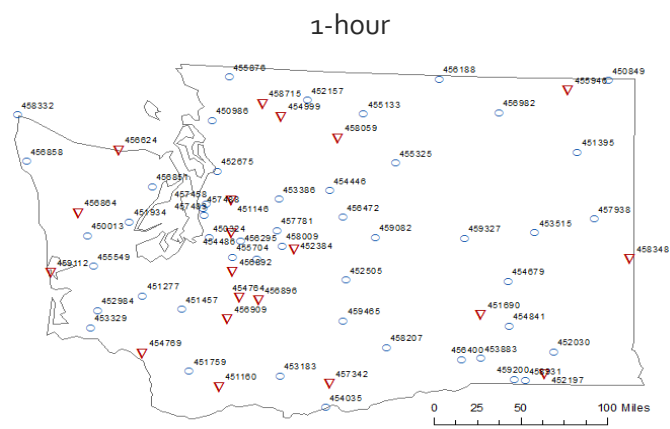
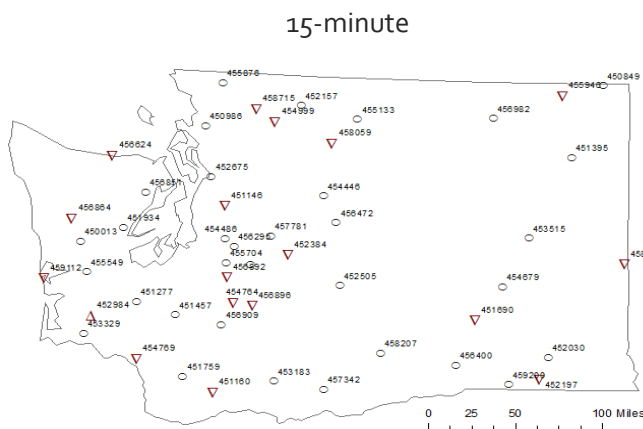
In addition to identifying potential measurement errors, the AM series for each station and duration was evaluated for presence of trend, correlation, and change in inter-annual variance. Like most statistical analyses, frequency analysis also requires stationarity and independence in the data. The Mann–Kendall statistics (Z) (Mann 1945, Kendall 1975), which uses the Z -test and less affected by outliers in data, was applied to investigate the stationarity and presence of linear trend in the AM series. When $|Z| > Z_{crit}$, the null hypothesis of no trend can be rejected and the data is

considered to have a significant trend. For the 95% confidence level or 5% significance level, $Z_{crit}=1.96$. The Breusch–Godfrey test (Breusch 1978, Godfrey 1978) was used to detect serial correlations in the AM series up to third order at the 5% significance level. The test is more general than the Durbin–Watson statistic, which is only valid for testing the possibility of a first-order autoregressive model (e.g. AR(1)) for the regression errors. Levene's test (Levene, 1960) was used to test for homogeneity of variance in the AM series at the 5% significance level. The test has been proven to be less sensitive to non-normality in data than some other commonly used tests. The test evaluates whether two sub-samples in a given population have equal or different variances. In our case we have divide the AM series to four sub-samples and evaluated the change in variances.

The results, in term of percentage of stations showing significant trend, correlation or change in variance, were presented in Table 2 for AM series with durations ranging from 15-minute to 10-day. For the sub-daily durations, the annual maximum precipitations showed decreasing trends for almost one third of the stations. Particularly, the maximum precipitations have decreased on the Cascade Mountain and Southeast region (Figure 9). About 7 to 8% of the stations showed increasing trends for longer duration storm exceeding 1-day, while only 3 to 4% stations showed decreasing trends for the same duration. Relatively few percentage of stations showed correlations (first, second and third orders) for all the durations we have considered. The change in inter-annual variability of the storms is relatively higher for shorter duration storm, with more than 15% of the stations showing significant change in storm annual variation over time. Similar trend, correlation and variance analyses were also conducted for each homogenous region identified in this study and little evidence of such trends and change in variance was identified for all the regions, allowing direct application of regional frequency analysis without the need for adjustment of the AM series.

Table 2. Trend, correlation and change variance for storms with durations ranging from 15-minute to 10-day.

Duration	Increasing Trend (%)	Decreasing Trend (%)	Correlation 1st order (%)	Correlation 2nd order (%)	Correlation 3rd order (%)	Change in Variance (%)
15 min	1.96	33.33	0	5.88	3.92	19.61
30 min	0	35.29	0	3.92	3.92	17.65
1 hour	0	28.99	0	3.92	3.92	17.65
2 hour	3.92	37.68	0	5.88	5.88	15.69
3 hour	1.96	34.78	0	7.84	3.92	15.69
6 hour	0	28.99	0	5.88	1.96	11.76
12 hour	1.96	21.74	0	0	1.96	9.80
24 hour	3.92	18.84	0	1.96	1.96	9.80
2 day	8.94	3.35	0	1.96	1.68	4.47
3 day	6.98	4.47	0	2.51	2.79	3.63
4 day	7.82	3.63	0	2.51	3.07	2.79
5 day	7.82	2.51	0	3.07	3.63	2.23
6 day	8.10	2.51	0	3.35	3.35	2.79
7 day	6.98	3.63	0	3.07	3.35	5.31
8 day	7.26	3.07	0	3.63	3.91	3.35
9 day	7.26	3.07	0	2.51	2.79	3.63
10 day	6.70	3.91	0	3.07	2.51	3.91



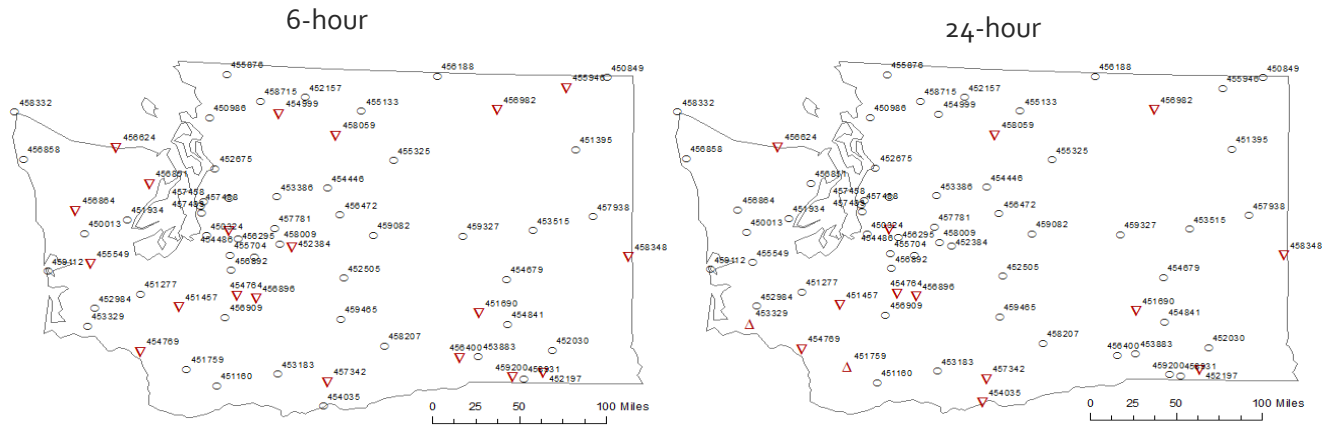


Figure 9. Locations of stations with significant decreasing trends in storms with 15-minute, 1-hour, 6-hour and 24-hour durations.

2.2.3. Seasonality of Extreme Precipitation

Seasonality of the extreme precipitation and their spatial variations were further analyzed based on the occurrence dates of the hourly storms. Such analysis is important to understand the main physical and climatological conditions that contribute to formation of extreme storm events at regional level, as well as to select or filter the extreme precipitation data for AM series. The results are presented in Figure 10, which shows noticeable seasonal and spatial variations in the occurrence of extreme precipitation in the state. The occurrence dates of the storms are often concentrated in certain period of a year and vary from region to region. In general, the storms with extreme precipitations seem to start from the Pacific Coast during November and progress eastward over time. For example, most of the extreme precipitations in Western Washington occur during November-January, with January being the month with large numbers of extreme precipitation records in Western Washington. February-April is relatively quiet season, with few records of extreme precipitation. In Eastern Washington, most of the extreme storm events happen during May-August, and then the extreme storms shift to the west for the rest of the months.



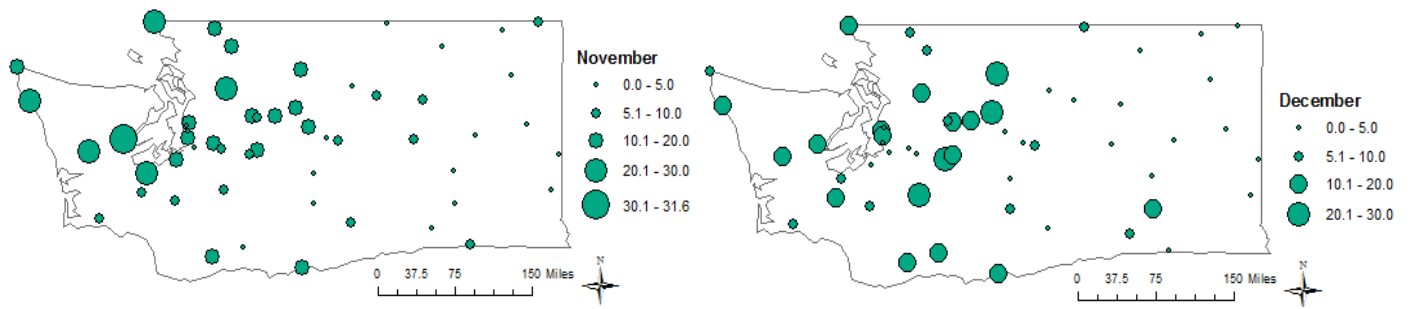


Figure 10. Seasonality of extreme precipitation occurrence across Washington State

3. Methodologies

Annual maximum precipitation series were extracted from the dataset for 15 minutes to 10 days duration after going through the initial screening process. The series were then used in Regional frequency analysis (RFA). Figure 11 describes the workflow applied in this study, which involves data pre-processing or screening, identifying initial and final homogenous regions, model selection and uncertainty analysis.

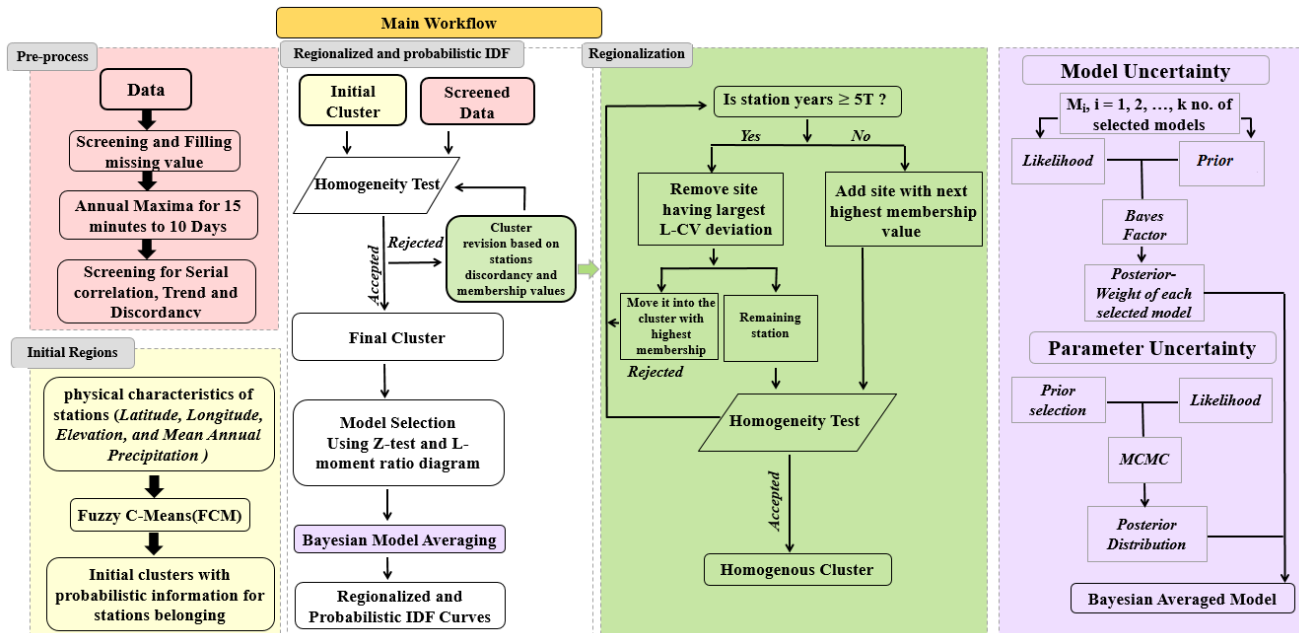


Figure 11. Work flow for regionalization and uncertainty methodologies.

3.1. Regional Frequency Approach (RFA)

Regional frequency approach (RFA) combines the data from a cluster of similar sites often called region or pooling group to improve the reliability of estimation of the quantiles (or probability of occurrence) of extreme events at any site in the group (Wallis J.R *et al*, 2007). The region should be homogenous with all sites in the region being similar and sufficiently sized in order to accurately transfer information among sites within a region (Burn and Goel, 2000). In this study, RFA based on L-moments method (Hosking and Wallis 1997) was used, which assumes an identical parent probability distribution with different scale factor for each site within a homogenous group. The scale factor, also known as “index-flood”, is often considered as the mean (μ) of the series (Hosking and Wallis 1997) and is used to weight quantiles (q) of regional distribution when calculating at-site quantiles (Q) as follow (Hosking and Wallis 1997):

$$Q_i(F) = q(F)\mu_i$$

L-moment, developed by Hosking (1990), is widely applied for regional frequency analysis of extreme hydrologic events. It is more robust for parameter estimation of probability distribution than ordinary moments as L-moments are not sensitive to the outliers of time series. The first four L-moments and associated ratios (i.e. L-covariance (L-Cv), L-skewness (L-Cs), and L-kurtosis(L-Ck)) are derived from linear combinations of probability weighted moments (PWMs) developed by Greenwood et al. (1979). Details of their derivations can be found in Hosking (1990).

3.1.1. Trend and Randomness Test

In frequency analysis it is necessary to test the assumptions that the observations at various sites are stationary, independent and identically distributed. In order to check the serial independence of the data autocorrelation test at various time lags was carried out. For a time series

with n observations, the critical values at $\alpha = 0.05$ can be calculated from $1.96/\sqrt{n}$ (Douglas et al. 2000). The non-parametric Mann–Kendall statistics (Z) (Mann, 1945; Kendall, 1975), which uses the Z -test, was applied to investigate the stationarity and presence of linear trend in the data. When $|Z| > Z_{crit}$, the null hypothesis of no trend can be rejected and the data is considered to have a significant trend. The test has been applied at 95 % confidence level ($Z_{crit} = 1.96$) in this study.

3.1.2. Discordancy measure

The discordancy measure aims at finding out sites that are abhorrently different from the region (Hosking and Wallis, 1993). If the L -moment ratios are represented by $t_{(i)}$, $t_{3(i)}$, and $t_{4(i)}$ for site i and u_i is a vector the ratios, $u_i = [t_{(i)}, t_{3(i)}, t_{4(i)}]^T$. The discordancy measure for a specific site i , D_i , can be calculated based on Hosking and Wallis (1997):

$$D_i = \frac{1}{3} M(u_i - U)^T A^{-1} (u_i - U)$$

$$U = \frac{1}{M} \sum_{i=1}^M u_i$$

$$A = \sum_{i=1}^M (u_i - U)(u_i - U)^T$$

where, M is total number of stations and superscript T refers to transpose of a vector. A site is called discordant when D_i is greater than a critical value, which depends on the number of stations with in a region. Large value of D_i The critical value is normally considered to be 3 if a region contains 15 or more sites (Hosking and Wallis 1997). Nevertheless, large value of D_i refers to close investigation of sites' data.

3.1.3. Initial Regions

Fuzzy C- Means (FCM) Clustering (Ruspini,1969; Dunn,1974) has been adopted to identify the initial regions. In this study, latitude/longitude, elevation, and mean annual precipitation have been used as attribute variables of the sites. The FCM algorithm is similar to the K-means algorithm except that instead of assigning each site to only one cluster, degree of membership is provided to each site into each clusters meaning sites on the edge of a cluster may be in that cluster to a lesser degree than points in the center of a cluster (Sadri and Burn, 2011). Thus each site can be a partial membership of any of the clusters. The working procedure of FCM algorithm involves:

1. Forming an initial set of k groups randomly.
2. Estimating the centroid of each group
3. Creating a new cluster by connecting each site with the closest centroid.
4. Recalculating the centroids for the new clusters.
5. Step 3 and 4 are repeated until convergence.

The objective of this algorithm is to achieve a minimized total intra-cluster variance (distance or squared error) function (D_v) (Ayvaza et al. 2007). If c_k denotes the centroid of all sites in cluster k when K is the total number of cluster and

$$D_v = \sum_{k=1}^K \sum_{x_i \in S_k} |x_i - c_k|^2$$

where x_i = standardized vector for site i . The degree of belonging of site i in the k th cluster is given by:

$$b_k(i) = 1/d_{(c_k,i)}$$

where $d_{(c_k,i)}$ is the distance of site i to the centroid of cluster k . Each station is assigned to the cluster with which it has the highest degree of membership. The coefficients are normalized so that the sum of membership of one site of interest to all different clusters is unity (Ayvaza et al., 2007).

3.1.4. Final Homogenous Regions:

It has been often the case that initial regions obtained from the clustering analyses may not fulfill the requirements of effective region which includes homogeneity and region size and therefore needs further corrections outlined by Hosking and Wallis (1997) which includes moving a site or few from one region to other, deleting sites, dividing or merging regions etc. The partial membership values from FCM reduces the amount of subjective judgment and complexity of deciding which site(s) can be moved from/to a region or different regions thus serve as an effective tool in RFA.

The size of the region has been defined considering 5T guideline recommended by Jacob et al. (1999), which states that a region should contain minimum of 5T station-years of data so that the T-year quantile gives reasonably accurate estimates. The target return period for the present study is 100 years. According to 5T guideline, summation of the station-years for a region should be at least 500 in order to estimate 100-year quantile accurately. The homogeneity of these regions has been assessed using L-moment based discordancy and heterogeneity measure. The heterogeneity measure compares dispersion of L-moments between sites within a region and expected dispersion limit for a homogenous region. The expected dispersion within a homogenous region can be obtained through simulation:

$$V = \frac{\sum_{i=1}^N n_i (t_{(i)} - t^R)^2}{\sum_{i=1}^N n_i}$$

where t^R and $t_{(i)}$ are the regional average L-moment ratio and the L-moment ratio for site i ; n_i is the sample size at station i , and N is the number of stations in a region. The simulated L-moment ratios were generated using Kappa distribution by considering large number of realizations of a homogeneous region using Monte Carlo simulations with equal number of sites and record lengths as the observed data.

$$H = \frac{V - \mu_v}{\sigma_v}$$

where V is the observed between-site dispersion of L-moment ratios; μ_v and σ_v are the mean and standard deviation of V obtained from a large number of simulated homogeneous regions. In this study, the critical value of H has been considered to be 2 because of additional variability coming from precipitation measurement. If an initial region failed to be homogeneous (i.e., $H > 2$), the region will be revised until it attained homogeneity by removing sites that were considered to be discordant ($D > 3$) and replacing them with other sites considering the partial membership values from FCM algorithm.

3.1.5. Identifying Appropriate Distribution

Once the homogenous regions are identified and validated, the next step is to determine appropriate probability distribution models for each region using Z -statistics (Z^{Dist}) based on L - C_k values for five commonly used extreme value distributions, namely Generalized extreme value

(GEV), Generalized Pareto (GP), Generalized logistic (GLO), Generalized normal (GNO) and Pearson type-3 (PE3) distributions developed by Hosking and Wallis (1997) :

$$Z^{Dist} = \frac{t_4^R - \tau_4^{Dist} + \beta_4}{\sigma_4}$$

where, t_4^R = regional average LC_k , τ_4^{Dist} = theoretical LC_k for the fitted distribution, β_4 is the bias and σ_4 is the standard deviation of the regional average LC_k . β_4 and σ_4 can be found using Monte Carlo simulation (Hosking and Wallis 1997). A practical criterion for determining the adequacy of fit which is $|Z^{Dist}| \leq 1.64$ at 90% confidence level. When no distribution falls within this criterion, Kappa was chosen to be the appropriate distribution.

3.2. Uncertainty Analysis using Bayesian Approaches

The main sources of uncertainty in extreme precipitation frequency analysis are considered to be the selection of appropriate distribution (model uncertainty) and estimation of the distribution parameters (parameter uncertainty). Bayesian approaches allow quantifying the combined model and parameter uncertainty by considering several extreme value distributions, instead of a single “best-fit” distribution, and by using the entire parameter probability distribution instead of using only the optimal set of parameters.

3.2.1. Parameter Uncertainty

Bayesian approach was used to estimate the posterior distribution of the parameters $p(\theta|D, M_i)$ for a given probability distribution model M_i and AM data D :

$$p(\theta|D, M_i) = \frac{p(D|\theta, M_i)p(\theta|M_i)}{\int p(D|\theta, M_i)p(\theta|M_i)d\theta}$$

where: $p(\theta|M_i)$ is the prior distribution of the parameters; $p(D|\theta, M_i)$ is the likelihood distribution, which measures the likelihood that the observed AM data D come from the given distribution model M_i with parameters θ . Since the integral in above equation is difficult to solve analytically, MCMC simulation using Metropolis-Hasting algorithm was used to generate a set of parameters that were used to compute the likelihood and the normalized factor (the denominator in Eq. 5). For an efficient implementation of the Metropolis-Hastings algorithm, a multivariate normal distribution was used as a proposal distribution (Reis Jr. and Stedinger, 2005). The variances of the proposal distribution were tuned using a trial-error method to get reasonable acceptance rate, which represents percentage of times a new sampled data is accepted. A high acceptance rate indicates poor mixing of the chain while a low acceptance rate means rejecting too many candidate samples resulting in an inefficient algorithm. Based on recommendations by Roberts et al. (1994) and Gamerman (1997), the acceptance rate in this study was kept approximately 0.3. After computing the posterior distribution of the model parameters, the posterior distribution of extreme precipitation quantiles $p(Q|D, M_i)$ for given model M_i and AMS data D was computed by marginalizing the prediction $p(Q|\theta, D, M_i)$ over the posterior parameters distribution.

$$p(Q|D, M_i) = \int_{\theta} p(Q|\theta, D, M_i)p(\theta|D, M_i)d\theta$$

The MCMC approach was used to sample from posterior distributions of the parameters and solve the integral. Credible intervals for estimated precipitation quantiles were calculated from the posterior distribution in order to have easily interpretable results (Congdon, 2001).

3.2.2. Model Uncertainty

Similar to their parameters, the models used to fit regional AMs were treated as random. Assuming that there are k probability distribution models (denoted as M_i , $i = 1, 2, \dots, k$) identified as appropriate model based on the Z-statistics, the posterior probability of models M_i given the sample AM series D can be estimated using the Bayesian approach:

$$p(M_i|D) = \frac{p(D|M_i)p(M_i)}{\sum_{j=1}^k p(M_j)p(D|M_j)}$$

where $p(D|M_i)$ and $p(M_i)$ are the likelihood function and prior probability, respectively. Prior probability for each selected model has been estimated based on the Z-statistic value z_i from regional frequency analysis:

$$p(M_i) = \frac{1/z_i}{\sum_{i=1}^k 1/z_i}$$

The likelihood distribution $p(D|M_i)$ is estimated by assuming that the AM data within a homogenous region are independent and identically distributed:

$$p(D|M_i) = \prod_j \prod_t p(D_{j,t}|M_i)$$

where, $D_{j,t}$ is the AM data from site j and time step t , $p(D_{j,t}|M_i)$ is the likelihood that $D_{j,t}$ come from the selected extreme value probability distribution M_i which has parameter θ . The posterior probability of the models was regarded as weight for the alternative models that were identified based on the Z-statistics, and can be estimated using the Bayes factor method (Kass and Raftery, 1995):

note Y

$$p(M_i|D) = \left[\frac{\sum_{j=1}^k p(M_j)B_{ji}}{p(M_i)} \right]^{-1}$$

where, B_{ji} is the Bayes factor, which is the likelihood ratio of the two alternative models M_j and M_i :

$$B_{ji} = \frac{p(D|M_j)}{p(D|M_i)}$$

The Bayes factor measures whether the observation data have increased or decreased the odds on the model M_j relative to the model M_i . Finally, the combined uncertainty from parameters and models was calculated using:

$$p(Q|D) = \sum_{i=1}^k p(M_i|D)p(Q|D, M_i)$$

where, $p(M_i|D)$ is the posterior probability of the selected model M_i and represents model uncertainty; $p(Q|D, M_i)$ denotes the prediction distribution of the quantiles Q resulted from parameter uncertainty for the given model M_i and data D .

3.3. Hydrologic Modeling

Even though the design risk levels for flooding and stormwater infrastructures are often defined through the return period and associated intensity of extreme rainfall events, the actual probabilities of occurrence of flooding and associated risk levels for design and operation of infrastructures are directly related to runoff, which also strongly depends on drainage characteristics, including land cover, soil type, topography, and river network. In this study, the Hydrologic Engineering Center Hydrologic Modeling System (HEC-HMS) model (USACE 2010) was used for selected watershed in Washington to develop IDF curves for peak runoff rates. The model uses rainfall intensities and durations derived from the regionalized rainfall IDF curves, along with readily available watershed data (e.g. soil, land cover, and digital elevation map) to

estimate runoff events. Other candidate and more traditional hydrologic models include the Rational Method and the Technical Release 55 (TR-55) method, which can predict peak discharge from a given storm event that is uniformly distributed over a homogeneous and relatively small drainage. The HEC-HMS model, on the other hand, can simulate peak discharge and hydrograph from multiple spatially and temporally varying storm events in a large basin with various drainage characteristics, as well as can directly simulate effects of snowmelt and accumulation on the hydrograph, making it suitable for this study. It also offers a variety of modeling options for computing runoff and flood routing along streams. Its ability to simulate the entire hydrograph and runoff volume also makes the model suitable for designing and evaluating effectiveness of volume-based stormwater management such as detention ponds and infiltration trenches. The watersheds delineated by Water Resource Inventory Areas (WRIA) were used for defining the drainage areas for the model. The model was applied for Yakima River Basin (WRIA 37, 38 and 39), Snohomish River Basin (WRIA 07), Puyallup-White River Basin (WRIA 10) and Green River Basin (WRIA 09). The basins were selected to represent the different climatic and drainage characteristics in Washington, and have to locate entirely in Washington to avoid data collections from other states and Canada.

3.3.1. HEC-HMS Modeling

Computation of Loss: HEC-HMS uses various methods (including the Green & Ampt, SCS Curve Number and Soil Moisture Accounting) to compute the rainfall excess (or direct runoff volume) from a given precipitation hyetograph. In this study, the SCS Curve Number method was used, which estimates the rainfall excess as a function of cumulative precipitation and curve number (CN) using the following equation:

$$P_e(t) = \frac{\left(P(t) - 0.2 \left(\frac{1000}{CN} - 10\right)\right)^2}{P(t) + 0.8 \left(\frac{1000}{CN} - 10\right)}$$

where P_e is accumulated rainfall excess at time t , P is accumulated rainfall depth at time t , and CN is the curve number, a measure of the ability of a watershed to storm precipitation to runoff. The HEC-GeoHMS software () was used to generate the gridded CN and composite CN for each sub-basin based on landuse, soil, percentage of impervious area and digital elevation maps.

Computation of Direct Runoff Hydrograph: HEC-HMS uses user-specified and synthetic Unit Hydrograph (UH) to simulate direct runoff hydrograph from rainfall excess. This study used the SCS synthetic UH method, which estimate the direct runoff discharge as a function of UH peak (Q_p) and time of peak (T_p) (also known as the time of rise). The time of peak is calculated using:

$$T_p = \frac{\Delta t}{t} + t_{lag}$$

where Δt is the rainfall excess duration and t_{lag} is the basin lag, defined as the time difference the center mass of rainfall excess and the peak of the UH. The basin lag time for each sub-basin was estimated using HEC-GeoHMS. The UH peak (Q_p) is computed using:

$$Q_p = 484 \frac{A}{T_p}$$

where A is sub-basin area. The dimensionless curvilinear SCS UH, which relates Q_t/Q_p and t/T_p , are then to estimate the direct runoff discharge Q_t at time t .

Computation of Baseflow Contribution: HEC-HMS uses constant, exponential recession and linear-reservoir volume methods to simulate groundwater or baseflow contribution to stream hydrograph. This study uses the exponential recession method, which relates the baseflow discharge at any time t (Q_t) to an initial baseflow at $t = 0$ or specified threshold discharge after the direct runoff contribution is completed (Q_o) as:

$$Q_t = Q_o k^t$$

where k is an exponential decaying constant. The parameters k and initial baseflow (in terms of discharge per unit area) and threshold discharge (in terms of ratio to peak discharge) were estimated using model calibration.

Modeling Channel Flow (Routing): Various routing methods are available in HEC-HMS, including: Lag, Muskingum, Modified Plus, Kinematic-wave and Muskingum Cunge methods. Since the routing in our study areas are mostly river routing with relatively small number of flood controlling dams, Muskingum method was used. Given the inflow hydrograph values (I_t for all t), an initial condition ($Q_{t=0}$), and the parameters K and X , HEC-HMS recursively computes the discharges of the routed hydrograph as follow:

$$O_t = \left(\frac{\Delta t - 2KX}{2K(1-X) + \Delta t} \right) I_t + \left(\frac{\Delta t + 2KX}{2K(1-X) + \Delta t} \right) I_{t-1} + \left(\frac{2K(1-X) - \Delta t}{2K(1-X) + \Delta t} \right) O_{t-1}$$

The parameters K and X for each river segment were estimated from model calibration.

Modeling Snowmelt: The runoff from all the watersheds considered in this study are often impacted by snowmelt from the mountains and higher altitudes, making it important to properly

simulate the snowmelt and associated volume of snow water equivalent (SWE) and the timing and magnitude of snowmelt, which impacts soil moisture, runoff, and streamflow. HEC-HMS simulate snowmelt using either the temperature index method or the gridded temperature index method. In this study the temperature index method (Anderson 1973) was used, which needs only air temperature and precipitation as inputs. The method uses the following basic equation:

$$M_s = C_m(T_a - T_b)$$

Where M_s is the snowmelt depth per period, C_m is a melt-rate coefficient, T_a is the air temperature, and T_b is the base temperature at which the snow begins to melt. If the air temperature is less than the base temperature, the amount of melt is zero. The melt-rate can be wet or dry melt-rate depending on the presence or absence of rainfall, respectively, during time intervals. When the rainfall during the time interval is greater than user specified “rain rate limit”, the time interval is considered to be wet, else it is considered as dry. For the dry condition, the melt-rate varies seasonally, typically increasing as snowmelt season progresses and when shortwave radiation and daylight hours increased. In order to calculate the dry melt-rate, first user defined functional relationship between the antecedent temperature index (ATI) and melt-rate is required (e.g. Table 3, which also used in this study). As the snowmelt season progresses, the ATI will be updated using user specified ATI-Meltrate Coefficient. The functional relationship is then used to estimate the dry melt-rate corresponding to the updated ATI. Calibration of the temperature index snowmelt method is recommended for watershed modeling (Daly et al. 1999). The user-specified parameters were calibrated for each watershed we have considered. Once the HEC-HMS model are calibrated with the historical rainfall and runoff data, specific storm events from the precipitation IDF curves will be used to estimate the associated runoff events.

Table 3. Melt-rate as a function of antecedent temperature index (ATI) (USACE 1991)

ATI (<i>F° day</i>)	Melt-rate (<i>in./F° day</i>)
0	0.025
100	0.03
200	0.05
300	0.04
1000	0.04

3.3.2. Yakima River Basin (YRB)

The YRB is one of the major basins in Washington State contributing to the Columbia River (Figure 12). The Yakima River stretches 215 mile from it headwaters at Keechelus Lake in the central Washington Cascades to Columbia River at Tri-city, draining approximately 6,155 square mile areas of mostly shrub (42.5%), forest (28.5%), and cultivated land (12.1%). The basin is one of the most intensively irrigated areas in the U.S. with approximately all the croplands are irrigated using both surface and groundwater (Ely et al. 2011). The average annual precipitation in the basin varies widely from 128 in. in the northwest to 6 in. the southeast sections of the basin (Figure). The precipitation spatial pattern resembles the basin's highly variable topography, which ranges in altitudes from 400 to nearly 8,000 feet above mean sea level. Despite being known for its water shortage and recurrent drought conditions, the basin was also affected by several historical storms and flooding events, mostly during spring season. From 1970 to 2015, significant portion of the basin were declared a federal flood disaster areas nine times (FEMA). In addition to these major flood events, the river also flood every two to five years on average (FEMA 2013). The southern east portion of the basin is generally prone to flash flooding caused by thunderstorms, combined with steep ravines, alluvial fans, dry or frozen ground, and lightly vegetated ground that does not absorb water.

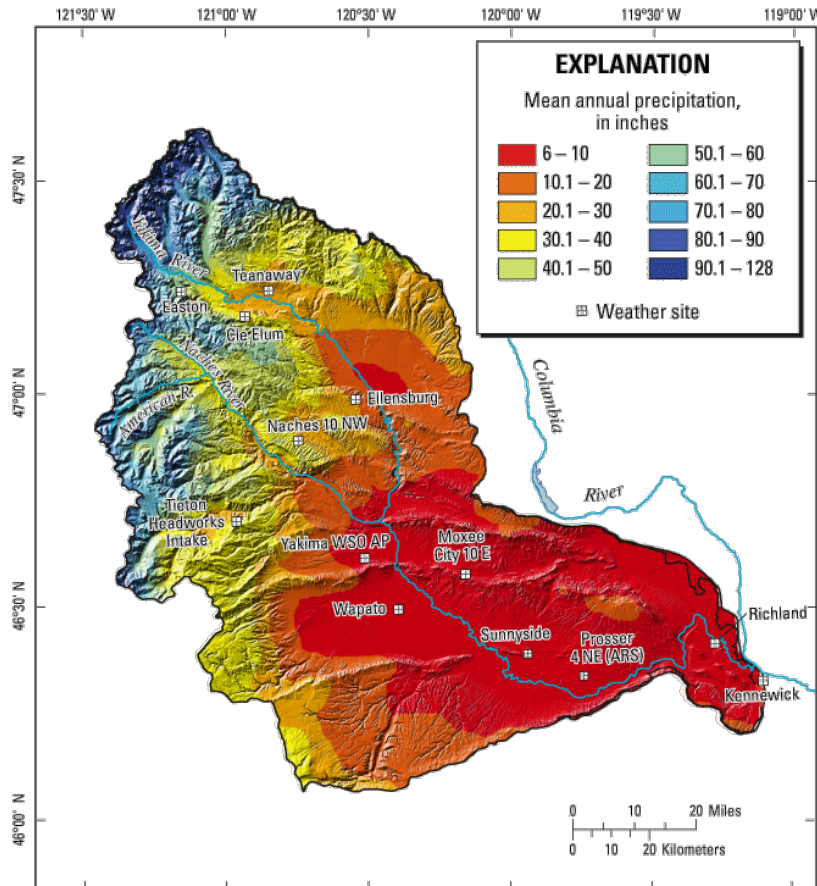


Figure 12. Yakima River Basin and distribution of mean annual precipitation (Source: USGS 2007).

The HEC-HMS model was constructed based on the January 9, 2009 storm which resulted in major floods throughout the basin. Figure 13 is the observed hydrograph near to the basin outlet, showing streamflow exceeding the flooding level for days. The resulted stream hydrographs of Yakima River at Kiona, WA (located close to the basin outlet) and at Umtanum, WA (located closed to were the city of Yakima) were used to calibrate and validate the model, respectively.

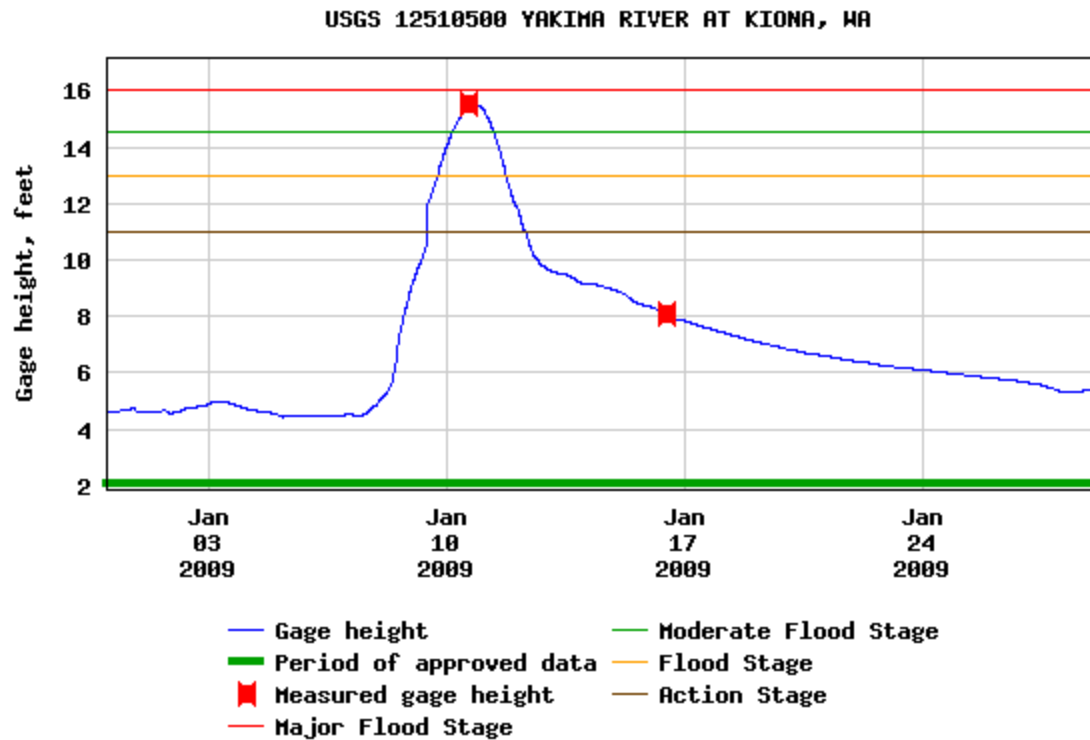


Figure 13. Yakima River stage near the basin outlet following the January 9, 2009 storm.

3.3.3. Snohomish River Basin (SRB)

The Snohomish River Basin is located just north of Seattle, draining approximately 1,978 square miles in both King and Snohomish counties of which 82 percent is forest, while most of the remaining areas are agriculture and residential. The two main tributaries, Skykomish and Snoqualmie rivers, originate in the Cascade Mountains and join near the City of Monroe where they become the Snohomish River that flows into the estuary near the City of Everett and finally discharge into Puget Sound. The basin is considered as the second largest basin draining into Puget Sound. Topography is generally lowlands in the western portion of the basin and mountainous terrain in the central and eastern areas. Precipitation is primarily dependent on elevation, with the lowlands receiving 30-40 inches a year, compared to over 150 inches in the mountainous areas (Figure 14). The basin is frequently impacted by floods caused by heavy rains and early melting

of mountain snow during the months of November-January. Since 2000 most of the areas in the basin were declared federal flood disaster zones eight times (FEMA).

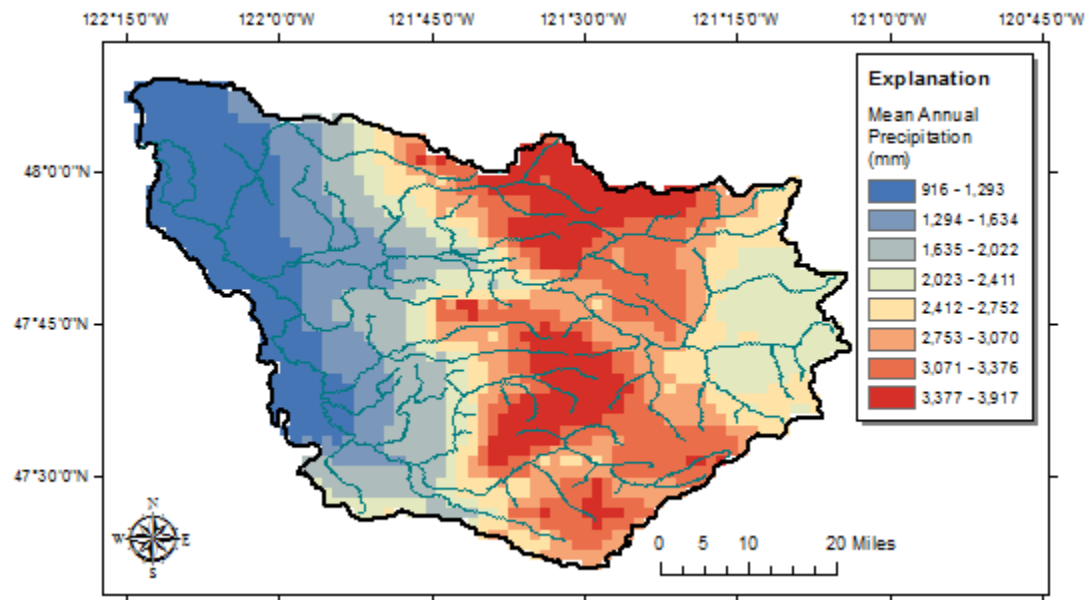


Figure 14. Snohomish River Basin and distribution of mean annual precipitation.

The HEC-HMS model was constructed based on the January 7, 2009 storm which resulted in major floods throughout the basin. Warmer air and heavy rains pummeled the region for multiple days causing massive flooding at near record levels on the Snohomish. Figure 15 is the observed hydrograph near to the basin outlet caused by the storm, showing streamflow exceeding the flooding level for days. Provisional data from USGS long-term stream gages indicate the resulted flood peak from this storm has recurrence intervals equal to or greater than 100 years. The model was calibrated using the observed hydrograph from this storm. December 8, 2015 storm and the stream hydrograph (Figure 16) were used to validate the model. This storm also caused a massive flooding throughout the basin.

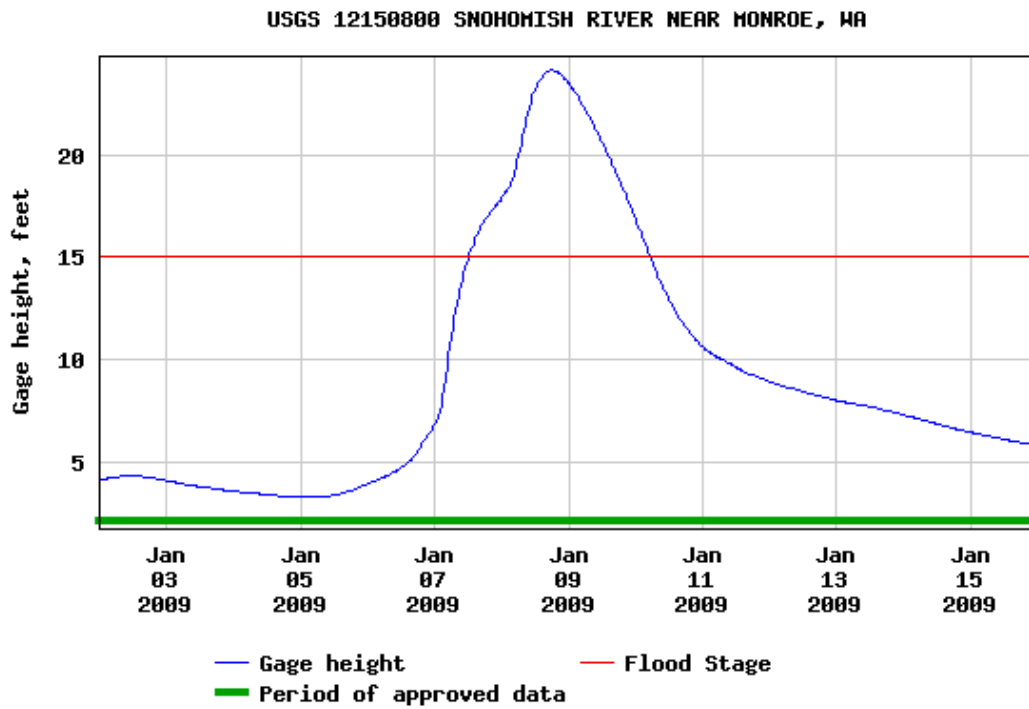


Figure 15. Snohomish River stage near the basin outlet following the January 7, 2009 storm. The stream hydrograph was used to calibrate the model.

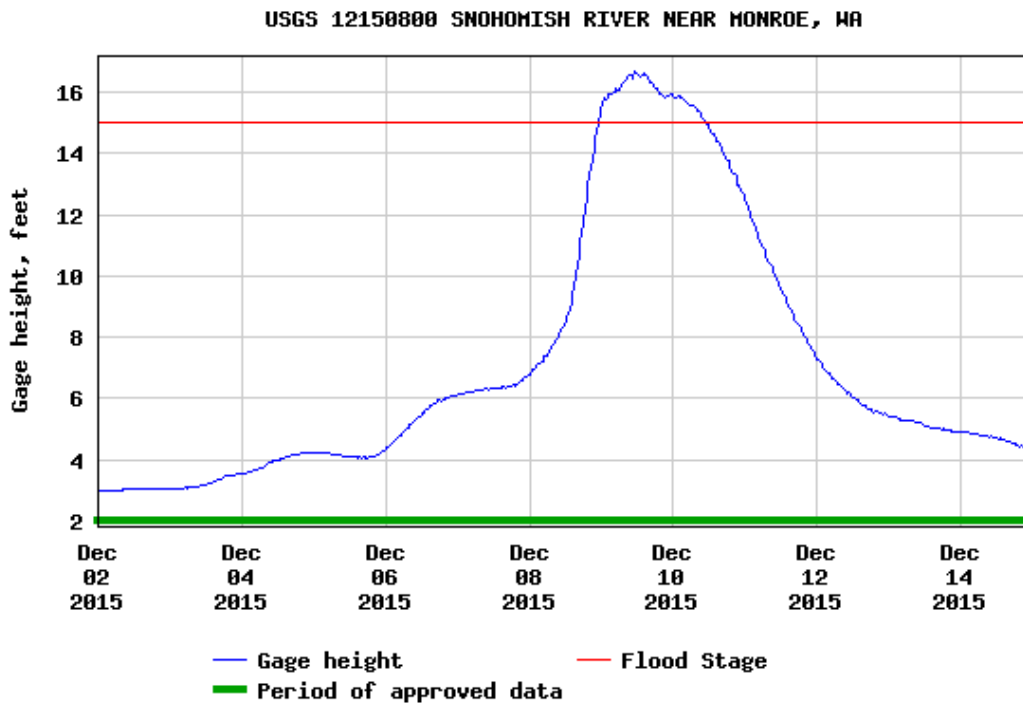


Figure 16. Snohomish River stage near the basin outlet following the December 08, 2015 storm. The stream hydrograph was used to validate the model.

3.3.4. Puyallup River Basin (PRB)

The Puyallup River and its two main tributaries, the White River and Carbon River, drain approximately 1,040 square miles (665,000 acres), which is predominately forest and mountainous in upstream portion of the basin while it is mostly urban and flat in the downstream (Figure). The river originates from Mount Rainier and crest of the Cascade Mountain range and flows through the city of Tacoma, third largest city in Washington, to Commencement Bay on Puget Sound. The annual mean precipitation ranges from 39 in. near Tacoma to 140 in. around Mount Rainier (Figure 17). Like most river basins in the Western Washington, the PRB is also frequently impacted by sever floods. Since 2000 most of the areas in the basin were declared federal flood disaster zones six times (FEMA).

The HEC-HMS model was constructed based on the January 7, 2009 storm which resulted in major floods throughout the basin. Heavy rain combined with melting snow have caused massive flooding, forcing the state to issue the largest evacuation order in the history of the state. Figure 18 is the observed hydrograph near to the basin outlet caused by the storm, showing streamflow cresting more than 2 feet above the flooding stage of 26.2 feet. Provisional data from USGS long-term stream gages indicate the resulted flood peak from this storm is the 2nd highest since 1914. The model was calibrated using the observed hydrograph from this storm. The December 8, 2015 storm and the stream hydrograph (Figure 19) were used to validate the model. This storm also caused a massive flooding, with the flood stage ranking 10th highest since 1914.

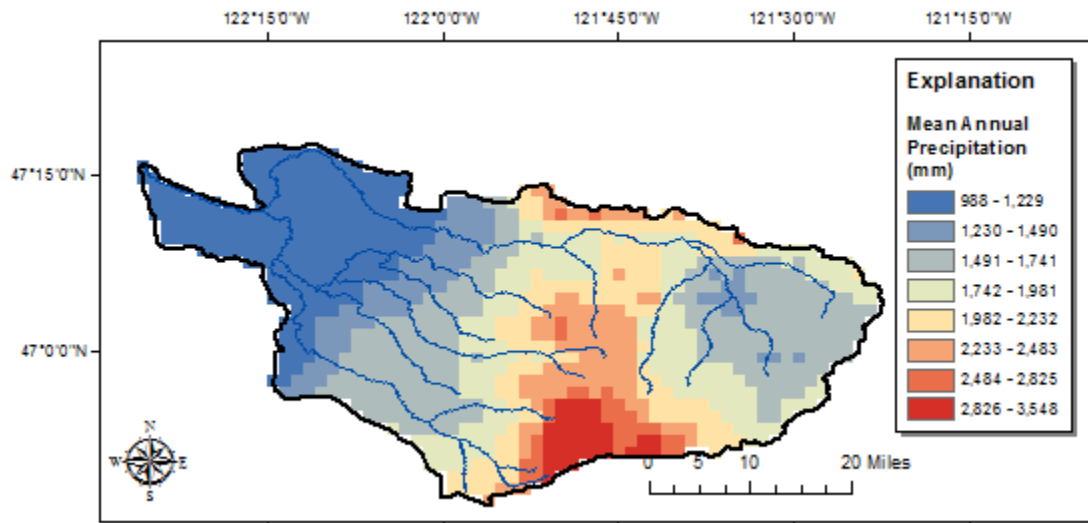


Figure 17. Puyallup River Basin and distribution of mean annual precipitation.

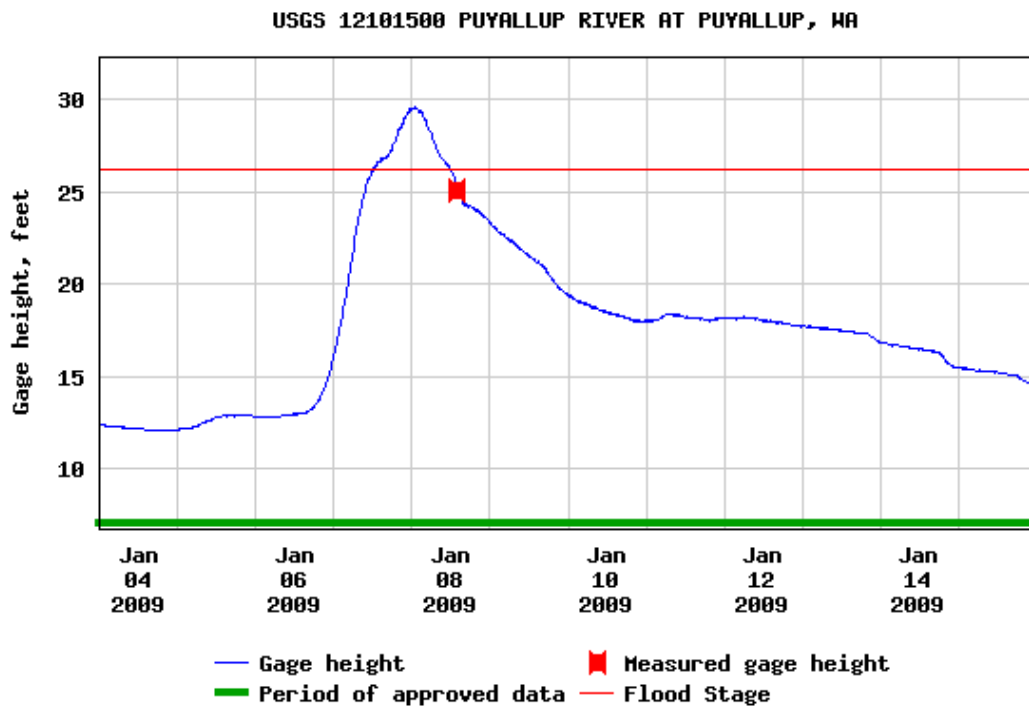


Figure 18. Puyallup River stage near the basin outlet following the January 7, 2009 storm. The stream hydrograph was used to calibrate the model.

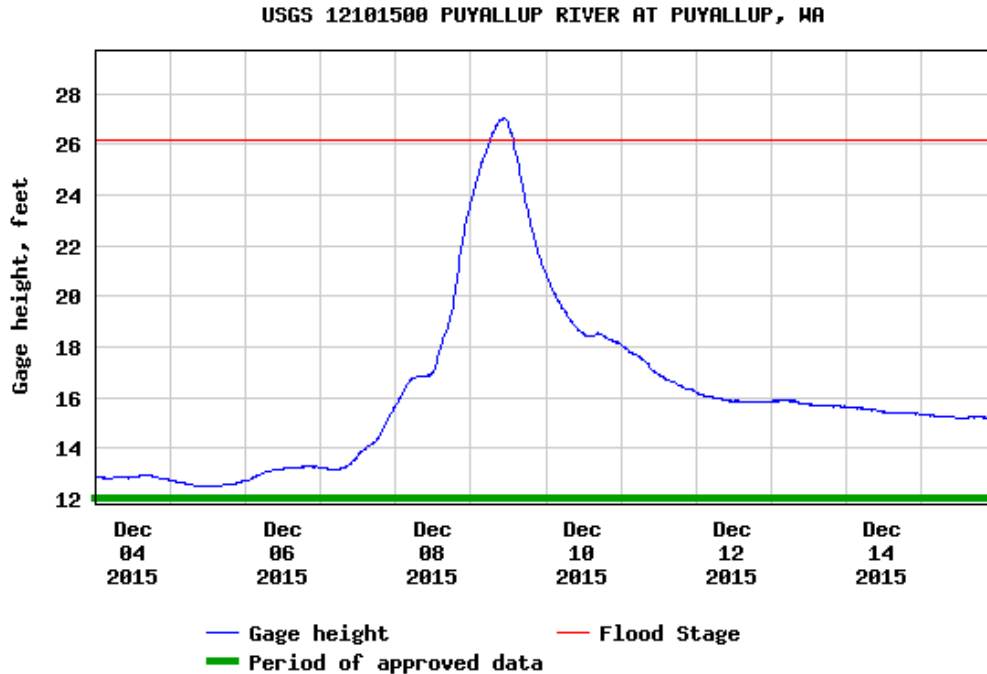


Figure 19. Puyallup River stage near the basin outlet following the December 08, 2015 storm. The stream hydrograph was used to validate the model.

3.3.5. Green-Duwamish River Basin (GRB)

The Green-Duwamish River originates in the Cascade Mountains and flow through steep sloped densely forested mountain terrain mountain terrain, before flowing through more gentle and urbanized area of southern Seattle and drains to Elliott Bay in the Puget Sound. The river flows for over 93 miles, draining approximately 484 square miles. It is the main source of drinking water for City of Tacoma, with much of the upper valley being restricted for public access. The mean annual precipitation increased from 36 in. in the west to 105 in. in the east portion of the basin (Figure 20). The basin is frequently affected by server storms resulted from heavy rains and early snow melt during early winter season, with majority the basin area declared federal flood disaster zones six times since 2000 (FEMA). The HEC-HMS model was constructed based on the January

7, 2009 storm which resulted in major floods throughout the basin. Figure 21 is the observed hydrograph near to the basin outlet caused by the storm, showing streamflow cresting more than flooding discharge for about a week. The model was calibrated using the observed hydrograph from this storm. The December 8, 2015 storm and the stream hydrograph (Figure 22) were used to validate the model. This storm also caused flooding in the basin, with the flow exceeding the flooding discharge for about three days.

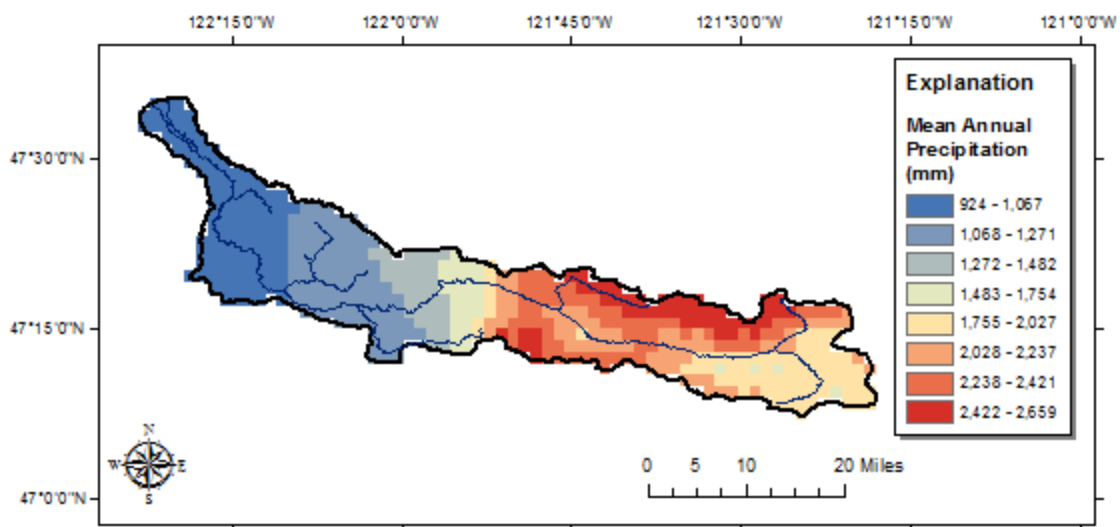


Figure 20. Green-Duwamish River Basin and distribution of mean annual precipitation.

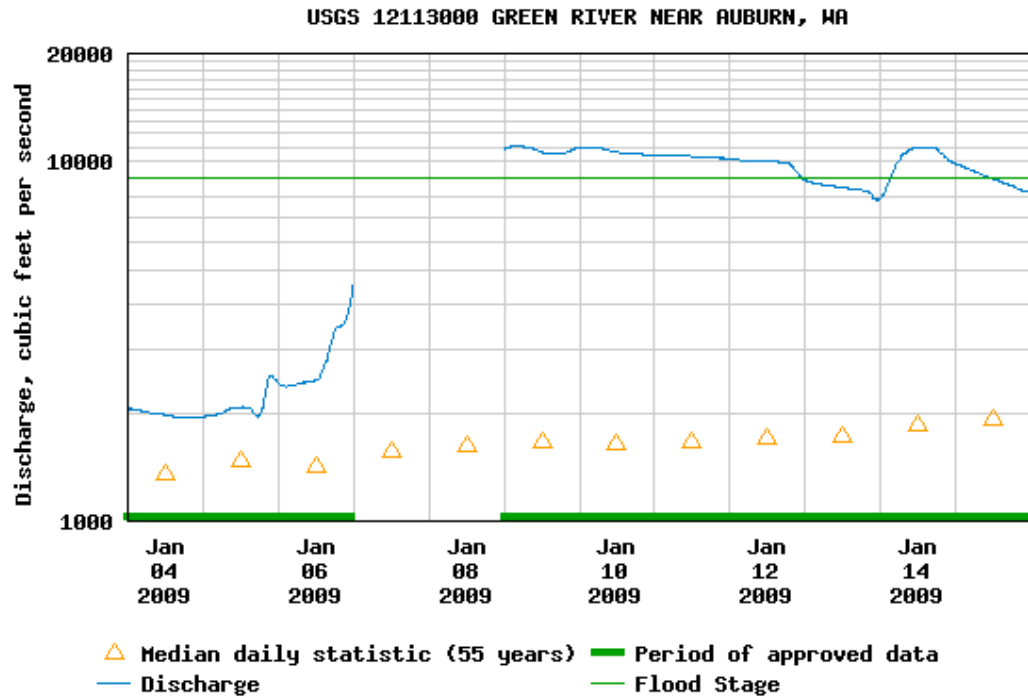


Figure 21. Green-Duwamish River stage near the basin outlet following the January 7, 2009 storm. The stream hydrograph was used to calibrate the model.

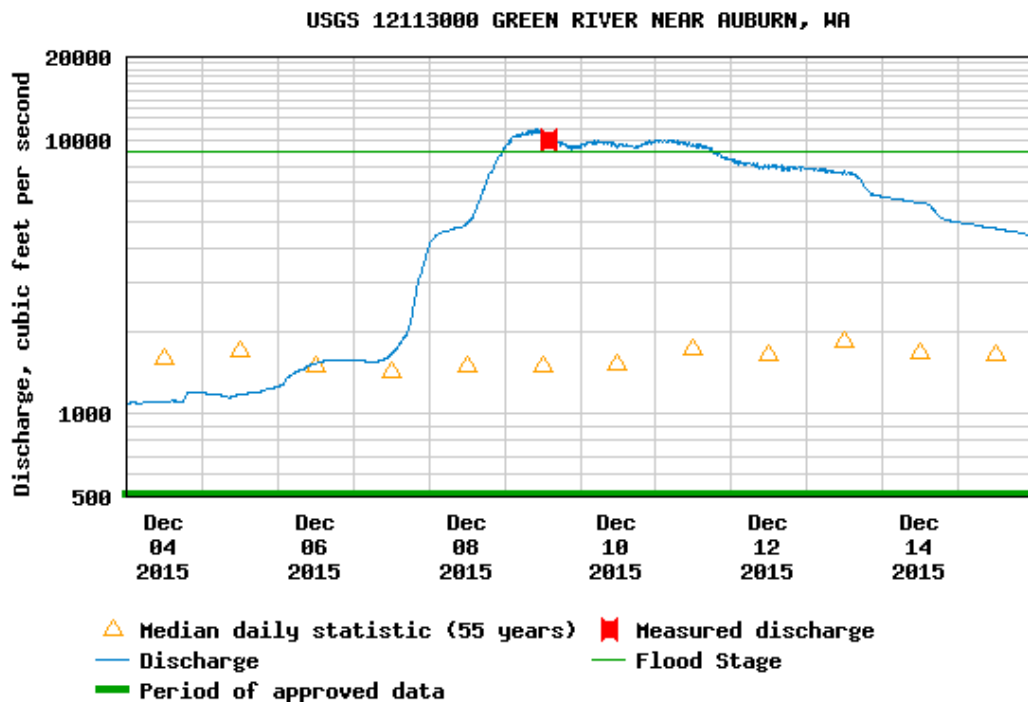


Figure 22. Green-Duwamish River stage near the basin outlet following the December 08, 2015 storm. The stream hydrograph was used to validate the model.

4. Results

In this chapter, the results from regional frequency analysis, uncertainty analysis and model combinations, comparison with previous works, future projection, and runoff of simulations will be presented. For brevity, representative results (figures and tables) and related discussion are presented, the remaining results can be found in the Appendices.

4.1. Identifying Homogeneous Regions

The purpose of this step is to form groups of stations that have climatologically homogeneity condition, whereby, apart from station-specific scale factors, the extreme precipitations at stations within a homogenous region can be characterized by identical frequency distributions. The grouping of stations involves two main steps: (1) identifying initial regions based on site characteristics such as latitude, longitude, elevation, and mean annual precipitation, and (2) refining the regions by moving around discordant stations from one region to another till all the regions satisfies the homogeneity statistics (H statistics). In this study, instead of deterministic initial grouping, which assumes a given station to belong to a region 100% and does not belong to any other regions, stochastic initial grouping, which assumes a given station to belong to various region with certain probabilities, were prepared using a fuzzy clustering technique. The probability information is critical during the refinement of the regions since it effectively and automatically guide the movement of discordant stations. In addition, unlike other similar studies, the regionalization was conducted for each storm duration considered, allowing for delineation of different regions for different durations of the storms, as it is often the case in reality. Figure 23 shows initial and final regions for one day extreme precipitations in Washington. As shown in the figure, the fuzzy clustering approach has resulted in 32 regions with most regions

being heterogeneous (H statistics ≥ 3), but after adjusting for discordant stations 26 homogenous regions (H statistics < 3) were identified.

The state of Washington is divided into 5, 6, and 26 homogenous regions for extreme precipitation with durations less than one hour, between one and 24 hours, and above 24 hours, respectively. The major difference in the number of regions for precipitation above 24 hours is mostly attributed to the relatively large number of daily stations used in the study. Otherwise, we expected more spatial relations (i.e., fewer regions) as storm duration increased. Thus, the homogenous regions for the longer duration storms can be lumped without losing their homogeneity. Table 4 shows the average number of stations in each region, indicating proportional division of the stations among the regions – an important attribute in regional frequency analysis. Figure 24 provides the homogenous regions for extreme precipitation with 1-hour duration, while the regions for the remaining durations are presented in Appendix A. Table 5 provides the mean L-CV and mean annual maximum precipitation for 15-min to 1-day storms for each region. As expected Region 1, which is located along the Cascade Mountain has higher 1-hour average extreme precipitation of 1.458 in., while Region 5 along the coast shows more variation (L-Cv = 0.593) in stations' maximum precipitations.

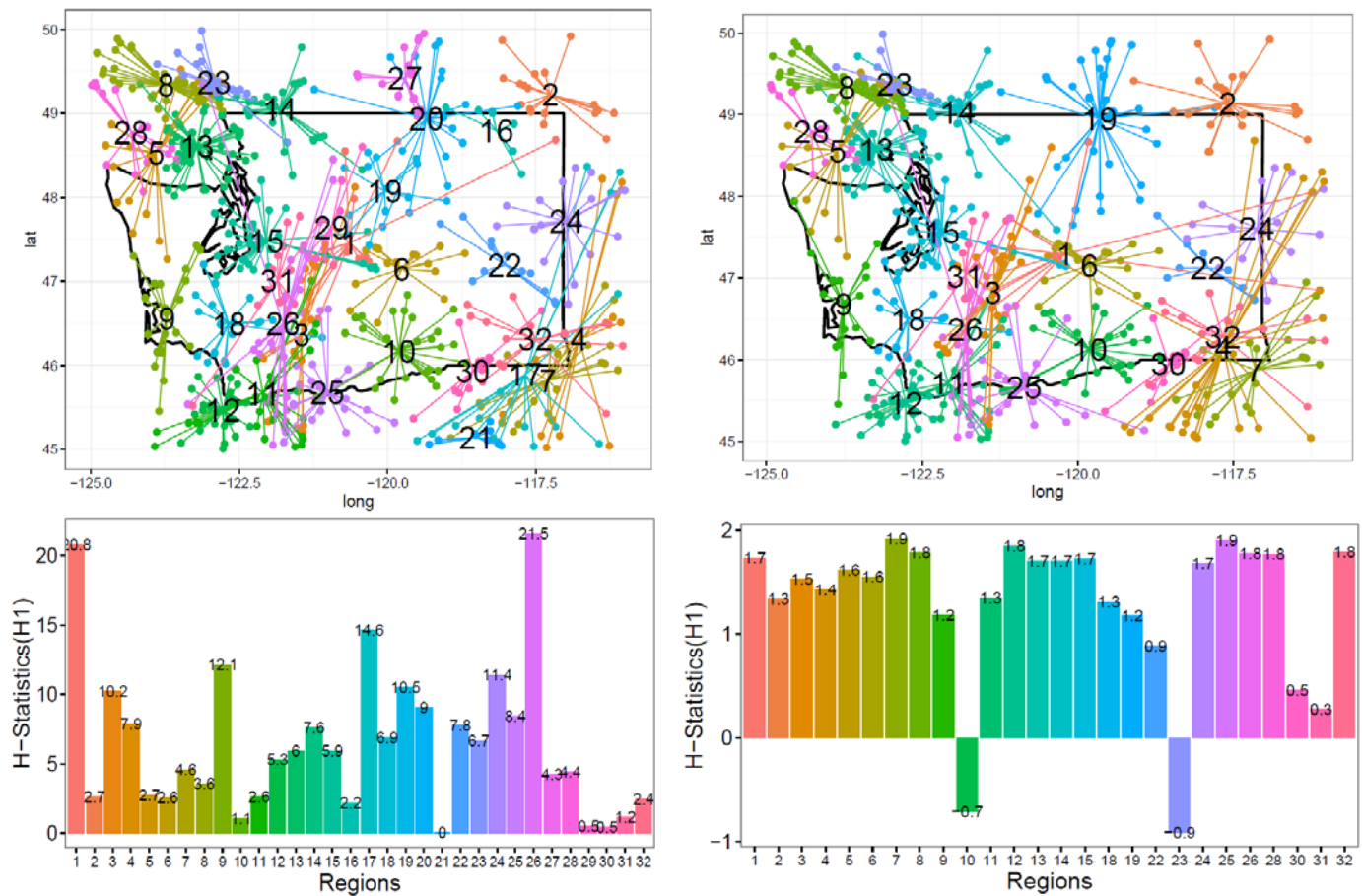


Figure 23. Initial and final regions, as well as corresponding H statistics for 1-day extreme precipitation in Washington.

Table 4. Average number of stations within each region.

Duration	No. of Regions	Avg. Number of Stations
15min	5	17.6
30min	5	17.2
60min	6	17.5
2hr	6	18.2
3hr	6	18.3
6hr	6	17.7
12hr	6	18.7
24hr	26	21.4
2 day	26	22.0
3 day	26	22.3
4 day	26	22.3
5 day	26	22.8
6 day	26	22.5
7 day	26	23.0
8 day	26	22.6
9 day	26	22.8
10 day	26	23.0

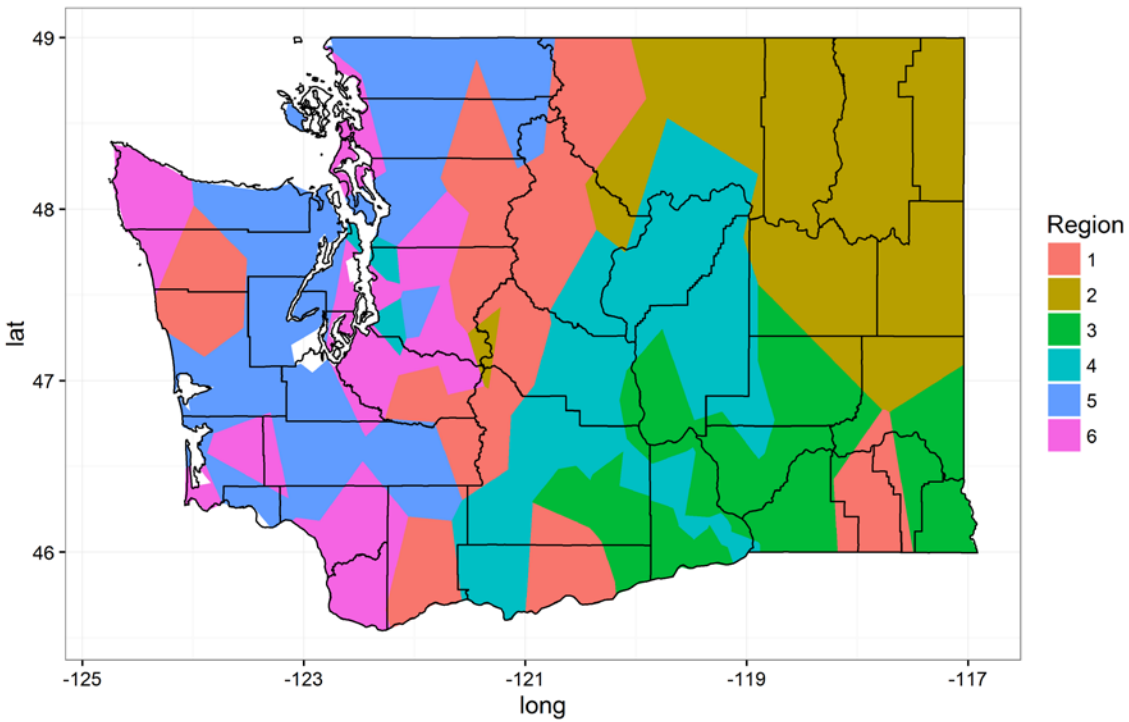


Figure 24. Climatologically homogenous regions for 1-hour extreme precipitation in Washington.

Table 5.L-CV and mean annual maximum precipitation for 15-min to 1-day storms

Duration	Statistics	Regions					
		1	2	3	4	5	6
15min	<i>Mean L-Cv</i>	0.337	0.269	0.305	0.494	0.439	
	<i>Mean index flood</i>	0.172	0.360	0.209	0.520	0.988	
30min	<i>Mean L-Cv</i>	0.320	0.234	0.284	0.450	0.414	
	<i>Mean index flood</i>	0.242	0.564	0.281	0.579	1.052	
60min	<i>Mean L-Cv</i>	0.519	0.263	0.384	0.291	0.593	0.173
	<i>Mean index flood</i>	1.458	0.415	0.314	0.346	0.950	0.483
2hr	<i>Mean L-Cv</i>	0.455	0.220	0.293	0.264	0.515	0.156
	<i>Mean index flood</i>	1.581	0.518	0.417	0.427	1.132	0.704
3hr	<i>Mean L-Cv</i>	0.399	0.179	0.277	0.197	0.421	0.132
	<i>Mean index flood</i>	1.706	0.606	0.523	0.507	1.176	0.859
6hr	<i>Mean L-Cv</i>	0.358	0.139	0.261	0.235	0.121	0.134
	<i>Mean index flood</i>	1.862	0.782	0.661	0.877	1.705	1.090
12hr	<i>Mean L-Cv</i>	0.256	0.162	0.264	0.244	0.297	0.129
	<i>Mean index flood</i>	2.824	1.002	0.786	0.941	2.305	1.731

4.2. Choosing Frequency Distribution.

In the standard regional frequency analysis, a single frequency distribution is fitted to the data from several sites in a homogeneous region. Because the “true” distribution of extreme rainfall is not known, a distribution must be chosen that not only provides a good fit to the data, but will also yield robust and accurate quantile estimates for each site in the region. In order to accomplish these modeling objection and incorporate uncertainty in selecting a distribution into the estimated

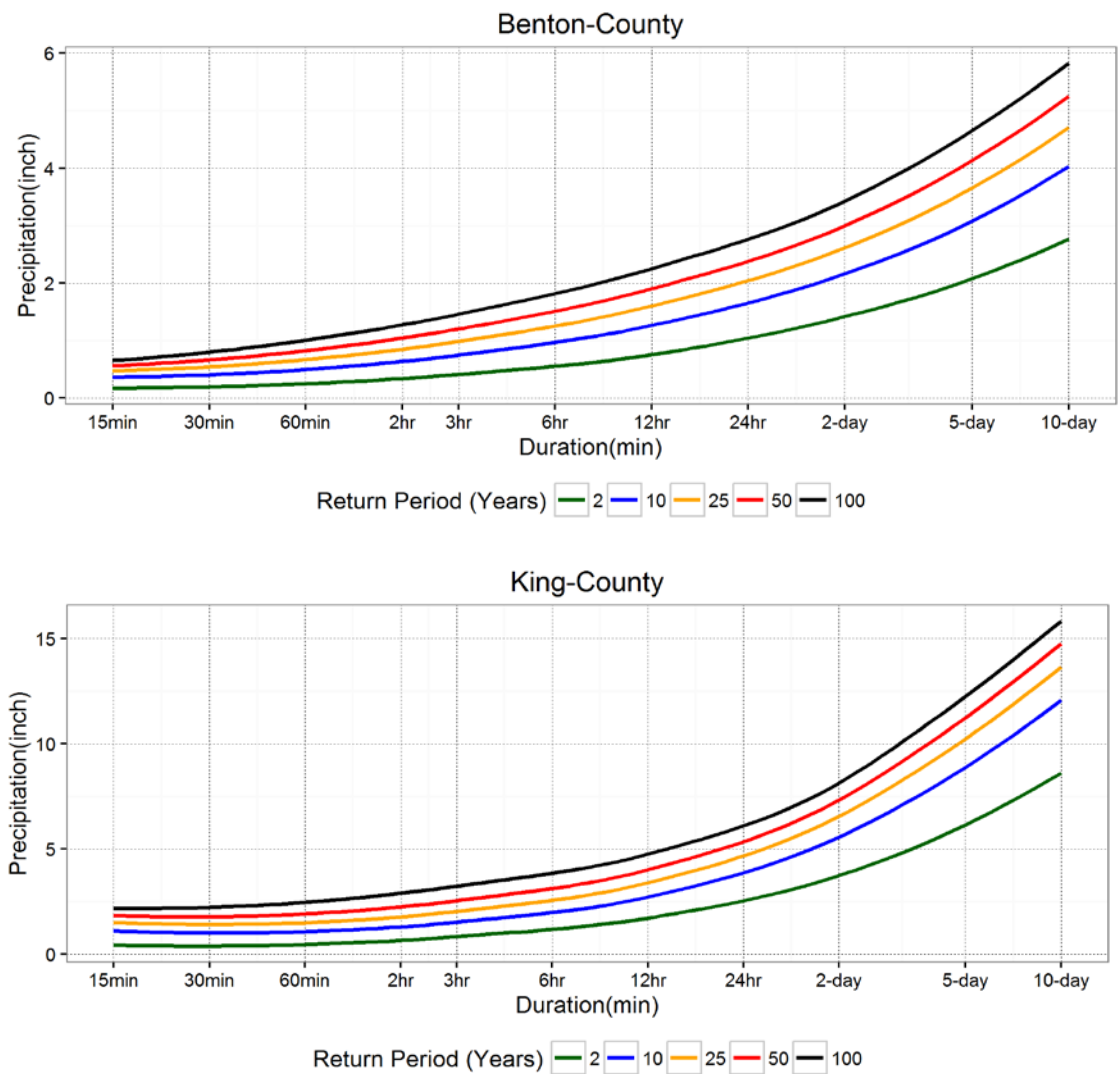
quantiles, we have adopted a Bayesian Model Averaging approach which allows selecting multiple appropriate distributions that fit the data reasonably well. The donut charts in Figure 25 showed the multiple distribution selected for each duration and region. The numbers in the chart represents the percentage of regions that use a given combinations of distributions. For example, for the 15-min storm events both the GNO and PE3 were found to be suitable for 40% of the regions (or 2 regions out of 5 total regions), while for the remaining 40% of the regions both GLO and GEV are suitable and for 20% of the region both GLO, GEV and GNO are suitable. Bayesian Averaging Method are used to combine the multiple distributions.



Figure 25. Selected frequency distributions for each duration and region. The numbers on the charts are the percentage of regions, which use the given combination of distributions

4.3. County Level IDF Curves

Once the regional level IDF curves are generated using the selected distributions, the next step is to determine representative IDF curves for the 39 counties in Washington using area weighted averaging approach. If a given county lays over multiple homogenous regions, the overlapping areas between the county and the regions are used to weight the IDF curves from the regions. Figure 26 provides IDF curves for Benton, Clark, King, Spokane and Yakima counties. For the remaining, the IDF curves are provided in Appendix (). The values with the associated 95% confidence intervals are provided in tabular form in Appendix ().



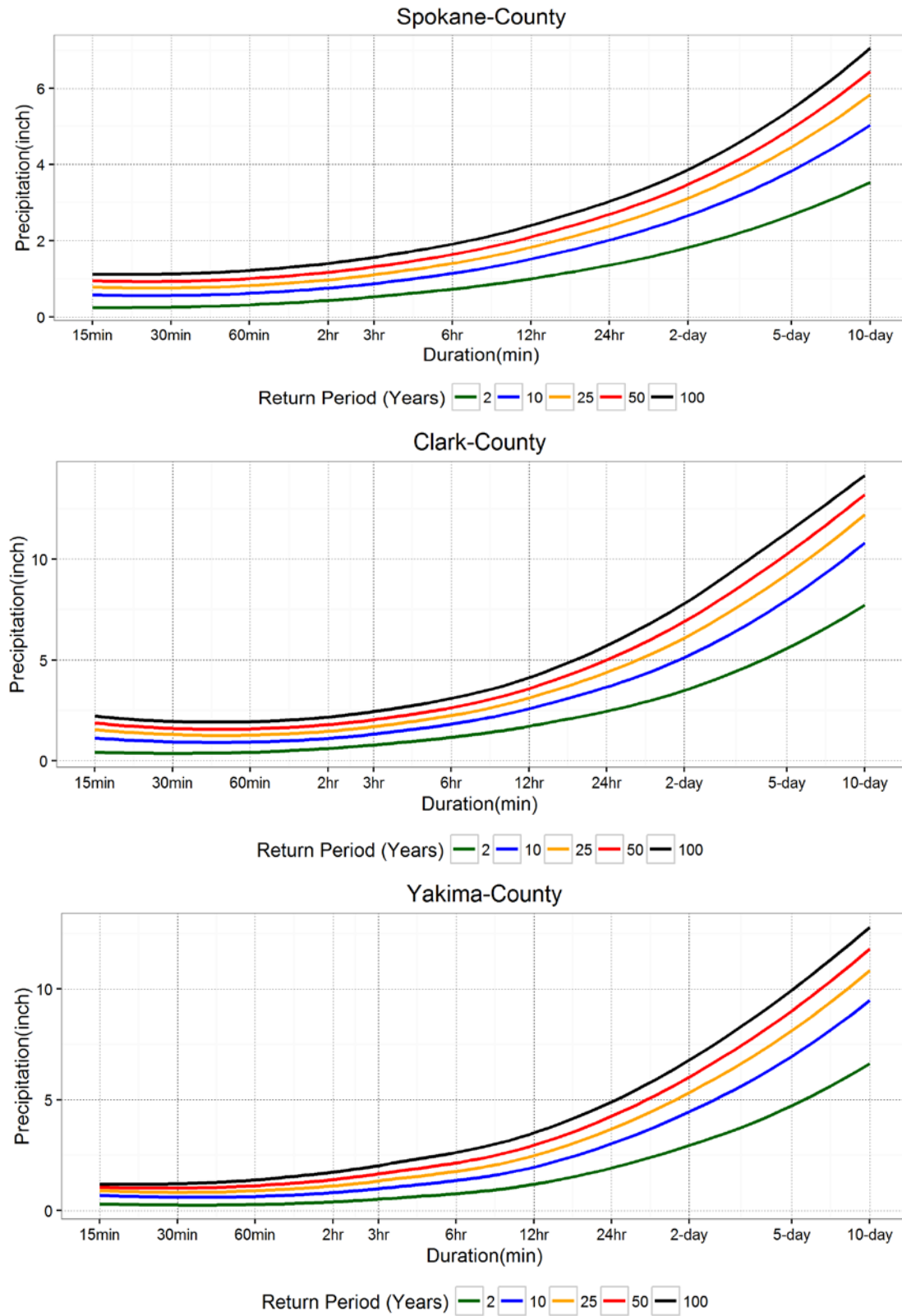
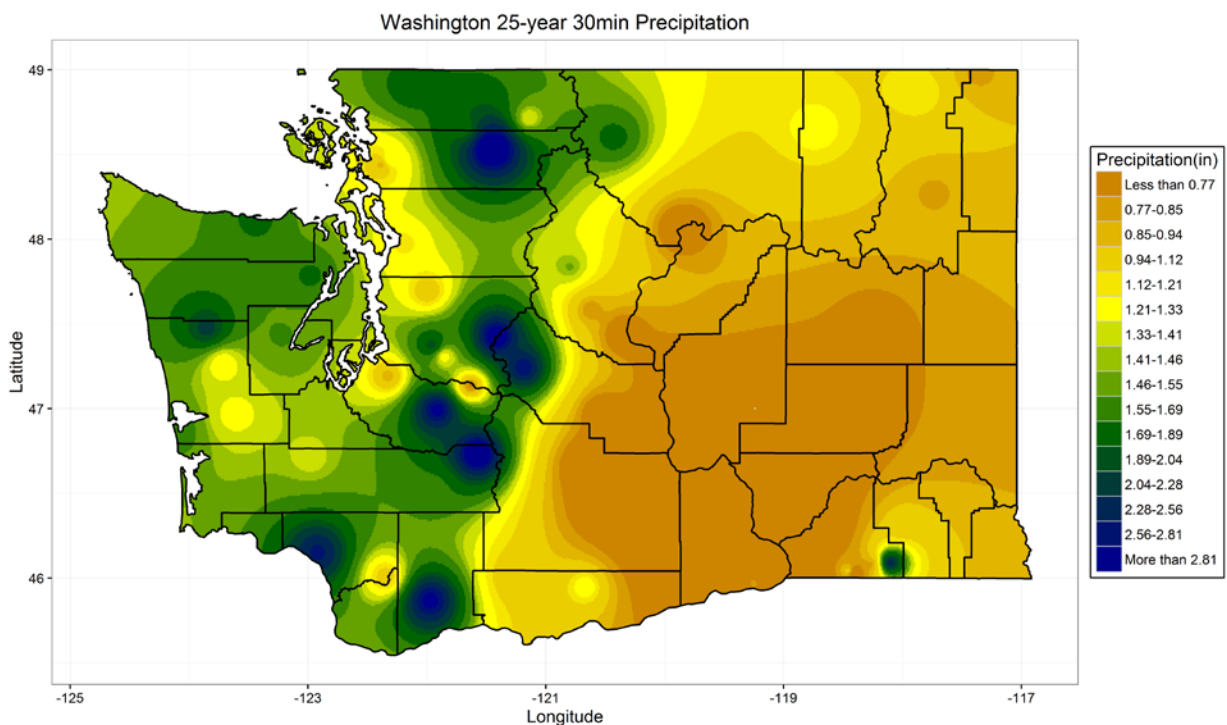


Figure 26. County-level IDF curves for selected counties in eastern and western Washington.

4.4. Spatial Maps of Extreme Precipitation

At regional scale, the precipitation value for a given duration and return period can be directly obtained from the regionally representative IDF curves. The at-site precipitation values for stations within a region can then be determined by multiply the regional precipitation value with scaling factors, also known as index-flood factors. In this study, the mean maximum precipitation values from the stations were used as scaling factors. The at-site extreme precipitations for a given duration and return period were then interpolated using Inverse Distance Weighting (IDW) method to generate the spatial maps. Figure 27 show the distribution of 30-minute and 24-hour extreme precipitations which have 25-year return period. The spatial distribution maps for other durations and return periods are provided in Appendix ().



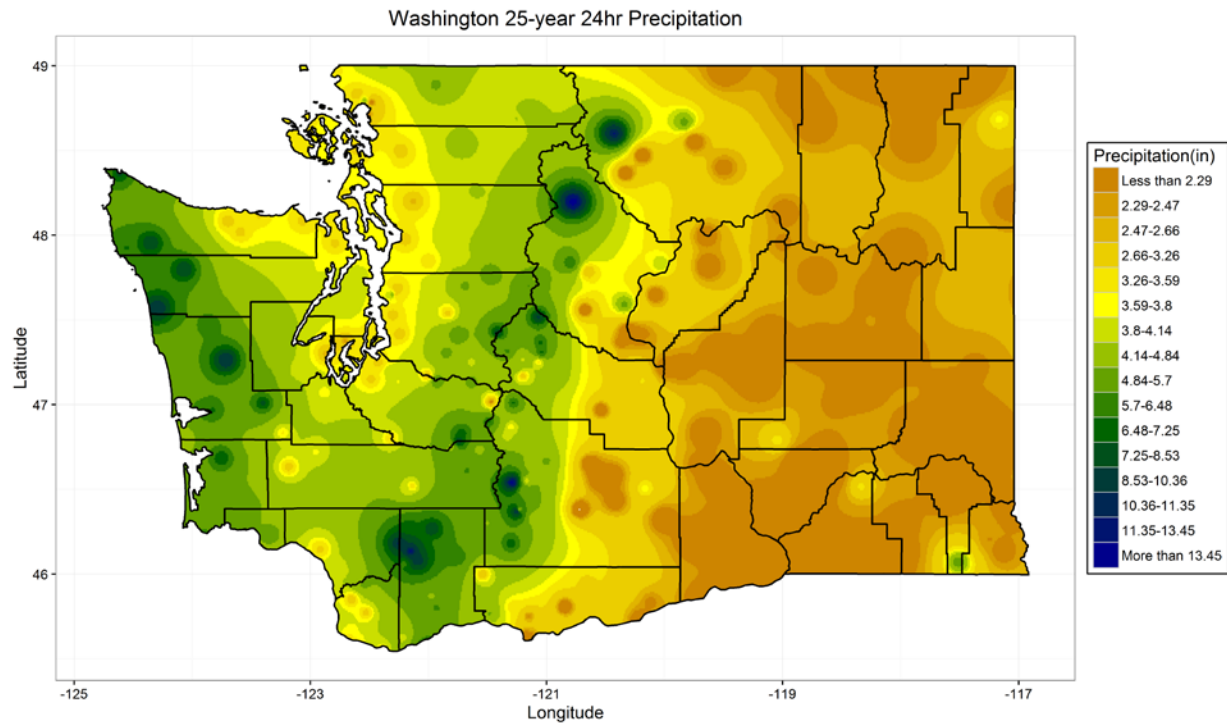


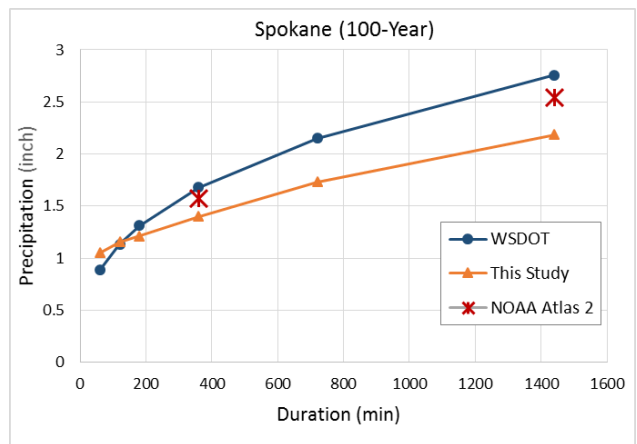
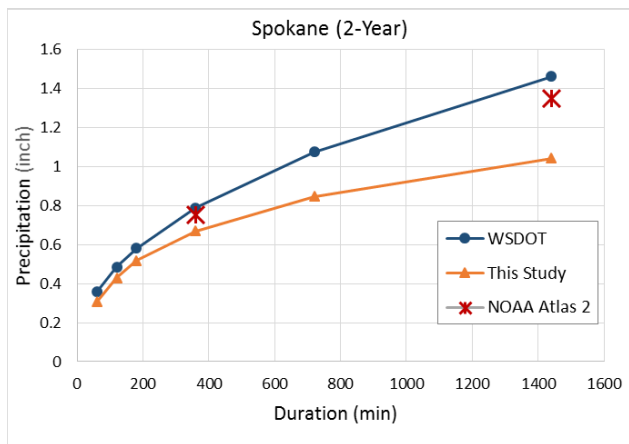
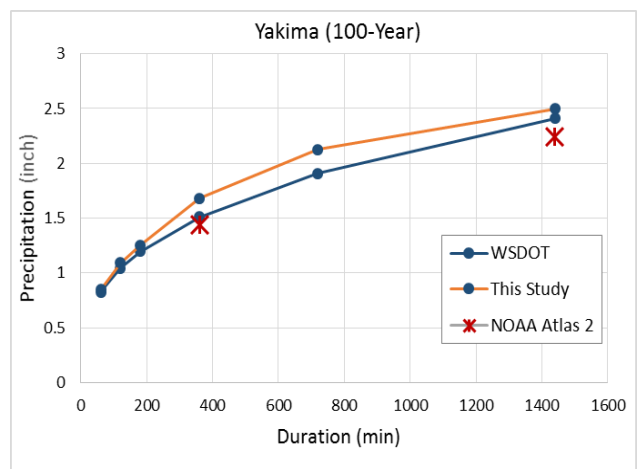
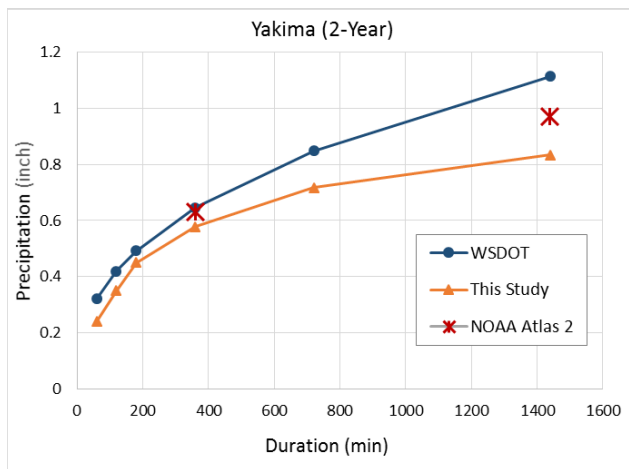
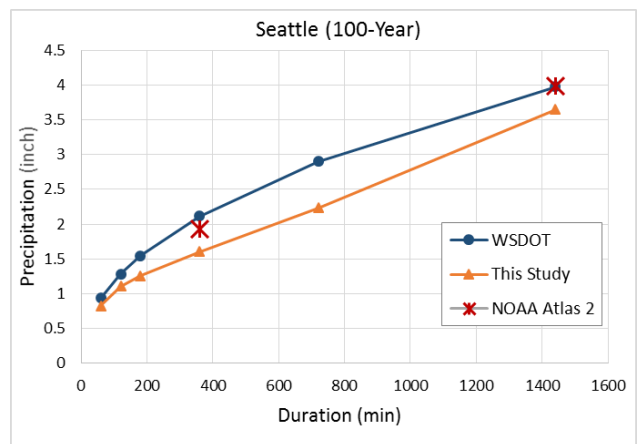
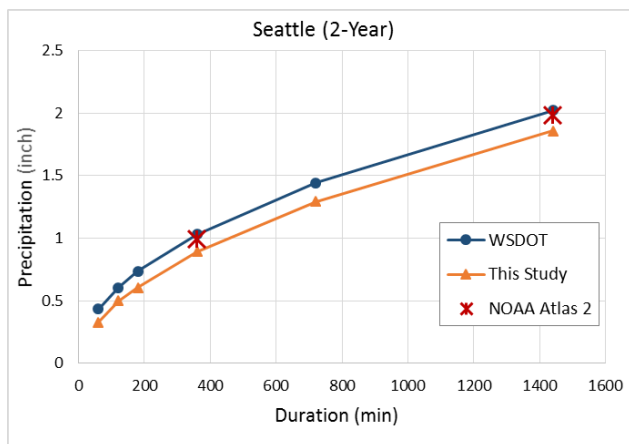
Figure 27. Distribution of 25-year extreme precipitations which have 30-minute and 24-hour durations.

4.5. Comparison with Currently Available IDF values

The IDF results from this study were compared with currently available IDF values for the state of Washington, which are obtained from the Washington State Department of Transportation (WSDOT), NOAA Atlas 2 and Wallis et al. (2007) spatial maps for 2-hour and 24-hour durations extreme precipitations. WSDOT (2015) provides an equation to estimate rainfall intensity as a function of time of concentration and two location-specific coefficients, which also varies with return periods. The coefficients for 2, 5, 10, 25, 50, and 100 years return periods are provided for most of the cities in Washington. NOAA Atlas 2 provides precipitation frequency estimates for 6-hour and 24-hour durations and 2-year and 100-year return periods at any given point with known latitude and longitude. Wallis et al. (2007) provides grids precipitation estimate for 2-hour and 24-hour durations and return periods of 6 months, 2 years, 10 years, 25 years, 50 years, 100 years and

500 years. The results from the first two comparisons (i.e., WSDOT and NOAA Atlas 2) are presented in Figure 28 for selected major cities in Washington. The comparison between this study and Wallis et al. (2007) results showed large differences along the mountains that need further examination and thus are not included in this report. To generate the spatial maps, Wallis et al. (2007) used the PRISM (Daly et al., 2002) mean annual precipitations estimates, which have relatively higher mean annual precipitations along the mountains than the mean annual precipitations obtained in this study using the IDW interpolation method. Some of the observed difference might be attributed to this difference in mean annual precipitation, interpolation methods and datasets used for the interpolation.

Overall, except for Walla Walla, the WSDOT estimates larger amount of precipitations for 2-year storms compared to this study and that of NOAA, while for the 100-year storms, this study estimated relatively large amount of precipitation in the southeast (Yakima, Walla Walla, and to some extent Kennewick) compared to the estimates by WSDOT and NOAA. Based on these preliminary observations, the current drainage systems designed based on WSDOT's estimate of precipitations are expected to be adequate for draining design storm with shorter return periods in most parts of the state. However, for design storm with larger return period, depending on locations, retrofitting of the drainage system might be required.



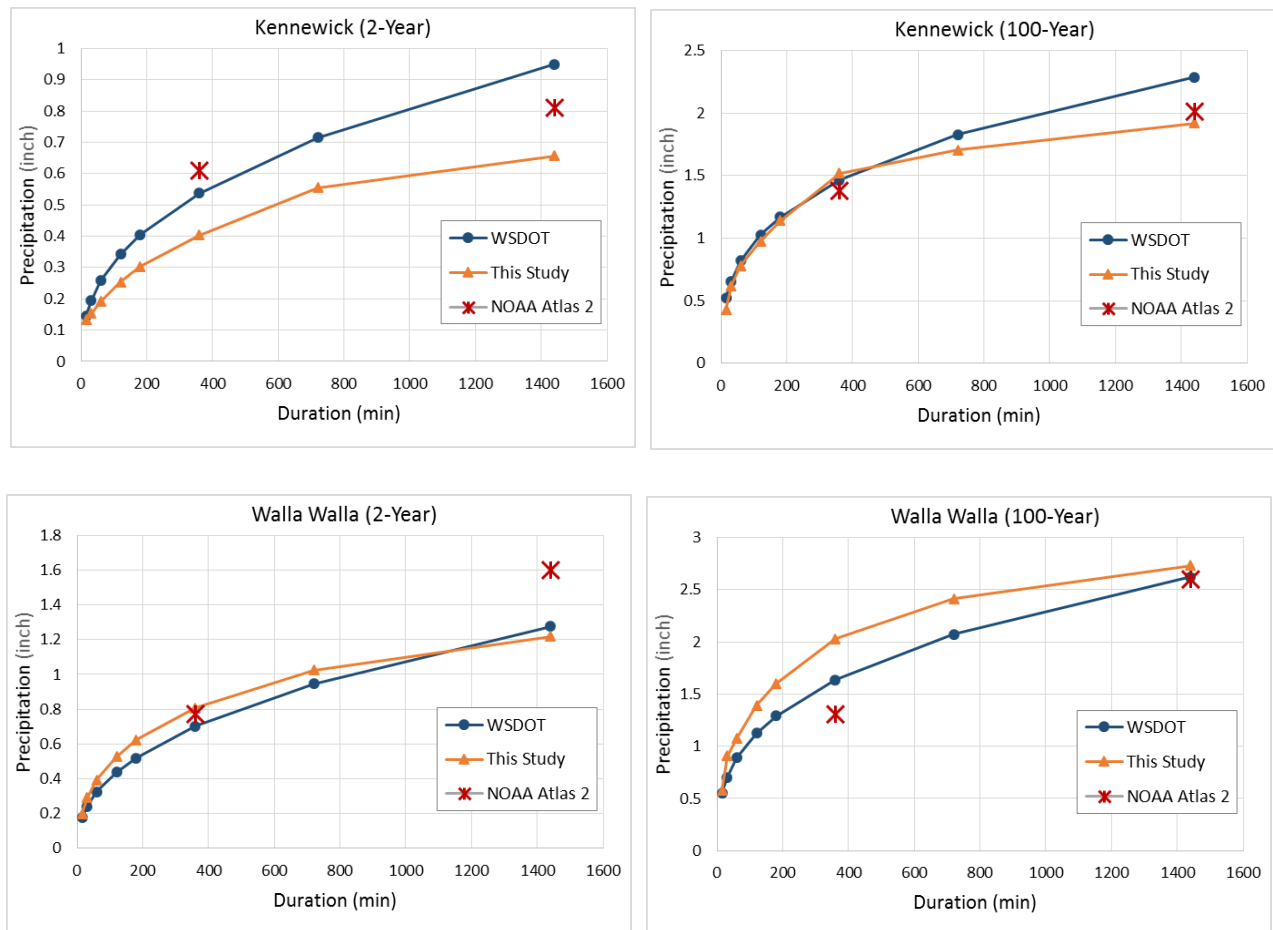


Figure 28. Comparisons of IDF curves from this study with that of WSDOT and NOAA-Atlas 2 for selected cities.

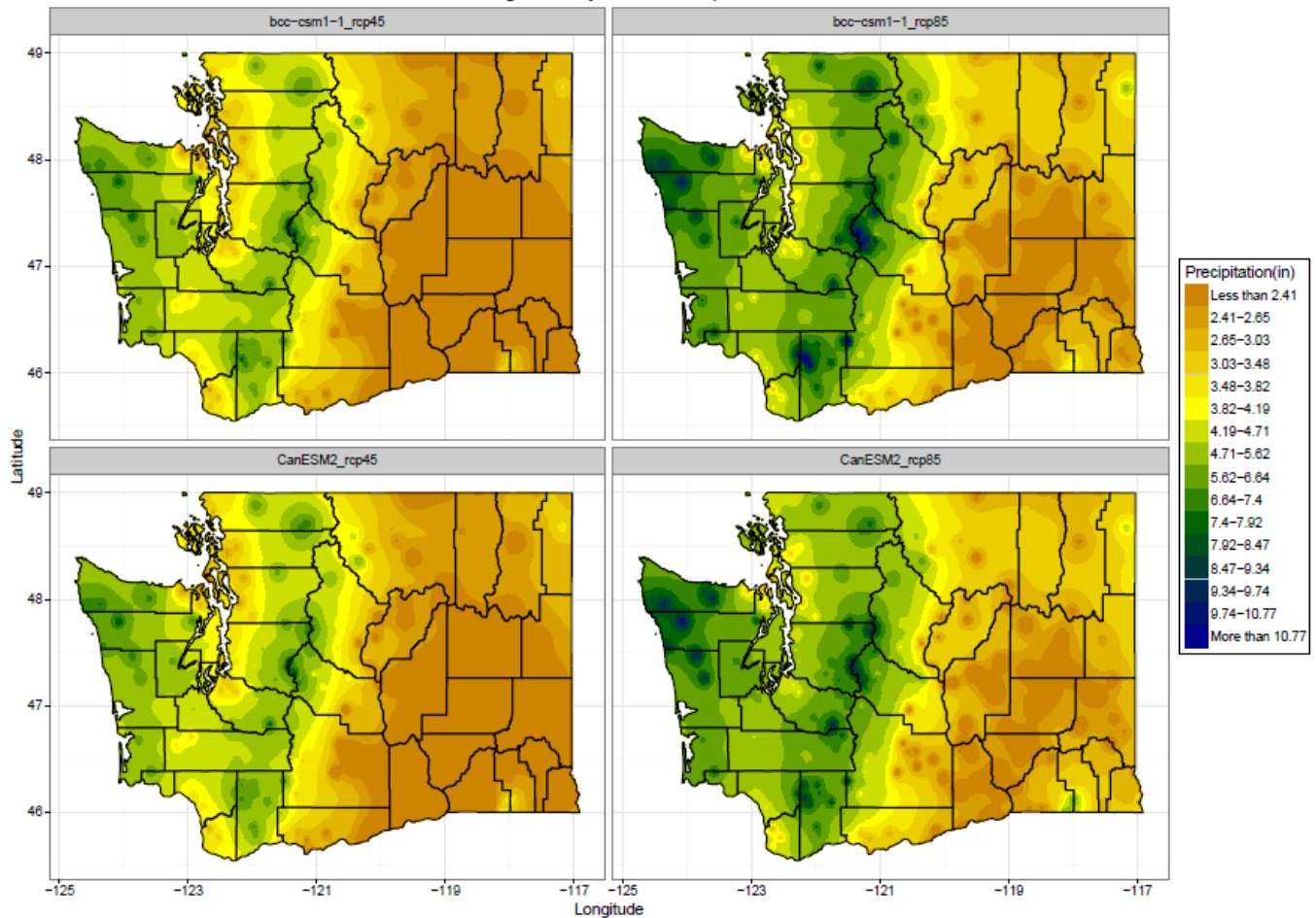
4.6. Climate Projections

Data from two climate models (BCC-CSM1.1 and CanESM2) and two scenarios (RCP 4.5 and RCP 8.5) were used for future projections of extreme precipitation. Figure 29 shows the projected extreme precipitation maps for 24-hour storm with 100-year return period. Compared to the historical estimate, the project extreme precipitations amount are smaller for most of the regions. This is contrary to what we have expected at the beginning of the study, and deems further

studies by including more climate models, addressing their uncertainty and limitations in projecting extreme storm events as most of the climate models are primarily designed to capture mean patterns.

Projected Precipitations

Washington 100-year 24hr Precipitation



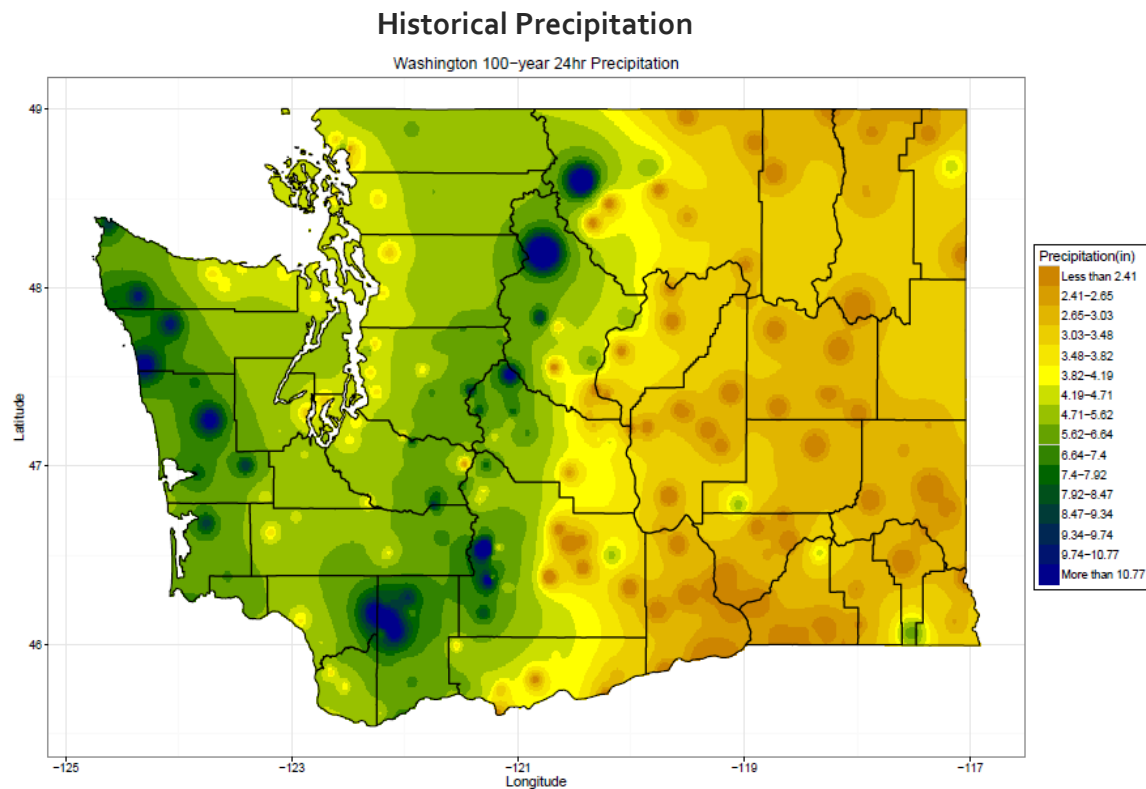
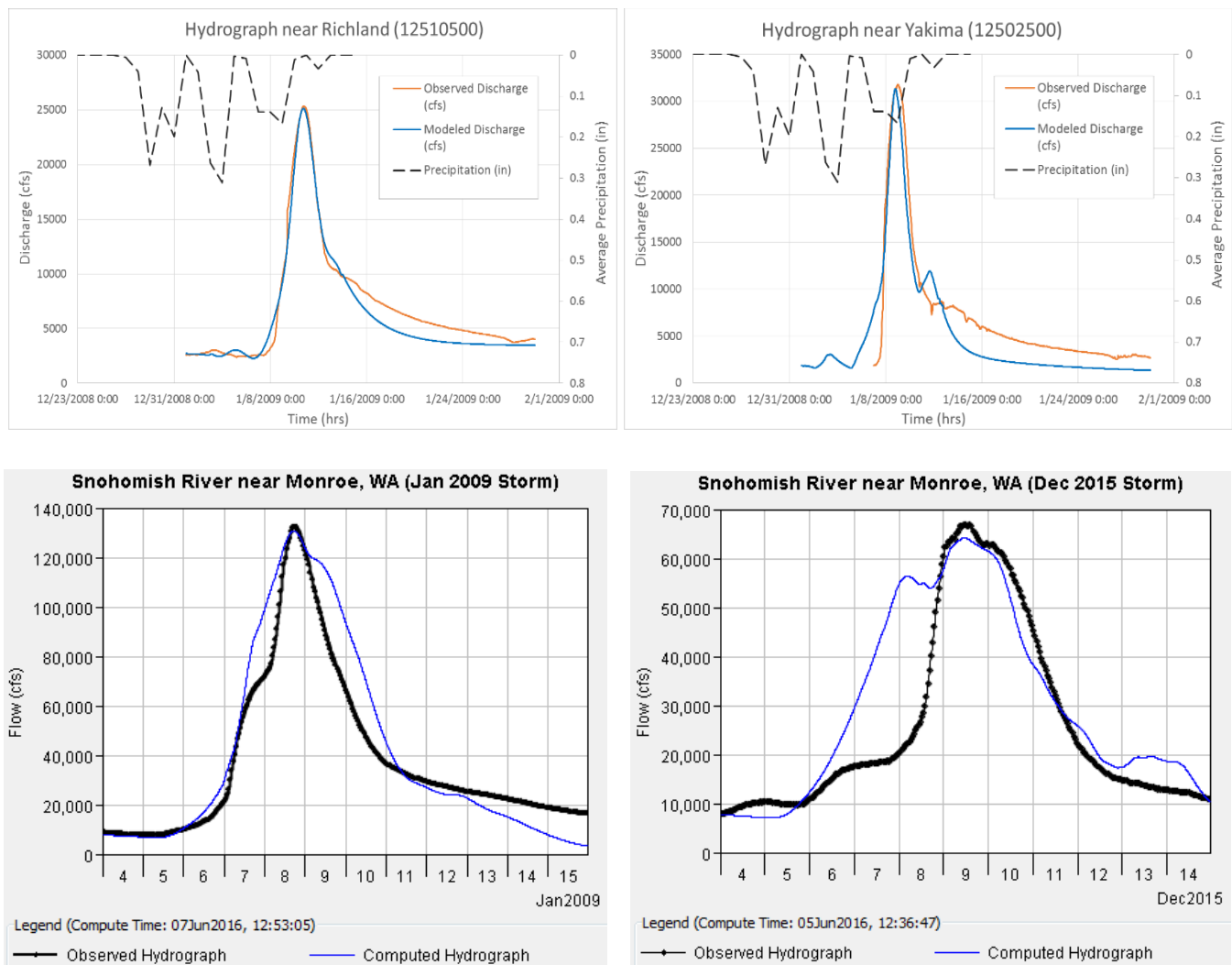


Figure 29. Extreme precipitation based on projected and historical data.

4.7. Runoff IDF Curves

In order to directly relate the extreme storm events with associated runoff and flooding risk, this study developed HEC-HMS models for selected watersheds located close to the cities of Seattle, Yakima and Tri-Cities. These watersheds include the Yakima River Basin (YRB), (SRB), Puyallup River Basin (PRB) and Green-Duwamish River Basin (GRB). Most of the basins were calibrated using the January 2009 storm and observed hydrographs near the basin outlets. The models were then validated based on the December 2015 storm and observed hydrographs. Figure 30 illustrates the calibration and validation results, showing reasonable fits between observed and computed hydrographs. Particular consideration was given in capturing the peak flow as the

models were intended to estimate the peak flows associated with storm events obtained from rainfall IDF curves. After the HEC-HMS models were calibrated and validated for each basin, the storm events obtained from IDF curves of the representative counties were used to estimate the peak runoff IDF curves. The results near to the basins outlets are presented in Figure 31. Since temperature data are not available for such simulation, the effect of snowmelt was neglected, potentially underestimating the expected peak flow if storm happen during snow melting season. The peak runoffs associated with the January 2009 storm, which affects the entire state, are included into the estimate runoff IDF curves to provide better perspective.



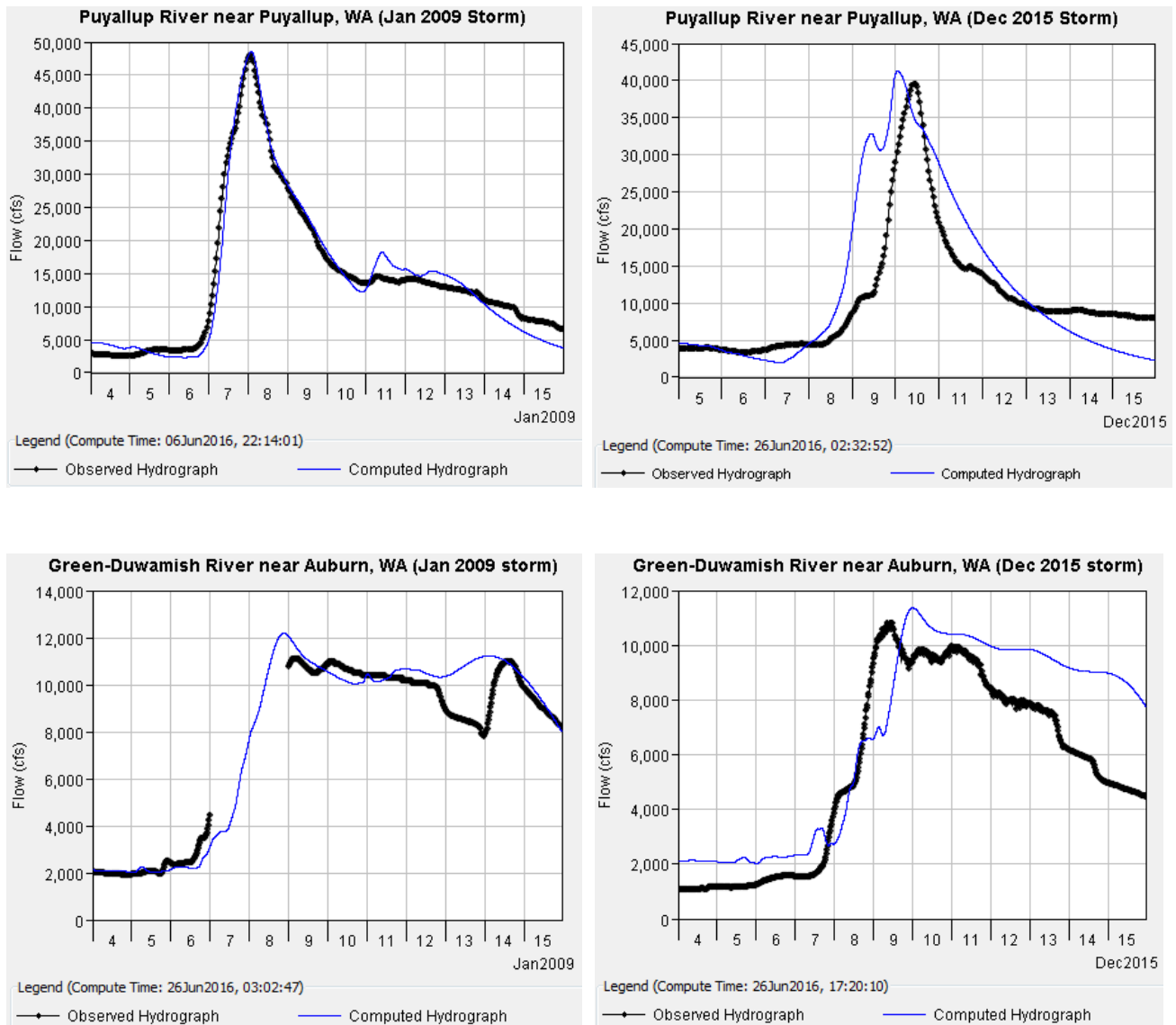
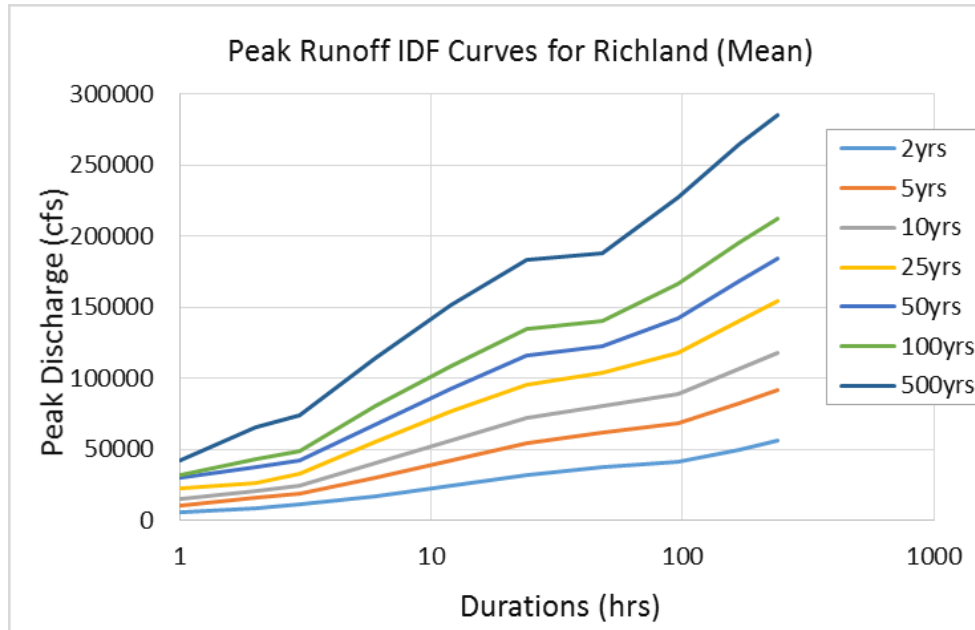
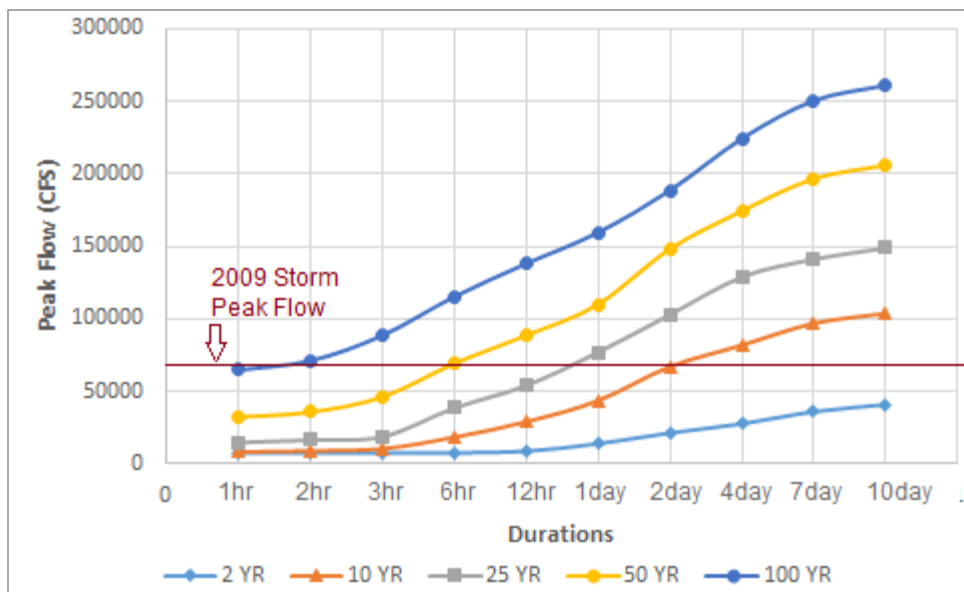


Figure 30. Calibration (left) and validation (right) results for the four watersheds considered.

Yakima River Basin



Snohomish River Basin



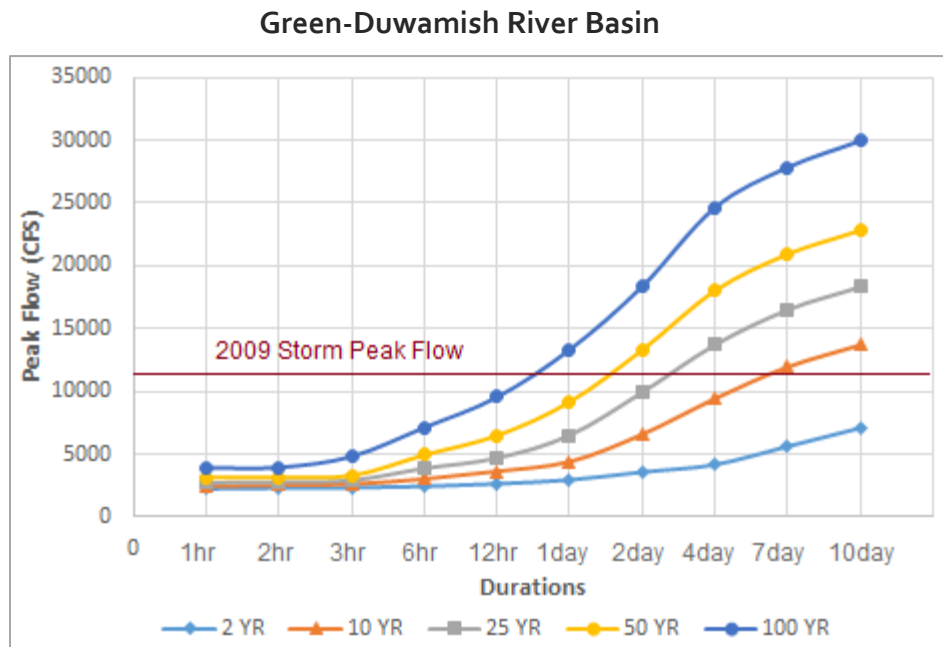
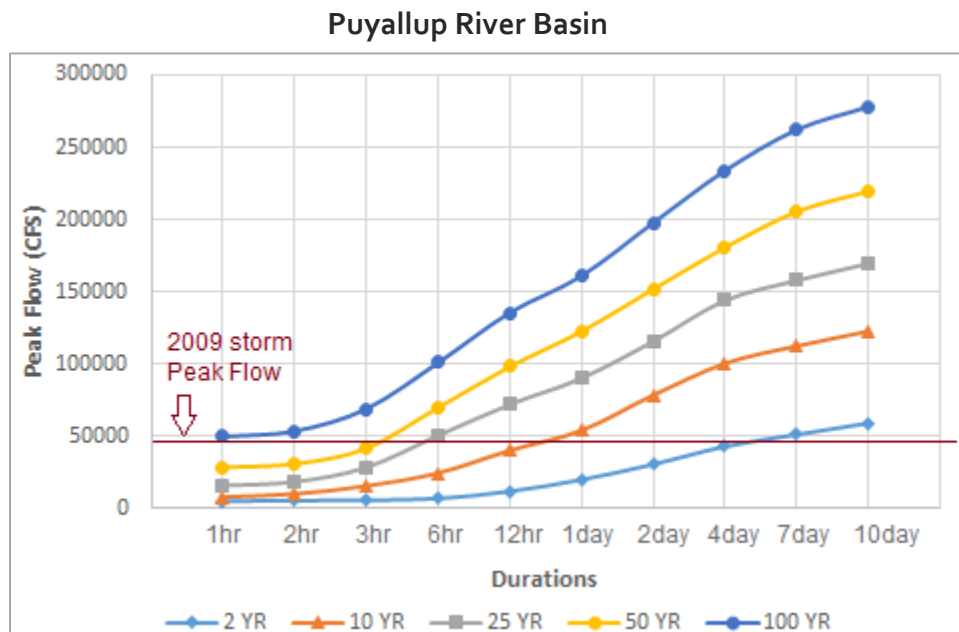


Figure 31. Runoff IDF curves for Yakima, Snohomish, Puyallup and Green-Duwamish watershed outlets.

References

- Arkell, R. E., and F. Richards, 1986, Short duration rainfall relations for the western United States. *AMS Conference on Climate and Water Management - A Critical Era*. Asheville, NC.
- Ayvaza, M. T.; H. Karahana, and M. M. Aral, 2007, Aquifer parameter and zone structure estimation using kernel-based fuzzy c-means clustering and genetic algorithm, *Journal of Hydrology*, 343(3–4), 240–253.
- Breusch, T. S., 1978, Testing for Autocorrelation in Dynamic Linear Models, *Australian Economic Papers*, 17: 334–355. doi:10.1111/j.1467-8454.1978.tb00635.x.
- Burn, D. H.; N. K. Goel, 2000, The formation of groups for regional flood frequency analysis, *Hydrological Sciences Journal*, 45(1), 97–112.
- Congdon, P., 2001. *Bayesian Statistical Modelling*, Wiley, West Sussex, Chichester, UK, p. 596.
- Dettinger, M.D., F.M. Ralph, T. Das, P.J. Neiman, and D. Cayan, 2011, Atmospheric rivers, floods, and the water resources of California. *Water* 3: 455-478.
- Douglas, E. M.; R. M. Vogel; C. N. Kroll, 2000, Trends in floods and low flows in the United States: impact of spatial correlation, *Journal of Hydrology*, 240,90–105.
- Dunn, J.C.,1974, A fuzzy relative of the ISODATA process and its use in detecting well-separated clusters, *Journal of Cybernetics*, 3,32-57.
- Federal Insurance and Mitigation Administration (FIMA) and Federal Emergency Management Agency (FEMA), 2013, *The impact of climate change and population growth on the National Flood Insurance Program through 2100*. Washington, DC.
- Gamerman, D., 1997, *Markov chain monte carlo-stochastic simulation for Bayesian inference*, Chapman & Hall, London, UK, p. 342.
- Godfrey, L. G., 1978, Testing Against General Autoregressive and Moving Average Error Models when the Regressors Include Lagged Dependent Variables". *Econometrica* 46: 1293–1301. JSTOR 1913829

- Greenwood, J. A., J. M. Landwehr; N. C. Matalas and J. R. Wallis, 1979, Probability weighted moments: definition and relation to parameters of several distributions expressible in inverse form, *Water Resources Research*, 15(5), 1049–1054.
- Groisman, P.Y., R.W. Knight, and T.R. Karl, 2012, Changes in intense precipitation over the central United States. *Journal of Hydrometeorology*, 13: 47–66.
- Hamlet, A. F., and D.P. Lettenmaier, 2007, Effects of 20th century warming and climate variability on flood risk in the western U.S., *Water Resources Research*, 43, W06427, doi:10.1029/2006WR005099.
- Hosking, J.R.M. 1990, L-Moments: analysis and estimation of distributions using linear combinations of order statistics. *Journal of the Royal Statistical Society: Series B*, 52(2): 105–124.
- Hosking, J. R. M., and J. R. Wallis, 1993, Some statistics useful in regional frequency analysis, *Water Resources Research*, 29(2), 271–281.
- Hosking, J.R.M., and J.R. Wallis, 1997, Regional Frequency Analysis, An Approach Based on L-moments, Cambridge University Press, Cambridge, UK, p. 224.
- Jakob, D., D. W. Reed and A. Robson, 1999. *Statistical procedures for flood frequency estimation, Chapter 16, Flood estimation*, Vol. 3, Institute of Hydrology, Wallingford, UK, p. 153–180.
- Janssen, E., D.J. Wuebbles, K.E. Kunkel, S.C. Olsen, and A. Goodman, 2014, Observational and model based trends and projections of extreme precipitation over the Contiguous United States. *Earth's Future*, doiI: 10.1002/2013EF000185
- Kendall, M.G., 1975, *Rank Correlation Measures*, Charles Griffin, London, UK, p. 272.
- Kass, R.E.; A.E. Raftery, 1995, Bayes factors, *Journal of the American Statistical Association*, 90(430):773–795
- Kunkel, K.E. et al., 2013, Monitoring and understanding trends in extreme storms: state of knowledge. *Bulletin of the American Meteorological Society*, 94: 499–514.
- Levene, H., 1960, *Robust testes for equality of variances. In Contributions to Probability and Statistics* (I. Olkin, ed.) 278–292. Stanford Univ. Press, Palo Alto, CA.

- Madsen, T., and E. Figdor, 2007, *When it rains, it pours: global warming and the rising frequency of extreme precipitation in the United States*. Environment America Research and Policy Center, Boston, MA.
- Mann, H.B., 1945, Non-parametric tests against trend, *Econometrica*, 13: 245–259.
- Mantua N, I. Tohver and A.F. Hamlet, 2010, Climate change impacts on streamflow extremes and summertime stream temperature and their possible consequences for freshwater salmon habitat in Washington State. *Climatic Change*, DOI: 10.1007/s10584-010-9845-2
- Mass, C., A. Skalenakis, and M. Warner, 2011, Extreme precipitation over the west coast of North America: Is there a trend? *Journal of Hydrometeorology*, 12: 310–318.
- Melillo, J. M., T.C. Richmond, and G.W. Yohe (Eds.), 2014, *Climate Change Impacts in the United States: The Third National Climate Assessment*. U.S. Global Change Research Program, 841 pp. doi:10.7930/J0Z31WJ2.
- Miller, J.F., 1964, *Two- to ten-day precipitation for return periods of 2 to 100 years in the contiguous United States*. Technical Paper No. 49, U.S. Weather Bureau and U.S. Department of Agriculture.
- Miller, J.F., R.H. Frederick, and R.J. Tracy, 1973, *Precipitation-frequency atlas of the western United States*. NOAA Atlas 2, 11 vols., National Weather Service, Silver Spring, MD.
- Mikkelsen P.S., H. Madsen, K. Arnbjerg-Nielsen, D. Rosbjerg, and P. Harrmoes, 2005, Selection of regional historical rainfall time series as input to urban drainage simulation at ungauged locations. *Atmospheric Research*, 77(1-4): 4-17.
- National Research Council (NRC), 2013, *A review of the draft 2013 National Climate Assessment*. The National Academies Press, Washington, DC.
- Neiman, P.J., L.J. Schick, F.M. Ralph, M. Hughes, and G.A. Wick, 2011, Flooding in Western Washington: the connection to atmospheric rivers. *Journal of Hydrometeorology*, 12: 1337–1358.
- Ralph, F.M., P.J. Neiman, G.A. Wick, S.I. Gutman, M.D. Dettinger, D.R. Cayan, and A.B. White (2006), Flooding on California's Russian River: role of atmospheric rivers, *Geophysical Research Letters*, 33, L13801, doi:10.1029/2006GL026689.

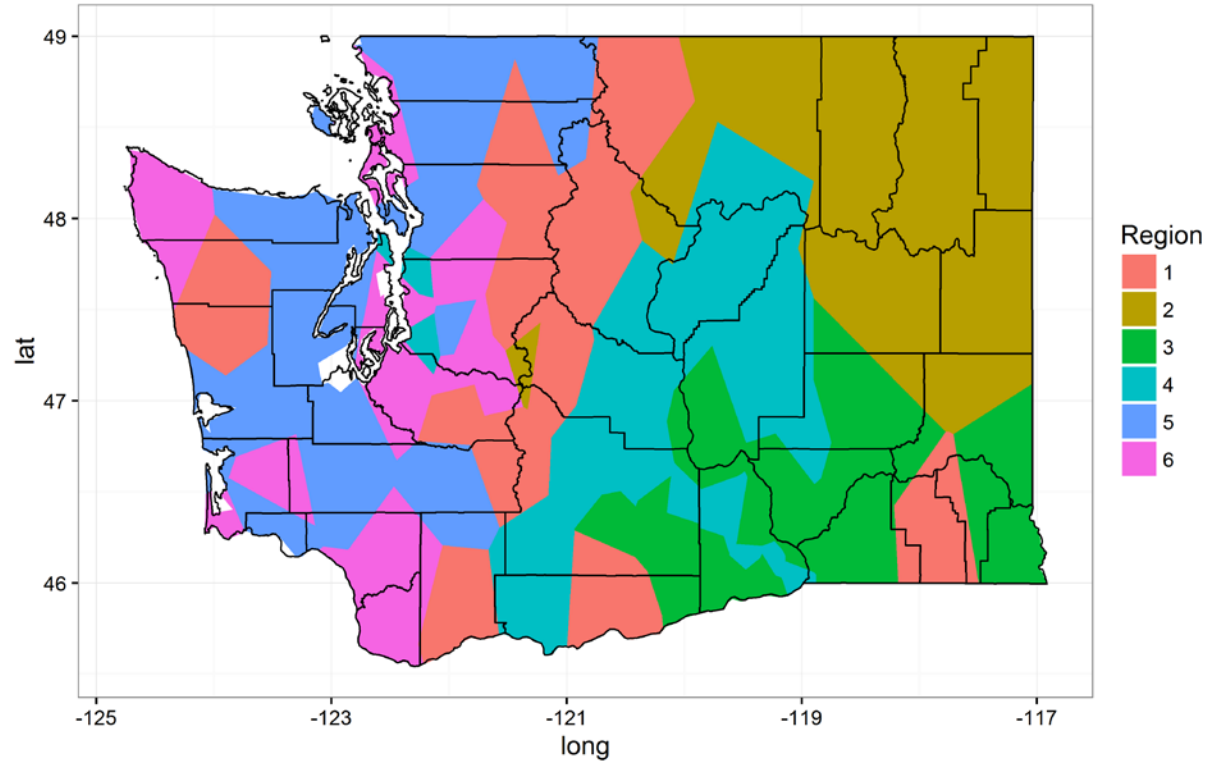
- Reis, D.S.; Jr, J.R. Stedinger, 2005, Bayesian MCMC flood frequency analysis with historical information, *Journal of Hydrology*, 313(1):97–116.
- Roberts, G.O.; A. Gelman; W.R. Gilks, 1994, Weak Convergence and Optimal Scaling of Random Walk Metropolis-Hastings Algorithms, *the Annals of Applied Probability*, 7(1), 110-120.
- Rosenberg, E.A., P.W. Keys, D.B. Booth, D. Hartley, J. Burkey, A.C. Steinemann, and D.P. Lettenmaier, 2010, Precipitation extremes and the impacts of climate change on stormwater infrastructure in Washington State. *Climatic Change*, doi:10.1007/s10584-010-9847-0.
- Ruspini, E. H., 1969. A new approach to clustering, *Information and Control*. 15, 22-32.
- Sadri, S. and D. H. Burn, 2011, A fuzzy C-means approach for regionalization using a bivariate homogeneity and discordancy approach, *Journal of Hydrology*, 401(3–4), 231–239.
- Salathé, E. P., L. R. Leung, Y. Qian, and Y. Zhang, 2010, Regional climate model projections for the state of Washington, *Climatic Change*, 102, 51–75, doi:10.1007/s10584-010-9849-y.
- Schaefer, M.G., B.L. Barker, G.H. Taylor, and J.R. Wallis, 2002, *Regional precipitation-frequency analysis and spatial mapping of precipitation for 24-hour and 2-hour durations in Western Washington*. Washington State Department of Transportation, Report WARD 544.1.
- Schaefer, M.G., B.L. Barker, G.H. Taylor, and J.R. Wallis, 2006, *Regional precipitation-frequency analysis and spatial mapping of precipitation for 24-hour and 2-hour durations in Eastern Washington*. Washington State Department of Transportation.
- Snober, A., G. Mauger, L. Whitely Binder, M. Krosby, and I. Tohver, 2013, *Climate Change Impacts and Adaptation in Washington State: Technical Summaries for Decision Makers*, Seattle: State of Knowledge Report prepared for the Washington State Department of Ecology, Climate Impacts Group, University of Washington, Seattle, WA.
- U.S. Environmental Protection Agency, 2014, *Climate change indicators in the United States, Third edition*. EPA 430-R-14-004. www.epa.gov/climatechange/indicators.
- Wallis, J. R.; M. G. Schaefer, B. L. Barker; G. H. Taylor 2007, Regional precipitation frequency analysis and spatial mapping for 2-hour and 24-hour durations for Washington State, *Hydrology and Earth System Sciences*, 11, 415-442.

Westra, S., L.V. Alexander, and F.W. Zwiers, 2013, Global increasing trends in annual maximum daily precipitation. *Journal of Climate*, 26:3904-3918.

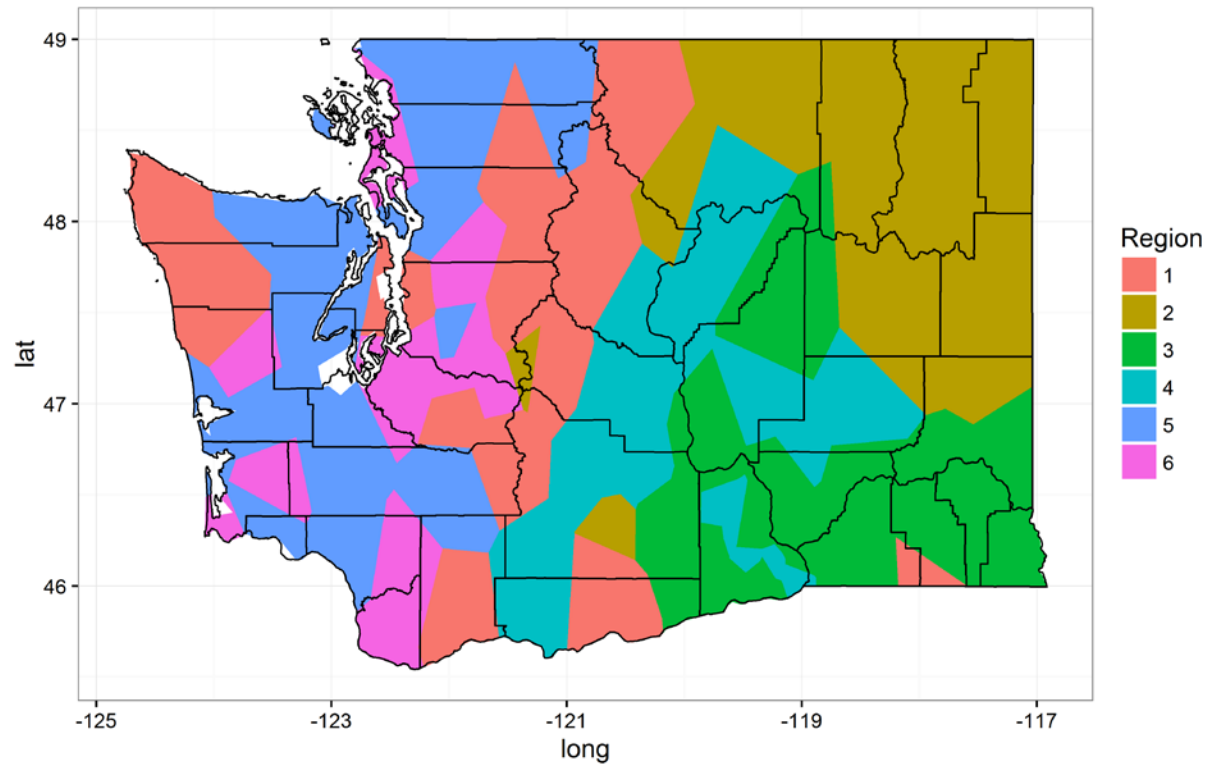
Appendix A

Maps of homogenous regions for various durations

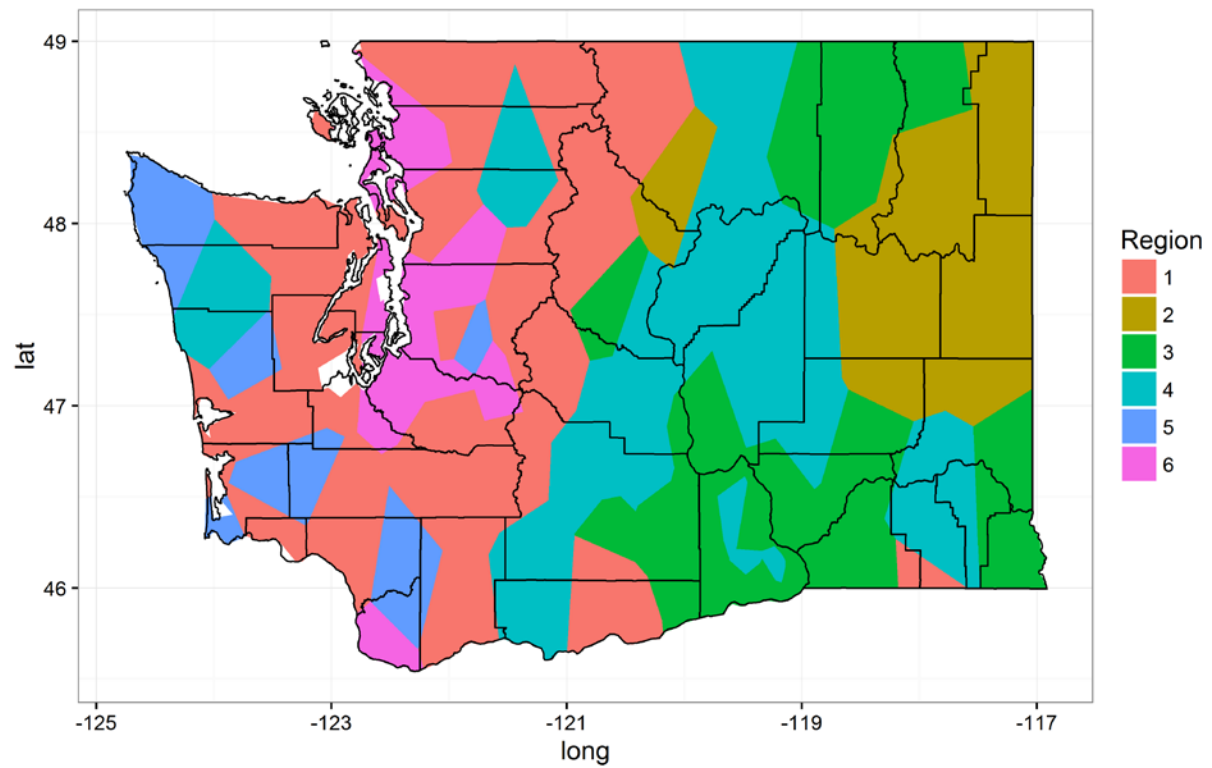
Duration: 60 Minutes



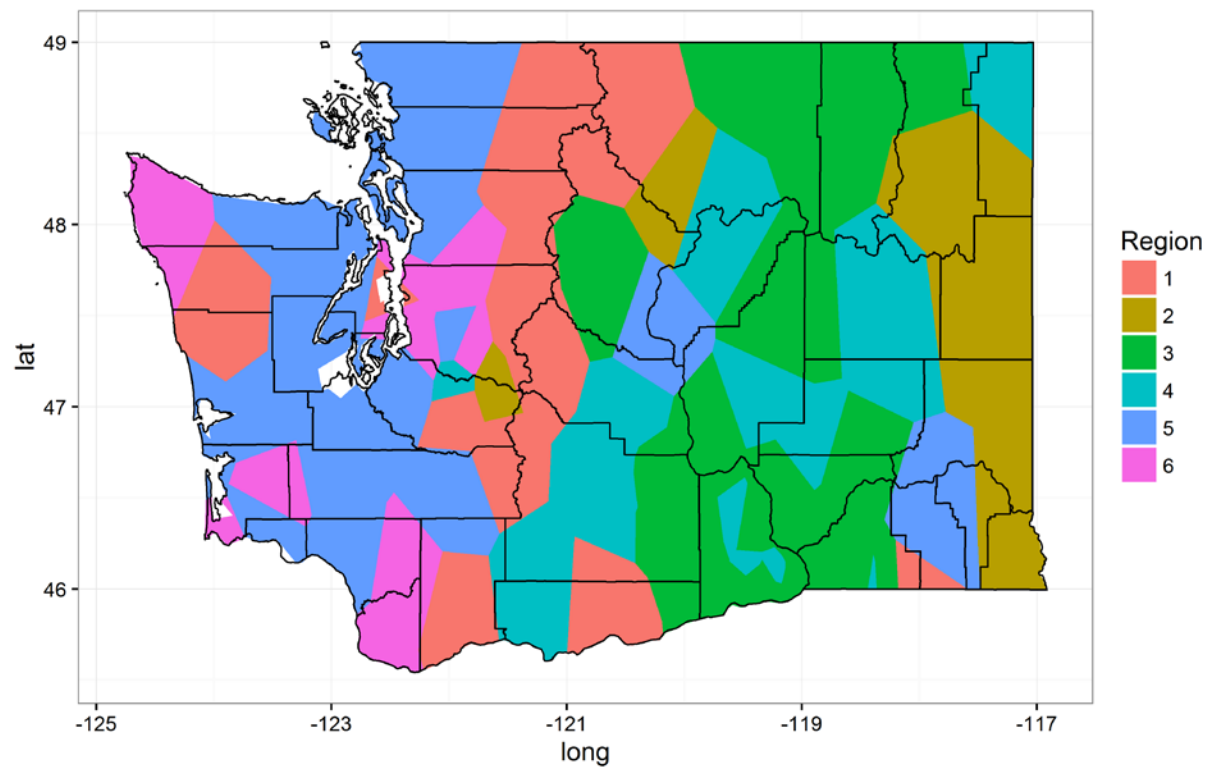
Duration: 2 hrs



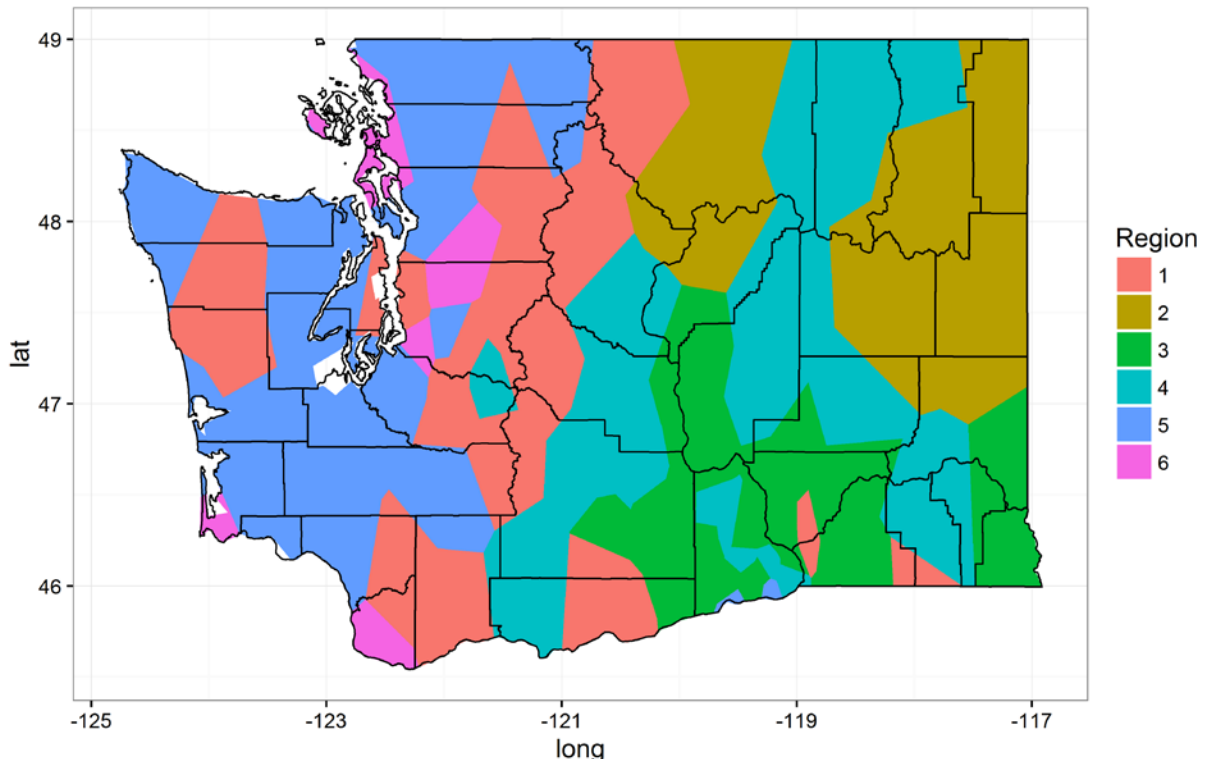
Duration: 3 hrs



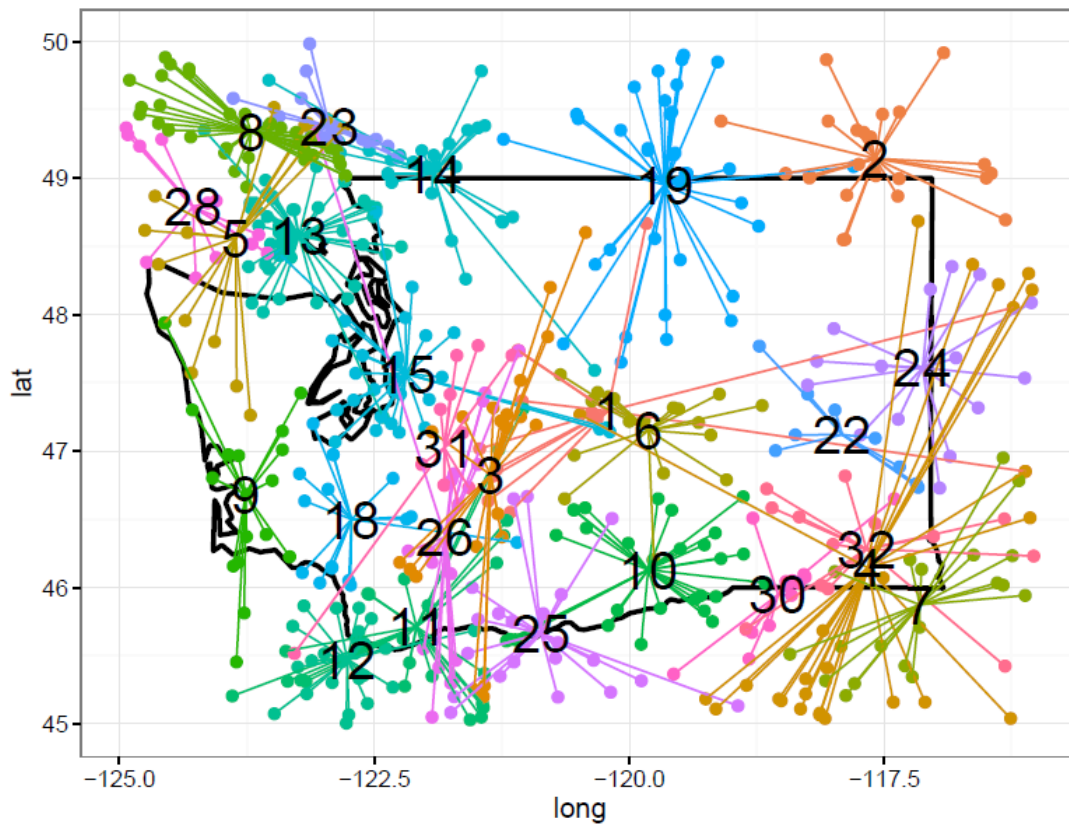
Duration: 6 hrs



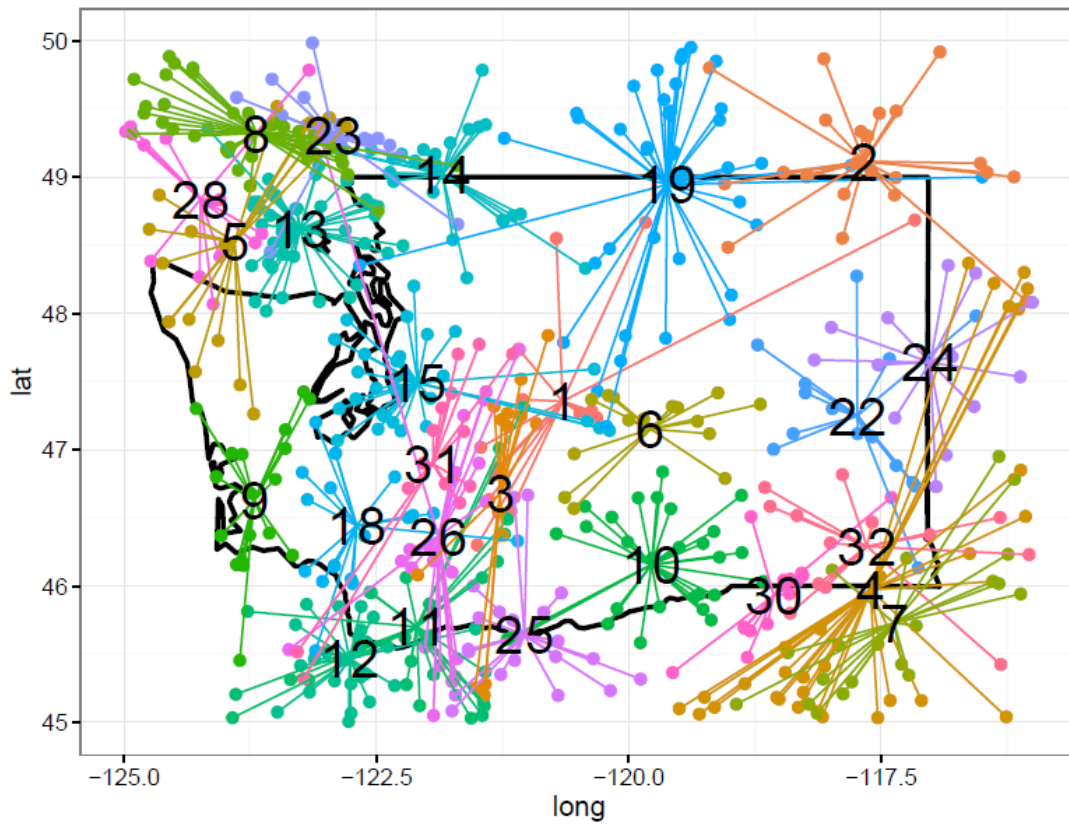
Duration: 12 hrs



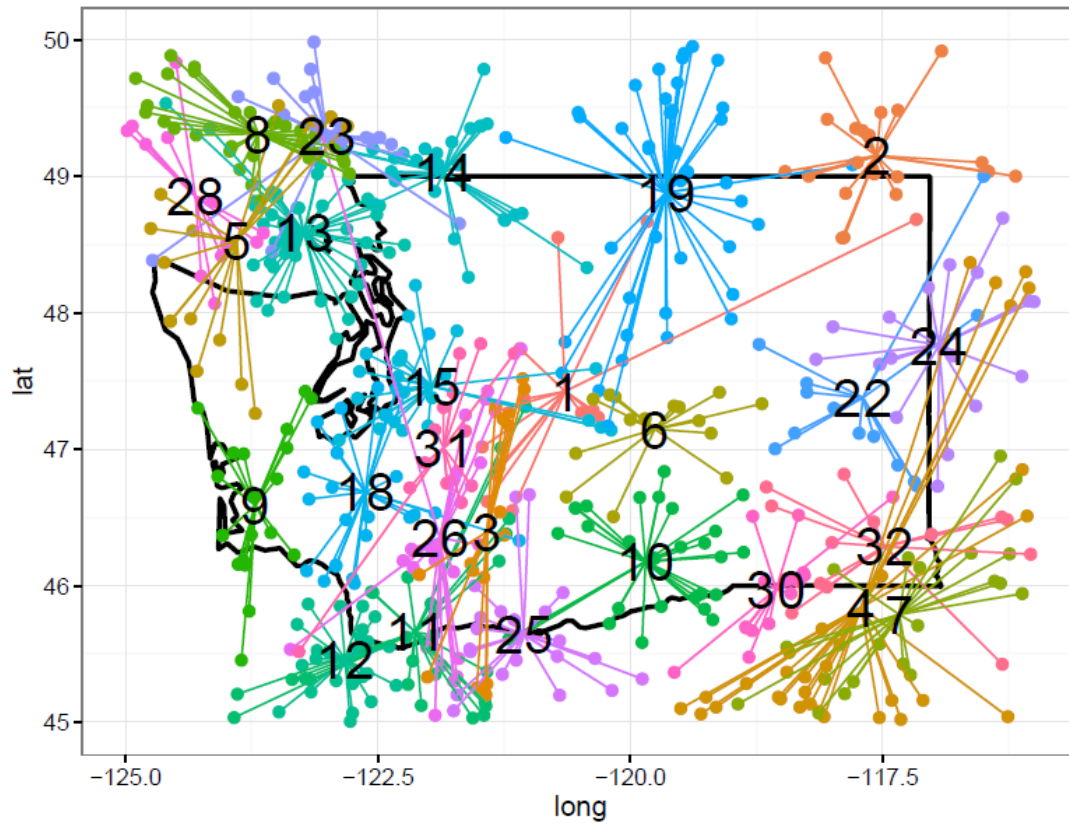
Duration: 24 hrs



Duration: 5-day

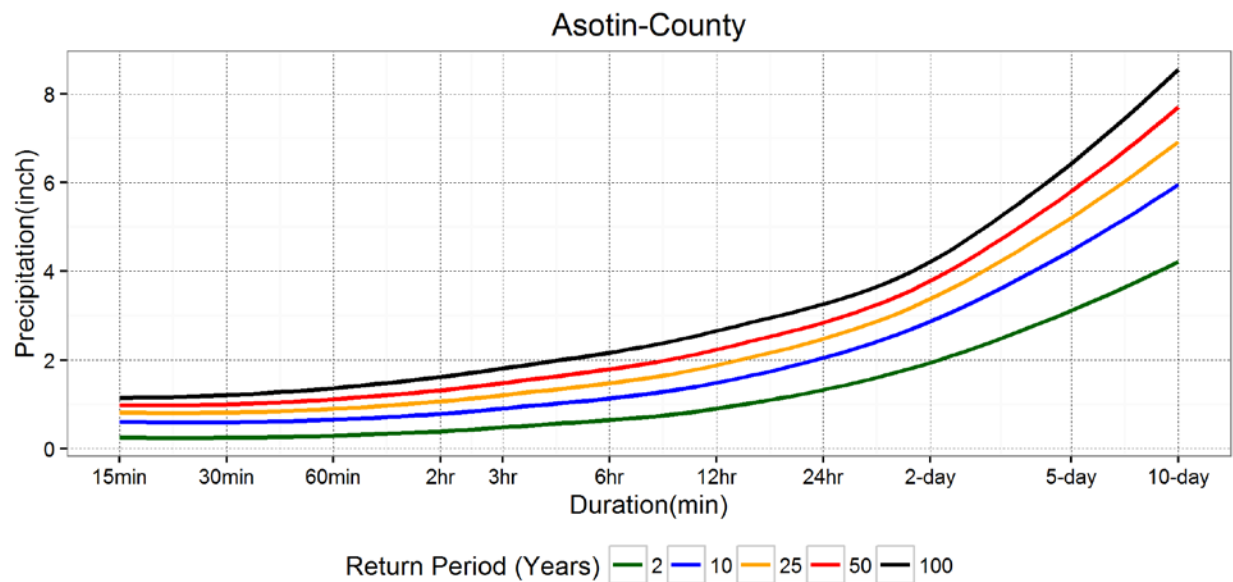
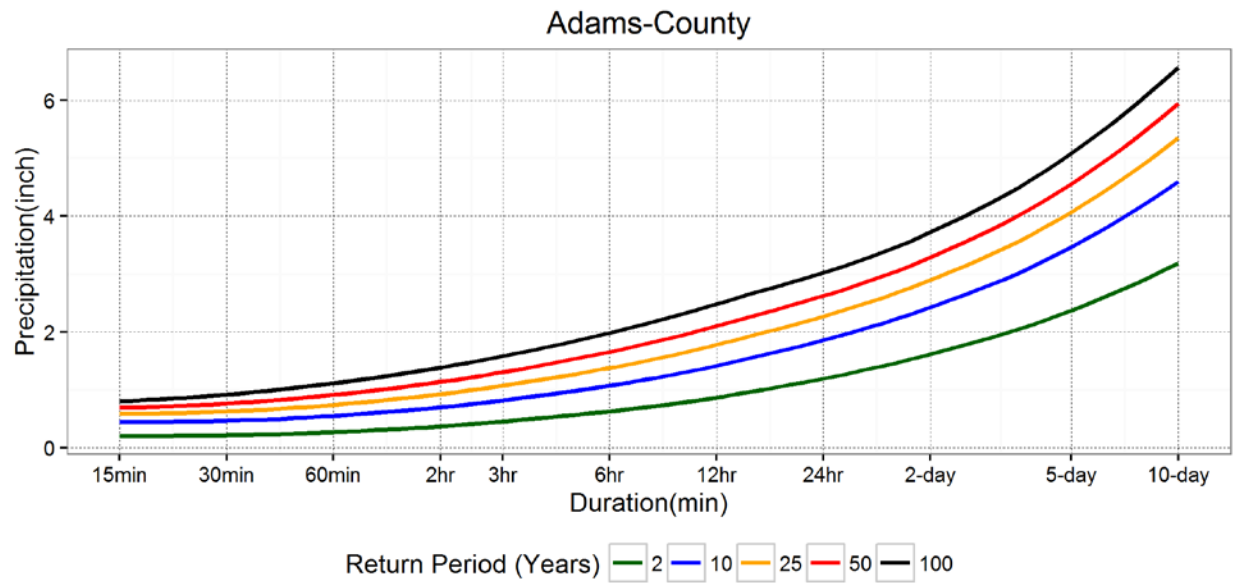


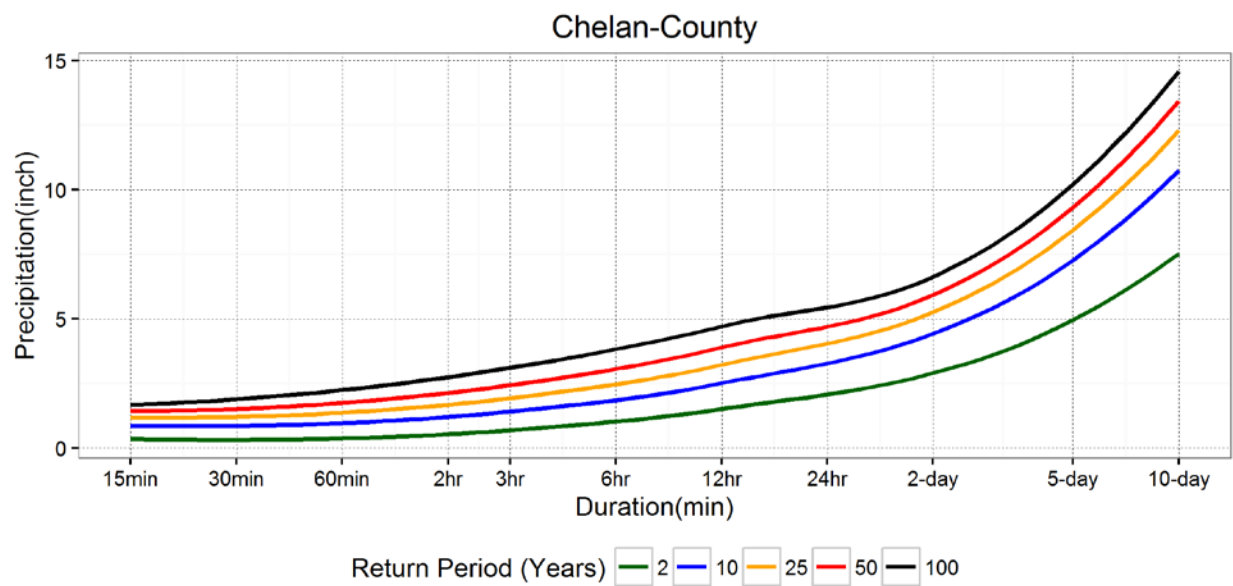
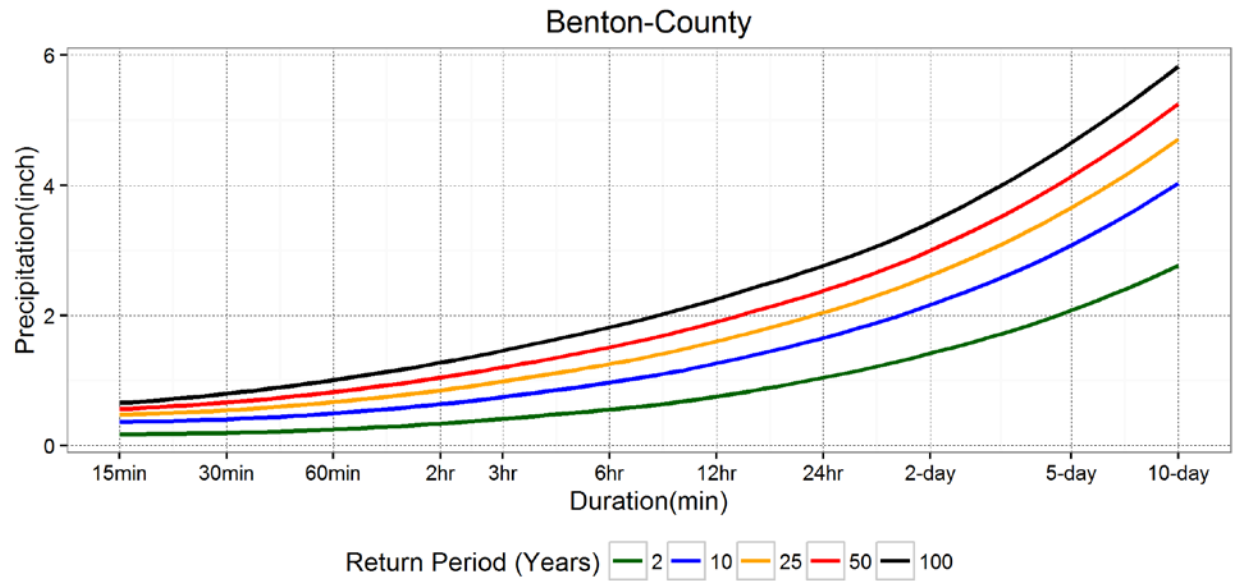
Duration: 10-day

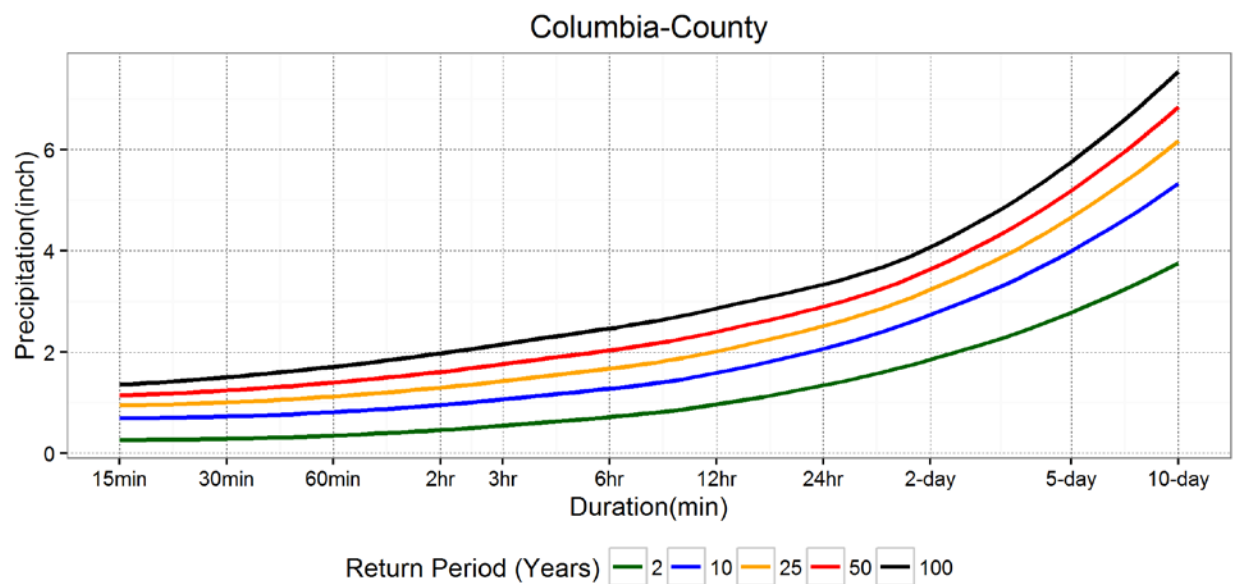
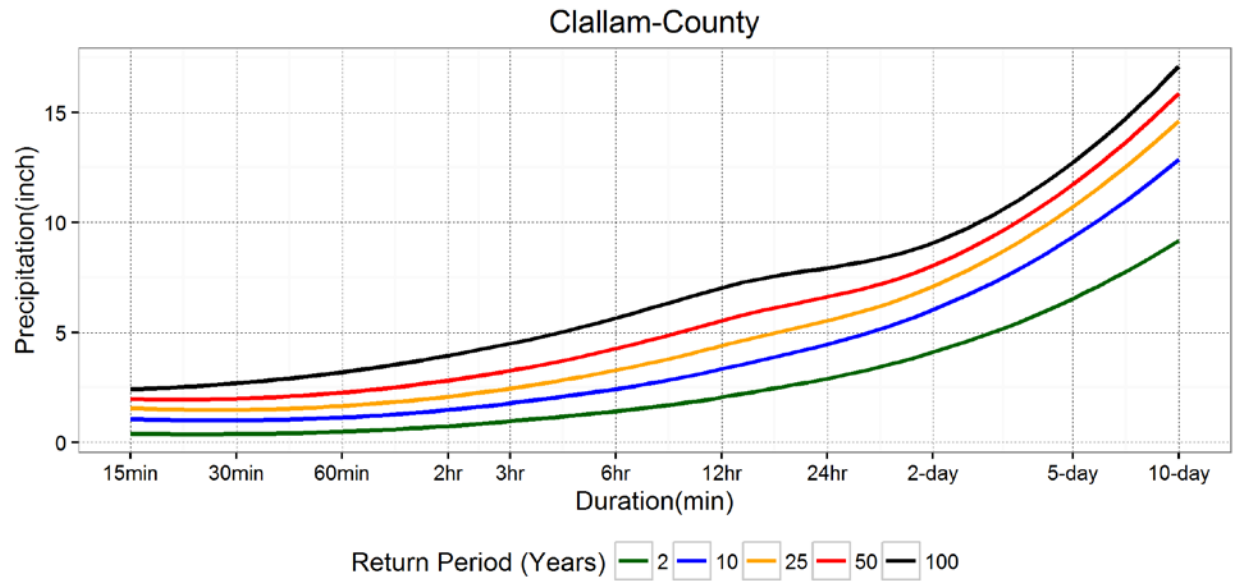


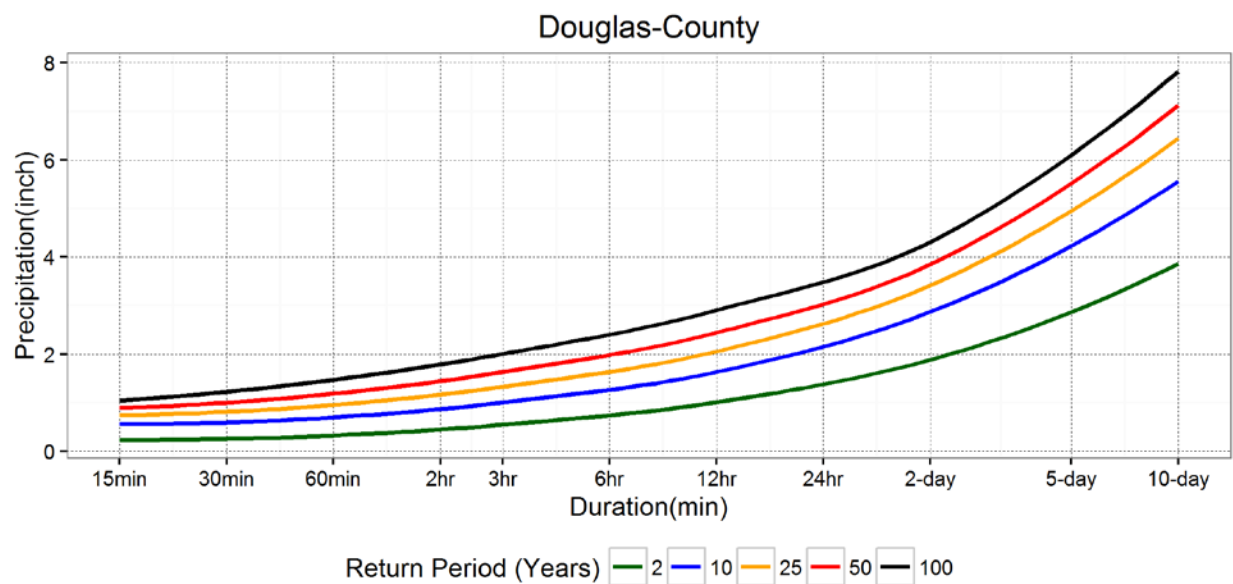
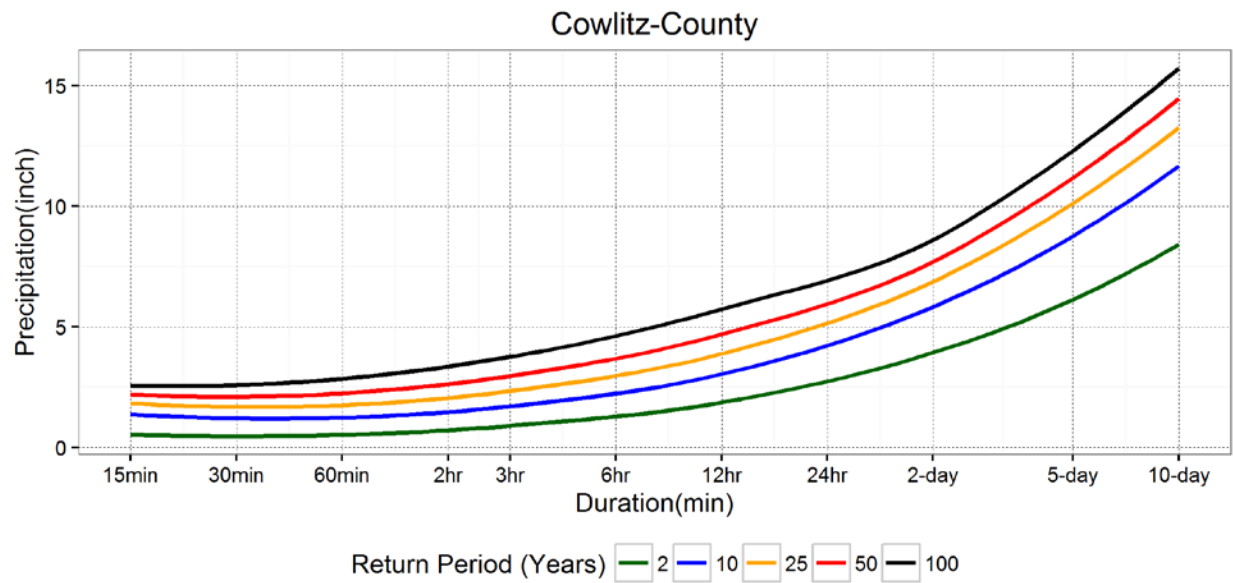
Appendix B.

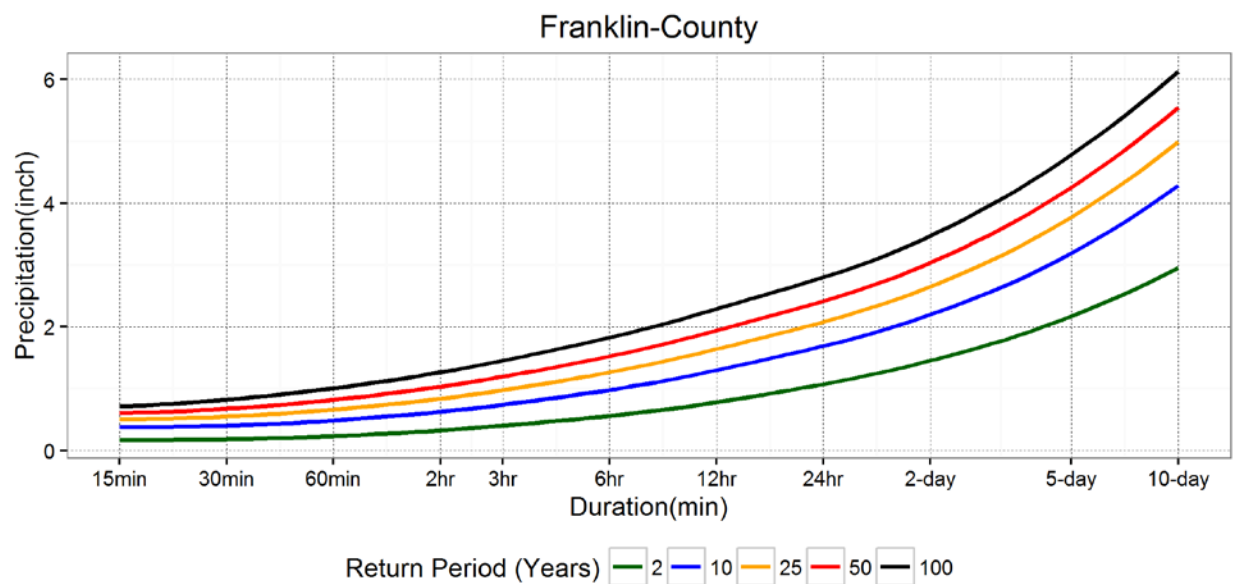
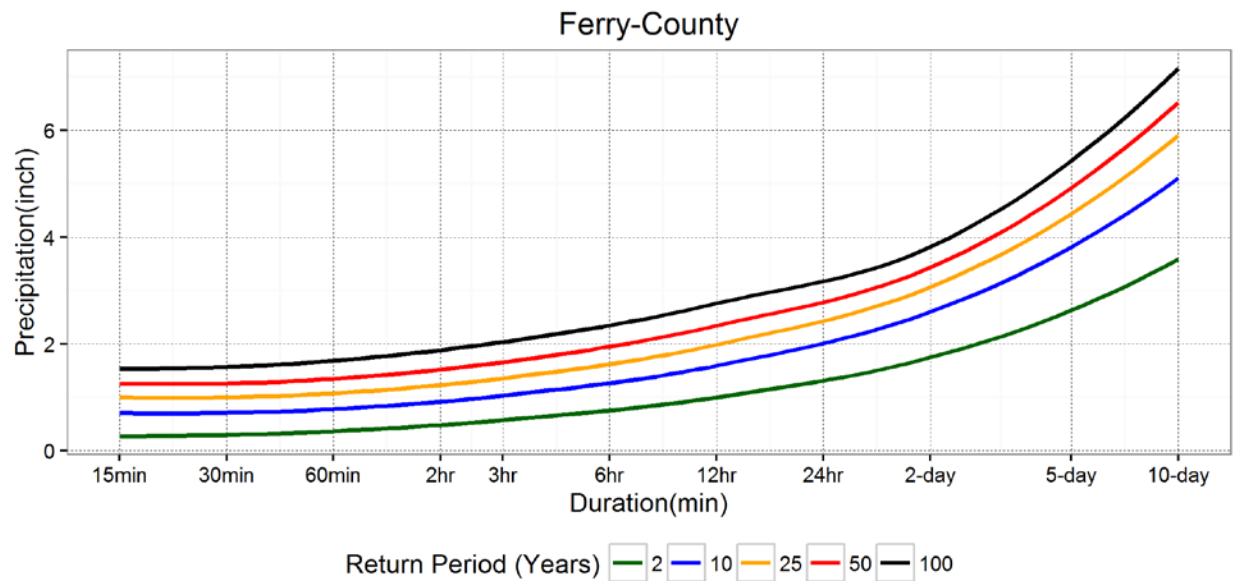
County level IDF curves

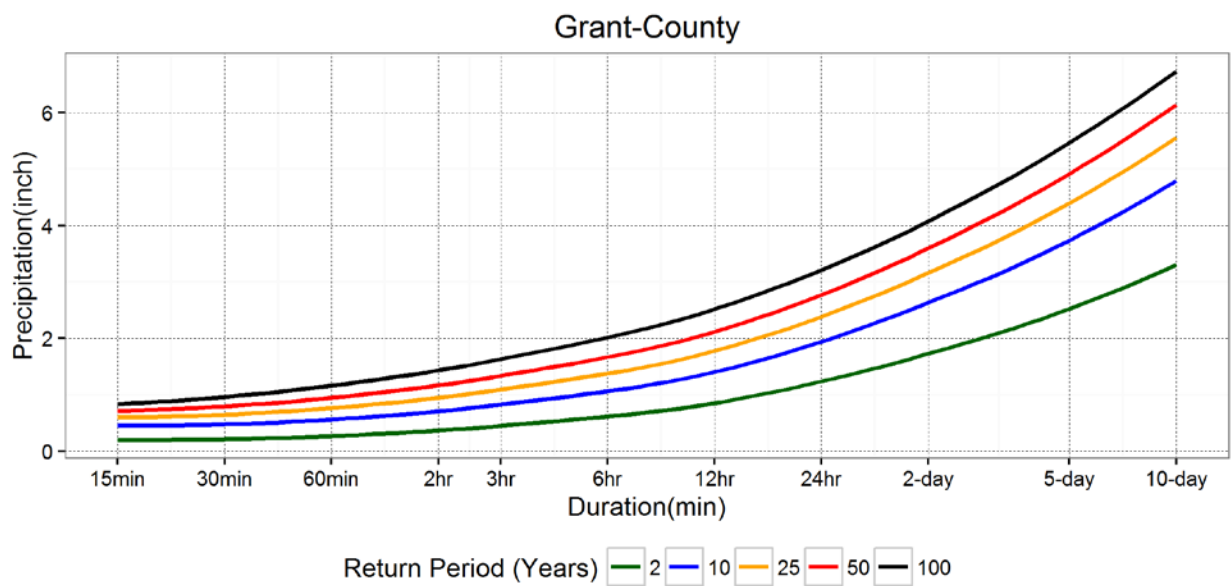
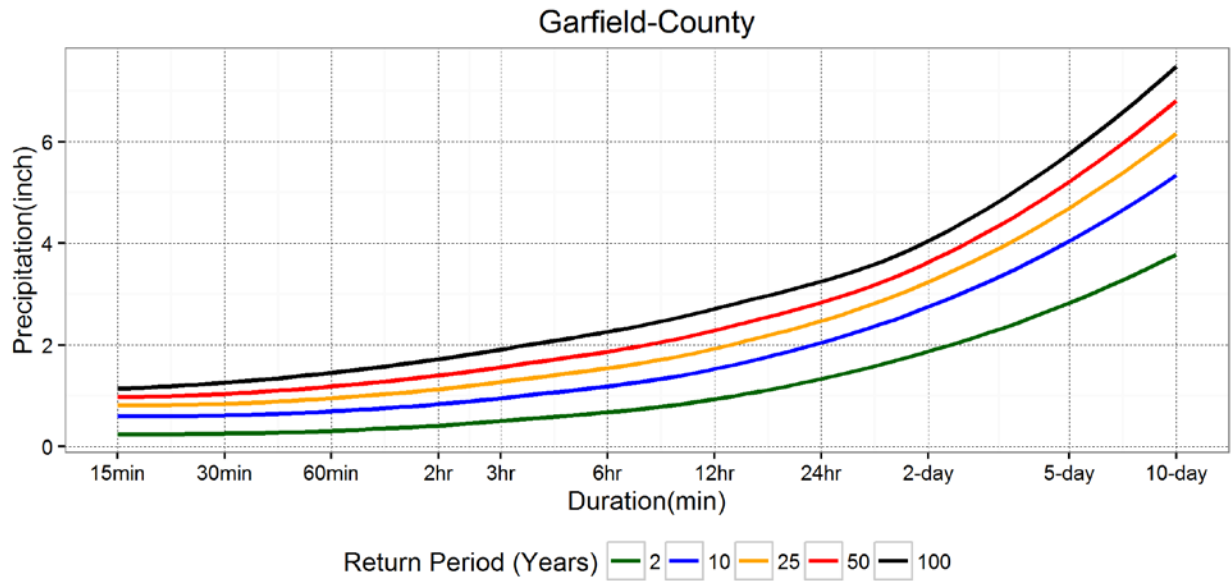


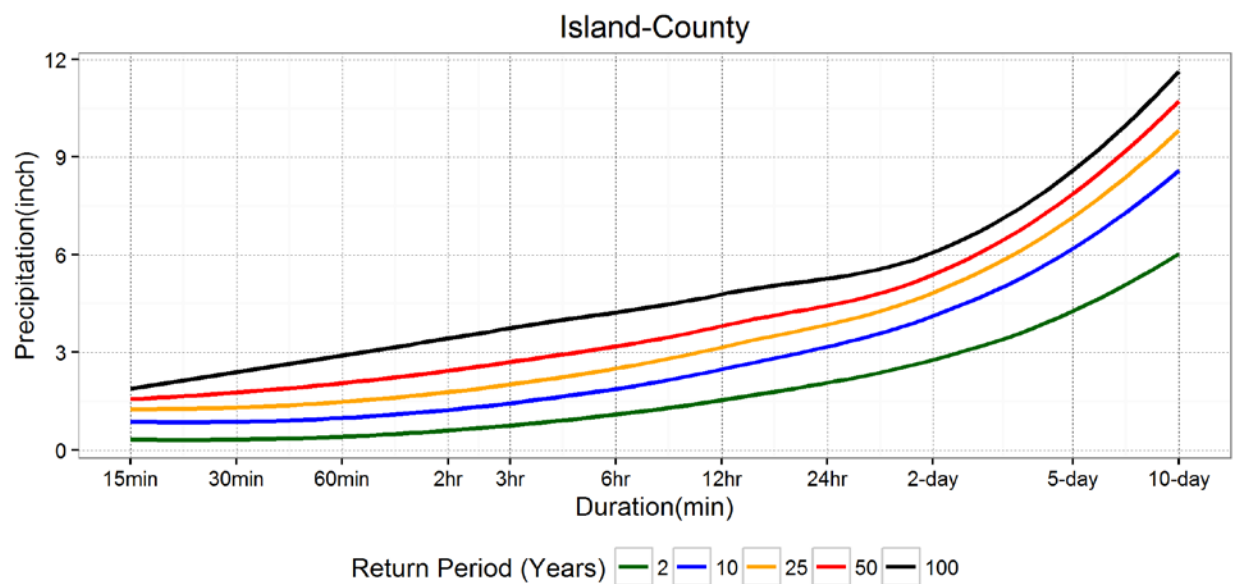
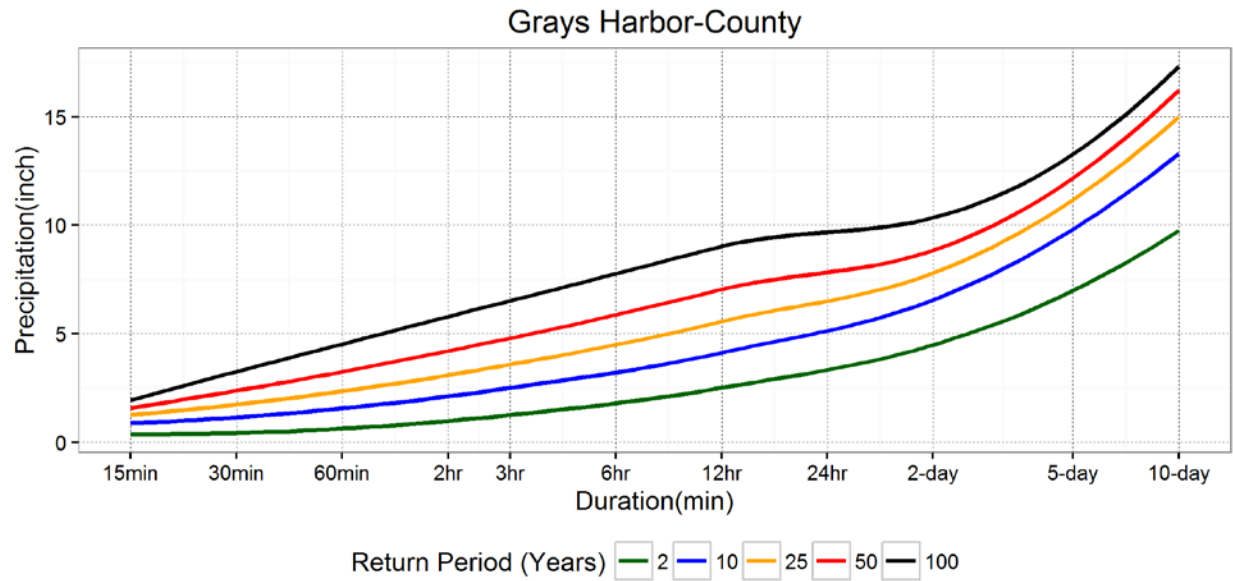


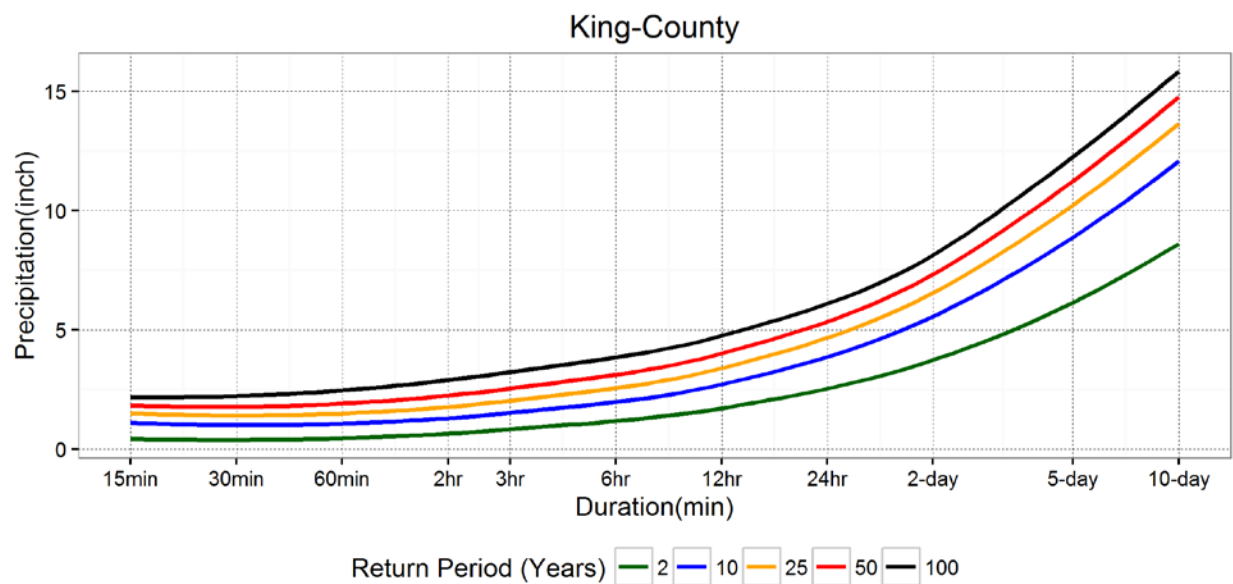
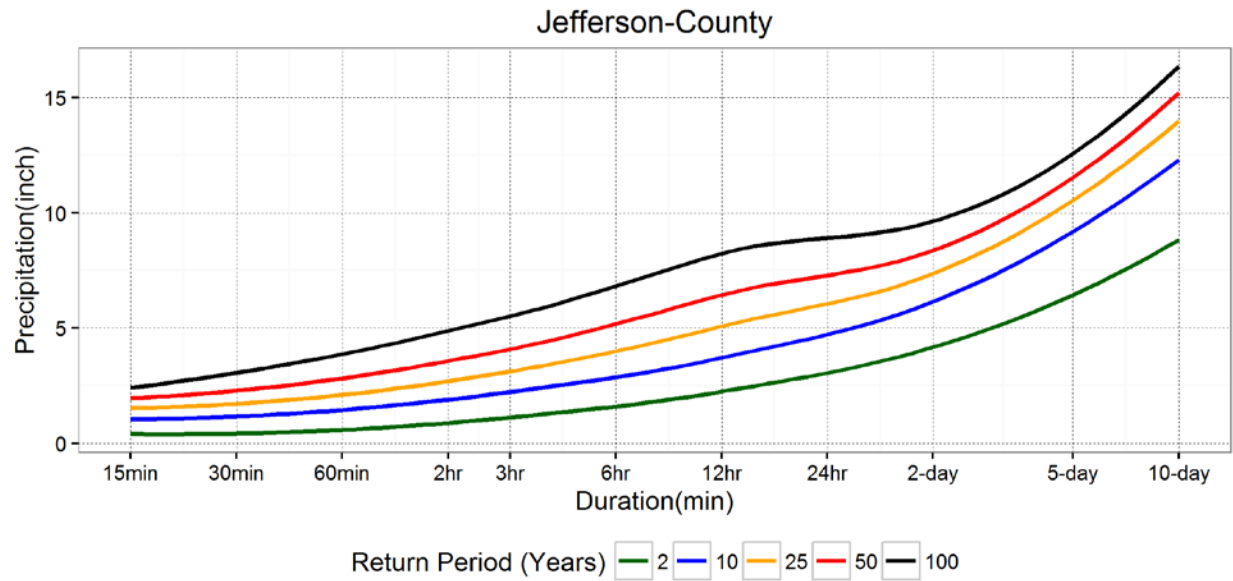


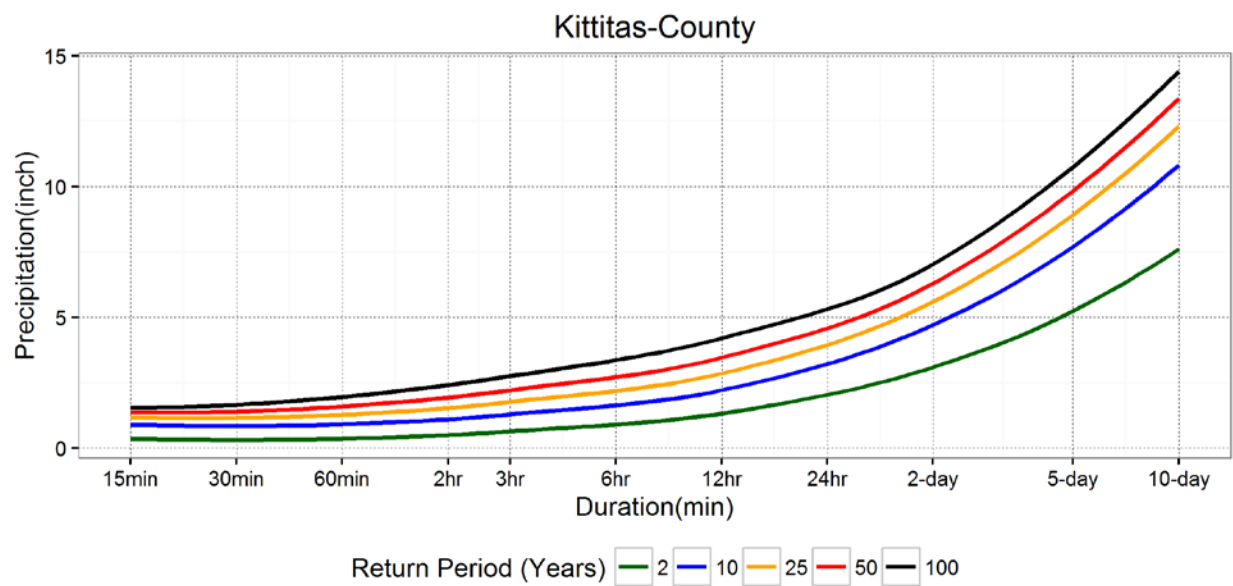
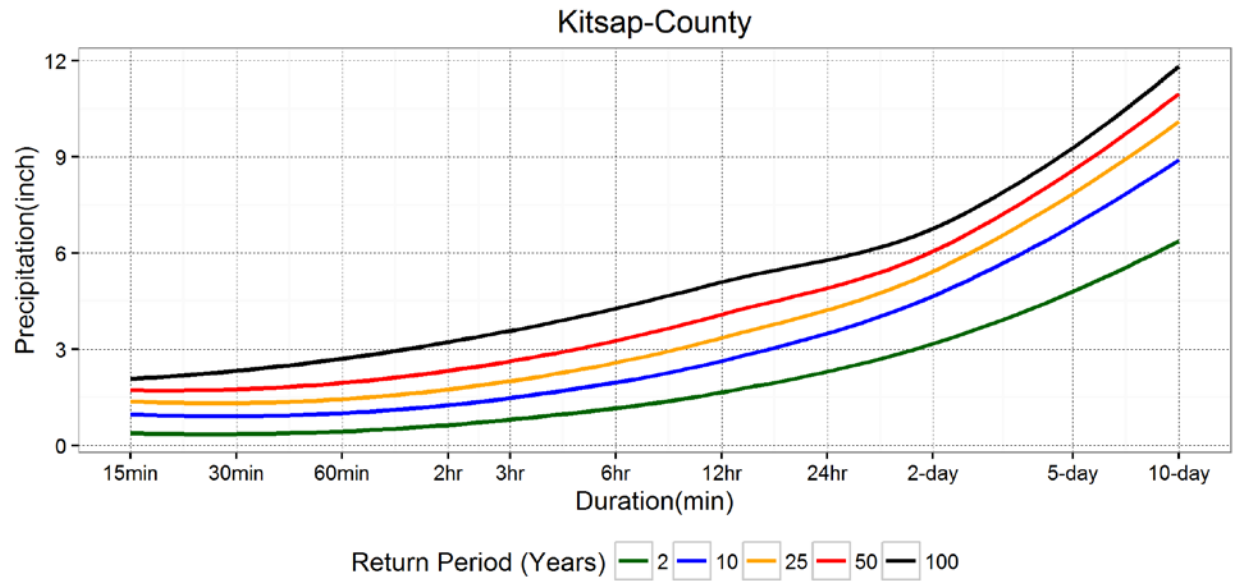


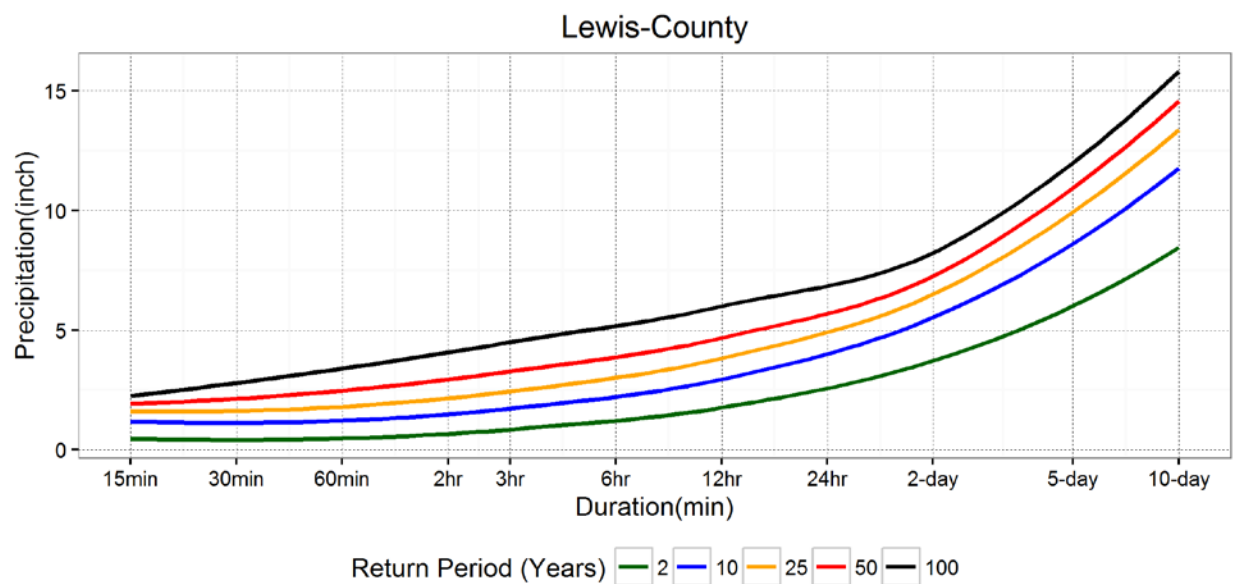
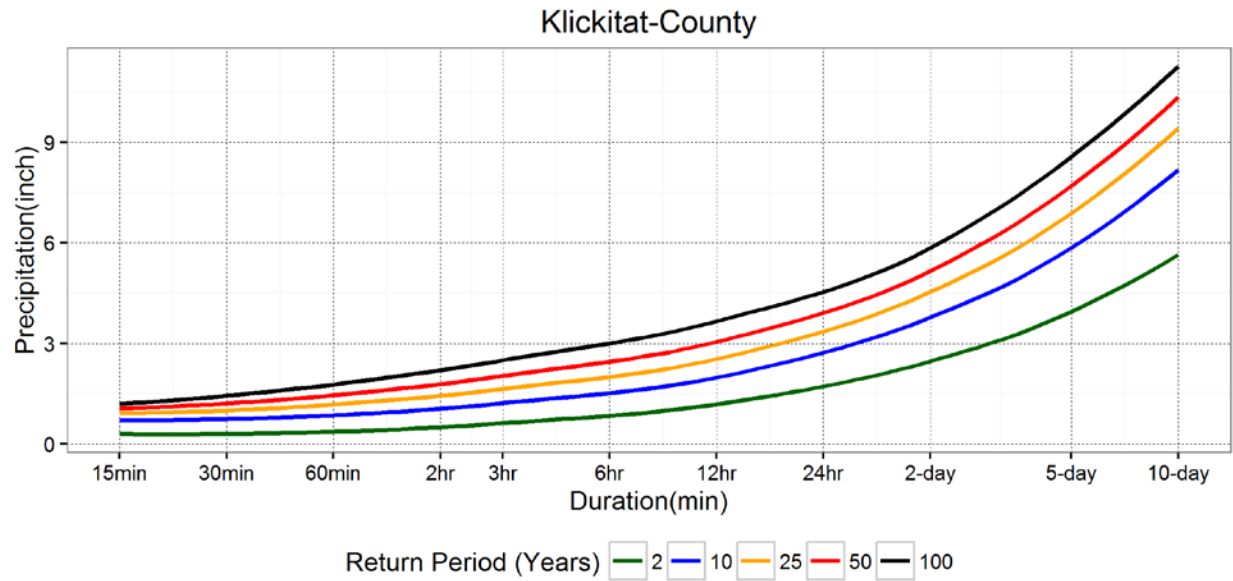


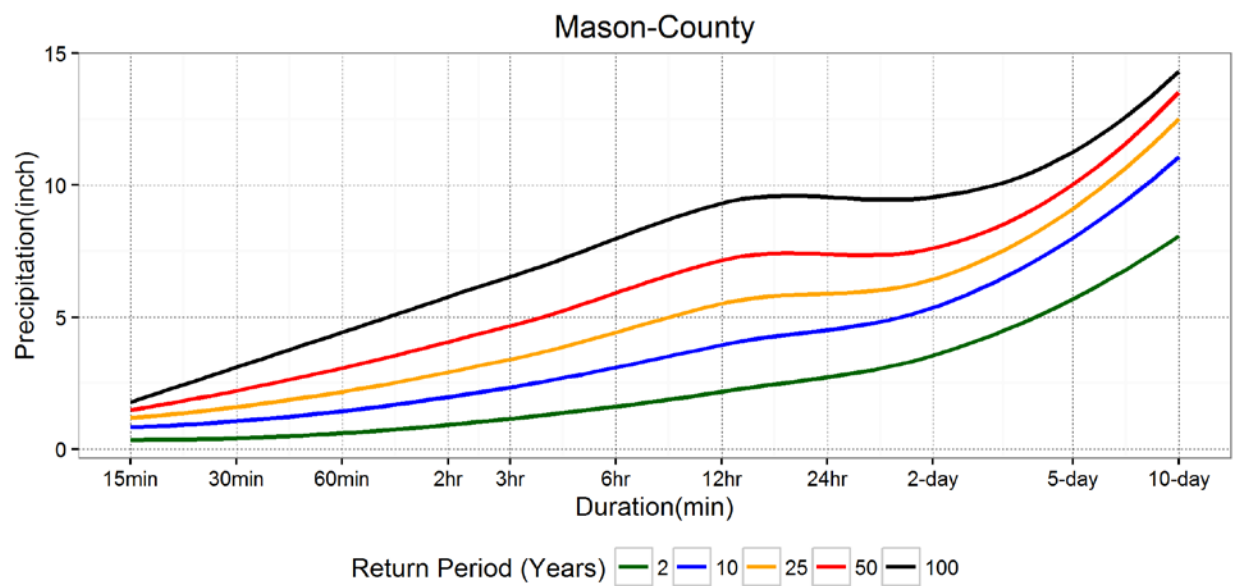
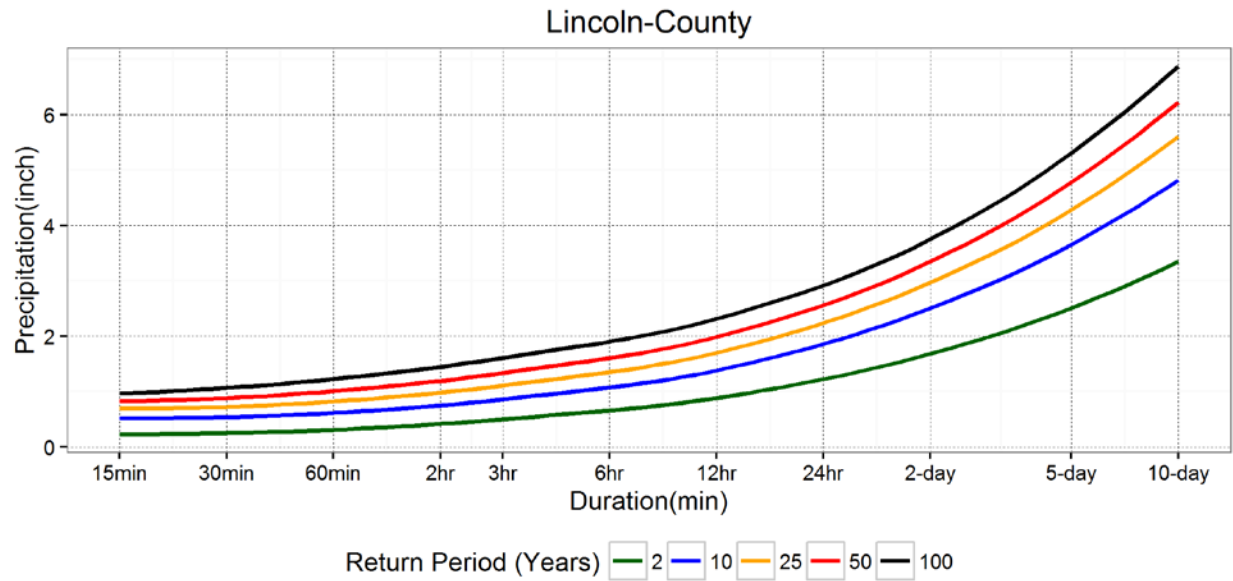


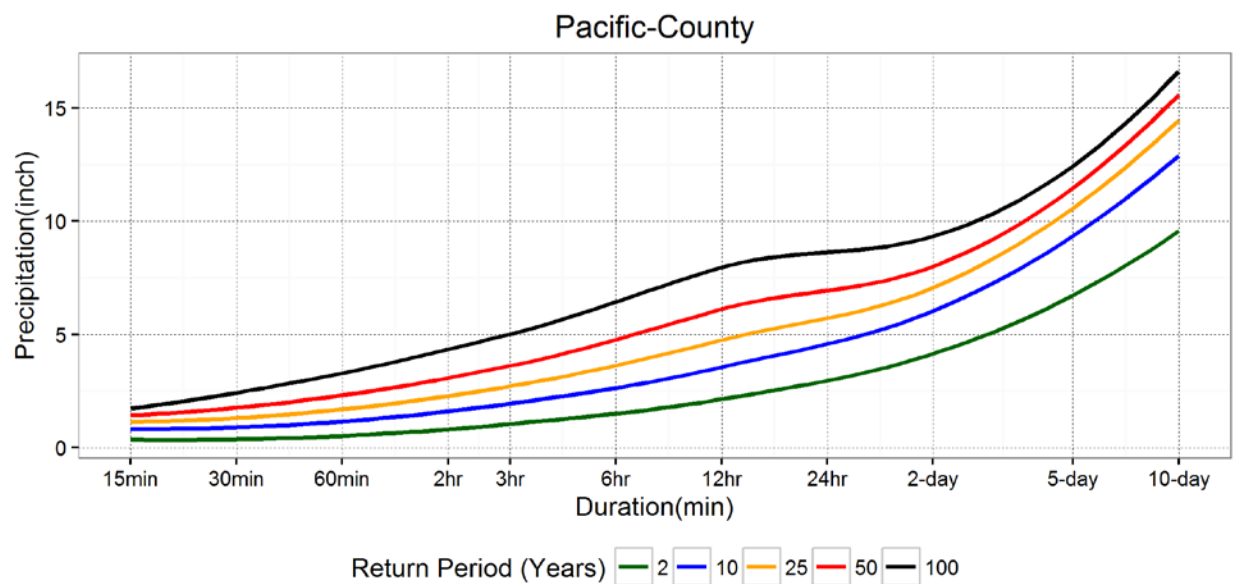
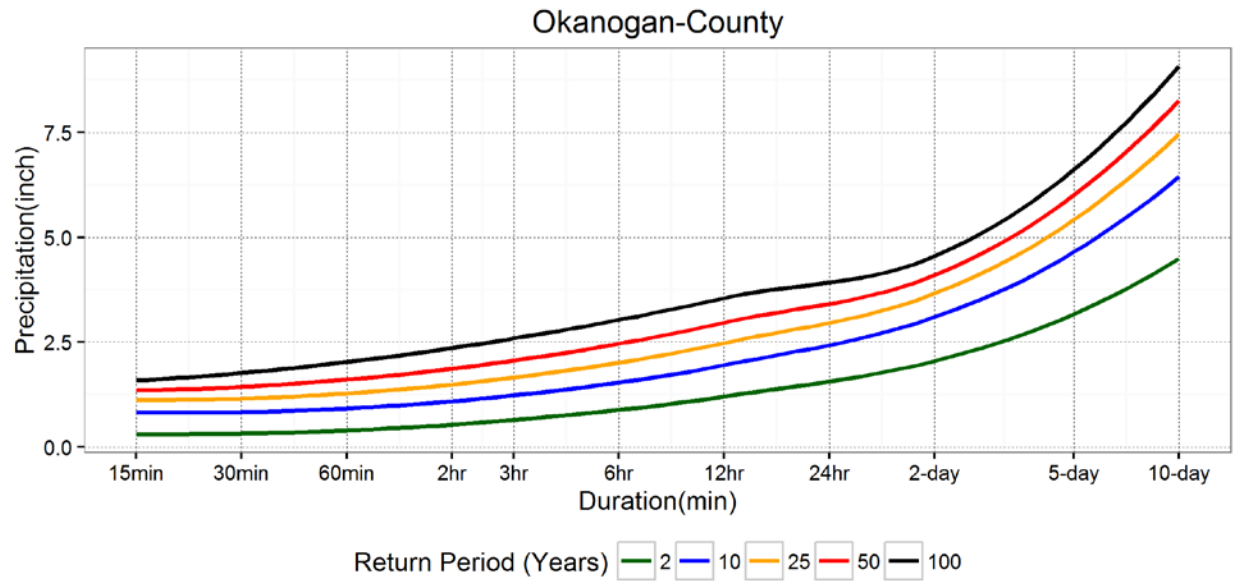


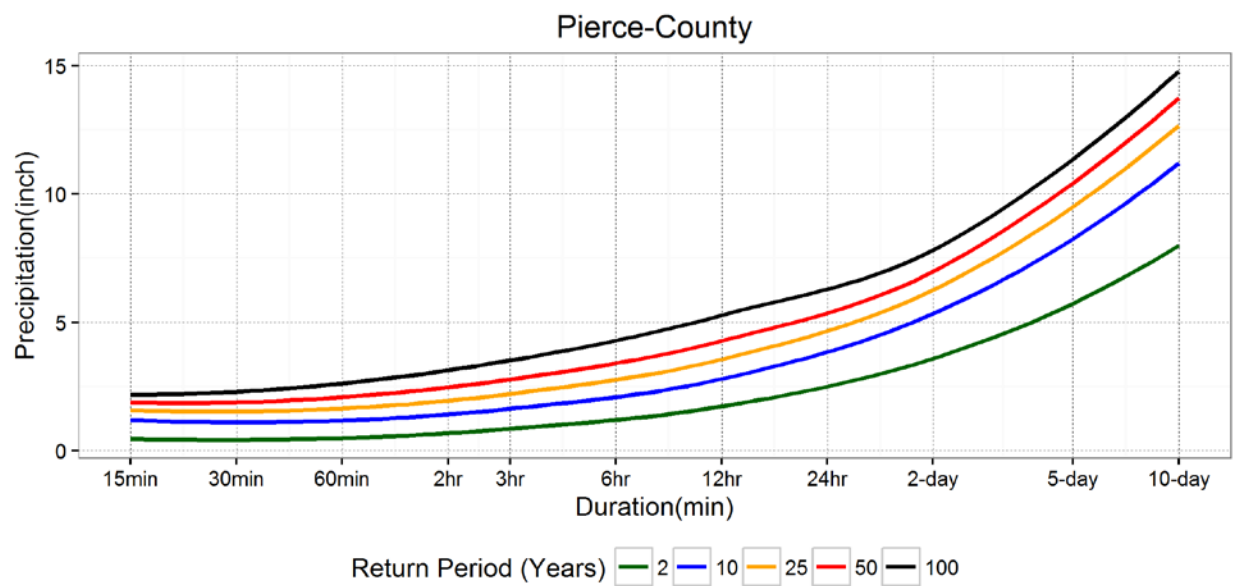
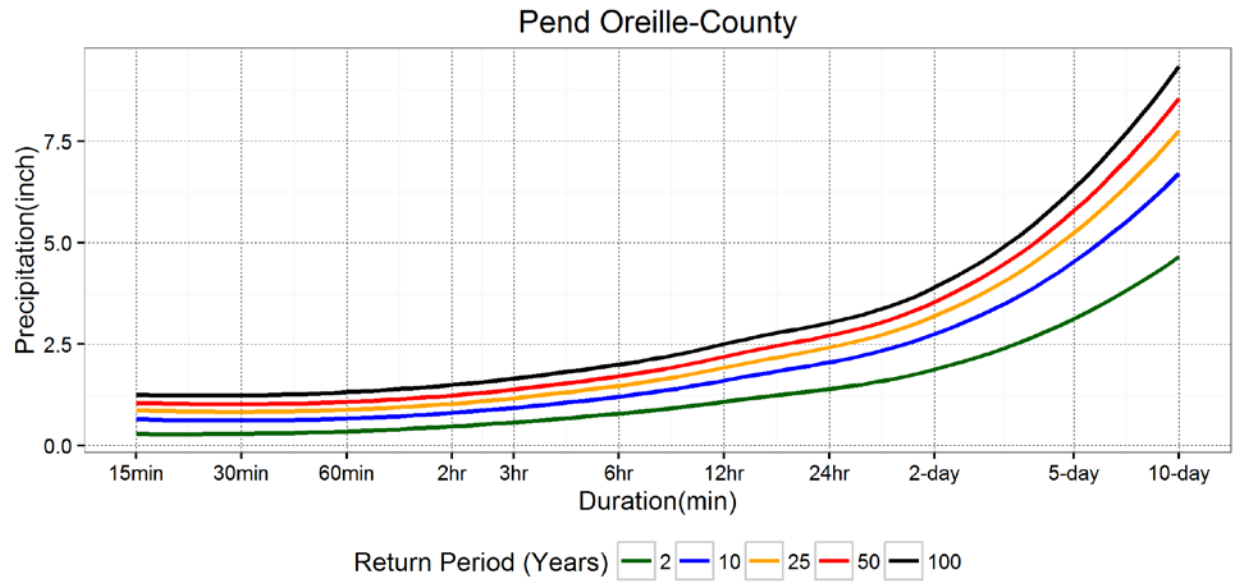


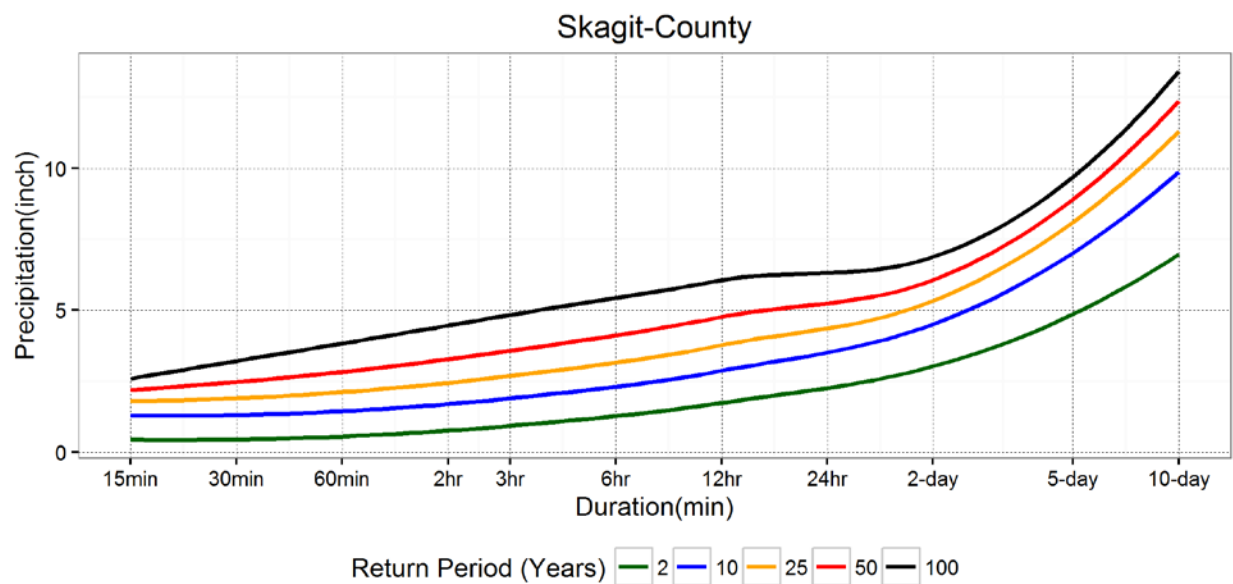
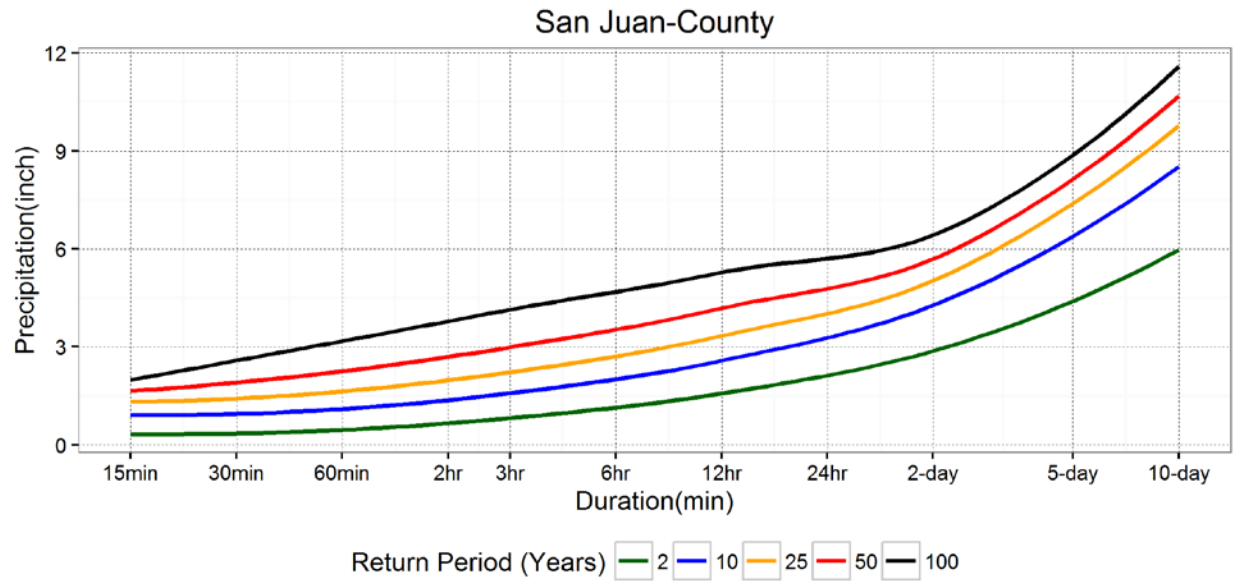


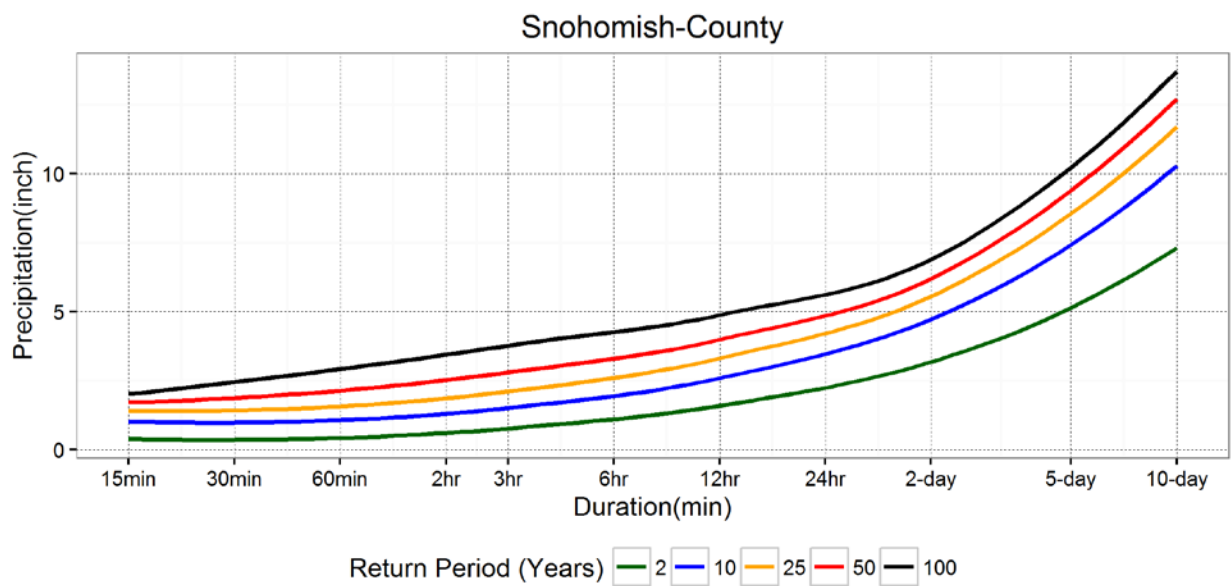
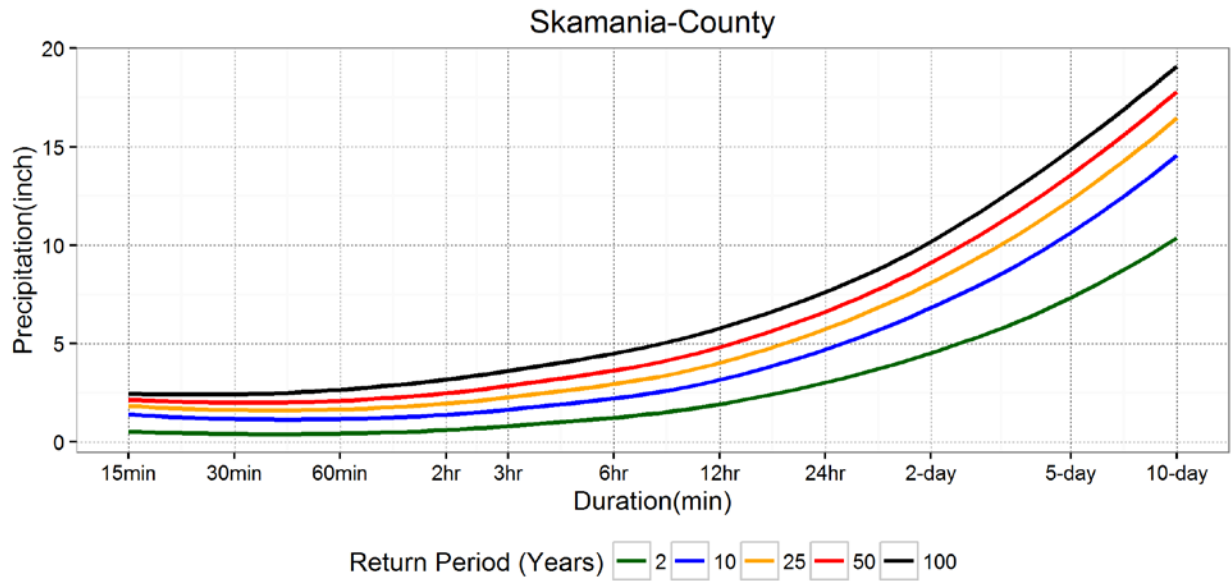


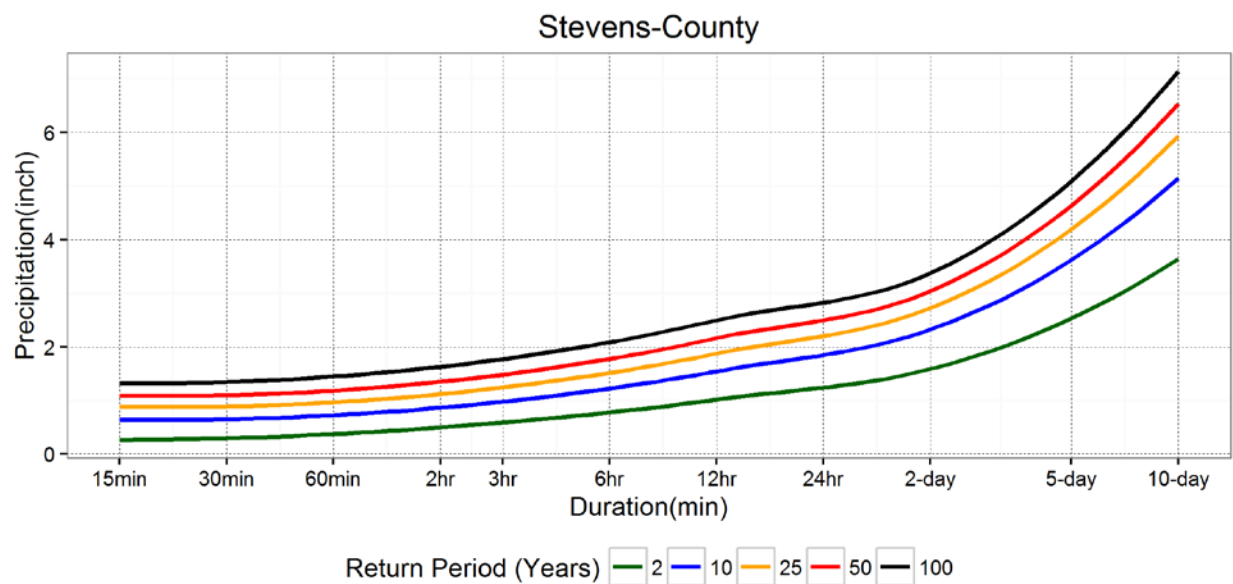
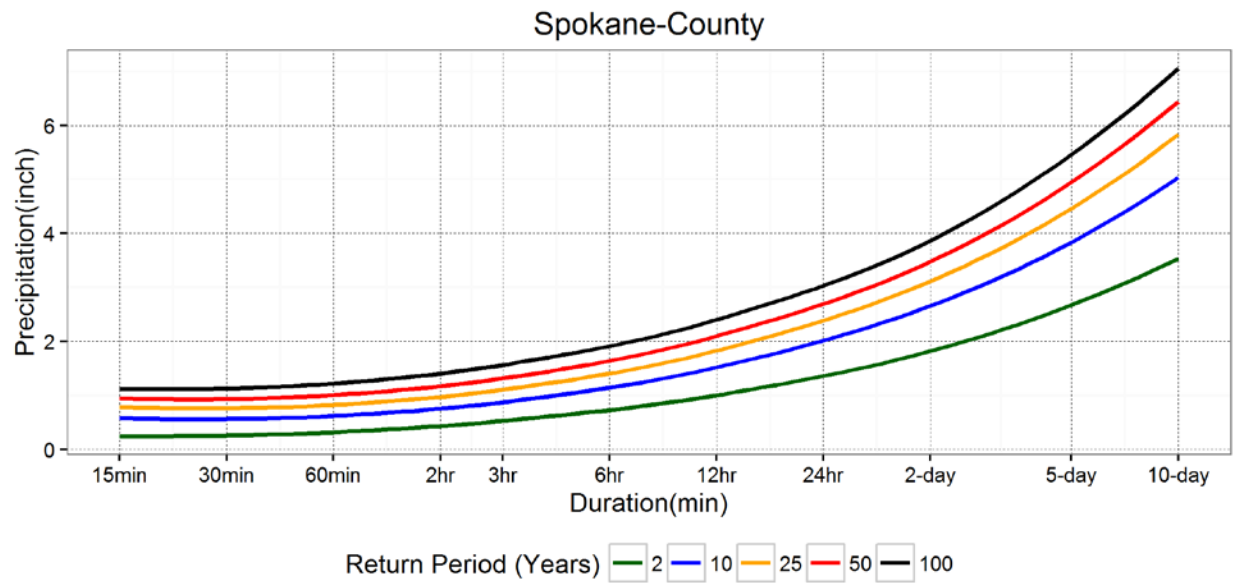


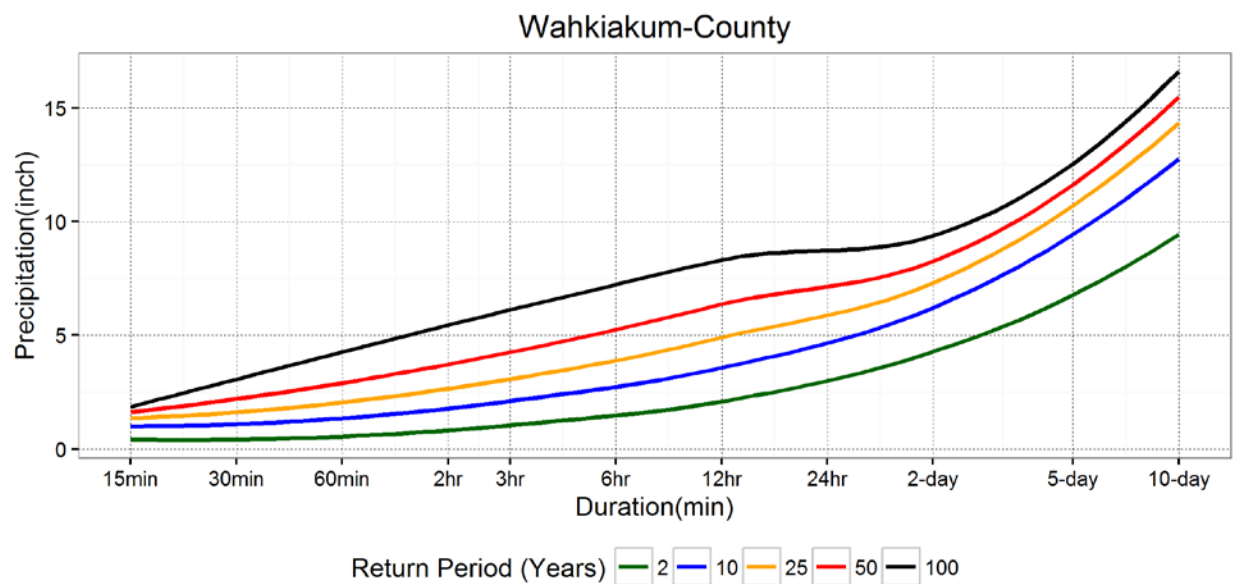
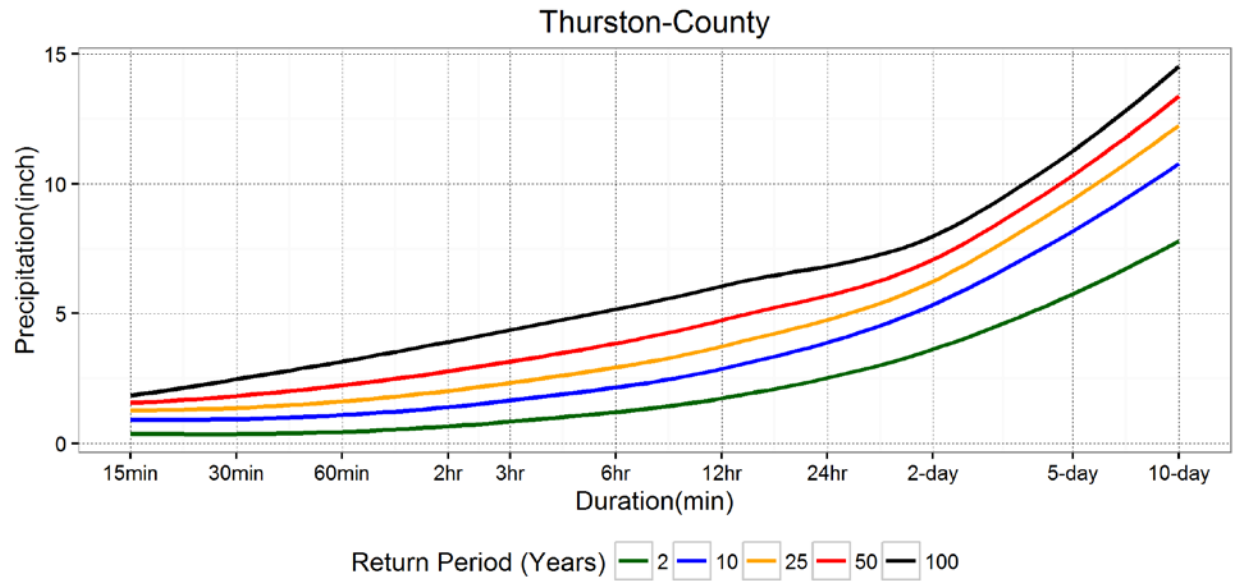


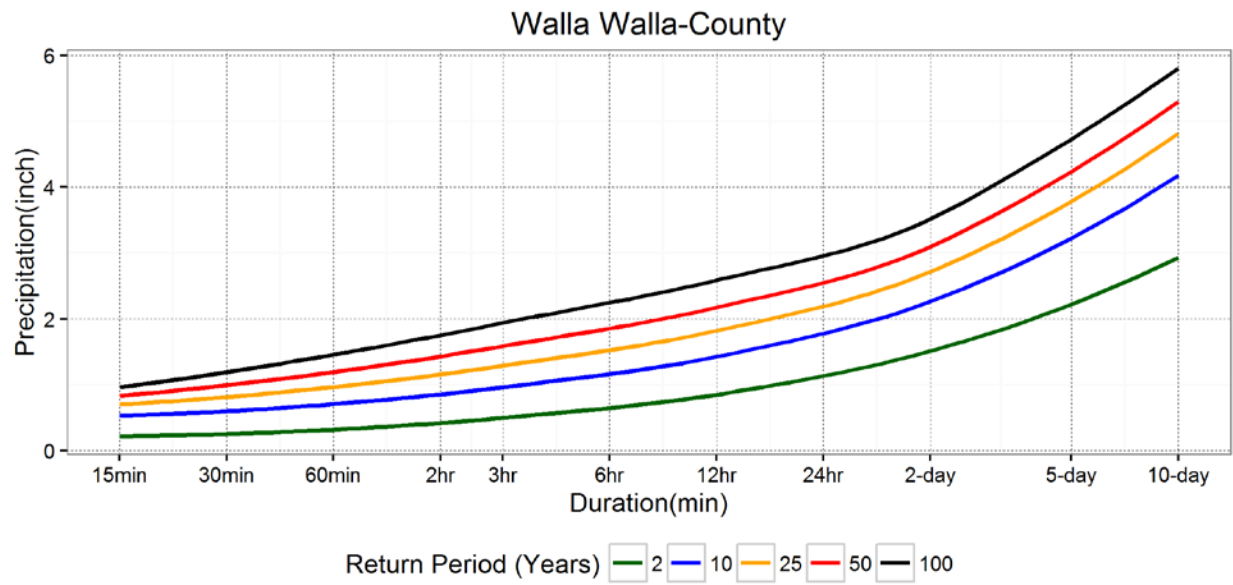












Appendix C.

Tables for county level IDF values and their 95% CI

County	Duration (min)	Return Period (Years)				
		2	10	25	50	100
Adams	15	0.181(0.174-0.19)	0.411(0.39-0.437)	0.546(0.512-0.589)	0.654(0.608-0.715)	0.77(0.707-0.851)
Adams	30	0.232(0.223-0.242)	0.495(0.469-0.526)	0.659(0.615-0.716)	0.797(0.732-0.882)	0.947(0.856-1.071)
Adams	60	0.301(0.291-0.312)	0.604(0.576-0.639)	0.813(0.764-0.875)	1.001(0.929-1.094)	1.224(1.121-1.36)
Adams	120	0.387(0.376-0.399)	0.696(0.668-0.732)	0.9(0.852-0.962)	1.079(1.008-1.169)	1.286(1.185-1.416)
Adams	180	0.486(0.473-0.5)	0.841(0.809-0.879)	1.068(1.015-1.131)	1.268(1.192-1.356)	1.501(1.395-1.621)
Adams	360	0.64(0.623-0.659)	1.115(1.073-1.165)	1.465(1.397-1.547)	1.79(1.693-1.906)	2.18(2.046-2.341)
Adams	720	0.794(0.775-0.814)	1.318(1.269-1.371)	1.677(1.597-1.763)	2.006(1.892-2.127)	2.401(2.24-2.566)
Adams	1440	1.255(1.235-1.276)	1.921(1.875-1.974)	2.309(2.232-2.4)	2.63(2.519-2.762)	2.982(2.827-3.169)
Adams	2880	1.707(1.68-1.734)	2.565(2.508-2.634)	3.061(2.967-3.175)	3.469(3.336-3.632)	3.916(3.733-4.141)
Adams	4320	1.854(1.827-1.882)	2.764(2.702-2.832)	3.29(3.188-3.404)	3.723(3.578-3.887)	4.197(3.998-4.426)
Adams	5760	2.15(2.119-2.182)	3.144(3.077-3.219)	3.717(3.611-3.841)	4.19(4.043-4.365)	4.71(4.508-4.951)
Adams	7200	2.279(2.247-2.314)	3.321(3.253-3.404)	3.91(3.801-4.042)	4.389(4.235-4.573)	4.909(4.699-5.156)
Adams	8640	2.537(2.5-2.577)	3.694(3.619-3.781)	4.31(4.195-4.448)	4.792(4.636-4.983)	5.297(5.089-5.553)
Adams	10080	2.693(2.653-2.734)	3.918(3.839-4.012)	4.57(4.45-4.719)	5.077(4.912-5.284)	5.607(5.387-5.886)
Adams	11520	2.915(2.871-2.96)	4.226(4.137-4.328)	4.94(4.8-5.107)	5.509(5.313-5.744)	6.117(5.85-6.44)
Adams	12960	3.109(3.063-3.156)	4.489(4.398-4.596)	5.237(5.093-5.411)	5.833(5.632-6.078)	6.468(6.193-6.808)
Adams	14400	3.212(3.165-3.261)	4.627(4.534-4.734)	5.382(5.236-5.556)	5.978(5.775-6.221)	6.608(6.333-6.938)
Asotin	15	0.213(0.204-0.223)	0.551(0.522-0.588)	0.758(0.708-0.824)	0.927(0.853-1.025)	1.109(1.005-1.248)
Asotin	30	0.276(0.265-0.289)	0.656(0.621-0.701)	0.885(0.824-0.965)	1.071(0.981-1.19)	1.27(1.144-1.44)
Asotin	60	0.336(0.325-0.35)	0.705(0.671-0.748)	0.952(0.893-1.025)	1.169(1.085-1.275)	1.422(1.305-1.573)
Asotin	120	0.446(0.433-0.46)	0.828(0.794-0.869)	1.076(1.021-1.143)	1.295(1.217-1.39)	1.55(1.442-1.681)
Asotin	180	0.52(0.504-0.537)	0.916(0.877-0.965)	1.171(1.107-1.252)	1.396(1.304-1.511)	1.659(1.53-1.815)
Asotin	360	0.662(0.643-0.684)	1.212(1.166-1.269)	1.633(1.557-1.726)	2.024(1.917-2.157)	2.496(2.347-2.68)
Asotin	720	0.863(0.843-0.885)	1.451(1.398-1.509)	1.857(1.769-1.951)	2.23(2.105-2.363)	2.679(2.504-2.86)
Asotin	1440	1.381(1.36-1.403)	2.069(2.02-2.123)	2.471(2.39-2.563)	2.805(2.688-2.938)	3.176(3.013-3.362)
Asotin	2880	1.861(1.833-1.889)	2.744(2.687-2.811)	3.219(3.13-3.328)	3.591(3.47-3.744)	3.981(3.818-4.188)

Asotin	4320	2.514(2.477-2.552)	3.681(3.605-3.769)	4.318(4.198-4.466)	4.824(4.657-5.033)	5.362(5.137-5.648)
Asotin	5760	2.672(2.634-2.709)	3.862(3.783-3.951)	4.529(4.405-4.675)	5.072(4.899-5.276)	5.661(5.425-5.941)
Asotin	7200	3.016(2.974-3.06)	4.339(4.256-4.442)	5.06(4.931-5.223)	5.634(5.451-5.859)	6.243(5.995-6.545)
Asotin	8640	3.648(3.598-3.701)	5.221(5.12-5.338)	6.068(5.91-6.249)	6.739(6.525-6.987)	7.451(7.162-7.781)
Asotin	10080	3.648(3.601-3.696)	5.221(5.128-5.337)	6.068(5.925-6.256)	6.739(6.539-7.001)	7.451(7.183-7.809)
Asotin	11520	3.907(3.857-3.964)	5.532(5.421-5.657)	6.453(6.268-6.661)	7.212(6.947-7.504)	8.042(7.671-8.448)
Asotin	12960	3.907(3.858-3.956)	5.532(5.428-5.647)	6.453(6.282-6.648)	7.212(6.967-7.49)	8.042(7.702-8.431)
Asotin	14400	4.182(4.125-4.237)	5.904(5.79-6.026)	6.827(6.646-7.026)	7.561(7.312-7.843)	8.343(8.007-8.729)
Benton	15	0.145(0.139-0.151)	0.323(0.308-0.342)	0.434(0.408-0.465)	0.525(0.489-0.57)	0.624(0.575-0.685)
Benton	30	0.204(0.197-0.212)	0.435(0.415-0.459)	0.58(0.546-0.621)	0.7(0.652-0.759)	0.83(0.765-0.911)
Benton	60	0.279(0.271-0.287)	0.541(0.518-0.569)	0.719(0.678-0.772)	0.877(0.815-0.958)	1.06(0.97-1.181)
Benton	120	0.361(0.352-0.371)	0.642(0.618-0.671)	0.83(0.79-0.88)	0.999(0.94-1.074)	1.199(1.114-1.306)
Benton	180	0.428(0.418-0.438)	0.745(0.718-0.775)	0.96(0.915-1.01)	1.158(1.091-1.228)	1.394(1.299-1.493)
Benton	360	0.544(0.529-0.561)	0.991(0.952-1.037)	1.319(1.256-1.396)	1.617(1.527-1.727)	1.966(1.841-2.118)
Benton	720	0.714(0.697-0.731)	1.217(1.172-1.265)	1.567(1.492-1.645)	1.89(1.783-2.001)	2.28(2.129-2.432)
Benton	1440	1.076(1.06-1.093)	1.681(1.645-1.724)	2.03(1.969-2.103)	2.315(2.227-2.42)	2.624(2.501-2.772)
Benton	2880	1.441(1.42-1.463)	2.204(2.156-2.258)	2.66(2.58-2.75)	3.046(2.934-3.174)	3.48(3.324-3.659)
Benton	4320	1.67(1.646-1.696)	2.529(2.473-2.59)	3.042(2.949-3.146)	3.478(3.344-3.624)	3.967(3.782-4.17)
Benton	5760	1.882(1.854-1.911)	2.794(2.737-2.859)	3.349(3.262-3.454)	3.817(3.698-3.961)	4.337(4.177-4.531)
Benton	7200	2.05(2.02-2.081)	3.022(2.963-3.092)	3.598(3.507-3.708)	4.074(3.948-4.224)	4.594(4.427-4.794)
Benton	8640	2.22(2.188-2.253)	3.292(3.224-3.365)	3.894(3.787-4.009)	4.386(4.236-4.546)	4.923(4.718-5.14)
Benton	10080	2.344(2.311-2.379)	3.474(3.404-3.553)	4.103(3.992-4.231)	4.612(4.458-4.793)	5.165(4.955-5.413)
Benton	11520	2.485(2.448-2.52)	3.65(3.58-3.73)	4.289(4.178-4.419)	4.805(4.651-4.988)	5.362(5.153-5.613)
Benton	12960	2.681(2.643-2.72)	3.907(3.832-3.99)	4.572(4.454-4.704)	5.106(4.943-5.292)	5.682(5.461-5.935)
Benton	14400	2.819(2.78-2.861)	4.092(4.017-4.18)	4.771(4.652-4.911)	5.31(5.147-5.504)	5.887(5.665-6.149)
Chelan	15	0.271(0.258-0.286)	0.762(0.716-0.823)	1.086(1.002-1.199)	1.363(1.238-1.534)	1.672(1.493-1.918)
Chelan	30	0.355(0.339-0.373)	0.867(0.816-0.932)	1.179(1.089-1.298)	1.435(1.302-1.613)	1.711(1.524-1.969)
Chelan	60	0.481(0.458-0.514)	1.207(1.133-1.298)	1.697(1.581-1.837)	2.14(1.986-2.325)	2.68(2.478-2.92)
Chelan	120	0.648(0.619-0.681)	1.349(1.275-1.441)	1.766(1.65-1.909)	2.14(1.983-2.333)	2.68(2.471-2.938)

Chelan	180	0.677(0.655-0.702)	1.349(1.287-1.426)	1.766(1.66-1.897)	2.14(1.988-2.397)	2.68(2.469-2.82)
Chelan	360	0.965(0.937-0.997)	1.825(1.758-1.908)	2.552(2.441-2.688)	3.281(3.125-3.473)	4.219(4.003-4.484)
Chelan	720	1.399(1.362-1.44)	2.319(2.23-2.426)	3.025(2.878-3.2)	3.702(3.495-3.949)	4.542(4.253-4.881)
Chelan	1440	2.374(2.338-2.412)	3.666(3.581-3.762)	4.413(4.269-4.576)	5.036(4.828-5.271)	5.732(5.438-6.063)
Chelan	2880	3.174(3.123-3.229)	4.82(4.715-4.946)	5.699(5.537-5.9)	6.38(6.16-6.657)	7.086(6.795-7.456)
Chelan	4320	3.477(3.423-3.537)	5.217(5.104-5.352)	6.149(5.971-6.365)	6.875(6.633-7.171)	7.633(7.309-8.031)
Chelan	5760	4.277(4.208-4.35)	6.314(6.183-6.474)	7.366(7.167-7.613)	8.166(7.902-8.496)	8.983(8.638-9.417)
Chelan	7200	4.614(4.542-4.688)	6.794(6.654-6.955)	7.913(7.702-8.159)	8.767(8.481-9.096)	9.64(9.271-10.071)
Chelan	8640	5.06(4.985-5.14)	7.414(7.27-7.584)	8.597(8.383-8.854)	9.481(9.196-9.823)	10.368(10.002-10.811)
Chelan	10080	6.43(6.326-6.54)	9.437(9.251-9.658)	10.927(10.661-11.258)	12.037(11.684-12.479)	13.151(12.695-13.725)
Chelan	11520	6.75(6.639-6.867)	9.782(9.581-10.018)	11.276(10.98-11.633)	12.394(12.004-12.864)	13.522(13.021-14.133)
Chelan	12960	7.355(7.241-7.476)	10.426(10.233-10.658)	11.887(11.604-12.228)	12.965(12.595-13.41)	14.044(13.569-14.612)
Chelan	14400	7.355(7.254-7.461)	10.426(10.256-10.635)	11.887(11.639-12.198)	12.965(12.64-13.374)	14.044(13.628-14.57)
Clallam	15	0.354(0.336-0.375)	0.986(0.918-1.078)	1.461(1.332-1.635)	1.894(1.699-2.163)	2.402(2.118-2.794)
Clallam	30	0.441(0.42-0.466)	1.092(1.017-1.193)	1.543(1.404-1.732)	1.94(1.733-2.229)	2.402(2.104-2.822)
Clallam	60	0.487(0.468-0.511)	1.227(1.174-1.294)	1.942(1.854-2.052)	2.749(2.625-2.902)	3.92(3.751-4.131)
Clallam	120	0.8(0.774-0.828)	1.463(1.386-1.556)	1.942(1.805-2.106)	2.749(2.547-2.991)	3.92(3.624-4.272)
Clallam	180	1.005(0.978-1.036)	1.726(1.654-1.821)	2.2(2.075-2.362)	2.749(2.565-2.592)	3.92(3.663-3.213)
Clallam	360	1.424(1.386-1.467)	2.398(2.317-2.501)	3.162(3.036-3.33)	3.913(3.739-4.147)	4.872(4.634-5.192)
Clallam	720	2.186(2.126-2.252)	3.749(3.608-3.921)	5.07(4.844-5.352)	6.398(6.08-6.796)	8.11(7.672-8.658)
Clallam	1440	2.747(2.707-2.788)	4.052(3.972-4.144)	5.07(4.948-5.219)	6.398(6.233-6.602)	8.11(7.892-8.384)
Clallam	2880	4.382(4.319-4.448)	6.445(6.324-6.591)	7.5(7.318-7.734)	8.294(8.048-8.616)	9.093(8.766-9.52)
Clallam	4320	5.059(4.989-5.133)	7.335(7.196-7.498)	8.495(8.285-8.75)	9.368(9.089-9.706)	10.247(9.887-10.688)
Clallam	5760	5.663(5.586-5.743)	8.143(7.996-8.32)	9.398(9.173-9.671)	10.336(10.038-10.704)	11.275(10.89-11.756)
Clallam	7200	6.459(6.371-6.551)	9.277(9.111-9.479)	10.718(10.464-11.032)	11.803(11.461-12.23)	12.897(12.451-13.458)
Clallam	8640	7.377(7.275-7.484)	10.504(10.314-10.738)	12.108(11.821-12.469)	13.307(12.925-13.794)	14.506(14.006-15.147)
Clallam	10080	7.427(7.33-7.526)	10.583(10.405-10.799)	12.168(11.909-12.505)	13.344(13-13.807)	14.512(14.06-15.118)
Clallam	11520	7.965(7.857-8.072)	11.266(11.077-11.492)	12.866(12.589-13.205)	14.033(13.67-14.485)	15.177(14.713-15.764)
Clallam	12960	8.724(8.613-8.838)	12.248(12.049-12.479)	13.895(13.606-14.25)	15.064(14.678-15.54)	16.185(15.687-16.799)
Clallam	14400	9.535(9.413-9.661)	13.272(13.065-13.533)	14.971(14.666-15.37)	16.151(15.748-16.692)	17.264(16.739-17.972)

Clark	15	0.367(0.35-0.386)	0.994(0.94-1.065)	1.359(1.262-1.49)	1.652(1.506-1.852)	1.967(1.756-2.259)
Clark	30	0.44(0.42-0.463)	1.092(1.025-1.182)	1.498(1.372-1.672)	1.84(1.649-2.116)	2.225(1.942-2.64)
Clark	60	0.455(0.441-0.474)	1.092(1.05-1.146)	1.498(1.427-1.586)	1.84(1.741-1.963)	2.225(2.09-2.395)
Clark	120	0.675(0.656-0.696)	1.146(1.096-1.209)	1.498(1.414-1.287)	1.84(1.72-1.607)	2.225(2.055-2.004)
Clark	180	0.844(0.824-0.867)	1.356(1.305-1.424)	1.67(1.583-1.786)	1.935(1.81-2.099)	2.23(2.057-2.456)
Clark	360	1.04(1.012-1.071)	1.663(1.607-1.735)	2.12(2.034-2.233)	2.555(2.438-2.709)	3.098(2.942-3.304)
Clark	720	1.871(1.829-1.914)	2.761(2.679-2.856)	3.321(3.202-3.469)	3.816(3.656-4.018)	4.397(4.185-4.667)
Clark	1440	2.417(2.383-2.451)	3.574(3.503-3.658)	4.222(4.107-4.363)	4.749(4.587-4.949)	5.322(5.096-5.601)
Clark	2880	3.648(3.597-3.7)	5.366(5.258-5.483)	6.301(6.134-6.492)	7.039(6.809-7.307)	7.818(7.506-8.183)
Clark	4320	4.271(4.215-4.329)	6.209(6.079-6.351)	7.347(7.135-7.587)	8.301(7.998-8.645)	9.362(8.94-9.843)
Clark	5760	4.852(4.791-4.918)	6.949(6.82-7.102)	8.152(7.942-8.404)	9.148(8.851-9.502)	10.242(9.832-10.735)
Clark	7200	5.599(5.529-5.671)	7.955(7.807-8.121)	9.286(9.044-9.558)	10.383(10.041-10.766)	11.584(11.115-12.111)
Clark	8640	6.132(6.051-6.212)	8.768(8.609-8.941)	10.167(9.921-10.442)	11.269(10.931-11.651)	12.431(11.986-12.946)
Clark	10080	6.517(6.422-6.614)	9.367(9.193-9.57)	10.766(10.514-11.077)	11.772(11.44-12.192)	12.746(12.313-13.298)
Clark	11520	7.1(7.005-7.196)	10.013(9.853-10.201)	11.388(11.159-11.664)	12.389(12.095-12.755)	13.374(12.997-13.84)
Clark	12960	7.283(7.192-7.382)	10.183(10.028-10.365)	11.517(11.296-11.785)	12.476(12.186-12.821)	13.41(13.043-13.845)
Clark	14400	7.767(7.664-7.87)	10.786(10.617-10.973)	12.145(11.912-12.412)	13.108(12.816-13.446)	14.038(13.677-14.458)
Columbia	15	0.231(0.221-0.243)	0.642(0.606-0.689)	0.905(0.84-0.993)	1.126(1.028-1.257)	1.367(1.228-1.555)
Columbia	30	0.297(0.285-0.312)	0.746(0.703-0.801)	1.019(0.943-1.118)	1.24(1.13-1.387)	1.478(1.323-1.686)
Columbia	60	0.4(0.384-0.421)	0.911(0.86-0.974)	1.231(1.148-1.333)	1.499(1.386-1.639)	1.797(1.645-1.985)
Columbia	120	0.501(0.484-0.519)	0.969(0.927-1.02)	1.261(1.194-1.342)	1.511(1.419-1.623)	1.797(1.673-1.947)
Columbia	180	0.571(0.553-0.591)	1.086(1.034-1.15)	1.436(1.346-1.546)	1.75(1.619-1.907)	2.12(1.936-2.338)
Columbia	360	0.734(0.714-0.757)	1.339(1.288-1.399)	1.809(1.725-1.909)	2.258(2.139-2.4)	2.812(2.646-3.009)
Columbia	720	0.934(0.911-0.958)	1.564(1.505-1.629)	2.008(1.91-2.116)	2.42(2.28-2.572)	2.917(2.72-3.125)
Columbia	1440	1.309(1.289-1.331)	1.973(1.927-2.025)	2.35(2.275-2.437)	2.655(2.548-2.781)	2.984(2.836-3.159)
Columbia	2880	2.004(1.972-2.038)	2.954(2.888-3.032)	3.476(3.371-3.601)	3.895(3.75-4.071)	4.346(4.15-4.583)
Columbia	4320	2.203(2.172-2.236)	3.227(3.159-3.308)	3.817(3.704-3.953)	4.304(4.144-4.499)	4.84(4.619-5.112)
Columbia	5760	2.405(2.37-2.439)	3.466(3.396-3.545)	4.06(3.95-4.188)	4.542(4.39-4.719)	5.064(4.858-5.305)
Columbia	7200	2.812(2.772-2.853)	4.043(3.966-4.138)	4.716(4.596-4.865)	5.252(5.085-5.456)	5.822(5.596-6.093)
Columbia	8640	2.891(2.85-2.933)	4.143(4.063-4.236)	4.813(4.688-4.958)	5.342(5.173-5.54)	5.902(5.675-6.165)

Columbia	10080	3.209(3.166-3.255)	4.571(4.484-4.68)	5.325(5.189-5.5)	5.934(5.742-6.177)	6.59(6.333-6.922)
Columbia	11520	3.371(3.324-3.419)	4.803(4.709-4.912)	5.574(5.425-5.749)	6.184(5.977-6.428)	6.829(6.547-7.162)
Columbia	12960	3.754(3.703-3.806)	5.32(5.22-5.438)	6.16(6.001-6.352)	6.823(6.601-7.091)	7.524(7.221-7.893)
Columbia	14400	3.754(3.702-3.806)	5.32(5.221-5.429)	6.16(6.008-6.331)	6.823(6.619-7.06)	7.524(7.254-7.841)
Cowlitz	15	0.447(0.426-0.471)	1.283(1.216-1.371)	1.751(1.63-1.913)	2.113(1.933-2.36)	2.491(2.23-2.851)
Cowlitz	30	0.535(0.509-0.565)	1.283(1.196-1.401)	1.77(1.604-2.006)	2.23(1.973-2.611)	2.775(2.389-3.357)
Cowlitz	60	0.535(0.518-0.557)	1.283(1.234-1.539)	1.77(1.689-1.871)	2.23(2.116-2.37)	2.775(2.621-2.968)
Cowlitz	120	0.828(0.799-0.859)	1.584(1.493-1.691)	2.132(1.967-2.326)	2.652(2.406-2.941)	3.298(2.933-3.725)
Cowlitz	180	1(0.972-1.032)	1.762(1.687-1.861)	2.273(2.142-2.443)	2.733(2.539-2.979)	3.298(3.023-3.643)
Cowlitz	360	1.161(1.127-1.199)	2.156(2.079-2.252)	3.011(2.889-3.169)	3.881(3.71-4.102)	5.016(4.782-5.32)
Cowlitz	720	1.916(1.866-1.969)	3.131(3.022-3.262)	4.092(3.921-4.304)	5.036(4.799-5.332)	6.235(5.912-6.64)
Cowlitz	1440	2.719(2.677-2.763)	4.082(3.994-4.186)	4.828(4.685-5.002)	5.425(5.223-5.67)	6.235(5.955-6.575)
Cowlitz	2880	4.094(4.032-4.16)	6.08(5.951-6.232)	7.149(6.951-7.397)	7.983(7.713-8.326)	8.852(8.491-9.316)
Cowlitz	4320	4.764(4.696-4.838)	6.978(6.829-7.147)	8.17(7.938-8.439)	9.107(8.789-9.475)	10.092(9.671-10.585)
Cowlitz	5760	5.444(5.365-5.527)	7.857(7.702-8.037)	9.119(8.88-9.403)	10.094(9.77-10.481)	11.104(10.675-11.626)
Cowlitz	7200	5.932(5.85-6.015)	8.429(8.265-8.617)	9.788(9.526-10.087)	10.878(10.515-11.294)	12.047(11.56-12.61)
Cowlitz	8640	6.889(6.791-6.987)	9.88(9.683-10.093)	11.479(11.173-11.815)	12.746(12.328-13.207)	14.093(13.536-14.712)
Cowlitz	10080	7.025(6.925-7.126)	9.984(9.798-10.184)	11.479(11.207-11.78)	12.746(12.389-13.149)	14.093(13.629-14.615)
Cowlitz	11520	7.359(7.255-7.461)	10.347(10.169-10.548)	11.802(11.543-12.101)	12.886(12.549-13.284)	14.093(13.656-14.261)
Cowlitz	12960	8.071(7.966-8.183)	11.21(11.03-11.42)	12.727(12.461-13.037)	13.858(13.504-14.266)	14.999(14.538-15.522)
Cowlitz	14400	8.621(8.508-8.737)	11.867(11.675-12.09)	13.42(13.138-13.755)	14.568(14.199-15.008)	15.719(15.243-16.285)
Douglas	15	0.206(0.197-0.216)	0.513(0.485-0.549)	0.701(0.653-0.764)	0.856(0.786-0.948)	1.023(0.927-1.153)
Douglas	30	0.271(0.26-0.284)	0.613(0.58-0.654)	0.822(0.763-0.898)	0.993(0.907-1.109)	1.18(1.058-1.348)
Douglas	60	0.357(0.343-0.374)	0.778(0.737-0.829)	1.075(1.006-1.16)	1.351(1.254-1.472)	1.692(1.558-1.862)
Douglas	120	0.477(0.461-0.495)	0.896(0.855-0.949)	1.164(1.095-1.252)	1.396(1.297-1.52)	1.692(1.555-1.866)
Douglas	180	0.557(0.541-0.575)	0.991(0.948-1.043)	1.269(1.198-1.356)	1.512(1.411-1.635)	1.794(1.654-1.962)
Douglas	360	0.749(0.729-0.772)	1.31(1.261-1.367)	1.741(1.662-1.835)	2.155(2.044-2.288)	2.67(2.516-2.853)
Douglas	720	0.99(0.965-1.016)	1.603(1.543-1.671)	2.04(1.943-2.152)	2.449(2.312-2.605)	2.946(2.756-3.158)
Douglas	1440	1.418(1.398-1.439)	2.179(2.133-2.231)	2.613(2.537-2.701)	2.968(2.858-3.096)	3.355(3.202-3.536)
Douglas	2880	1.875(1.848-1.903)	2.844(2.787-2.91)	3.378(3.287-3.484)	3.801(3.676-3.951)	4.25(4.08-4.452)

Douglas	4320	2.273(2.241-2.306)	3.421(3.352-3.499)	4.057(3.946-4.186)	4.564(4.41-4.745)	5.103(4.894-5.352)
Douglas	5760	2.549(2.513-2.587)	3.785(3.713-3.87)	4.448(4.338-4.585)	4.965(4.816-5.153)	5.502(5.303-5.756)
Douglas	7200	2.946(2.905-2.989)	4.36(4.278-4.456)	5.115(4.986-5.268)	5.701(5.524-5.913)	6.311(6.077-6.596)
Douglas	8640	3.044(3.002-3.089)	4.492(4.409-4.592)	5.245(5.118-5.4)	5.819(5.647-6.03)	6.405(6.18-6.686)
Douglas	10080	3.317(3.27-3.365)	4.857(4.766-4.962)	5.679(5.541-5.843)	6.324(6.137-6.55)	7.004(6.755-7.306)
Douglas	11520	3.477(3.427-3.527)	5.045(4.951-5.156)	5.882(5.737-6.058)	6.543(6.345-6.785)	7.243(6.977-7.57)
Douglas	12960	3.715(3.664-3.768)	5.342(5.245-5.454)	6.191(6.041-6.367)	6.855(6.65-7.095)	7.552(7.278-7.872)
Douglas	14400	3.892(3.834-3.952)	5.594(5.491-5.718)	6.458(6.305-6.649)	7.101(6.896-7.359)	7.743(7.474-8.081)
Ferry	15	0.246(0.235-0.26)	0.661(0.619-0.716)	0.953(0.877-1.056)	1.212(1.098-1.366)	1.507(1.345-1.729)
Ferry	30	0.318(0.303-0.334)	0.762(0.714-0.824)	1.057(0.971-1.17)	1.31(1.184-1.477)	1.591(1.415-1.83)
Ferry	60	0.372(0.357-0.391)	0.797(0.754-0.853)	1.11(1.036-1.203)	1.41(1.305-1.543)	1.792(1.645-1.978)
Ferry	120	0.499(0.483-0.518)	0.921(0.878-0.975)	1.201(1.129-1.29)	1.447(1.345-1.573)	1.792(1.65-1.967)
Ferry	180	0.577(0.561-0.593)	1.014(0.973-1.062)	1.303(1.235-1.382)	1.561(1.463-1.674)	1.866(1.729-2.022)
Ferry	360	0.78(0.759-0.804)	1.327(1.279-1.387)	1.729(1.651-1.827)	2.1(1.991-2.237)	2.547(2.398-2.735)
Ferry	720	0.984(0.96-1.01)	1.583(1.525-1.65)	2.002(1.906-2.112)	2.391(2.255-2.544)	2.862(2.671-3.069)
Ferry	1440	1.332(1.314-1.35)	2.008(1.967-2.053)	2.394(2.327-2.47)	2.709(2.613-2.82)	3.052(2.919-3.207)
Ferry	2880	1.779(1.755-1.804)	2.649(2.6-2.708)	3.116(3.039-3.21)	3.479(3.373-3.609)	3.855(3.714-4.031)
Ferry	4320	2.08(2.052-2.109)	3.072(3.014-3.138)	3.607(3.517-3.714)	4.025(3.902-4.175)	4.46(4.294-4.664)
Ferry	5760	2.364(2.334-2.396)	3.451(3.39-3.524)	4.038(3.943-4.156)	4.498(4.367-4.662)	4.979(4.803-5.202)
Ferry	7200	2.601(2.567-2.636)	3.777(3.71-3.855)	4.403(4.298-4.527)	4.889(4.745-5.062)	5.395(5.203-5.627)
Ferry	8640	2.818(2.78-2.855)	4.089(4.016-4.172)	4.753(4.642-4.884)	5.262(5.112-5.442)	5.784(5.588-6.024)
Ferry	10080	2.99(2.951-3.031)	4.304(4.228-4.392)	5.001(4.886-5.14)	5.544(5.388-5.735)	6.111(5.903-6.368)
Ferry	11520	3.275(3.231-3.321)	4.682(4.596-4.783)	5.45(5.313-5.611)	6.063(5.873-6.288)	6.718(6.46-7.023)
Ferry	12960	3.466(3.42-3.515)	4.938(4.847-5.043)	5.716(5.574-5.883)	6.319(6.125-6.549)	6.948(6.687-7.257)
Ferry	14400	3.608(3.556-3.662)	5.134(5.037-5.248)	5.919(5.773-6.096)	6.504(6.307-6.745)	7.088(6.828-7.407)
Franklin	15	0.147(0.141-0.153)	0.344(0.327-0.367)	0.471(0.441-0.51)	0.578(0.534-0.635)	0.696(0.635-0.774)
Franklin	30	0.197(0.19-0.206)	0.435(0.412-0.462)	0.585(0.547-0.633)	0.711(0.657-0.781)	0.849(0.775-0.946)
Franklin	60	0.269(0.261-0.277)	0.531(0.508-0.56)	0.709(0.669-0.762)	0.868(0.808-0.947)	1.053(0.966-1.17)
Franklin	120	0.352(0.343-0.361)	0.631(0.608-0.659)	0.817(0.778-0.866)	0.986(0.928-1.057)	1.184(1.102-1.285)
Franklin	180	0.423(0.413-0.434)	0.743(0.716-0.774)	0.962(0.915-1.014)	1.162(1.093-1.236)	1.402(1.304-1.506)

Franklin	360	0.553(0.537-0.571)	1.009(0.97-1.057)	1.348(1.284-1.427)	1.656(1.565-1.768)	2.019(1.892-2.174)
Franklin	720	0.736(0.719-0.754)	1.241(1.196-1.288)	1.579(1.506-1.655)	1.886(1.781-1.993)	2.251(2.105-2.398)
Franklin	1440	1.118(1.101-1.136)	1.727(1.688-1.773)	2.08(2.015-2.159)	2.369(2.275-2.483)	2.683(2.551-2.843)
Franklin	2880	1.554(1.531-1.578)	2.357(2.304-2.418)	2.84(2.752-2.943)	3.25(3.124-3.398)	3.712(3.535-3.919)
Franklin	4320	1.668(1.644-1.693)	2.498(2.443-2.561)	3(2.906-3.107)	3.427(3.292-3.581)	3.91(3.721-4.126)
Franklin	5760	1.938(1.909-1.967)	2.846(2.787-2.913)	3.392(3.299-3.501)	3.851(3.722-4.003)	4.362(4.187-4.569)
Franklin	7200	2.08(2.05-2.113)	3.042(2.982-3.114)	3.597(3.503-3.712)	4.052(3.922-4.209)	4.545(4.369-4.755)
Franklin	8640	2.438(2.404-2.475)	3.576(3.504-3.658)	4.214(4.098-4.344)	4.733(4.572-4.913)	5.297(5.077-5.541)
Franklin	10080	2.438(2.403-2.475)	3.576(3.505-3.66)	4.214(4.101-4.348)	4.733(4.576-4.92)	5.297(5.085-5.552)
Franklin	11520	2.658(2.619-2.697)	3.881(3.805-3.968)	4.541(4.423-4.683)	5.065(4.902-5.264)	5.622(5.402-5.893)
Franklin	12960	2.859(2.818-2.899)	4.15(4.071-4.241)	4.844(4.719-4.988)	5.393(5.22-5.595)	5.975(5.743-6.251)
Franklin	14400	2.995(2.953-3.039)	4.334(4.252-4.429)	5.041(4.913-5.191)	5.594(5.419-5.802)	6.176(5.941-6.457)
Garfield	15	0.211(0.202-0.221)	0.55(0.521-0.588)	0.763(0.711-0.831)	0.938(0.861-1.04)	1.129(1.021-1.273)
Garfield	30	0.274(0.263-0.287)	0.655(0.619-0.7)	0.886(0.824-0.968)	1.076(0.984-1.197)	1.28(1.151-1.452)
Garfield	60	0.349(0.337-0.365)	0.75(0.711-0.797)	1.014(0.95-1.094)	1.246(1.156-1.36)	1.515(1.39-1.675)
Garfield	120	0.458(0.444-0.473)	0.86(0.824-0.904)	1.118(1.059-1.19)	1.343(1.261-1.444)	1.603(1.49-1.742)
Garfield	180	0.534(0.518-0.552)	0.966(0.924-1.017)	1.251(1.18-1.338)	1.505(1.402-1.628)	1.803(1.659-1.973)
Garfield	360	0.69(0.67-0.711)	1.25(1.203-1.308)	1.68(1.602-1.775)	2.085(1.974-2.219)	2.577(2.424-2.763)
Garfield	720	0.893(0.871-0.916)	1.493(1.437-1.553)	1.911(1.82-2.01)	2.297(2.168-2.437)	2.763(2.581-2.954)
Garfield	1440	1.339(1.318-1.361)	2.008(1.962-2.061)	2.381(2.306-2.469)	2.679(2.573-2.804)	2.997(2.852-3.17)
Garfield	2880	1.914(1.884-1.944)	2.81(2.751-2.88)	3.297(3.205-3.412)	3.685(3.556-3.847)	4.097(3.923-4.317)
Garfield	4320	2.311(2.279-2.346)	3.37(3.3-3.451)	3.96(3.845-4.096)	4.436(4.276-4.629)	4.951(4.733-5.216)
Garfield	5760	2.514(2.479-2.55)	3.612(3.54-3.694)	4.224(4.11-4.356)	4.718(4.561-4.903)	5.253(5.039-5.506)
Garfield	7200	2.734(2.696-2.774)	3.91(3.836-4.001)	4.541(4.427-4.683)	5.039(4.881-5.233)	5.563(5.352-5.822)
Garfield	8640	2.968(2.926-3.011)	4.23(4.15-4.324)	4.887(4.765-5.032)	5.398(5.232-5.594)	5.929(5.71-6.189)
Garfield	10080	3.287(3.243-3.334)	4.662(4.574-4.774)	5.413(5.276-5.592)	6.013(5.821-6.262)	6.654(6.397-6.993)
Garfield	11520	3.574(3.525-3.625)	5.051(4.953-5.166)	5.851(5.693-6.038)	6.487(6.266-6.748)	7.164(6.862-7.519)
Garfield	12960	3.586(3.537-3.635)	5.077(4.98-5.191)	5.884(5.729-6.071)	6.527(6.309-6.79)	7.212(6.913-7.576)
Garfield	14400	3.793(3.739-3.847)	5.361(5.259-5.473)	6.156(6.002-6.33)	6.761(6.554-7.002)	7.384(7.109-7.704)
Grant	15	0.173(0.166-0.182)	0.408(0.387-0.435)	0.549(0.514-0.594)	0.663(0.613-0.727)	0.785(0.717-0.874)

Grant	30	0.231(0.221-0.241)	0.504(0.478-0.536)	0.672(0.627-0.731)	0.812(0.746-0.9)	0.964(0.87-1.09)
Grant	60	0.311(0.3-0.323)	0.649(0.618-0.689)	0.885(0.831-0.954)	1.102(1.024-1.202)	1.366(1.256-1.508)
Grant	120	0.404(0.392-0.417)	0.739(0.708-0.778)	0.958(0.906-1.024)	1.151(1.076-1.246)	1.374(1.268-1.508)
Grant	180	0.482(0.469-0.496)	0.844(0.811-0.884)	1.08(1.024-1.145)	1.288(1.208-1.381)	1.532(1.42-1.659)
Grant	360	0.632(0.615-0.651)	1.106(1.065-1.155)	1.46(1.392-1.54)	1.792(1.696-1.906)	2.197(2.063-2.355)
Grant	720	0.811(0.791-0.832)	1.35(1.3-1.405)	1.726(1.643-1.816)	2.074(1.955-2.2)	2.493(2.327-2.667)
Grant	1440	1.221(1.202-1.241)	1.891(1.847-1.943)	2.29(2.214-2.378)	2.627(2.516-2.754)	3.006(2.85-3.188)
Grant	2880	1.803(1.776-1.831)	2.748(2.688-2.817)	3.293(3.195-3.405)	3.741(3.603-3.899)	4.233(4.043-4.45)
Grant	4320	2.029(1.999-2.061)	3.068(2.998-3.144)	3.671(3.555-3.799)	4.171(4.006-4.355)	4.723(4.496-4.98)
Grant	5760	2.326(2.29-2.363)	3.442(3.373-3.525)	4.056(3.949-4.187)	4.542(4.397-4.723)	5.055(4.863-5.299)
Grant	7200	2.494(2.457-2.533)	3.691(3.615-3.781)	4.347(4.229-4.491)	4.866(4.703-5.066)	5.414(5.197-5.682)
Grant	8640	2.63(2.591-2.671)	3.882(3.805-3.975)	4.542(4.424-4.687)	5.054(4.893-5.252)	5.584(5.371-5.85)
Grant	10080	2.83(2.787-2.874)	4.177(4.092-4.275)	4.889(4.76-5.045)	5.443(5.267-5.659)	6.02(5.784-6.31)
Grant	11520	3(2.953-3.047)	4.39(4.302-4.495)	5.122(4.986-5.292)	5.691(5.506-5.929)	6.286(6.039-6.608)
Grant	12960	3.224(3.175-3.274)	4.68(4.588-4.786)	5.434(5.292-5.601)	6.016(5.822-6.245)	6.62(6.361-6.929)
Grant	14400	3.369(3.319-3.422)	4.866(4.773-4.979)	5.626(5.485-5.804)	6.201(6.011-6.444)	6.787(6.536-7.11)
Grays Harbor	15	0.347(0.33-0.367)	0.859(0.798-0.941)	1.25(1.135-1.406)	1.616(1.44-1.858)	2.056(1.799-2.414)
Grays Harbor	30	0.454(0.432-0.48)	1.053(0.977-1.157)	1.493(1.346-1.702)	1.901(1.674-2.241)	2.394(2.051-2.913)
Grays Harbor	60	0.62(0.587-0.664)	1.86(1.761-1.981)	2.971(2.817-3.157)	4.182(3.977-4.428)	5.905(5.638-6.222)
Grays Harbor	120	1.002(0.962-1.046)	1.996(1.881-2.135)	2.971(2.775-3.204)	4.182(3.901-4.516)	5.905(5.506-6.378)
Grays Harbor	180	1.208(1.164-1.258)	2.398(2.268-2.563)	3.204(2.978-3.491)	4.182(3.852-3.658)	5.905(5.445-4.523)
Grays Harbor	360	1.839(1.79-1.894)	3.166(3.055-3.301)	4.212(4.036-4.434)	5.243(4.997-5.555)	6.558(6.219-6.987)
Grays Harbor	720	2.681(2.605-2.767)	4.66(4.474-4.89)	6.346(6.041-6.728)	8.036(7.604-8.576)	10.197(9.599-10.946)
Grays Harbor	1440	3.257(3.209-3.309)	4.787(4.693-4.909)	6.346(6.197-6.544)	8.036(7.83-8.309)	10.197(9.921-10.569)
Grays Harbor	2880	4.529(4.463-4.601)	6.596(6.47-6.75)	7.629(7.444-7.866)	8.398(8.154-8.715)	10.197(9.88-7.272)
Grays Harbor	4320	5.621(5.542-5.706)	8.097(7.935-8.282)	9.343(9.102-9.632)	10.276(9.96-10.657)	11.214(10.813-11.705)
Grays Harbor	5760	6.23(6.144-6.321)	8.929(8.762-9.128)	10.308(10.048-10.615)	11.345(11.001-11.759)	12.388(11.942-12.936)
Grays Harbor	7200	6.902(6.809-6.999)	9.746(9.578-9.96)	11.191(10.935-11.529)	12.281(11.935-12.747)	13.383(12.929-13.996)
Grays Harbor	8640	7.319(7.219-7.418)	10.282(10.1-10.489)	11.737(11.471-12.055)	12.818(12.467-13.242)	13.902(13.45-14.456)
Grays Harbor	10080	8.185(8.077-8.293)	11.335(11.149-11.55)	12.835(12.569-13.158)	13.928(13.586-14.358)	15.003(14.568-15.555)

Grays Harbor	11520	8.769(8.654-8.885)	12.092(11.9-12.32)	13.656(13.377-13.997)	14.791(14.426-15.239)	15.905(15.438-16.483)
Grays Harbor	12960	9.31(9.189-9.431)	12.745(12.546-12.973)	14.328(14.048-14.666)	15.463(15.098-15.904)	16.567(16.106-17.12)
Grays Harbor	14400	9.944(9.811-10.082)	13.464(13.227-13.753)	15.135(14.782-15.584)	16.318(15.844-16.93)	17.446(16.822-18.255)
Island	15	0.284(0.27-0.301)	0.81(0.755-0.885)	1.199(1.095-1.34)	1.551(1.393-1.768)	1.96(1.731-2.277)
Island	30	0.366(0.348-0.387)	0.932(0.869-1.016)	1.316(1.2-1.47)	1.646(1.476-1.877)	2.019(1.779-2.35)
Island	60	0.395(0.379-0.415)	1.04(0.994-1.096)	1.672(1.597-1.766)	2.392(2.287-2.523)	3.443(3.299-3.622)
Island	120	0.635(0.613-0.659)	1.196(1.13-1.275)	1.672(1.554-1.813)	2.392(2.217-2.6)	3.443(3.185-3.747)
Island	180	0.778(0.755-0.804)	1.423(1.358-1.507)	1.86(1.746-2.005)	2.392(2.224-2.177)	3.443(3.206-2.72)
Island	360	1.094(1.063-1.129)	1.944(1.875-2.03)	2.645(2.535-2.784)	3.347(3.195-3.539)	4.253(4.046-4.515)
Island	720	1.526(1.486-1.569)	2.523(2.434-2.632)	3.326(3.184-3.503)	4.12(3.922-4.366)	5.131(4.861-5.469)
Island	1440	2.091(2.065-2.116)	3.099(3.046-3.156)	3.642(3.559-3.736)	4.12(4.005-4.253)	5.131(4.978-5.313)
Island	2880	2.988(2.951-3.027)	4.445(4.371-4.531)	5.187(5.076-5.32)	5.745(5.597-5.923)	6.306(6.115-6.538)
Island	4320	3.4(3.359-3.443)	4.995(4.912-5.09)	5.821(5.694-5.969)	6.447(6.275-6.649)	7.083(6.856-7.352)
Island	5760	3.7(3.657-3.746)	5.411(5.325-5.512)	6.297(6.163-6.456)	6.969(6.786-7.188)	7.65(7.409-7.943)
Island	7200	4.062(4.013-4.111)	5.926(5.83-6.032)	6.888(6.742-7.052)	7.619(7.419-7.843)	8.362(8.1-8.659)
Island	8640	4.387(4.329-4.448)	6.349(6.238-6.48)	7.379(7.211-7.581)	8.156(7.93-8.429)	8.939(8.643-9.302)
Island	10080	4.975(4.917-5.035)	7.202(7.092-7.325)	8.32(8.157-8.51)	9.151(8.933-9.41)	9.979(9.692-10.319)
Island	11520	5.63(5.565-5.696)	8.104(7.988-8.24)	9.324(9.152-9.535)	10.224(9.993-10.509)	11.114(10.811-11.489)
Island	12960	5.793(5.728-5.861)	8.243(8.13-8.378)	9.405(9.238-9.605)	10.245(10.026-10.508)	11.114(10.834-11.447)
Island	14400	6.093(6.025-6.165)	8.611(8.493-8.753)	9.792(9.62-10.005)	10.639(10.415-10.92)	11.462(11.174-11.822)
Jefferson	15	0.37(0.352-0.393)	1.02(0.948-1.117)	1.516(1.38-1.701)	1.973(1.766-2.258)	2.513(2.212-2.93)
Jefferson	30	0.47(0.447-0.497)	1.139(1.059-1.247)	1.614(1.463-1.823)	2.041(1.813-2.366)	2.539(2.207-3.022)
Jefferson	60	0.57(0.542-0.607)	1.593(1.509-1.698)	2.477(2.344-2.639)	3.422(3.244-3.636)	4.747(4.513-5.025)
Jefferson	120	0.9(0.863-0.941)	1.825(1.719-1.953)	2.477(2.299-2.691)	3.422(3.168-3.724)	4.747(4.388-5.171)
Jefferson	180	1.111(1.073-1.155)	2.136(2.025-2.279)	2.823(2.63-3.069)	3.429(3.147-3.782)	4.747(4.356-4.085)
Jefferson	360	1.629(1.584-1.678)	2.872(2.769-2.996)	3.872(3.707-4.075)	4.864(4.632-5.149)	6.133(5.813-6.527)
Jefferson	720	2.45(2.381-2.527)	4.247(4.081-4.451)	5.777(5.506-6.115)	7.314(6.932-7.791)	9.287(8.758-9.947)
Jefferson	1440	2.875(2.835-2.918)	4.247(4.165-4.346)	5.777(5.649-5.936)	7.314(7.138-7.533)	9.287(9.052-9.584)
Jefferson	2880	4.268(4.207-4.332)	6.265(6.15-6.41)	7.293(7.118-7.524)	8.068(7.831-8.389)	9.287(8.97-6.511)
Jefferson	4320	5.111(5.041-5.185)	7.446(7.304-7.614)	8.651(8.435-8.918)	9.564(9.275-9.921)	10.49(10.115-10.957)

Jefferson	5760	5.928(5.847-6.014)	8.584(8.421-8.777)	9.952(9.699-10.254)	10.985(10.649-11.392)	12.029(11.593-12.563)
Jefferson	7200	6.341(6.257-6.429)	9.09(8.932-9.286)	10.499(10.257-10.808)	11.566(11.236-11.99)	12.646(12.214-13.208)
Jefferson	8640	6.886(6.794-6.983)	9.795(9.625-10.004)	11.265(11.01-11.587)	12.361(12.02-12.793)	13.455(13.011-14.026)
Jefferson	10080	7.313(7.22-7.408)	10.357(10.189-10.561)	11.864(11.62-12.178)	12.976(12.654-13.402)	14.076(13.655-14.631)
Jefferson	11520	7.866(7.76-7.968)	11.096(10.913-11.314)	12.669(12.4-13.002)	13.821(13.466-14.269)	14.956(14.496-15.544)
Jefferson	12960	8.428(8.32-8.538)	11.775(11.589-11.992)	13.357(13.089-13.685)	14.495(14.142-14.932)	15.602(15.151-16.159)
Jefferson	14400	9.111(8.994-9.232)	12.601(12.408-12.847)	14.227(13.946-14.601)	15.38(15.011-15.884)	16.486(16.007-17.143)
King	15	0.357(0.34-0.377)	0.966(0.909-1.042)	1.355(1.25-1.497)	1.684(1.526-1.902)	2.053(1.823-2.372)
King	30	0.45(0.429-0.475)	1.156(1.086-1.249)	1.585(1.456-1.76)	1.937(1.744-2.207)	2.323(2.044-2.719)
King	60	0.511(0.49-0.539)	1.175(1.111-1.254)	1.668(1.566-1.793)	2.147(2.008-2.317)	2.769(2.584-2.996)
King	120	0.723(0.698-0.752)	1.341(1.274-1.424)	1.725(1.617-1.86)	2.147(1.997-2.334)	2.769(2.563-3.024)
King	180	0.845(0.819-0.874)	1.501(1.431-1.593)	1.919(1.798-2.075)	2.274(2.101-2.495)	2.769(2.532-2.73)
King	360	1.224(1.189-1.263)	2.119(2.045-2.212)	2.843(2.728-2.993)	3.565(3.405-3.772)	4.493(4.277-4.773)
King	720	1.786(1.742-1.833)	2.802(2.706-2.915)	3.535(3.386-3.718)	4.224(4.019-4.48)	5.069(4.788-5.417)
King	1440	2.455(2.418-2.493)	3.673(3.597-3.76)	4.332(4.208-4.474)	4.855(4.683-5.055)	5.415(5.18-5.69)
King	2880	3.757(3.7-3.816)	5.557(5.448-5.686)	6.465(6.305-6.662)	7.143(6.931-7.406)	7.821(7.549-8.163)
King	4320	4.781(4.713-4.858)	7.038(6.893-7.208)	8.24(8.012-8.509)	9.178(8.864-9.545)	10.158(9.738-10.649)
King	5760	5.417(5.335-5.505)	7.922(7.761-8.12)	9.252(8.996-9.571)	10.287(9.938-10.725)	11.366(10.899-11.96)
King	7200	6.089(6-6.183)	8.813(8.638-9.013)	10.2(9.935-10.506)	11.265(10.909-11.674)	12.368(11.903-12.903)
King	8640	6.828(6.723-6.935)	9.878(9.691-10.099)	11.355(11.079-11.688)	12.434(12.069-12.875)	13.495(13.031-14.069)
King	10080	7.17(7.06-7.28)	10.297(10.111-10.516)	11.782(11.518-12.108)	12.853(12.509-13.286)	13.896(13.455-14.453)
King	11520	7.601(7.484-7.718)	10.8(10.61-11.033)	12.286(12.018-12.63)	13.351(13.003-13.802)	14.383(13.942-14.962)
King	12960	8.284(8.161-8.409)	11.646(11.448-11.884)	13.18(12.901-13.527)	14.271(13.913-14.719)	15.322(14.875-15.893)
King	14400	8.695(8.57-8.829)	12.095(11.899-12.338)	13.618(13.341-13.974)	14.693(14.339-15.151)	15.726(15.282-16.304)
Kitsap	15	0.335(0.319-0.355)	0.891(0.832-0.971)	1.292(1.18-1.442)	1.652(1.484-1.885)	2.074(1.829-2.415)
Kitsap	30	0.419(0.399-0.443)	1.041(0.971-1.134)	1.461(1.332-1.638)	1.828(1.633-2.1)	2.246(1.966-2.645)
Kitsap	60	0.419(0.403-0.438)	1.041(0.998-1.096)	1.541(1.469-1.632)	2.157(2.055-2.285)	3.043(2.903-3.22)
Kitsap	120	0.654(0.633-0.677)	1.184(1.123-1.258)	1.554(1.446-1.686)	2.157(1.997-2.351)	3.043(2.808-3.324)
Kitsap	180	0.805(0.784-0.83)	1.388(1.33-1.464)	1.772(1.672-1.902)	2.157(2.01-2.086)	3.043(2.836-2.582)
Kitsap	360	1.189(1.155-1.227)	2.098(2.024-2.191)	2.845(2.728-2.994)	3.592(3.43-3.799)	4.557(4.336-4.838)

Kitsap	720	1.725(1.68-1.772)	2.797(2.701-2.914)	3.637(3.486-3.825)	4.459(4.25-4.721)	5.499(5.214-5.856)
Kitsap	1440	2.224(2.199-2.253)	3.236(3.185-3.297)	3.805(3.721-3.899)	4.459(4.343-4.587)	5.499(5.343-5.669)
Kitsap	2880	3.248(3.209-3.289)	4.782(4.707-4.872)	5.561(5.451-5.699)	6.144(5.997-6.328)	6.728(6.538-6.968)
Kitsap	4320	3.662(3.62-3.71)	5.327(5.246-5.428)	6.169(6.044-6.323)	6.799(6.632-7.006)	7.432(7.216-7.701)
Kitsap	5760	4.478(4.424-4.535)	6.47(6.369-6.589)	7.468(7.315-7.652)	8.21(8.005-8.459)	8.951(8.682-9.281)
Kitsap	7200	5.046(4.987-5.107)	7.213(7.105-7.333)	8.252(8.093-8.429)	9.016(8.807-9.248)	9.778(9.513-10.073)
Kitsap	8640	5.056(4.996-5.12)	7.247(7.141-7.379)	8.313(8.156-8.509)	9.093(8.884-9.35)	9.861(9.592-10.199)
Kitsap	10080	5.187(5.123-5.251)	7.359(7.247-7.486)	8.412(8.249-8.603)	9.183(8.969-9.436)	9.943(9.667-10.271)
Kitsap	11520	5.941(5.868-6.013)	8.322(8.203-8.467)	9.443(9.271-9.657)	10.253(10.028-10.535)	11.044(10.756-11.407)
Kitsap	12960	6.315(6.241-6.391)	8.817(8.695-8.962)	9.988(9.815-10.198)	10.832(10.61-11.106)	11.656(11.374-12.004)
Kitsap	14400	6.315(6.244-6.393)	8.817(8.698-8.963)	9.988(9.814-10.208)	10.832(10.603-11.124)	11.656(11.359-12.033)
Kittitas	15	0.288(0.275-0.303)	0.8(0.76-0.852)	1.083(1.013-1.175)	1.297(1.196-1.434)	1.516(1.373-1.711)
Kittitas	30	0.364(0.348-0.381)	0.916(0.87-0.976)	1.215(1.132-1.324)	1.44(1.318-1.606)	1.67(1.496-1.91)
Kittitas	60	0.452(0.432-0.479)	1.059(0.995-1.137)	1.448(1.348-1.572)	1.785(1.648-1.951)	2.174(1.992-2.394)
Kittitas	120	0.597(0.573-0.625)	1.199(1.138-1.277)	1.558(1.461-1.679)	1.852(1.721-2.016)	2.174(1.999-2.393)
Kittitas	180	0.686(0.661-0.713)	1.328(1.258-1.416)	1.741(1.621-1.89)	2.093(1.923-2.302)	2.488(2.257-2.773)
Kittitas	360	0.919(0.892-0.949)	1.746(1.682-1.825)	2.447(2.341-2.577)	3.152(3.002-3.335)	4.061(3.853-4.314)
Kittitas	720	1.327(1.293-1.364)	2.21(2.124-2.31)	2.875(2.734-3.04)	3.508(3.308-3.742)	4.287(4.007-4.609)
Kittitas	1440	2.088(2.056-2.121)	3.203(3.13-3.286)	3.826(3.703-3.965)	4.337(4.161-4.536)	4.901(4.654-5.181)
Kittitas	2880	3.046(2.995-3.101)	4.601(4.498-4.724)	5.432(5.273-5.626)	6.08(5.863-6.345)	6.756(6.468-7.109)
Kittitas	4320	4.074(4.007-4.148)	6.131(5.992-6.301)	7.238(7.019-7.515)	8.107(7.806-8.487)	9.018(8.614-9.53)
Kittitas	5760	4.606(4.527-4.69)	6.797(6.646-6.98)	7.923(7.697-8.204)	8.783(8.485-9.152)	9.663(9.278-10.144)
Kittitas	7200	5.18(5.094-5.272)	7.633(7.467-7.822)	8.856(8.613-9.137)	9.779(9.457-10.147)	10.719(10.31-11.19)
Kittitas	8640	5.891(5.794-5.996)	8.62(8.442-8.835)	9.951(9.688-10.267)	10.933(10.587-11.346)	11.91(11.471-12.439)
Kittitas	10080	6.032(5.931-6.138)	8.869(8.691-9.082)	10.246(9.994-10.563)	11.255(10.924-11.675)	12.252(11.827-12.793)
Kittitas	11520	6.355(6.244-6.469)	9.216(9.022-9.446)	10.588(10.306-10.933)	11.594(11.226-12.048)	12.592(12.124-13.176)
Kittitas	12960	7.449(7.328-7.58)	10.554(10.354-10.797)	11.988(11.7-12.341)	13.024(12.651-13.479)	14.04(13.566-14.614)
Kittitas	14400	7.874(7.742-8.011)	11.075(10.868-11.329)	12.53(12.238-12.896)	13.568(13.194-14.038)	14.574(14.105-15.165)
Klickitat	15	0.247(0.236-0.259)	0.637(0.607-0.677)	0.853(0.8-0.922)	1.017(0.942-1.118)	1.185(1.08-1.326)
Klickitat	30	0.309(0.297-0.323)	0.737(0.7-0.784)	0.978(0.913-1.063)	1.165(1.069-1.295)	1.361(1.224-1.548)

Klickitat	60	0.436(0.417-0.46)	1.009(0.951-1.081)	1.375(1.282-1.489)	1.686(1.56-1.841)	2.042(1.873-2.249)
Klickitat	120	0.559(0.538-0.585)	1.125(1.069-1.196)	1.462(1.373-1.574)	1.74(1.618-1.892)	2.045(1.882-2.25)
Klickitat	180	0.662(0.639-0.686)	1.242(1.181-1.317)	1.611(1.508-1.739)	1.927(1.781-2.105)	2.282(2.083-2.524)
Klickitat	360	0.832(0.808-0.858)	1.551(1.493-1.621)	2.141(2.046-2.256)	2.724(2.589-2.886)	3.464(3.276-3.69)
Klickitat	720	1.172(1.143-1.204)	1.955(1.881-2.04)	2.532(2.409-2.672)	3.076(2.901-3.275)	3.743(3.498-4.016)
Klickitat	1440	1.726(1.699-1.754)	2.698(2.637-2.768)	3.248(3.147-3.368)	3.691(3.549-3.866)	4.169(3.971-4.414)
Klickitat	2880	2.548(2.509-2.591)	3.889(3.805-3.989)	4.618(4.486-4.777)	5.195(5.016-5.41)	5.806(5.568-6.09)
Klickitat	4320	3.127(3.079-3.179)	4.73(4.626-4.855)	5.631(5.465-5.84)	6.357(6.124-6.649)	7.135(6.817-7.537)
Klickitat	5760	3.447(3.394-3.504)	5.132(5.02-5.262)	6.114(5.933-6.325)	6.932(6.678-7.225)	7.836(7.486-8.237)
Klickitat	7200	3.888(3.831-3.949)	5.733(5.613-5.871)	6.791(6.596-7.009)	7.664(7.391-7.969)	8.623(8.254-9.039)
Klickitat	8640	4.235(4.172-4.303)	6.272(6.137-6.419)	7.403(7.188-7.634)	8.32(8.023-8.638)	9.316(8.915-9.744)
Klickitat	10080	4.478(4.408-4.549)	6.66(6.532-6.815)	7.778(7.59-8.021)	8.626(8.374-8.957)	9.49(9.161-9.93)
Klickitat	11520	4.803(4.728-4.877)	7.074(6.94-7.229)	8.212(8.015-8.446)	9.068(8.806-9.383)	9.935(9.595-10.35)
Klickitat	12960	5.58(5.496-5.671)	8.071(7.928-8.247)	9.281(9.07-9.544)	10.179(9.899-10.529)	11.08(10.718-11.534)
Klickitat	14400	5.858(5.768-5.949)	8.418(8.264-8.599)	9.648(9.426-9.922)	10.556(10.264-10.918)	11.464(11.09-11.931)
Lewis	15	0.396(0.378-0.418)	1.086(1.023-1.17)	1.518(1.402-1.674)	1.879(1.704-2.119)	2.28(2.026-2.631)
Lewis	30	0.491(0.468-0.518)	1.221(1.145-1.324)	1.679(1.537-1.879)	2.068(1.85-2.384)	2.507(2.183-2.982)
Lewis	60	0.491(0.468-0.521)	1.326(1.258-1.411)	2.066(1.959-2.198)	2.865(2.719-3.042)	3.99(3.797-4.224)
Lewis	120	0.755(0.725-0.789)	1.529(1.44-1.637)	2.066(1.913-2.249)	2.865(2.642-3.128)	3.99(3.672-4.366)
Lewis	180	0.899(0.87-0.933)	1.692(1.609-1.799)	2.223(2.078-2.407)	2.865(2.654-2.783)	3.99(3.695-3.449)
Lewis	360	1.224(1.188-1.264)	2.294(2.212-2.397)	3.217(3.085-3.386)	4.157(3.973-4.394)	5.383(5.13-5.708)
Lewis	720	1.753(1.704-1.807)	3.025(2.909-3.166)	4.097(3.909-4.33)	5.173(4.908-5.501)	6.554(6.187-7.007)
Lewis	1440	2.628(2.587-2.671)	3.937(3.853-4.036)	4.621(4.486-4.785)	5.173(4.985-5.405)	6.554(6.298-6.873)
Lewis	2880	3.724(3.666-3.785)	5.514(5.399-5.651)	6.446(6.273-6.664)	7.157(6.926-7.454)	7.883(7.58-8.278)
Lewis	4320	4.611(4.542-4.686)	6.756(6.609-6.924)	7.897(7.668-8.162)	8.786(8.474-9.146)	9.714(9.303-10.194)
Lewis	5760	5.433(5.349-5.522)	7.887(7.724-8.081)	9.165(8.913-9.47)	10.149(9.811-10.562)	11.165(10.719-11.717)
Lewis	7200	5.902(5.817-5.991)	8.444(8.271-8.644)	9.819(9.546-10.137)	10.918(10.54-11.358)	12.093(11.586-12.686)
Lewis	8640	6.631(6.53-6.732)	9.543(9.347-9.76)	11.065(10.765-11.405)	12.252(11.844-12.714)	13.496(12.957-14.11)
Lewis	10080	6.833(6.732-6.936)	9.728(9.544-9.93)	11.171(10.902-11.475)	12.259(11.905-12.664)	13.496(13.038-14.019)
Lewis	11520	7.523(7.413-7.633)	10.601(10.41-10.819)	12.102(11.828-12.426)	13.224(12.864-13.651)	14.356(13.89-14.906)

Lewis	12960	8.108(7.995-8.225)	11.286(11.096-11.509)	12.809(12.531-13.138)	13.94(13.572-14.37)	15.075(14.6-15.626)
Lewis	14400	8.609(8.489-8.733)	11.889(11.689-12.129)	13.449(13.156-13.81)	14.598(14.213-15.072)	15.744(15.25-16.354)
Lincoln	15	0.206(0.198-0.216)	0.477(0.453-0.509)	0.637(0.597-0.689)	0.766(0.709-0.84)	0.903(0.827-1.004)
Lincoln	30	0.265(0.254-0.277)	0.572(0.542-0.609)	0.763(0.711-0.832)	0.922(0.845-1.026)	1.097(0.987-1.247)
Lincoln	60	0.33(0.317-0.345)	0.663(0.628-0.709)	0.9(0.839-0.98)	1.122(1.032-1.238)	1.394(1.266-1.559)
Lincoln	120	0.426(0.414-0.44)	0.761(0.729-0.802)	0.988(0.933-1.056)	1.188(1.11-1.286)	1.421(1.312-1.557)
Lincoln	180	0.518(0.504-0.533)	0.879(0.846-0.92)	1.1(1.046-1.165)	1.289(1.214-1.38)	1.505(1.402-1.627)
Lincoln	360	0.69(0.672-0.71)	1.114(1.074-1.163)	1.416(1.352-1.494)	1.694(1.606-1.804)	2.03(1.909-2.179)
Lincoln	720	0.876(0.854-0.899)	1.375(1.325-1.433)	1.712(1.632-1.805)	2.021(1.909-2.149)	2.389(2.234-2.562)
Lincoln	1440	1.211(1.193-1.23)	1.83(1.791-1.878)	2.183(2.117-2.263)	2.47(2.374-2.586)	2.78(2.648-2.942)
Lincoln	2880	1.652(1.627-1.678)	2.463(2.411-2.525)	2.907(2.825-3.008)	3.258(3.145-3.4)	3.63(3.477-3.823)
Lincoln	4320	2.08(2.05-2.111)	3.091(3.026-3.163)	3.655(3.55-3.773)	4.105(3.959-4.273)	4.585(4.386-4.817)
Lincoln	5760	2.335(2.303-2.368)	3.407(3.338-3.486)	4.024(3.912-4.156)	4.534(4.375-4.721)	5.092(4.873-5.352)
Lincoln	7200	2.449(2.416-2.485)	3.55(3.479-3.636)	4.171(4.056-4.309)	4.677(4.514-4.87)	5.225(5.002-5.488)
Lincoln	8640	2.62(2.583-2.658)	3.794(3.72-3.879)	4.416(4.304-4.552)	4.901(4.749-5.088)	5.406(5.204-5.657)
Lincoln	10080	2.828(2.786-2.871)	4.1(4.019-4.196)	4.766(4.643-4.919)	5.273(5.106-5.484)	5.79(5.569-6.074)
Lincoln	11520	3.056(3.011-3.103)	4.417(4.325-4.524)	5.16(5.013-5.334)	5.747(5.542-5.993)	6.37(6.09-6.708)
Lincoln	12960	3.241(3.193-3.29)	4.673(4.578-4.785)	5.449(5.298-5.631)	6.062(5.852-6.319)	6.71(6.423-7.067)
Lincoln	14400	3.405(3.355-3.457)	4.905(4.805-5.021)	5.714(5.555-5.902)	6.347(6.127-6.612)	7.014(6.713-7.375)
Mason	15	0.371(0.353-0.391)	0.861(0.801-0.94)	1.222(1.112-1.372)	1.559(1.39-1.793)	1.968(1.718-2.317)
Mason	30	0.448(0.426-0.473)	1.057(0.982-1.159)	1.493(1.351-1.695)	1.892(1.672-2.215)	2.366(2.038-2.855)
Mason	60	0.482(0.458-0.511)	1.482(1.417-1.563)	2.521(2.416-2.651)	3.735(3.59-3.914)	5.537(5.341-5.779)
Mason	120	0.886(0.852-0.923)	1.758(1.652-1.883)	2.521(2.329-2.746)	3.735(3.447-4.07)	5.537(5.112-6.032)
Mason	180	1.115(1.08-1.155)	2.102(2.002-2.231)	2.784(2.609-3.007)	3.735(3.474-3.319)	5.537(5.167-4.202)
Mason	360	1.675(1.625-1.73)	3.194(3.079-3.338)	4.523(4.337-4.758)	5.884(5.623-6.215)	7.666(7.307-8.123)
Mason	720	2.48(2.409-2.559)	4.385(4.214-4.596)	6.053(5.773-6.402)	7.75(7.355-8.243)	9.953(9.406-10.635)
Mason	1440	2.501(2.466-2.538)	4.385(4.317-4.471)	6.053(5.944-6.191)	7.75(7.6-7.941)	9.953(9.75-10.211)
Mason	2880	3.719(3.668-3.774)	5.441(5.343-5.561)	6.308(6.163-6.49)	7.75(7.559-5.025)	9.953(9.707-5.606)
Mason	4320	4.321(4.263-4.384)	6.217(6.101-6.348)	7.16(6.989-7.361)	7.862(7.638-8.127)	9.953(9.669-7.943)
Mason	5760	5.088(5.021-5.159)	7.296(7.168-7.445)	8.408(8.213-8.637)	9.237(8.979-9.547)	10.067(9.732-10.479)

Mason	7200	5.704(5.629-5.78)	8.054(7.92-8.216)	9.234(9.032-9.485)	10.124(9.851-10.465)	11.027(10.671-11.474)
Mason	8640	6.174(6.093-6.255)	8.713(8.565-8.881)	9.97(9.751-10.227)	10.912(10.62-11.252)	11.863(11.486-12.31)
Mason	10080	6.563(6.477-6.648)	9.167(9.018-9.333)	10.422(10.206-10.671)	11.344(11.065-11.675)	12.26(11.902-12.684)
Mason	11520	7.26(7.169-7.354)	10.023(9.867-10.204)	11.34(11.114-11.607)	12.309(12.013-12.659)	13.275(12.893-13.723)
Mason	12960	7.878(7.781-7.977)	10.807(10.645-10.993)	12.184(11.95-12.457)	13.19(12.884-13.546)	14.188(13.796-14.637)
Mason	14400	8.023(7.922-8.13)	10.905(10.721-11.125)	12.292(12.014-12.633)	13.292(12.917-13.754)	14.265(13.771-14.875)
Okanogan	15	0.272(0.259-0.287)	0.765(0.722-0.822)	1.07(0.993-1.174)	1.321(1.206-1.477)	1.592(1.429-1.816)
Okanogan	30	0.345(0.329-0.363)	0.874(0.825-0.938)	1.185(1.096-1.302)	1.432(1.302-1.608)	1.695(1.51-1.947)
Okanogan	60	0.417(0.398-0.442)	0.983(0.925-1.057)	1.385(1.29-1.501)	1.761(1.632-1.921)	2.234(2.06-2.447)
Okanogan	120	0.561(0.538-0.586)	1.109(1.051-1.181)	1.453(1.36-1.568)	1.761(1.633-1.919)	2.234(2.06-2.448)
Okanogan	180	0.654(0.633-0.677)	1.218(1.16-1.289)	1.59(1.492-1.711)	1.918(1.777-2.09)	2.3(2.104-2.536)
Okanogan	360	0.846(0.822-0.872)	1.529(1.472-1.597)	2.083(1.991-2.195)	2.63(2.501-2.788)	3.327(3.148-3.543)
Okanogan	720	1.17(1.139-1.203)	1.885(1.814-1.97)	2.419(2.304-2.557)	2.927(2.766-3.121)	3.554(3.332-3.818)
Okanogan	1440	1.729(1.704-1.754)	2.651(2.594-2.713)	3.169(3.076-3.274)	3.591(3.458-3.744)	4.051(3.865-4.265)
Okanogan	2880	2.025(1.996-2.056)	3.05(2.99-3.119)	3.596(3.504-3.707)	4.02(3.894-4.173)	4.458(4.291-4.662)
Okanogan	4320	2.552(2.514-2.591)	3.802(3.725-3.889)	4.462(4.344-4.6)	4.97(4.813-5.159)	5.494(5.286-5.745)
Okanogan	5760	2.695(2.658-2.735)	3.967(3.894-4.055)	4.636(4.526-4.774)	5.15(5.001-5.338)	5.679(5.481-5.93)
Okanogan	7200	3.19(3.145-3.236)	4.701(4.611-4.805)	5.501(5.361-5.665)	6.118(5.926-6.345)	6.754(6.5-7.058)
Okanogan	8640	3.267(3.222-3.315)	4.808(4.718-4.913)	5.606(5.47-5.769)	6.212(6.029-6.432)	6.828(6.59-7.116)
Okanogan	10080	3.735(3.681-3.79)	5.437(5.335-5.554)	6.331(6.178-6.512)	7.027(6.822-7.271)	7.754(7.485-8.077)
Okanogan	11520	4.128(4.067-4.191)	5.985(5.868-6.124)	6.966(6.787-7.187)	7.733(7.49-8.036)	8.537(8.214-8.944)
Okanogan	12960	4.404(4.341-4.469)	6.316(6.199-6.451)	7.293(7.115-7.503)	8.045(7.805-8.328)	8.825(8.508-9.195)
Okanogan	14400	4.404(4.338-4.474)	6.316(6.196-6.46)	7.293(7.115-7.514)	8.045(7.808-8.341)	8.825(8.516-9.211)
Pacific	15	0.301(0.287-0.318)	0.719(0.672-0.784)	1.017(0.928-1.137)	1.288(1.153-1.476)	1.612(1.413-1.891)
Pacific	30	0.443(0.422-0.468)	1.046(0.974-1.143)	1.467(1.331-1.66)	1.847(1.637-2.157)	2.296(1.982-2.766)
Pacific	60	0.481(0.463-0.503)	1.211(1.163-1.271)	1.965(1.885-2.067)	2.842(2.727-2.987)	4.139(3.98-4.343)
Pacific	120	0.846(0.82-0.875)	1.529(1.448-1.627)	2.03(1.881-2.209)	2.842(2.616-3.111)	4.139(3.803-4.537)
Pacific	180	1.081(1.054-1.112)	1.824(1.753-1.919)	2.316(2.192-2.479)	2.842(2.657-2.747)	4.139(3.877-3.443)
Pacific	360	1.559(1.516-1.607)	2.68(2.59-2.797)	3.588(3.449-3.779)	4.494(4.3-4.759)	5.661(5.397-6.024)
Pacific	720	2.213(2.149-2.283)	3.94(3.788-4.127)	5.471(5.224-5.78)	7.04(6.692-7.476)	9.089(8.608-9.691)

Pacific	1440	2.978(2.934-3.024)	4.383(4.299-4.494)	5.471(5.337-5.651)	7.04(6.854-7.29)	9.089(8.838-9.43)
Pacific	2880	4.127(4.069-4.191)	5.994(5.88-6.127)	6.911(6.748-7.105)	7.588(7.378-7.839)	9.089(8.823-6.626)
Pacific	4320	5.211(5.139-5.289)	7.407(7.262-7.564)	8.473(8.262-8.71)	9.258(8.989-9.567)	10.04(9.706-10.43)
Pacific	5760	6.05(5.969-6.133)	8.583(8.433-8.761)	9.864(9.633-10.135)	10.823(10.517-11.191)	11.785(11.386-12.28)
Pacific	7200	6.667(6.578-6.759)	9.318(9.164-9.513)	10.636(10.405-10.937)	11.619(11.311-12.031)	12.606(12.205-13.141)
Pacific	8640	7.38(7.28-7.475)	10.272(10.093-10.46)	11.657(11.402-11.944)	12.678(12.345-13.056)	13.7(13.28-14.188)
Pacific	10080	7.621(7.518-7.722)	10.453(10.281-10.64)	11.757(11.515-12.033)	12.695(12.388-13.055)	13.7(13.318-14.154)
Pacific	11520	8.502(8.398-8.614)	11.569(11.4-11.771)	12.957(12.717-13.25)	13.951(13.637-14.325)	14.917(14.522-15.387)
Pacific	12960	9.147(9.032-9.262)	12.385(12.203-12.593)	13.831(13.575-14.131)	14.857(14.53-15.24)	15.851(15.442-16.322)
Pacific	14400	9.809(9.676-9.947)	13.124(12.871-13.421)	14.719(14.331-15.184)	15.838(15.312-16.475)	16.896(16.197-17.745)
Pend Oreille	15	0.252(0.242-0.265)	0.584(0.553-0.625)	0.787(0.735-0.855)	0.954(0.881-1.051)	1.135(1.036-1.268)
Pend Oreille	30	0.317(0.304-0.331)	0.682(0.645-0.729)	0.917(0.851-1.003)	1.115(1.017-1.246)	1.335(1.197-1.525)
Pend Oreille	60	0.367(0.352-0.384)	0.703(0.662-0.757)	0.946(0.873-1.039)	1.176(1.071-1.314)	1.463(1.31-1.66)
Pend Oreille	120	0.477(0.463-0.493)	0.826(0.79-0.871)	1.071(1.011-1.146)	1.29(1.204-1.396)	1.544(1.425-1.692)
Pend Oreille	180	0.564(0.548-0.58)	0.923(0.889-0.965)	1.129(1.077-1.195)	1.3(1.229-1.389)	1.544(1.449-1.66)
Pend Oreille	360	0.854(0.832-0.878)	1.27(1.228-1.325)	1.537(1.472-1.624)	1.772(1.683-1.891)	2.045(1.925-2.204)
Pend Oreille	720	1.038(1.012-1.067)	1.548(1.493-1.614)	1.873(1.787-1.977)	2.163(2.044-2.304)	2.501(2.34-2.69)
Pend Oreille	1440	1.413(1.393-1.433)	2.087(2.045-2.135)	2.464(2.394-2.542)	2.768(2.67-2.878)	3.096(2.964-3.247)
Pend Oreille	2880	2.184(2.149-2.223)	3.196(3.129-3.276)	3.705(3.604-3.824)	4.086(3.953-4.244)	4.47(4.301-4.674)
Pend Oreille	4320	2.184(2.16-2.208)	3.196(3.147-3.252)	3.705(3.629-3.795)	4.086(3.983-4.212)	4.47(4.333-4.641)
Pend Oreille	5760	2.493(2.456-2.533)	3.603(3.532-3.69)	4.183(4.074-4.317)	4.632(4.485-4.811)	5.097(4.905-5.332)
Pend Oreille	7200	3.146(3.096-3.198)	4.573(4.474-4.693)	5.317(5.165-5.504)	5.888(5.678-6.142)	6.474(6.201-6.81)
Pend Oreille	8640	3.448(3.396-3.507)	4.975(4.872-5.096)	5.747(5.594-5.926)	6.33(6.129-6.563)	6.922(6.666-7.221)
Pend Oreille	10080	3.653(3.595-3.714)	5.253(5.142-5.382)	6.055(5.889-6.249)	6.65(6.432-6.905)	7.244(6.964-7.575)
Pend Oreille	11520	4.277(4.203-4.352)	6.188(6.045-6.366)	7.213(6.991-7.503)	8.011(7.705-8.415)	8.84(8.431-9.387)
Pend Oreille	12960	4.441(4.364-4.521)	6.419(6.277-6.591)	7.432(7.213-7.7)	8.191(7.895-8.554)	8.954(8.563-9.427)
Pend Oreille	14400	4.639(4.558-4.724)	6.688(6.54-6.868)	7.715(7.489-7.993)	8.472(8.169-8.847)	9.221(8.826-9.712)
Pierce	15	0.382(0.364-0.403)	1.055(0.997-1.131)	1.448(1.344-1.588)	1.763(1.607-1.975)	2.1(1.876-2.41)
Pierce	30	0.479(0.457-0.504)	1.253(1.183-1.347)	1.691(1.562-1.868)	2.036(1.841-2.31)	2.402(2.119-2.806)
Pierce	60	0.535(0.512-0.567)	1.262(1.19-1.351)	1.772(1.658-1.91)	2.247(2.095-2.43)	2.843(2.644-3.083)

Pierce	120	0.74(0.712-0.772)	1.421(1.349-1.513)	1.833(1.717-1.978)	2.247(2.088-2.445)	2.843(2.628-3.108)
Pierce	180	0.848(0.819-0.88)	1.588(1.508-1.691)	2.068(1.93-2.244)	2.481(2.283-2.73)	2.949(2.677-3.291)
Pierce	360	1.225(1.19-1.265)	2.194(2.116-2.291)	3.001(2.878-3.158)	3.813(3.642-4.031)	4.864(4.632-5.161)
Pierce	720	1.769(1.723-1.819)	2.908(2.801-3.036)	3.796(3.625-4.006)	4.658(4.418-4.953)	5.739(5.408-6.143)
Pierce	1440	2.454(2.417-2.491)	3.675(3.6-3.761)	4.316(4.195-4.456)	4.814(4.647-5.011)	5.739(5.511-6.01)
Pierce	2880	3.59(3.536-3.647)	5.3(5.196-5.423)	6.165(6.012-6.353)	6.812(6.61-7.063)	7.461(7.201-7.788)
Pierce	4320	4.59(4.525-4.665)	6.722(6.584-6.883)	7.844(7.629-8.095)	8.714(8.421-9.053)	9.617(9.23-10.068)
Pierce	5760	5.096(5.019-5.179)	7.446(7.296-7.63)	8.669(8.435-8.958)	9.608(9.292-9.999)	10.575(10.158-11.098)
Pierce	7200	5.628(5.548-5.713)	8.114(7.954-8.297)	9.399(9.153-9.683)	10.397(10.063-10.781)	11.44(11-11.948)
Pierce	8640	6.31(6.215-6.409)	9.123(8.949-9.327)	10.502(10.244-10.81)	11.522(11.18-11.93)	12.538(12.099-13.07)
Pierce	10080	6.476(6.379-6.573)	9.272(9.104-9.465)	10.608(10.37-10.896)	11.58(11.269-11.961)	12.538(12.139-13.027)
Pierce	11520	7.142(7.034-7.249)	10.117(9.941-10.33)	11.511(11.262-11.827)	12.518(12.195-12.936)	13.502(13.09-14.04)
Pierce	12960	7.606(7.496-7.717)	10.674(10.496-10.886)	12.09(11.838-12.401)	13.106(12.781-13.509)	14.092(13.683-14.607)
Pierce	14400	8.23(8.115-8.354)	11.447(11.26-11.677)	12.914(12.647-13.255)	13.963(13.618-14.405)	14.981(14.545-15.544)
San Juan	15	0.307(0.292-0.326)	0.877(0.818-0.956)	1.293(1.182-1.442)	1.665(1.498-1.896)	2.097(1.855-2.433)
San Juan	30	0.391(0.373-0.414)	0.995(0.928-1.083)	1.399(1.277-1.561)	1.746(1.567-1.989)	2.136(1.883-2.485)
San Juan	60	0.426(0.407-0.449)	1.143(1.092-1.208)	1.838(1.754-1.943)	2.625(2.507-2.77)	3.767(3.608-3.965)
San Juan	120	0.682(0.658-0.709)	1.313(1.239-1.401)	1.838(1.707-1.994)	2.625(2.431-2.854)	3.767(3.485-4.101)
San Juan	180	0.837(0.812-0.867)	1.552(1.479-1.645)	2.037(1.91-2.198)	2.625(2.438-2.401)	3.767(3.504-2.998)
San Juan	360	1.177(1.144-1.215)	2.111(2.035-2.204)	2.883(2.763-3.035)	3.657(3.49-3.868)	4.656(4.427-4.945)
San Juan	720	1.646(1.602-1.693)	2.756(2.656-2.878)	3.661(3.501-3.86)	4.559(4.334-4.838)	5.704(5.396-6.087)
San Juan	1440	2.054(2.028-2.077)	3.049(2.998-3.102)	3.661(3.582-3.751)	4.559(4.451-4.685)	5.704(5.562-5.877)
San Juan	2880	2.967(2.93-3.005)	4.419(4.346-4.503)	5.155(5.045-5.284)	5.707(5.561-5.88)	6.261(6.073-6.485)
San Juan	4320	3.518(3.478-3.561)	5.18(5.096-5.272)	6.04(5.913-6.186)	6.692(6.52-6.891)	7.351(7.122-7.616)
San Juan	5760	3.993(3.949-4.04)	5.824(5.734-5.926)	6.767(6.627-6.928)	7.478(7.288-7.7)	8.196(7.945-8.49)
San Juan	7200	4.158(4.108-4.208)	6.079(5.98-6.188)	7.086(6.933-7.257)	7.852(7.642-8.087)	8.628(8.351-8.941)
San Juan	8640	4.818(4.752-4.886)	6.949(6.822-7.097)	8.097(7.904-8.327)	8.969(8.708-9.281)	9.849(9.506-10.264)
San Juan	10080	5.178(5.118-5.238)	7.52(7.405-7.647)	8.715(8.541-8.914)	9.607(9.374-9.882)	10.5(10.19-10.864)
San Juan	11520	5.342(5.281-5.404)	7.697(7.586-7.827)	8.872(8.705-9.075)	9.739(9.514-10.015)	10.598(10.301-10.962)
San Juan	12960	5.808(5.744-5.875)	8.275(8.16-8.411)	9.45(9.277-9.655)	10.297(10.069-10.568)	11.122(10.829-11.47)

San Juan	14400	5.982(5.916-6.051)	8.472(8.354-8.611)	9.643(9.471-9.854)	10.482(10.257-10.761)	11.294(11.004-11.653)
Skagit	15	0.409(0.389-0.433)	1.246(1.173-1.344)	1.779(1.643-1.962)	2.222(2.018-2.502)	2.707(2.413-3.113)
Skagit	30	0.491(0.468-0.518)	1.333(1.253-1.437)	1.827(1.683-2.017)	2.222(2.011-2.505)	2.707(2.411-3.111)
Skagit	60	0.536(0.508-0.574)	1.53(1.445-1.634)	2.369(2.238-2.528)	3.256(3.081-3.465)	4.489(4.262-4.757)
Skagit	120	0.788(0.753-0.828)	1.666(1.566-1.788)	2.369(2.201-2.569)	3.256(3.018-3.537)	4.489(4.156-4.881)
Skagit	180	0.928(0.892-0.967)	1.871(1.767-2.003)	2.509(2.328-2.738)	3.256(2.992-3.059)	4.489(4.123-3.769)
Skagit	360	1.301(1.265-1.341)	2.336(2.251-2.438)	3.179(3.041-3.346)	4.019(3.825-4.252)	5.096(4.828-5.417)
Skagit	720	1.789(1.739-1.844)	3.068(2.95-3.212)	4.144(3.953-4.382)	5.221(4.952-5.556)	6.601(6.23-7.064)
Skagit	1440	2.262(2.232-2.291)	3.363(3.302-3.432)	4.144(4.047-4.257)	5.221(5.086-5.381)	6.601(6.419-6.82)
Skagit	2880	3.23(3.189-3.275)	4.822(4.737-4.924)	5.643(5.513-5.8)	6.263(6.09-6.475)	6.891(6.667-7.166)
Skagit	4320	3.64(3.592-3.692)	5.365(5.266-5.476)	6.256(6.103-6.43)	6.933(6.728-7.167)	7.621(7.353-7.929)
Skagit	5760	4.139(4.088-4.196)	6.025(5.921-6.148)	6.998(6.837-7.19)	7.733(7.516-7.995)	8.478(8.193-8.827)
Skagit	7200	4.912(4.847-4.976)	7.152(7.024-7.292)	8.319(8.119-8.537)	9.206(8.933-9.506)	10.108(9.75-10.51)
Skagit	8640	5.216(5.145-5.288)	7.513(7.379-7.668)	8.696(8.496-8.938)	9.585(9.315-9.913)	10.476(10.124-10.908)
Skagit	10080	5.725(5.651-5.799)	8.213(8.078-8.368)	9.448(9.25-9.686)	10.359(10.098-10.68)	11.263(10.924-11.685)
Skagit	11520	6.39(6.308-6.471)	9.114(8.969-9.285)	10.452(10.237-10.718)	11.436(11.152-11.795)	12.408(12.039-12.88)
Skagit	12960	6.445(6.365-6.525)	9.114(8.973-9.276)	10.452(10.246-10.692)	11.436(11.168-11.75)	12.408(12.069-12.808)
Skagit	14400	7.097(7.009-7.19)	10.045(9.891-10.23)	11.45(11.227-11.725)	12.464(12.174-12.829)	13.453(13.08-13.922)
Skamania	15	0.421(0.402-0.444)	1.219(1.157-1.301)	1.665(1.553-1.815)	2.007(1.841-2.234)	2.36(2.122-2.688)
Skamania	30	0.496(0.473-0.521)	1.305(1.234-1.398)	1.749(1.62-1.925)	2.092(1.898-2.364)	2.448(2.166-2.851)
Skamania	60	0.554(0.528-0.591)	1.377(1.293-1.479)	1.931(1.802-2.087)	2.432(2.261-2.637)	3.043(2.821-3.305)
Skamania	120	0.758(0.725-0.795)	1.557(1.472-1.663)	2.031(1.898-2.197)	2.432(2.25-2.655)	3.043(2.8-3.34)
Skamania	180	0.903(0.871-0.94)	1.735(1.642-1.853)	2.274(2.114-2.476)	2.734(2.506-3.019)	3.25(2.939-3.641)
Skamania	360	1.127(1.094-1.165)	2.151(2.073-2.248)	3.039(2.913-3.198)	3.945(3.768-4.169)	5.127(4.882-5.435)
Skamania	720	1.882(1.833-1.934)	3.052(2.941-3.186)	3.938(3.759-4.157)	4.785(4.535-5.092)	5.833(5.488-6.254)
Skamania	1440	3.145(3.096-3.196)	4.837(4.73-4.959)	5.731(5.556-5.935)	6.431(6.184-6.721)	7.174(6.83-7.578)
Skamania	2880	4.624(4.549-4.704)	6.902(6.745-7.08)	8.098(7.861-8.375)	9.021(8.704-9.392)	9.976(9.56-10.463)
Skamania	4320	5.516(5.432-5.609)	8.196(8.011-8.41)	9.67(9.374-10.017)	10.844(10.435-11.322)	12.093(11.541-12.74)
Skamania	5760	6.718(6.609-6.834)	9.858(9.638-10.12)	11.541(11.198-11.959)	12.863(12.398-13.433)	14.253(13.63-15.022)
Skamania	7200	7.277(7.168-7.39)	10.516(10.299-10.761)	12.219(11.886-12.6)	13.557(13.104-14.071)	14.965(14.371-15.646)

Skamania	8640	7.835(7.711-7.96)	11.356(11.122-11.614)	13.108(12.762-13.495)	14.422(13.967-14.935)	15.75(15.169-16.413)
Skamania	10080	8.537(8.403-8.672)	12.379(12.144-12.65)	14.226(13.899-14.628)	15.568(15.144-16.104)	16.883(16.343-17.573)
Skamania	11520	8.889(8.744-9.027)	12.71(12.476-12.979)	14.49(14.157-14.891)	15.767(15.343-16.3)	17.006(16.472-17.693)
Skamania	12960	10.044(9.891-10.206)	14.116(13.87-14.41)	15.957(15.609-16.386)	17.262(16.813-17.816)	18.517(17.951-19.222)
Skamania	14400	10.726(10.56-10.897)	14.923(14.663-15.23)	16.795(16.435-17.236)	18.12(17.665-18.676)	19.396(18.831-20.089)
Snohomish	15	0.324(0.309-0.343)	0.924(0.867-1)	1.326(1.22-1.469)	1.672(1.512-1.891)	2.062(1.832-2.381)
Snohomish	30	0.405(0.386-0.427)	1.045(0.979-1.13)	1.444(1.325-1.602)	1.774(1.599-2.013)	2.136(1.888-2.481)
Snohomish	60	0.46(0.439-0.488)	1.206(1.143-1.284)	1.838(1.738-1.961)	2.506(2.369-2.671)	3.432(3.251-3.651)
Snohomish	120	0.677(0.65-0.707)	1.344(1.269-1.435)	1.838(1.711-1.99)	2.506(2.325-2.722)	3.432(3.177-3.736)
Snohomish	180	0.791(0.765-0.82)	1.47(1.398-1.561)	1.92(1.796-2.078)	2.506(2.325-2.39)	3.432(3.182-2.932)
Snohomish	360	1.101(1.069-1.136)	2.011(1.938-2.1)	2.773(2.656-2.919)	3.54(3.377-3.744)	4.532(4.308-4.811)
Snohomish	720	1.568(1.526-1.613)	2.597(2.502-2.712)	3.417(3.264-3.605)	4.22(4.007-4.484)	5.236(4.942-5.598)
Snohomish	1440	2.319(2.287-2.352)	3.449(3.383-3.524)	4.065(3.958-4.188)	4.556(4.407-4.729)	5.236(5.032-5.473)
Snohomish	2880	3.33(3.284-3.38)	4.947(4.855-5.057)	5.776(5.639-5.945)	6.401(6.217-6.628)	7.031(6.794-7.328)
Snohomish	4320	3.89(3.839-3.948)	5.717(5.61-5.843)	6.674(6.505-6.871)	7.409(7.18-7.678)	8.166(7.864-8.523)
Snohomish	5760	4.454(4.394-4.519)	6.484(6.366-6.628)	7.541(7.357-7.767)	8.349(8.1-8.658)	9.178(8.848-9.592)
Snohomish	7200	5.065(4.997-5.135)	7.332(7.198-7.482)	8.491(8.286-8.723)	9.375(9.097-9.688)	10.281(9.917-10.695)
Snohomish	8640	5.572(5.494-5.653)	8.044(7.9-8.213)	9.279(9.066-9.54)	10.195(9.91-10.544)	11.106(10.738-11.563)
Snohomish	10080	6.111(6.025-6.196)	8.759(8.61-8.932)	10.045(9.832-10.309)	10.984(10.704-11.338)	11.908(11.547-12.369)
Snohomish	11520	6.566(6.475-6.657)	9.324(9.169-9.509)	10.64(10.417-10.919)	11.596(11.305-11.967)	12.533(12.159-13.015)
Snohomish	12960	7.08(6.984-7.176)	9.965(9.803-10.153)	11.318(11.086-11.595)	12.296(11.997-12.658)	13.254(12.875-13.715)
Snohomish	14400	7.294(7.199-7.396)	10.212(10.053-10.406)	11.571(11.342-11.859)	12.545(12.248-12.923)	13.49(13.111-13.975)
Spokane	15	0.218(0.208-0.229)	0.523(0.496-0.559)	0.71(0.663-0.771)	0.862(0.795-0.951)	1.027(0.935-1.15)
Spokane	30	0.279(0.267-0.291)	0.622(0.588-0.664)	0.835(0.777-0.912)	1.013(0.927-1.128)	1.207(1.085-1.374)
Spokane	60	0.33(0.317-0.346)	0.644(0.608-0.691)	0.867(0.804-0.949)	1.076(0.984-1.196)	1.333(1.2-1.505)
Spokane	120	0.447(0.434-0.462)	0.783(0.749-0.825)	1.015(0.959-1.085)	1.222(1.142-1.321)	1.461(1.35-1.6)
Spokane	180	0.566(0.549-0.584)	0.928(0.892-0.973)	1.134(1.08-1.205)	1.305(1.231-1.401)	1.495(1.396-1.619)
Spokane	360	0.74(0.72-0.761)	1.136(1.097-1.186)	1.405(1.343-1.484)	1.647(1.562-1.756)	1.935(1.82-2.081)
Spokane	720	0.922(0.899-0.947)	1.4(1.351-1.46)	1.712(1.633-1.806)	1.992(1.883-2.12)	2.322(2.173-2.493)
Spokane	1440	1.408(1.388-1.428)	2.095(2.053-2.145)	2.475(2.406-2.558)	2.776(2.679-2.895)	3.097(2.963-3.261)

Spokane	2880	1.956(1.929-1.985)	2.87(2.814-2.936)	3.345(3.259-3.447)	3.708(3.593-3.846)	4.08(3.931-4.264)
Spokane	4320	2.065(2.038-2.094)	3.006(2.952-3.071)	3.506(3.42-3.608)	3.893(3.774-4.035)	4.293(4.134-4.486)
Spokane	5760	2.327(2.296-2.358)	3.335(3.27-3.408)	3.908(3.804-4.026)	4.379(4.233-4.545)	4.894(4.693-5.122)
Spokane	7200	2.579(2.545-2.614)	3.676(3.607-3.76)	4.29(4.179-4.423)	4.789(4.631-4.975)	5.33(5.114-5.581)
Spokane	8640	2.953(2.916-2.991)	4.203(4.127-4.287)	4.883(4.765-5.015)	5.425(5.263-5.607)	6.002(5.788-6.247)
Spokane	10080	3.141(3.097-3.187)	4.498(4.412-4.601)	5.207(5.075-5.37)	5.738(5.558-5.962)	6.27(6.031-6.572)
Spokane	11520	3.275(3.228-3.323)	4.682(4.59-4.79)	5.428(5.283-5.601)	5.997(5.796-6.237)	6.577(6.306-6.903)
Spokane	12960	3.436(3.387-3.486)	4.912(4.817-5.025)	5.693(5.543-5.873)	6.284(6.078-6.534)	6.884(6.605-7.223)
Spokane	14400	3.437(3.388-3.488)	4.912(4.816-5.023)	5.693(5.542-5.87)	6.284(6.077-6.53)	6.884(6.605-7.215)
Stevens	15	0.252(0.241-0.265)	0.608(0.573-0.654)	0.841(0.781-0.921)	1.04(0.953-1.156)	1.261(1.141-1.424)
Stevens	30	0.316(0.302-0.331)	0.702(0.661-0.754)	0.955(0.883-1.05)	1.171(1.065-1.314)	1.412(1.262-1.618)
Stevens	60	0.369(0.354-0.387)	0.725(0.684-0.78)	0.983(0.911-1.077)	1.229(1.123-1.366)	1.536(1.384-1.731)
Stevens	120	0.485(0.47-0.502)	0.852(0.814-0.899)	1.106(1.043-1.184)	1.332(1.243-1.443)	1.594(1.47-1.749)
Stevens	180	0.548(0.533-0.565)	0.919(0.884-0.962)	1.146(1.09-1.214)	1.341(1.264-1.435)	1.594(1.489-1.719)
Stevens	360	0.873(0.85-0.898)	1.337(1.292-1.396)	1.641(1.572-1.735)	1.909(1.813-2.038)	2.219(2.09-2.393)
Stevens	720	0.977(0.953-1.004)	1.499(1.445-1.563)	1.844(1.757-1.945)	2.154(2.033-2.294)	2.522(2.355-2.709)
Stevens	1440	1.287(1.271-1.305)	1.912(1.873-1.955)	2.275(2.211-2.348)	2.576(2.484-2.682)	2.91(2.781-3.057)
Stevens	2880	1.699(1.677-1.723)	2.488(2.442-2.542)	2.901(2.83-2.987)	3.218(3.122-3.336)	3.543(3.417-3.7)
Stevens	4320	1.857(1.833-1.883)	2.697(2.648-2.754)	3.14(3.065-3.232)	3.482(3.38-3.609)	3.835(3.697-4.005)
Stevens	5760	2.173(2.145-2.202)	3.118(3.062-3.185)	3.634(3.545-3.741)	4.042(3.919-4.192)	4.476(4.309-4.68)
Stevens	7200	2.427(2.395-2.46)	3.473(3.41-3.548)	4.032(3.934-4.15)	4.47(4.333-4.633)	4.928(4.745-5.148)
Stevens	8640	2.857(2.821-2.895)	4.068(3.995-4.149)	4.701(4.591-4.829)	5.192(5.043-5.365)	5.699(5.504-5.931)
Stevens	10080	3.014(2.973-3.056)	4.287(4.21-4.376)	4.939(4.824-5.079)	5.427(5.273-5.619)	5.919(5.715-6.175)
Stevens	11520	3.328(3.282-3.376)	4.718(4.627-4.825)	5.47(5.326-5.642)	6.062(5.862-6.302)	6.686(6.414-7.011)
Stevens	12960	3.512(3.462-3.564)	4.981(4.885-5.094)	5.748(5.599-5.927)	6.327(6.123-6.572)	6.912(6.64-7.24)
Stevens	14400	3.566(3.514-3.62)	5.039(4.941-5.154)	5.792(5.642-5.972)	6.347(6.145-6.593)	6.912(6.644-7.239)
Thurston	15	0.344(0.328-0.363)	0.846(0.793-0.917)	1.184(1.086-1.317)	1.483(1.333-1.688)	1.831(1.613-2.136)
Thurston	30	0.43(0.41-0.454)	1.038(0.97-1.131)	1.446(1.317-1.629)	1.806(1.607-2.096)	2.224(1.928-2.662)
Thurston	60	0.436(0.417-0.46)	1.175(1.121-1.242)	1.88(1.793-1.989)	2.674(2.552-2.823)	3.822(3.657-4.025)
Thurston	120	0.721(0.695-0.749)	1.39(1.311-1.484)	1.88(1.741-2.046)	2.674(2.468-2.916)	3.822(3.522-4.175)

Thurston	180	0.868(0.842-0.898)	1.592(1.518-1.686)	2.079(1.952-2.243)	2.674(2.485-2.53)	3.822(3.557-3.157)
Thurston	360	1.3(1.263-1.342)	2.337(2.254-2.44)	3.201(3.069-3.369)	4.069(3.886-4.304)	5.192(4.942-5.514)
Thurston	720	1.79(1.741-1.844)	3.075(2.959-3.216)	4.157(3.97-4.389)	5.244(4.98-5.571)	6.642(6.278-7.093)
Thurston	1440	2.395(2.361-2.431)	3.514(3.447-3.596)	4.157(4.051-4.29)	5.244(5.097-5.428)	6.642(6.442-6.891)
Thurston	2880	3.712(3.66-3.766)	5.467(5.366-5.592)	6.386(6.233-6.586)	7.086(6.88-7.359)	7.799(7.528-8.166)
Thurston	4320	4.541(4.48-4.608)	6.611(6.485-6.758)	7.676(7.485-7.903)	8.484(8.228-8.789)	9.307(8.976-9.707)
Thurston	5760	5.006(4.936-5.077)	7.204(7.075-7.353)	8.304(8.11-8.532)	9.124(8.867-9.43)	9.946(9.612-10.35)
Thurston	7200	5.783(5.709-5.86)	8.185(8.037-8.354)	9.46(9.226-9.728)	10.468(10.145-10.84)	11.537(11.105-12.039)
Thurston	8640	6.372(6.288-6.457)	9.11(8.943-9.296)	10.566(10.306-10.86)	11.715(11.356-12.118)	12.931(12.45-13.476)
Thurston	10080	6.721(6.633-6.81)	9.464(9.301-9.638)	10.852(10.608-11.114)	11.909(11.588-12.259)	12.993(12.575-13.446)
Thurston	11520	7.085(6.994-7.177)	9.879(9.717-10.062)	11.262(11.024-11.534)	12.307(11.993-12.667)	13.372(12.961-13.836)
Thurston	12960	7.399(7.308-7.494)	10.239(10.083-10.42)	11.622(11.393-11.888)	12.658(12.353-13.007)	13.705(13.309-14.152)
Thurston	14400	7.813(7.718-7.912)	10.713(10.549-10.908)	12.114(11.87-12.412)	13.152(12.825-13.551)	14.191(13.764-14.711)
Wahkiakum	15	0.361(0.344-0.381)	0.955(0.9-1.028)	1.319(1.218-1.454)	1.621(1.47-1.828)	1.957(1.737-2.262)
Wahkiakum	30	0.493(0.47-0.52)	1.167(1.088-1.274)	1.632(1.482-1.845)	2.05(1.819-2.39)	2.542(2.197-3.058)
Wahkiakum	60	0.493(0.473-0.516)	1.336(1.284-1.401)	2.306(2.22-2.414)	3.464(3.342-3.617)	5.205(5.036-5.419)
Wahkiakum	120	0.883(0.851-0.918)	1.738(1.631-1.862)	2.389(2.189-2.621)	3.464(3.158-3.816)	5.205(4.746-5.736)
Wahkiakum	180	1.127(1.096-1.164)	2.034(1.946-2.149)	2.661(2.506-2.859)	3.464(3.232-3.318)	5.205(4.872-4.248)
Wahkiakum	360	1.542(1.495-1.594)	2.989(2.882-3.125)	4.277(4.105-4.5)	5.605(5.362-5.918)	7.351(7.018-7.783)
Wahkiakum	720	2.159(2.096-2.228)	3.856(3.707-4.039)	5.366(5.124-5.668)	6.915(6.574-7.342)	8.941(8.47-9.531)
Wahkiakum	1440	2.849(2.807-2.893)	4.191(4.111-4.298)	5.366(5.237-5.538)	6.915(6.736-7.156)	8.941(8.7-9.27)
Wahkiakum	2880	4.405(4.343-4.474)	6.394(6.271-6.539)	7.367(7.191-7.577)	8.085(7.858-8.354)	8.941(8.656-6.374)
Wahkiakum	4320	5.324(5.25-5.404)	7.575(7.425-7.736)	8.676(8.458-8.922)	9.494(9.213-9.814)	10.313(9.962-10.719)
Wahkiakum	5760	6.167(6.085-6.253)	8.751(8.597-8.932)	10.06(9.823-10.335)	11.042(10.728-11.418)	12.03(11.621-12.537)
Wahkiakum	7200	6.617(6.529-6.708)	9.245(9.09-9.438)	10.564(10.331-10.864)	11.556(11.244-11.969)	12.562(12.153-13.101)
Wahkiakum	8640	7.393(7.292-7.488)	10.301(10.119-10.491)	11.714(11.452-12.005)	12.768(12.425-13.155)	13.835(13.398-14.337)
Wahkiakum	10080	7.405(7.304-7.503)	10.301(10.132-10.485)	11.714(11.473-11.985)	12.768(12.463-13.123)	13.835(13.453-14.284)
Wahkiakum	11520	8.45(8.346-8.561)	11.507(11.338-11.708)	12.899(12.657-13.19)	13.899(13.585-14.271)	14.876(14.479-15.344)
Wahkiakum	12960	9.151(9.035-9.266)	12.395(12.212-12.603)	13.854(13.596-14.155)	14.896(14.565-15.28)	15.912(15.497-16.385)
Wahkiakum	14400	9.727(9.596-9.862)	13.043(12.795-13.331)	14.64(14.262-15.092)	15.771(15.259-16.387)	16.849(16.171-17.669)

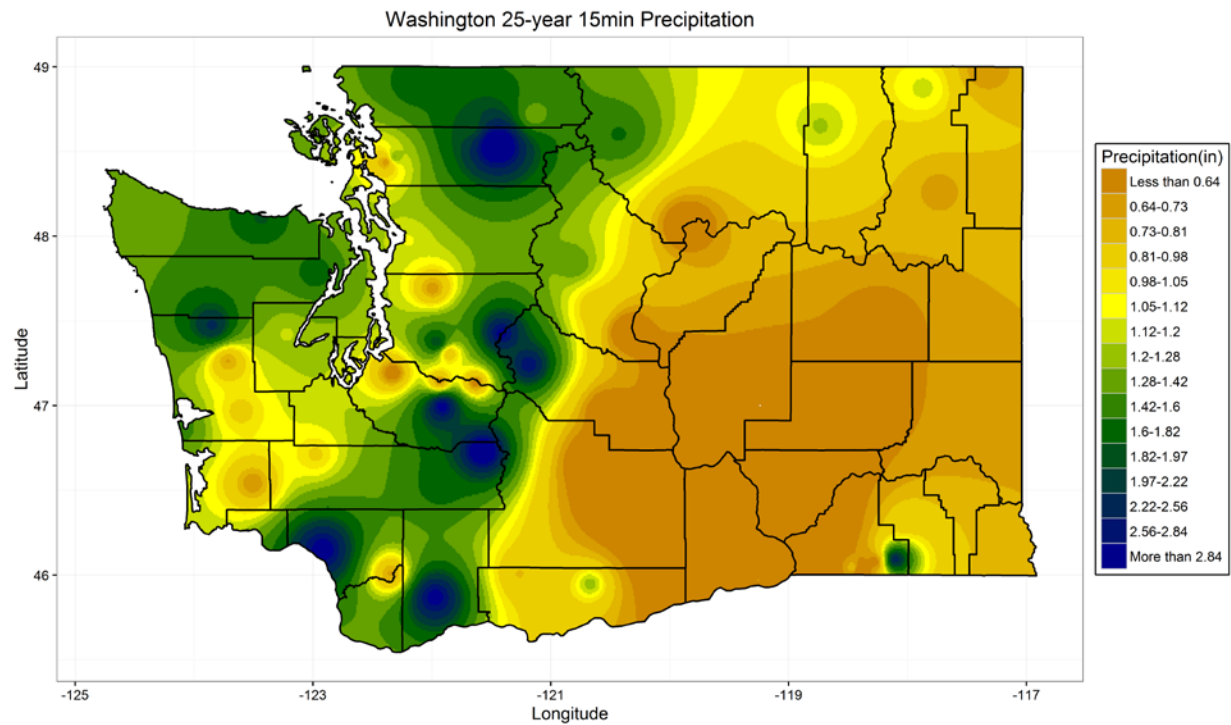
Walla Walla	15	0.201(0.193-0.21)	0.508(0.484-0.54)	0.692(0.65-0.748)	0.84(0.778-0.921)	0.996(0.909-1.11)
Walla Walla	30	0.263(0.253-0.274)	0.618(0.587-0.657)	0.829(0.775-0.899)	0.999(0.92-1.104)	1.181(1.07-1.329)
Walla Walla	60	0.349(0.337-0.364)	0.75(0.712-0.798)	1.006(0.943-1.086)	1.223(1.133-1.336)	1.465(1.341-1.623)
Walla Walla	120	0.445(0.431-0.46)	0.847(0.812-0.89)	1.102(1.046-1.17)	1.323(1.245-1.418)	1.577(1.471-1.705)
Walla Walla	180	0.519(0.505-0.535)	0.964(0.921-1.013)	1.268(1.196-1.352)	1.545(1.438-1.664)	1.872(1.722-2.038)
Walla Walla	360	0.648(0.629-0.67)	1.227(1.179-1.285)	1.678(1.6-1.775)	2.102(1.992-2.24)	2.617(2.463-2.807)
Walla Walla	720	0.845(0.825-0.866)	1.427(1.374-1.483)	1.826(1.74-1.918)	2.192(2.069-2.321)	2.63(2.459-2.807)
Walla Walla	1440	1.137(1.12-1.157)	1.735(1.695-1.783)	2.078(2.012-2.159)	2.356(2.261-2.473)	2.653(2.522-2.818)
Walla Walla	2880	1.556(1.531-1.581)	2.329(2.277-2.391)	2.776(2.691-2.879)	3.144(3.024-3.293)	3.549(3.383-3.754)
Walla Walla	4320	1.785(1.76-1.812)	2.646(2.587-2.714)	3.167(3.066-3.287)	3.613(3.466-3.787)	4.117(3.911-4.364)
Walla Walla	5760	1.938(1.909-1.967)	2.825(2.765-2.893)	3.353(3.254-3.466)	3.797(3.657-3.959)	4.291(4.098-4.515)
Walla Walla	7200	2.306(2.273-2.341)	3.342(3.277-3.423)	3.925(3.823-4.052)	4.396(4.253-4.57)	4.901(4.708-5.133)
Walla Walla	8640	2.374(2.34-2.41)	3.435(3.367-3.512)	4.003(3.897-4.127)	4.451(4.305-4.622)	4.925(4.728-5.153)
Walla Walla	10080	2.551(2.515-2.589)	3.681(3.61-3.769)	4.3(4.188-4.439)	4.797(4.641-4.989)	5.331(5.122-5.59)
Walla Walla	11520	2.61(2.572-2.648)	3.752(3.681-3.836)	4.349(4.239-4.481)	4.812(4.661-4.996)	5.331(5.129-5.58)
Walla Walla	12960	2.886(2.846-2.927)	4.113(4.038-4.202)	4.744(4.629-4.885)	5.23(5.071-5.427)	5.733(5.518-6.001)
Walla Walla	14400	2.929(2.888-2.972)	4.163(4.087-4.251)	4.781(4.666-4.916)	5.249(5.093-5.433)	5.733(5.526-5.979)
Whatcom	15	0.364(0.346-0.386)	1.085(1.014-1.182)	1.602(1.467-1.785)	2.06(1.855-2.341)	2.584(2.289-2.993)
Whatcom	30	0.451(0.429-0.477)	1.183(1.105-1.286)	1.658(1.517-1.844)	2.06(1.854-2.335)	2.584(2.297-2.974)
Whatcom	60	0.461(0.437-0.491)	1.469(1.402-1.552)	2.505(2.398-2.637)	3.709(3.562-3.888)	5.492(5.295-5.731)
Whatcom	120	0.778(0.745-0.814)	1.632(1.528-1.755)	2.505(2.318-2.723)	3.709(3.43-4.031)	5.492(5.082-5.965)
Whatcom	180	0.942(0.909-0.978)	1.837(1.743-1.957)	2.505(2.341-2.454)	3.709(3.467-3.128)	5.492(5.151-3.967)
Whatcom	360	1.278(1.238-1.321)	2.549(2.455-2.664)	3.686(3.532-3.877)	4.86(4.642-5.129)	6.403(6.101-6.776)
Whatcom	720	1.902(1.847-1.963)	3.398(3.265-3.562)	4.722(4.504-4.995)	6.077(5.768-6.462)	7.841(7.414-8.373)
Whatcom	1440	2.3(2.271-2.33)	3.398(3.338-3.467)	4.722(4.629-4.834)	6.077(5.948-6.233)	7.841(7.669-8.055)
Whatcom	2880	3.308(3.267-3.354)	4.928(4.841-5.031)	5.763(5.631-5.923)	6.394(6.218-6.608)	7.841(7.614-5.174)
Whatcom	4320	3.843(3.793-3.896)	5.654(5.551-5.769)	6.588(6.427-6.765)	7.293(7.08-7.532)	8.008(7.73-8.321)
Whatcom	5760	4.38(4.329-4.439)	6.35(6.244-6.474)	7.367(7.204-7.564)	8.137(7.914-8.406)	8.914(8.62-9.275)
Whatcom	7200	5.055(4.99-5.119)	7.332(7.202-7.47)	8.525(8.322-8.741)	9.431(9.153-9.732)	10.35(9.984-10.756)
Whatcom	8640	5.416(5.345-5.486)	7.774(7.64-7.927)	8.989(8.789-9.232)	9.902(9.631-10.235)	10.819(10.464-11.258)

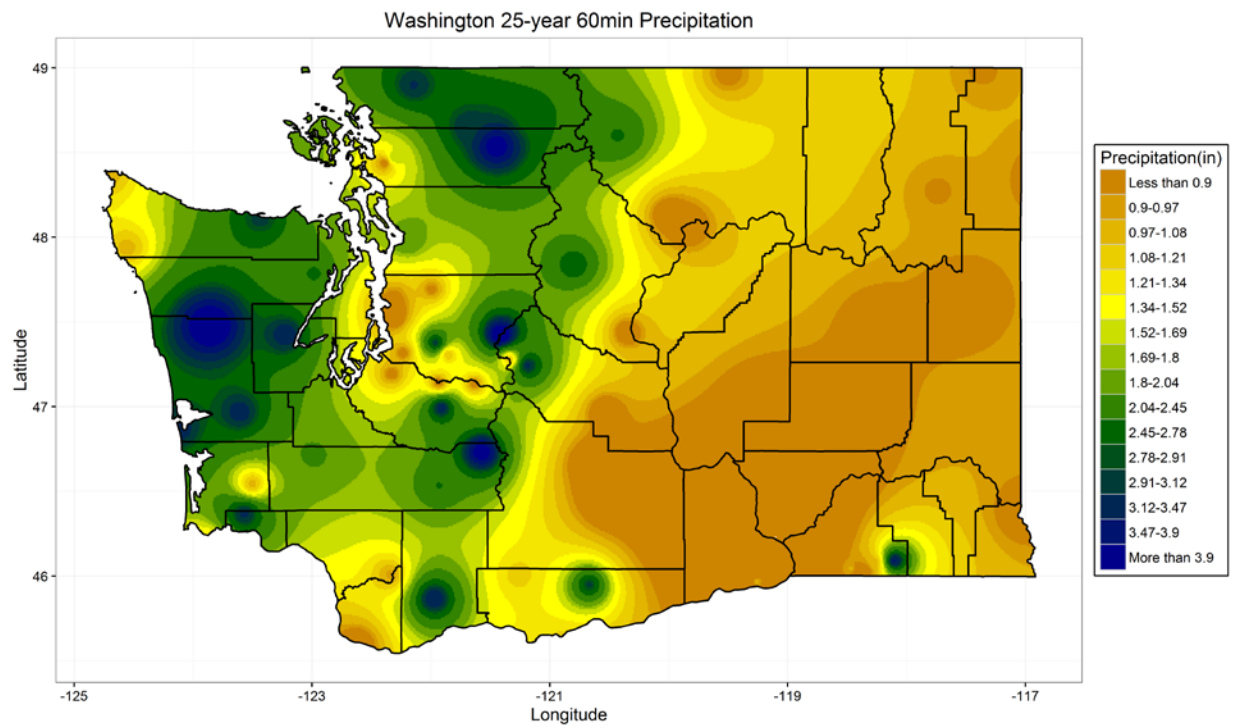
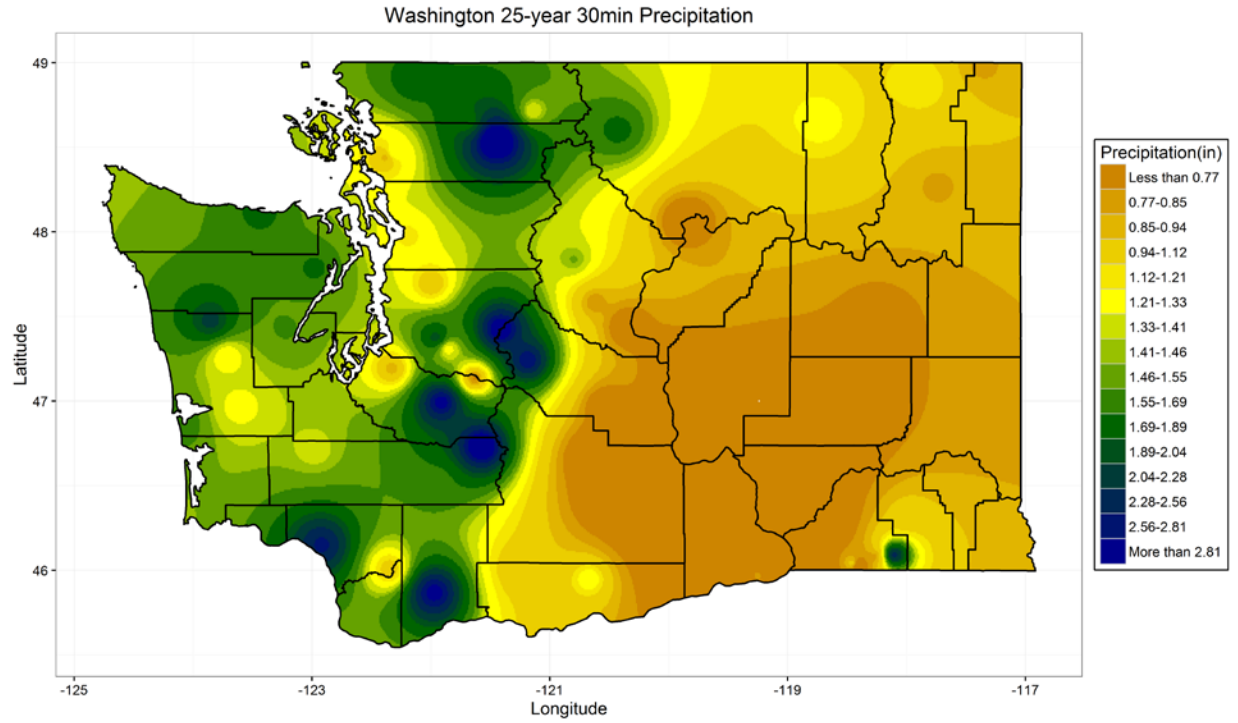
Whatcom	10080	5.893(5.818-5.964)	8.393(8.259-8.546)	9.636(9.442-9.877)	10.555(10.297-10.88)	11.466(11.131-11.898)
Whatcom	11520	6.481(6.403-6.559)	9.193(9.051-9.357)	10.524(10.315-10.78)	11.501(11.225-11.847)	12.465(12.107-12.922)
Whatcom	12960	6.649(6.569-6.727)	9.371(9.227-9.531)	10.67(10.461-10.908)	11.615(11.344-11.927)	12.543(12.201-12.941)
Whatcom	14400	7.056(6.972-7.145)	9.973(9.824-10.15)	11.373(11.159-11.637)	12.385(12.106-12.736)	13.372(13.011-13.824)
Whitman	15	0.201(0.192-0.211)	0.497(0.471-0.531)	0.68(0.635-0.739)	0.83(0.765-0.916)	0.993(0.902-1.114)
Whitman	30	0.261(0.251-0.273)	0.597(0.566-0.638)	0.805(0.749-0.877)	0.976(0.894-1.084)	1.162(1.047-1.317)
Whitman	60	0.33(0.318-0.343)	0.685(0.65-0.727)	0.929(0.871-1.003)	1.151(1.066-1.258)	1.416(1.298-1.569)
Whitman	120	0.437(0.424-0.451)	0.801(0.768-0.843)	1.041(0.985-1.11)	1.252(1.173-1.35)	1.498(1.387-1.634)
Whitman	180	0.525(0.51-0.541)	0.922(0.884-0.968)	1.178(1.115-1.255)	1.405(1.314-1.513)	1.669(1.543-1.817)
Whitman	360	0.685(0.666-0.706)	1.2(1.155-1.255)	1.587(1.514-1.677)	1.948(1.845-2.074)	2.384(2.242-2.558)
Whitman	720	0.884(0.863-0.907)	1.453(1.4-1.513)	1.847(1.761-1.944)	2.211(2.088-2.346)	2.649(2.477-2.832)
Whitman	1440	1.209(1.191-1.229)	1.815(1.775-1.864)	2.157(2.09-2.238)	2.431(2.335-2.549)	2.722(2.591-2.887)
Whitman	2880	1.597(1.573-1.622)	2.361(2.311-2.423)	2.781(2.702-2.883)	3.114(3.004-3.259)	3.467(3.317-3.665)
Whitman	4320	1.95(1.923-1.979)	2.871(2.81-2.94)	3.395(3.295-3.51)	3.82(3.679-3.985)	4.28(4.087-4.509)
Whitman	5760	2.154(2.125-2.185)	3.117(3.052-3.19)	3.685(3.578-3.807)	4.162(4.01-4.336)	4.695(4.483-4.938)
Whitman	7200	2.309(2.277-2.343)	3.322(3.255-3.405)	3.905(3.796-4.037)	4.386(4.23-4.571)	4.916(4.7-5.167)
Whitman	8640	2.459(2.424-2.496)	3.537(3.467-3.617)	4.113(4.006-4.241)	4.565(4.419-4.742)	5.04(4.845-5.278)
Whitman	10080	2.624(2.585-2.663)	3.773(3.698-3.864)	4.382(4.268-4.526)	4.85(4.694-5.049)	5.334(5.127-5.603)
Whitman	11520	2.79(2.749-2.832)	4.007(3.922-4.103)	4.68(4.543-4.837)	5.219(5.026-5.442)	5.797(5.531-6.105)
Whitman	12960	2.973(2.929-3.016)	4.268(4.18-4.371)	4.985(4.845-5.156)	5.561(5.363-5.805)	6.178(5.906-6.521)
Whitman	14400	3.127(3.082-3.173)	4.491(4.398-4.595)	5.241(5.091-5.411)	5.842(5.631-6.085)	6.486(6.196-6.82)
Yakima	15	0.222(0.213-0.233)	0.568(0.54-0.604)	0.765(0.717-0.829)	0.919(0.85-1.012)	1.08(0.983-1.209)
Yakima	30	0.289(0.277-0.302)	0.675(0.641-0.718)	0.898(0.838-0.976)	1.074(0.985-1.193)	1.26(1.134-1.433)
Yakima	60	0.371(0.357-0.389)	0.819(0.776-0.873)	1.12(1.049-1.209)	1.388(1.288-1.512)	1.705(1.569-1.877)
Yakima	120	0.49(0.473-0.51)	0.939(0.895-0.995)	1.218(1.146-1.31)	1.456(1.354-1.583)	1.722(1.583-1.899)
Yakima	180	0.585(0.567-0.604)	1.055(1.008-1.112)	1.352(1.273-1.448)	1.607(1.496-1.741)	1.897(1.745-2.079)
Yakima	360	0.758(0.737-0.781)	1.38(1.329-1.442)	1.874(1.789-1.975)	2.353(2.233-2.496)	2.952(2.786-3.152)
Yakima	720	1.054(1.028-1.082)	1.761(1.695-1.836)	2.273(2.164-2.397)	2.755(2.599-2.929)	3.343(3.123-3.581)
Yakima	1440	2.047(2.015-2.081)	3.158(3.086-3.24)	3.77(3.651-3.908)	4.261(4.093-4.46)	4.792(4.559-5.071)
Yakima	2880	2.93(2.883-2.982)	4.427(4.326-4.545)	5.25(5.091-5.438)	5.906(5.688-6.164)	6.606(6.313-6.952)

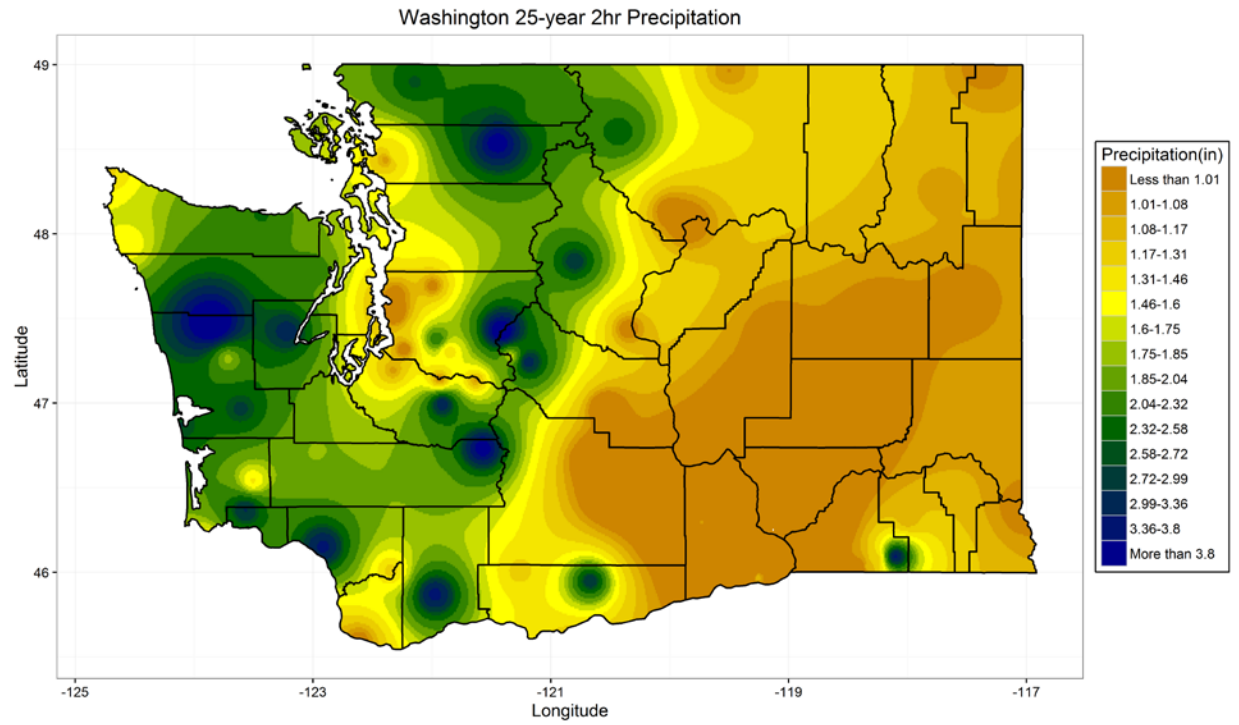
Yakima	4320	3.701(3.642-3.766)	5.562(5.433-5.714)	6.599(6.392-6.848)	7.434(7.146-7.78)	8.331(7.94-8.802)
Yakima	5760	4.243(4.173-4.317)	6.261(6.122-6.427)	7.36(7.145-7.62)	8.234(7.944-8.584)	9.163(8.779-9.628)
Yakima	7200	4.682(4.608-4.762)	6.876(6.726-7.051)	8.06(7.828-8.33)	9.001(8.683-9.366)	10.001(9.584-10.486)
Yakima	8640	5.057(4.976-5.144)	7.421(7.264-7.603)	8.637(8.399-8.911)	9.571(9.252-9.936)	10.538(10.122-11.014)
Yakima	10080	5.417(5.329-5.509)	7.973(7.813-8.162)	9.245(9.015-9.53)	10.194(9.891-10.576)	11.148(10.758-11.647)
Yakima	11520	5.932(5.834-6.032)	8.618(8.445-8.82)	9.931(9.678-10.236)	10.907(10.576-11.314)	11.887(11.462-12.416)
Yakima	12960	6.374(6.274-6.482)	9.095(8.926-9.299)	10.386(10.139-10.687)	11.334(11.01-11.729)	12.277(11.861-12.784)
Yakima	14400	6.805(6.695-6.918)	9.637(9.457-9.853)	10.963(10.705-11.281)	11.93(11.597-12.344)	12.888(12.466-13.415)

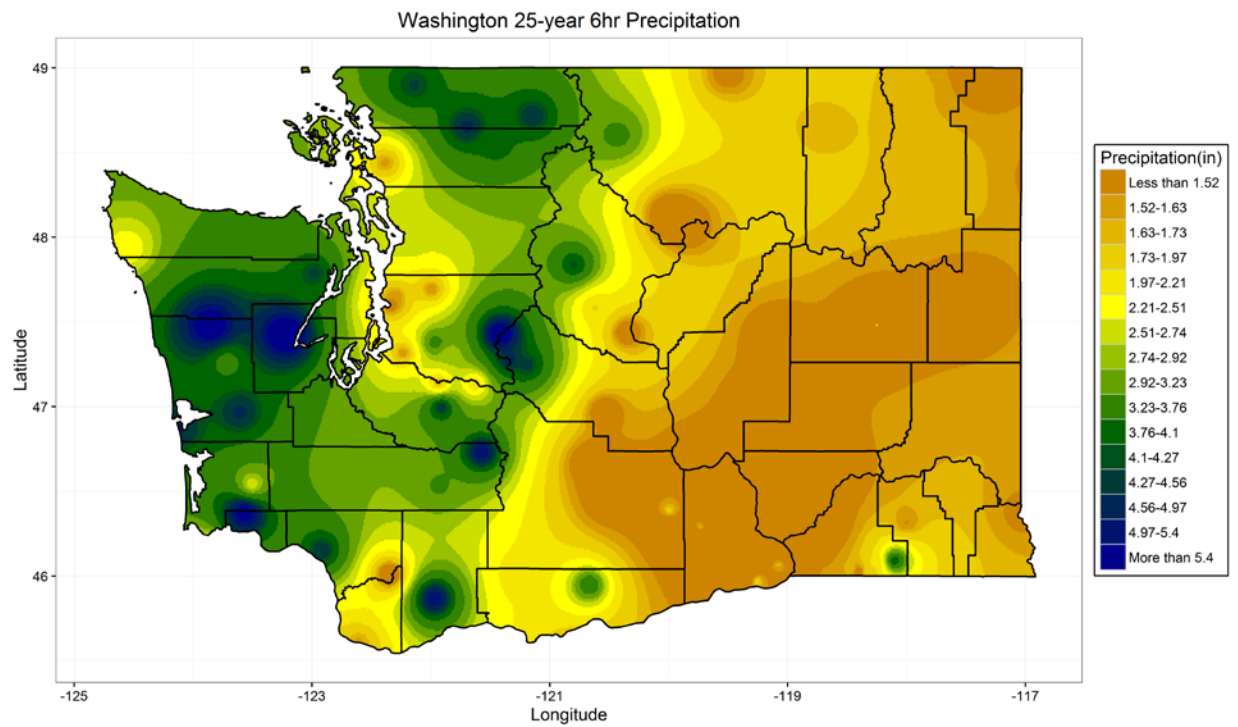
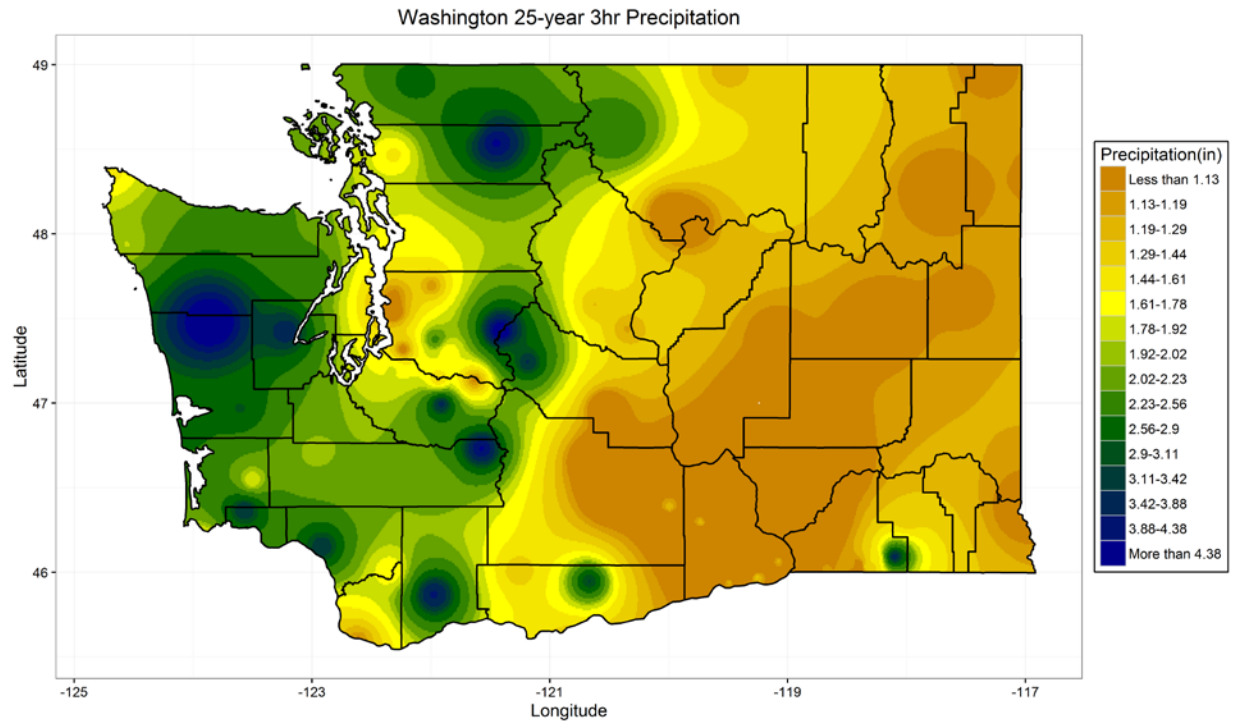
Appendix D

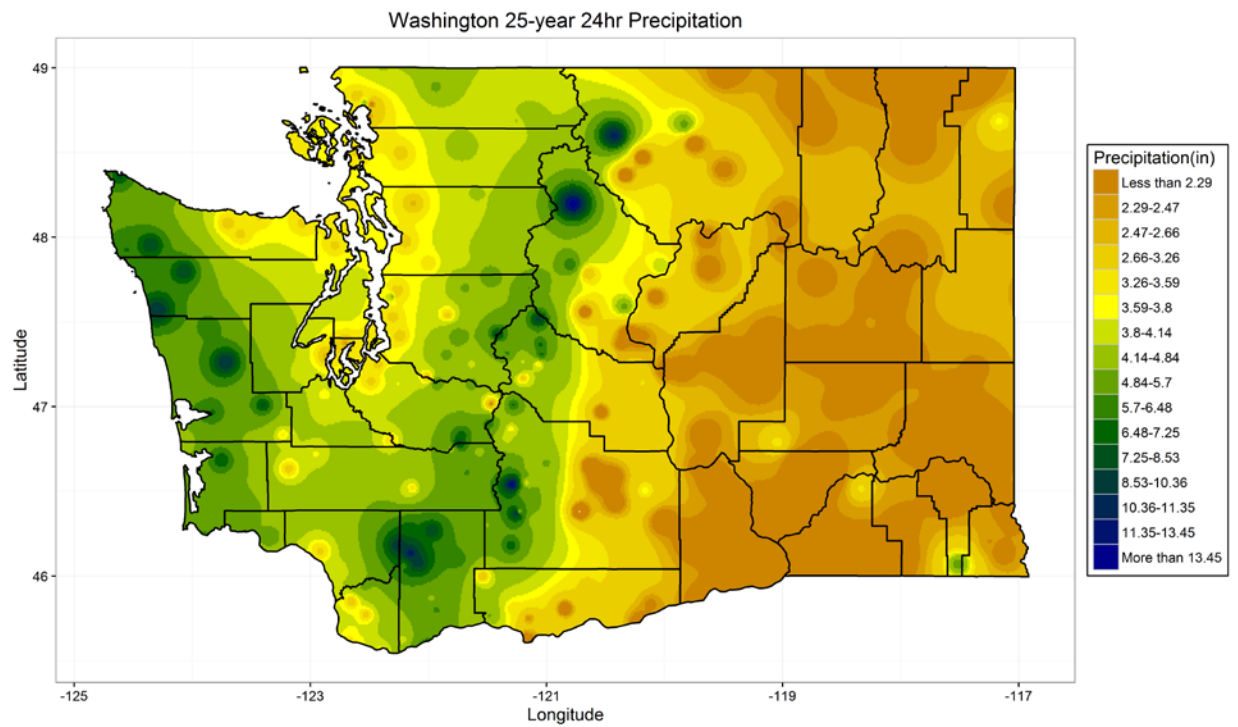
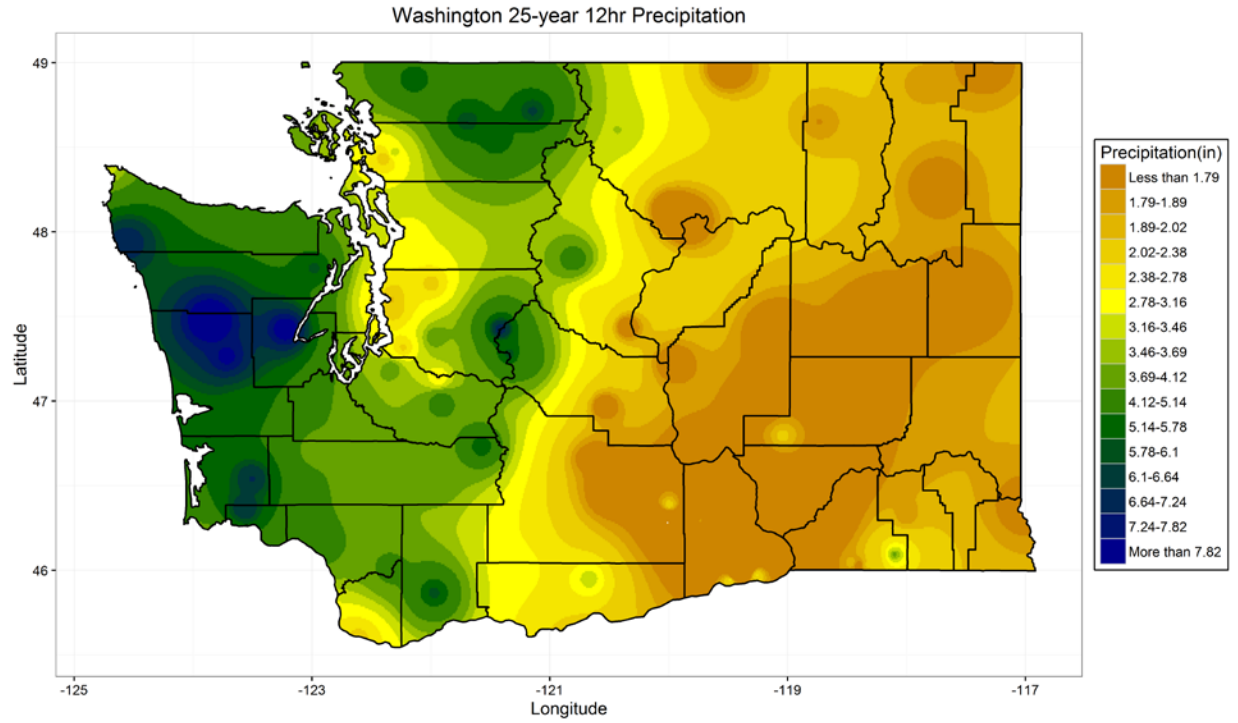
Spatial maps of the extreme precipitation

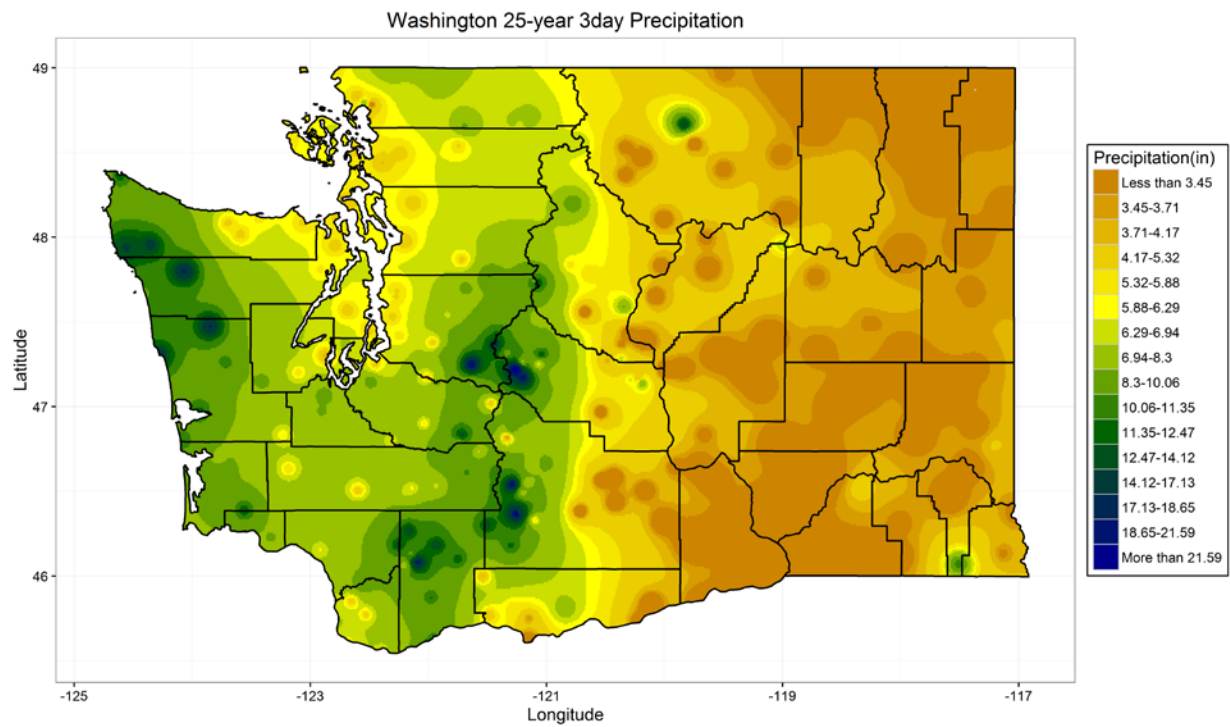
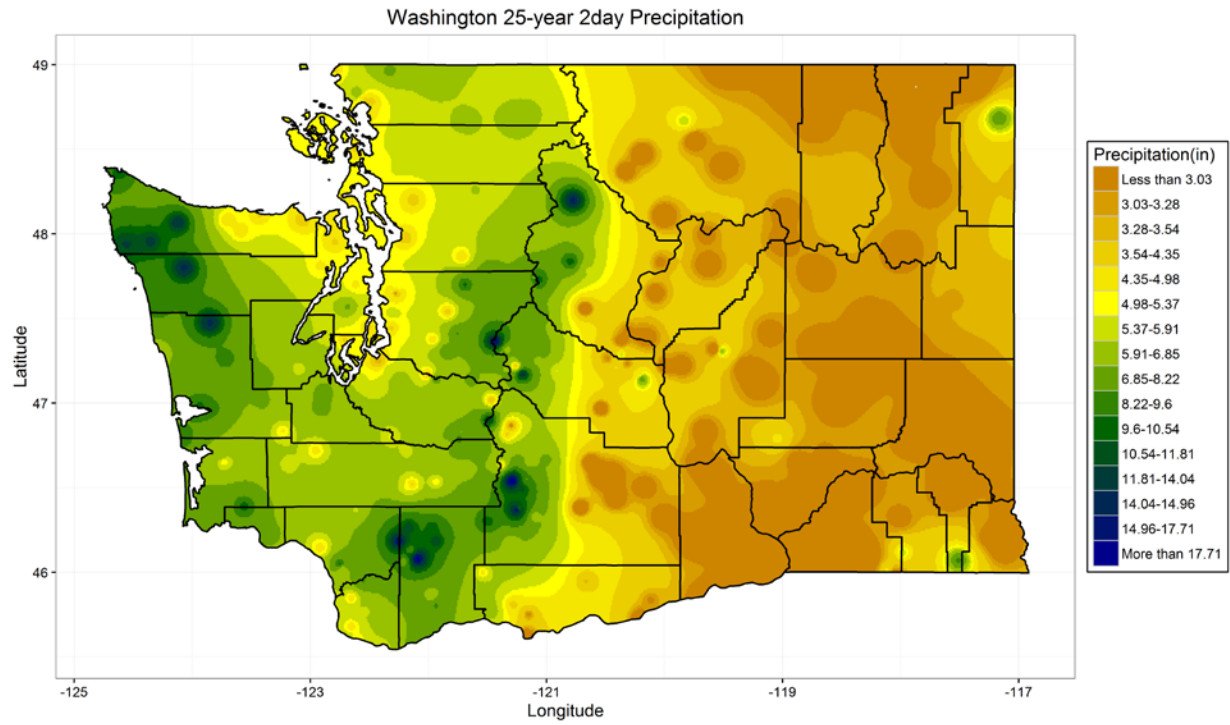


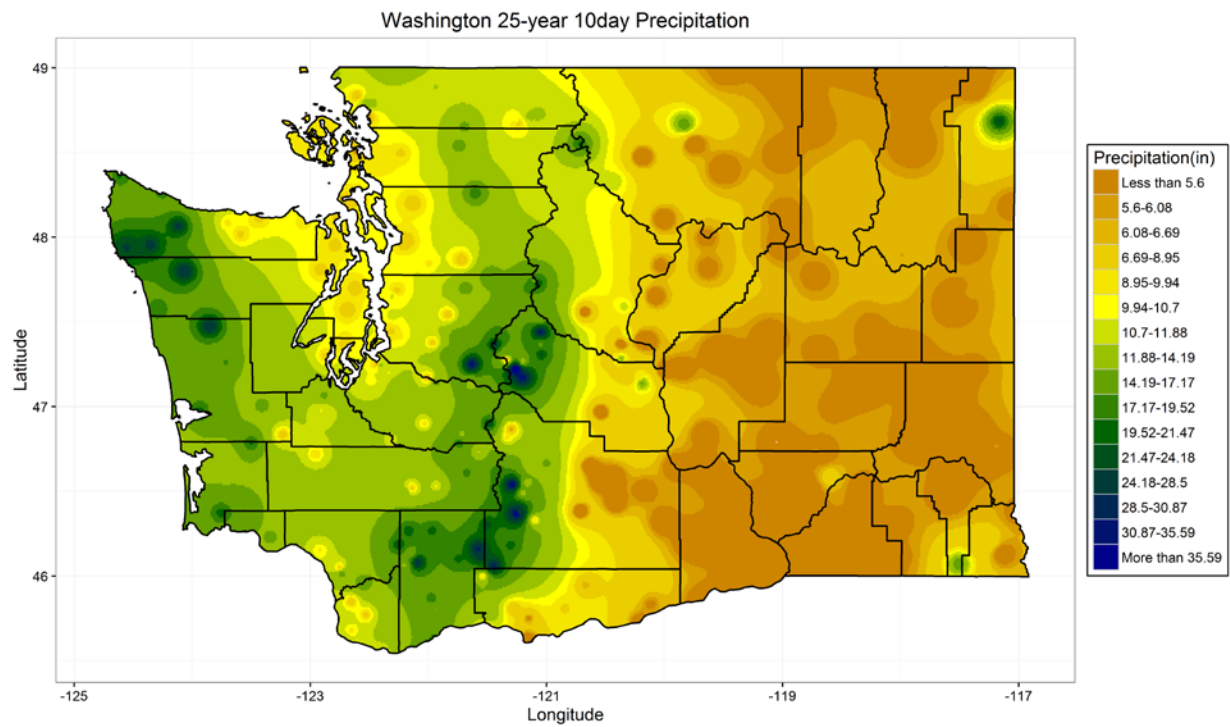
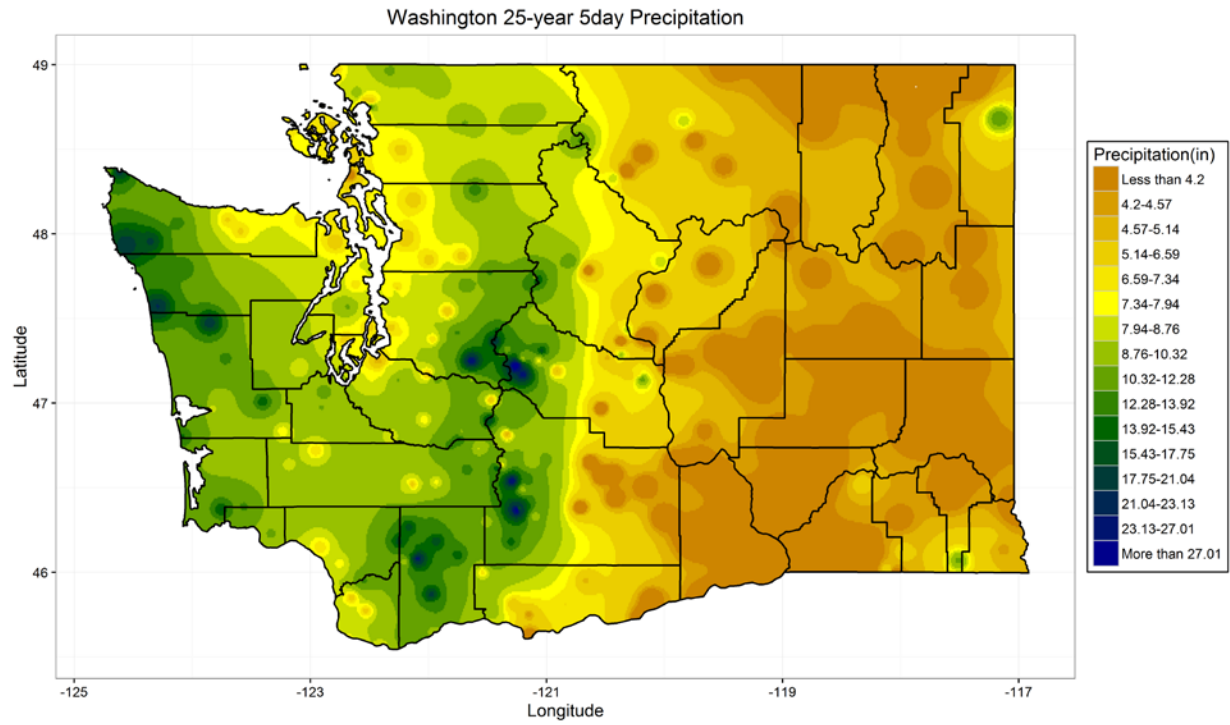


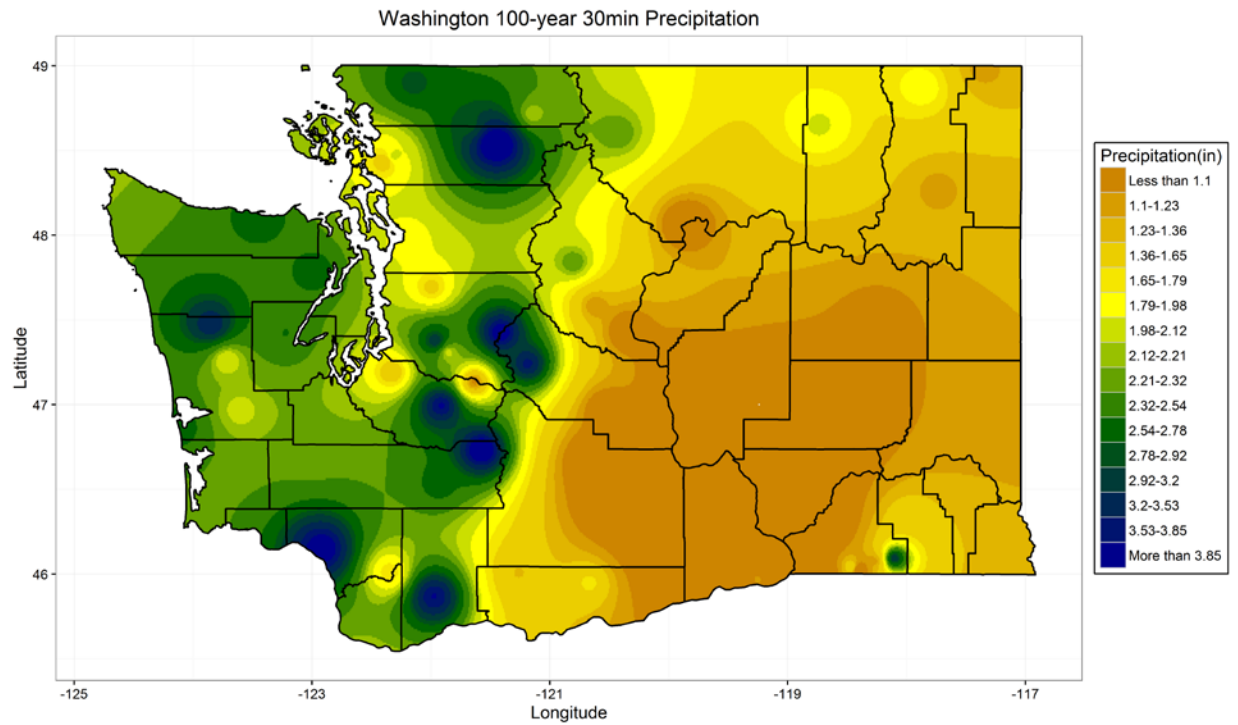
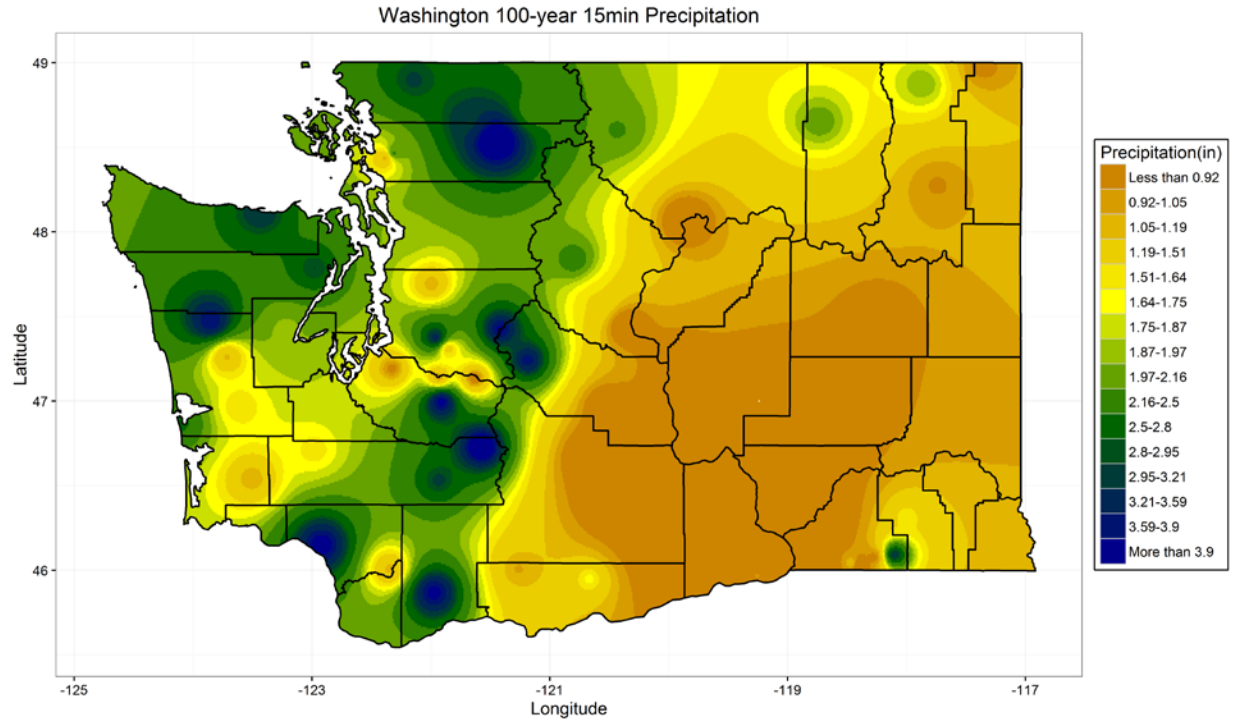


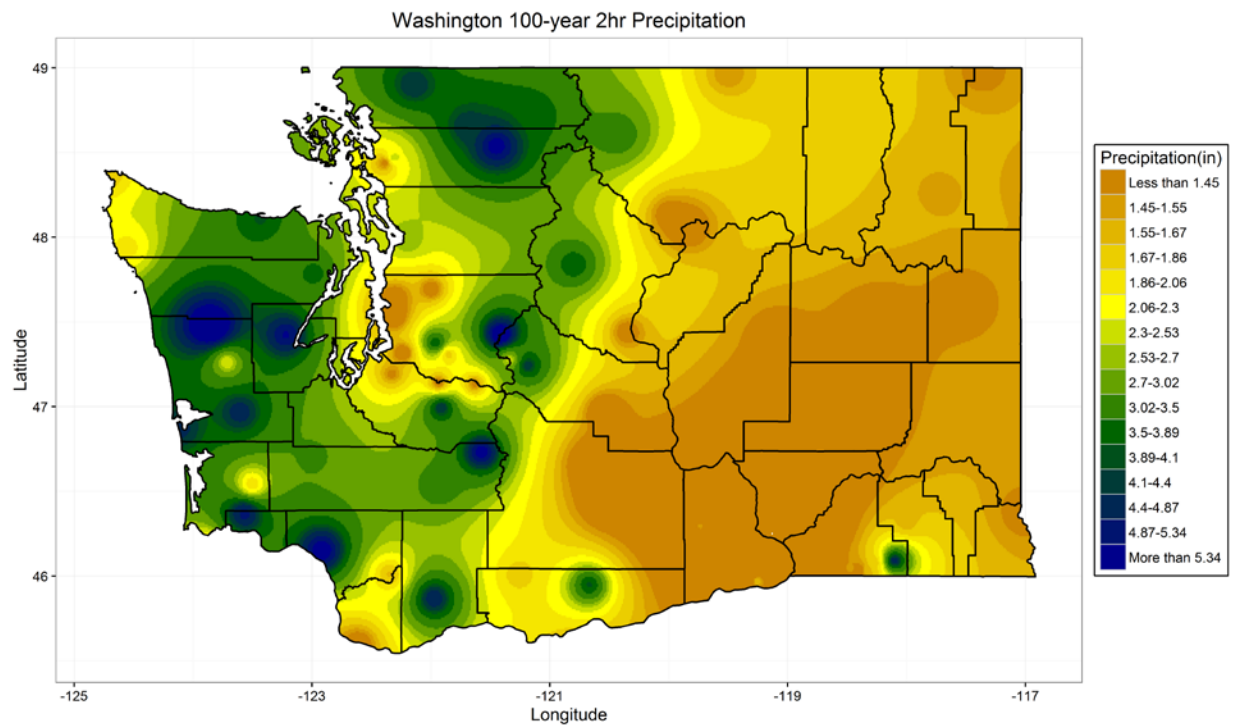
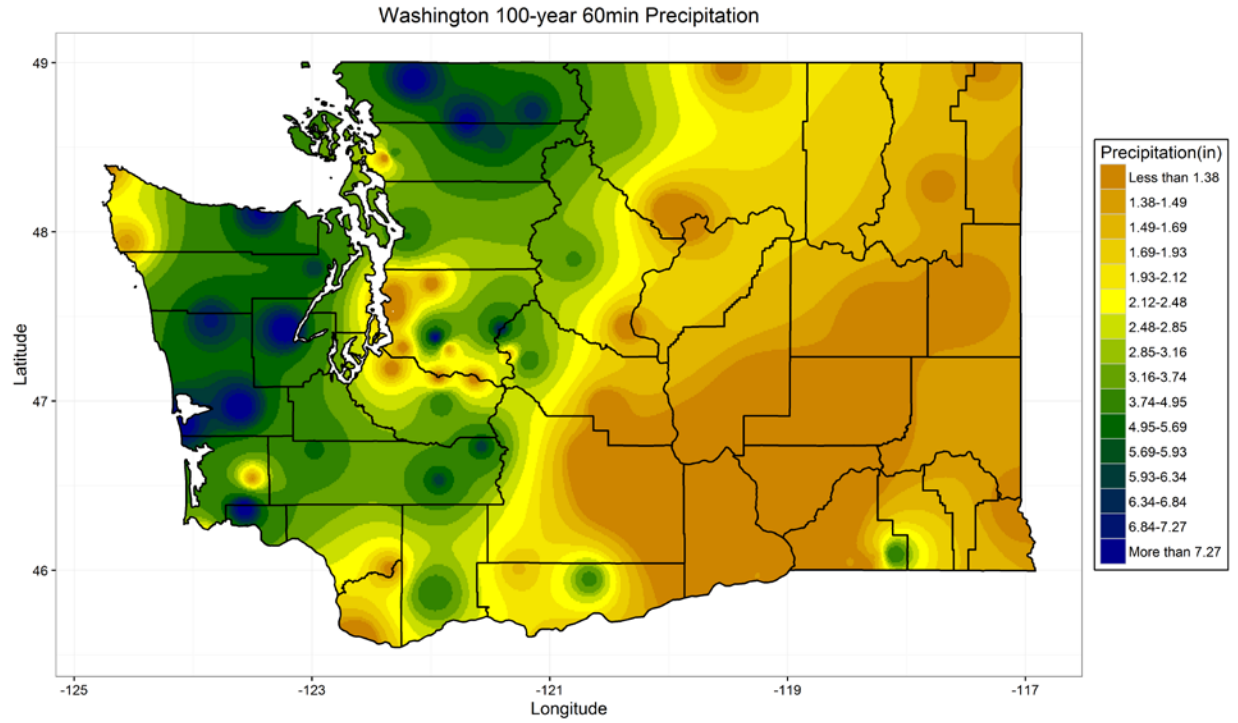


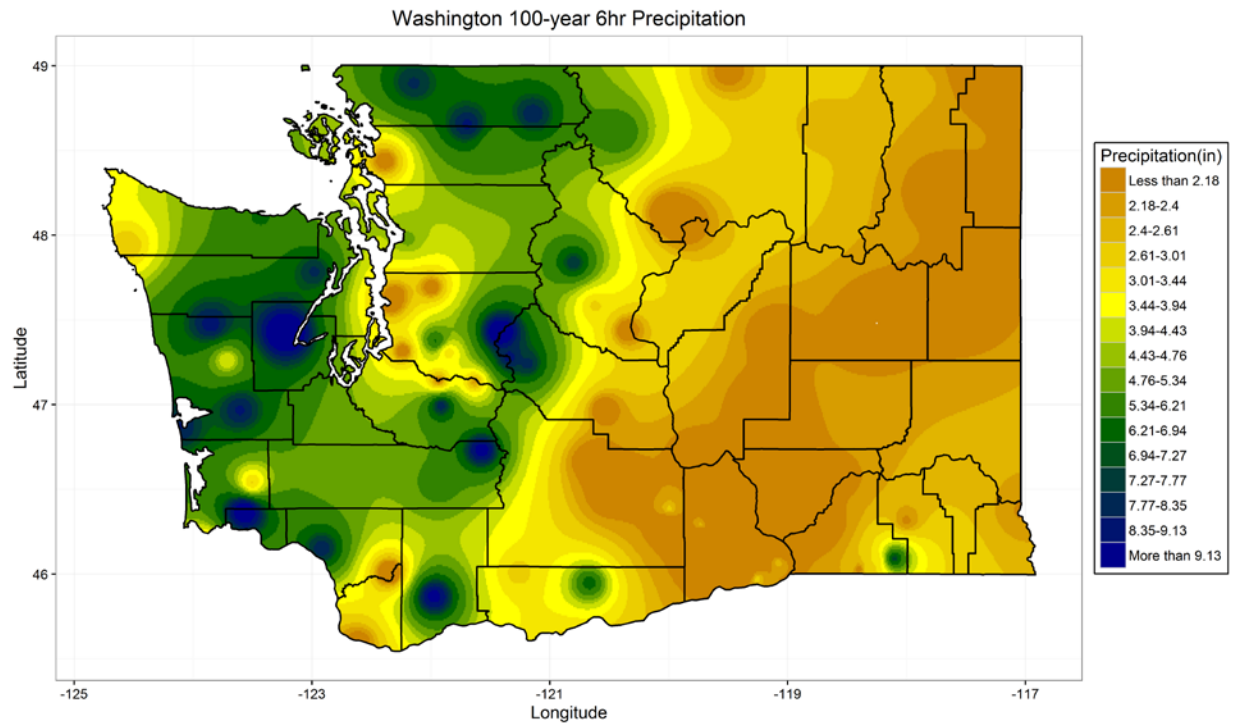
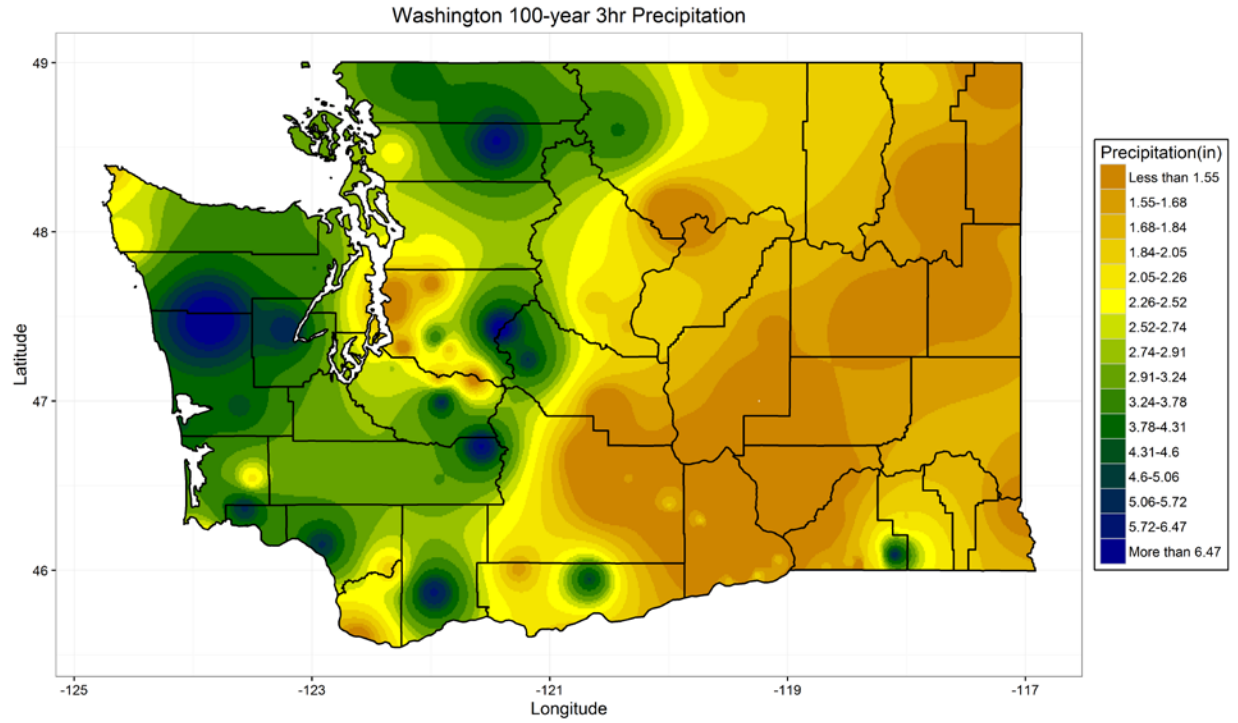


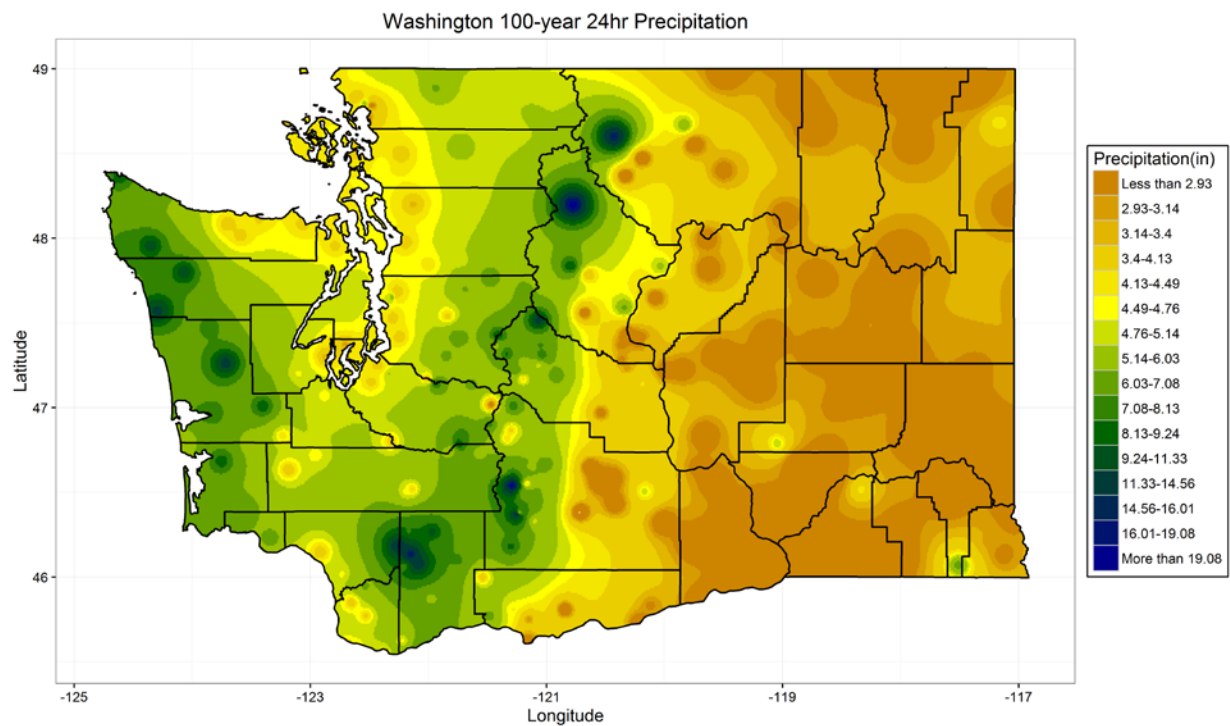
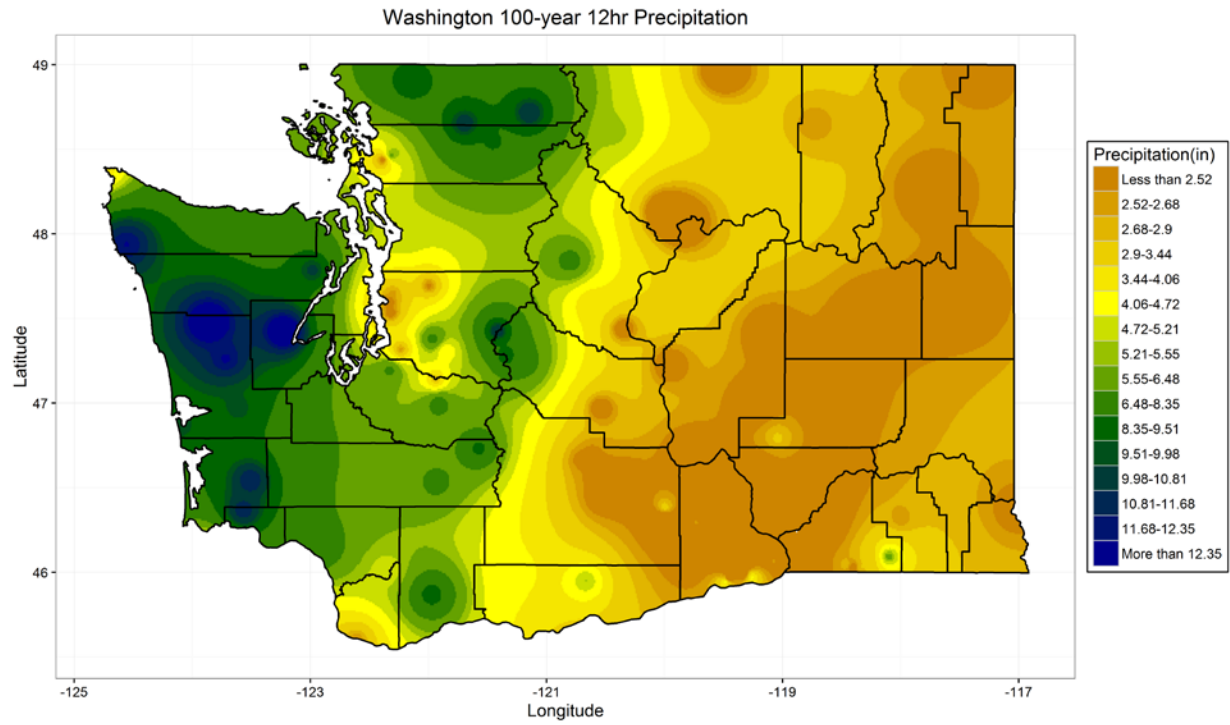


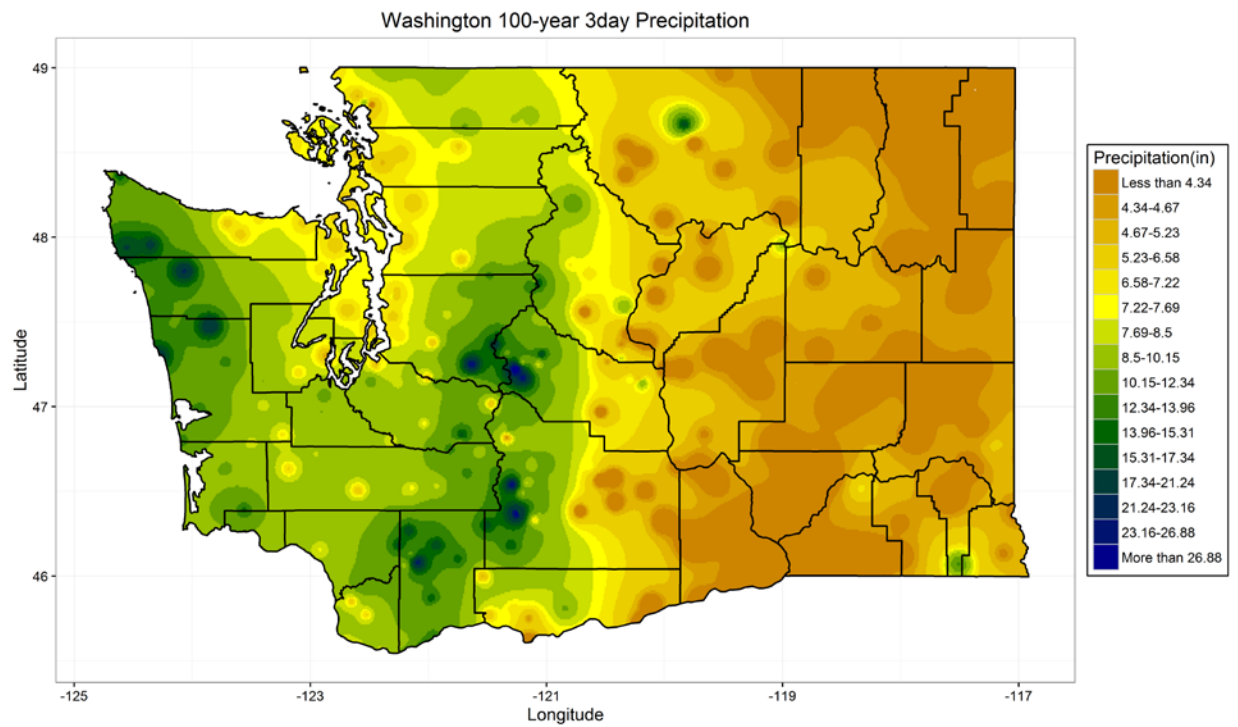
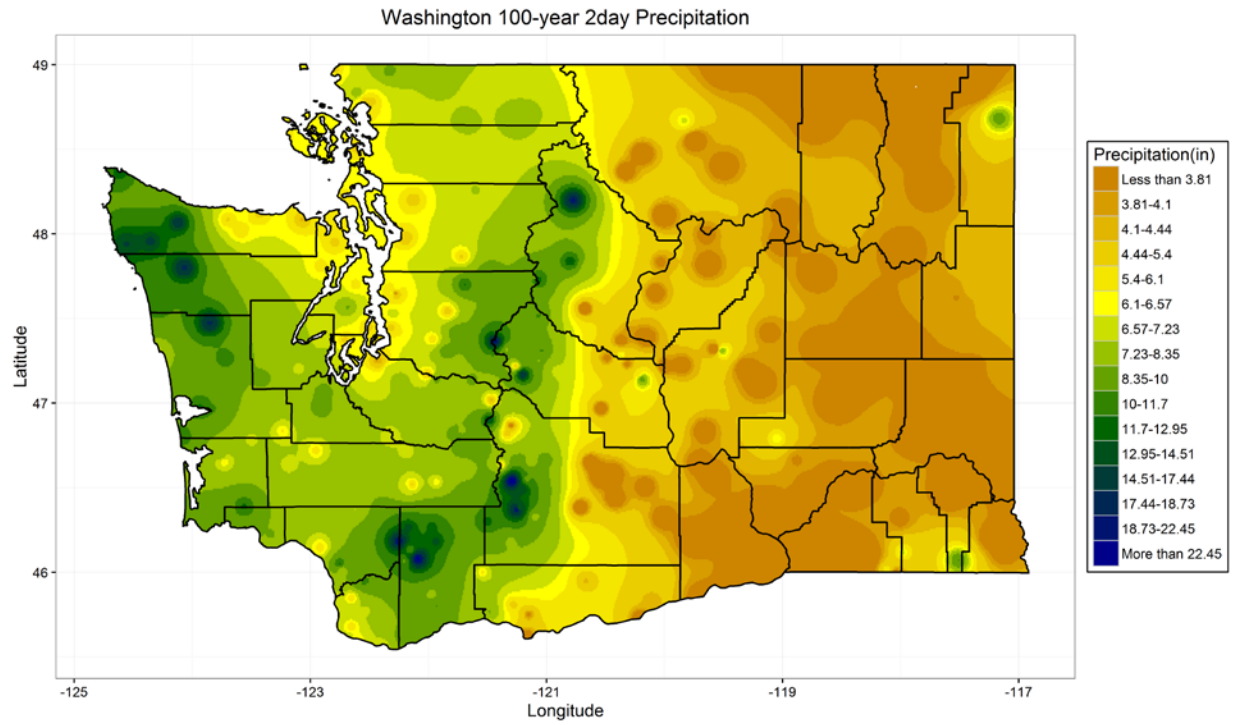


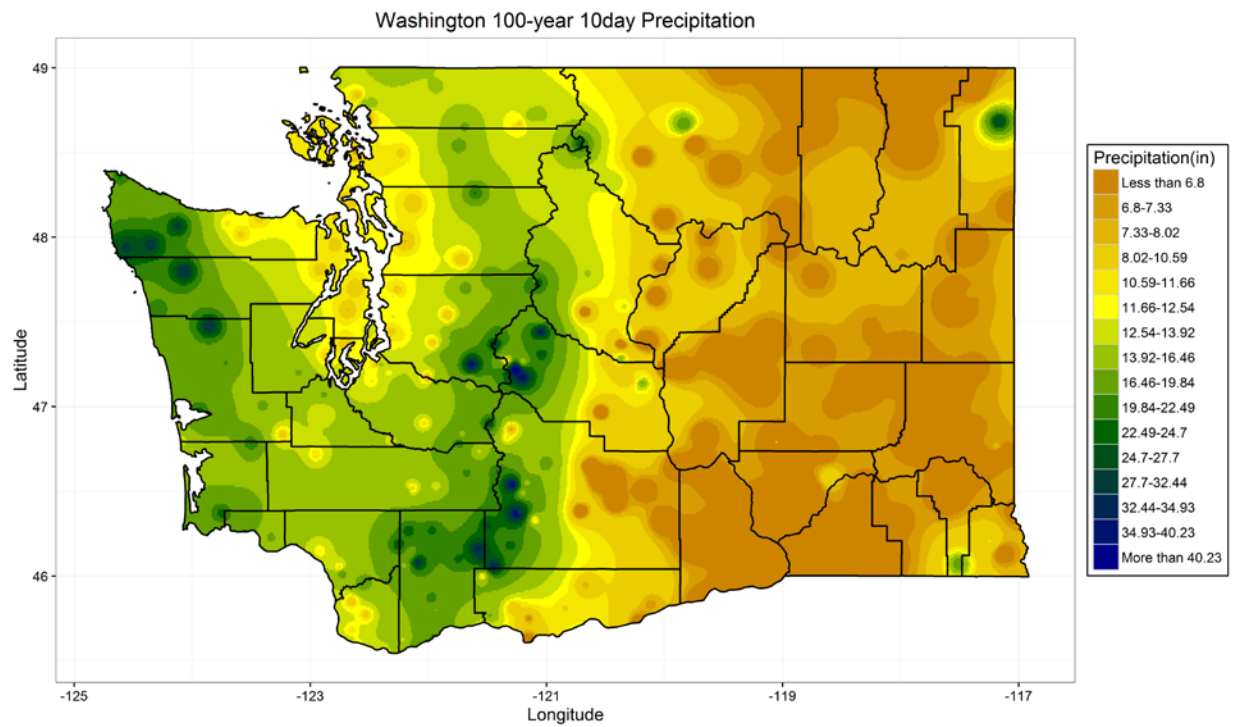
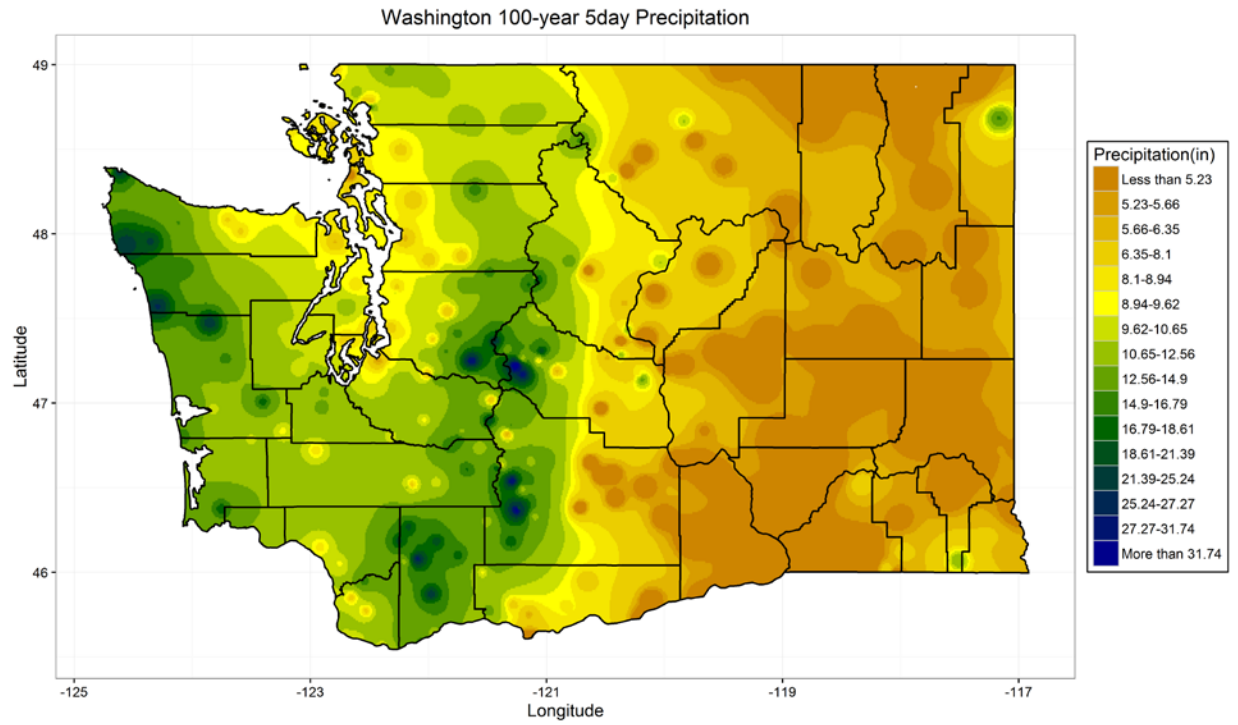












Bedload dynamics at the confluence of large rivers

Basic Information

Title:	Bedload dynamics at the confluence of large rivers
Project Number:	2015WA404B
Start Date:	3/1/2015
End Date:	2/28/2016
Funding Source:	104B
Congressional District:	5
Research Category:	Engineering
Focus Category:	Geomorphological Processes, Sediments, Hydrology
Descriptors:	None
Principal Investigators:	John Eric Petrie, Balasingam Muhunthan

Publications

1. Shehata, Mahmoud, John Petrie, 2016, Hydrodynamics in the confluence of the Snake and Clearwater Rivers, in River Flow 2016, International Conference on Fluvial Hydraulics, IAHR, St. Louis, MO.
2. Shehata, Mahmoud, John Petrie, 2016, Mixing zone hydrodynamics in a large confluence: a case study at the confluence of the Snake and Clearwater Rivers, BioEarth Annual Meeting, Washington State University (February 2016).
3. Shehata, Mahmoud, John Petrie, 2016, Mixing zone hydrodynamics in a large confluence: a case study at the confluence of the Snake and Clearwater Rivers, Pacific Northwest Water Research Symposium, Oregon State University (April 2016).

Bedload dynamics at the confluence of large rivers

Basic Information

Title:	Bedload dynamics at the confluence of large rivers
Project Number:	2015WA404B
Start Date:	3/1/2015
End Date:	2/28/2016
Funding Source:	104B
Congressional District:	Washington, 5
Research Category:	Water Quality
Focus Category:	Geomorphological Processes, Sediments, Hydrology
Descriptors:	None
Principal Investigators:	John Petrie, Balasingam Muhunthan

Publications

1. Shehata, M., J. Petrie, 2016, Hydrodynamics in the confluence of the Snake and Clearwater Rivers, in River Flow 2016, International Conference on Fluvial Hydraulics, IAHR, St. Louis, MO.
2. Shehata, M., J. Petrie, 2016, Mixing zone hydrodynamics in a large confluence: a case study at the confluence of the Snake and Clearwater Rivers, BioEarth Annual Meeting, Washington State University (February 2016).
3. Shehata, M., J. Petrie, 2016, Mixing zone hydrodynamics in a large confluence: a case study at the confluence of the Snake and Clearwater Rivers, Pacific Northwest Water Research Symposium, Oregon State University (April 2016).
4. Shehata, M. and J. Petrie, Hydrodynamics at a large river confluence under low flow conditions. (In preparation)

1. PROBLEM AND RESEARCH OBJECTIVES

1.1 Introduction

Rivers in the Pacific Northwest provide numerous benefits to society including hydropower, transportation, irrigation, and recreation. These human uses are often in conflict with natural fluvial and biological processes. Nowhere is this conflict more evident than the confluence of the Snake and Clearwater Rivers at the border of Washington and Idaho. These rivers have been impacted by humans in a myriad of ways including hydropower dams built upstream and downstream of the confluence, a levee system protecting the cities of Clarkston, WA and Lewiston, ID, and commercial ports in both cities. The lower Granite Dam creates a reservoir which begins near the downstream end of the confluence. Monitoring of the riverbed elevation since dam construction shows significant sediment deposited in the vicinity of the confluence of the Snake and Clearwater Rivers. This sedimentation has adverse effects on the navigability of shipping channels and the capacity of the rivers to pass floods. The historical solution to sedimentation problems at this location has been dredging (USACE 2014). Questions regarding the environmental impacts of dredging, particularly with respect to national water quality standards and endangered species, led to a lawsuit by environmental groups in 2002. The response to the lawsuit was the development of the Lower Snake River Programmatic Sediment Management Plan (USACE 2014), an adaptive plan that embraces a range of approaches to address sediment-related problems. Among the potential remediation actions are dredging, reservoir drawdown to flush sediments, and hydraulic structures such as dikes and weirs. These potential activities require careful consideration as each alternative may have unforeseen impacts. For example, drawdown of the reservoir in 1992 led to a local marina filing for bankruptcy (W. Keefer, personal communication, November 17, 2014). Knowledge of flow and sediment dynamics in the vicinity of the confluence is needed to predict channel response and evaluate alternatives to improve water quality, protect habitat, as well as protect infrastructure. Thus, the results of this project will assist reservoir operators, port managers, fish biologists, and town managers.

Confluences are important features of river networks providing diverse flow conditions that influence physical channel processes and biological processes (Benda et al. 2004). Despite the importance of confluences to the fluvial environment, research on confluence dynamics received little attention until the end of the last century (Rice et al. 2008). Beginning with the work of Mosley (1976) and Best (1986, 1987, 1988), research has expanded and embraced a range of approaches from laboratory experiments (Best 1988; Leite Ribeiro et al. 2012) to field studies (Biron et al. 1993, 2002; Rhoads & Kenworthy 1998; Rhoads & Sukhodolov 2001; Sukhodolov & Rhoads 2001) and numerical investigations (Bradbrook et al. 2000; Constantinescu et al. 2011, 2012). While these studies and others form the basis of our understanding of confluence dynamics, the vast majority of investigations consider confluences of small channels (channel width < 10 m). Only recently have confluences of large rivers (channel width > 100 m), such as the Snake and Clearwater Rivers, been the subject of detailed investigations (e.g., Lane et al. 2008; Szupiany et al. 2009). These studies suggest important differences between small and large channels. To build a more complete understanding of confluences dynamics embracing the full range of scales requires significantly more observations from large channels (Parsons et al. 2008).

Confluence dynamics are influenced by the geometry of the joining channels as well as differences in the flow and sediment load. While the flows are of similar order of magnitude, recent

measurements have found that the Snake River carries more sediment than the Clearwater River with the Snake contributing as much as 90% of the sediment that deposits in the lower Granite Reservoir (Clark et al. 2013, see Figure 1). This difference in load has implications for sedimentation at the confluence as sediment transport is the link between flow structure and bed morphology (Best & Rhoads 2008). The total sediment load is often divided into the suspended load—finer material that moves in suspension—and bedload—coarser material that moves along the channel bottom. This study focuses on bedload due to evidence that much of the deposited material is coarse (Boll et al. 2010). At present, no direct observations of bedload dynamics have been reported in confluences of large rivers and only two studies have presented similar results for small channel confluences (Boyer et al. 2006; Rhoads 1996). Thus, this study seeks to make a fundamental contribution to our knowledge of confluence dynamics while addressing problems facing the confluence of the Snake and Clearwater Rivers.



Figure 1: The confluence of the Snake and Clearwater Rivers illustrating the difference in sediment load. The arrows indicate the direction of flow. (Photo courtesy of Wanda Keefer, Port of Clarkston)

1.2 Objectives

Our long-term goal is to develop a detailed understanding of flow and sediment processes and the resulting morphology at confluences of large rivers. The overarching goal of this project is to collect and analyze field data of flow and bedload transport in the confluence of the Snake and Clearwater Rivers. We propose to use state-of-the-art techniques to measure 3D velocity and bedload velocity using an acoustic Doppler current profiler (ADCP) at locations in the confluence region. The specific project objectives are:

1. *Quantify the 3D flow field at the confluence of two large rivers.* A boat-mounted ADCP will be used to measure velocity throughout the confluence of the Snake and Clearwater Rivers. Two survey methodologies will be used that allow for both spatially-rich and temporally-rich

velocity data. These measurements will be compared with previous measurements obtained at confluences of small rivers to clarify the role of scale on the flow field.

2. *Quantify bedload dynamics at the confluence of two large rivers.* Bedload transport characteristics will be measured at the field site using traditional, intrusive and cutting edge, nonintrusive methods. A Helley-Smith sampler will provide bulk measurements of the transport rate and the grain size distribution of the transported material. ADCP measurements and high resolution positioning will be used to determine the speed and direction of the transported bed material.
3. *Map spatial distribution of flow and sediment dynamics at the field site.* Results from the previous objectives will be compiled to produce vectors maps of flow and bedload transport. Viewing flow and sediment transport together at the field site allows the identification of regions where bedload is likely to be deposited and potential feedbacks between processes. These maps will be used to evaluate existing conceptual models for small channels confluences and contribute to the development of new models for large channel confluences.

1.3 Study area description

A field study was conducted in the large confluence of the Snake and the Clearwater Rivers adjacent to the towns of Clarkston, WA and Lewiston, ID (see Figure 2) during the period of July 8-14, 2015. This confluence supports many purposes including commercial navigation, a downstream hydropower facility, as well as fish and wildlife conservation. As a consequence, the natural state of the confluence has been altered over time by a number of dredging operations performed to maintain the minimum navigable depth and adequate level of flood protection for the adjacent towns. The confluence is also influenced by backwater effects from the Lower Granite Reservoir (USACE 2014).

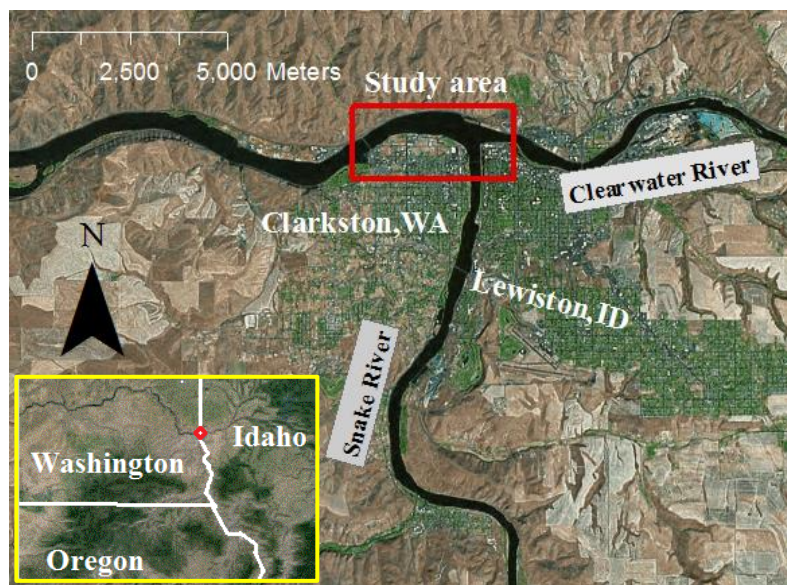


Figure 2: Location of the study site.

The average widths of the Snake and the Clearwater Rivers approaching the confluence are on the order of 300 m and the width increases to approximately 700 m in the confluence central zone. The two confluent rivers intersect at an angle of about 80 degrees. Two bridges exist at distances of ~450 m and ~600 m from the confluence upstream corner in the Snake and Clearwater Rivers, respectively. Another bridge crosses the post confluence region at a distance of ~3200 m from the upstream corner. The study area ends before the downstream bridge to avoid its artificial influence on the flow hydrodynamics.

In 2010, underwater video and surficial sediment cores were taken in the two confluent rivers and in the confluence zone by the USGS in cooperation with the USACE (Braun et al. 2012). The results indicate that the bed sediment in the confluence zone ranges from fine to medium sands with sizes mainly less than 0.5 mm in the regions near to the confluence upstream and downstream corners. The bed surface becomes coarser in the confluence central zone, which consists mainly of boulders, cobbles and gravels. Fine materials (silt and clay) were typically found to account for less than 20% and 40% of the surficial sediments in the Snake and Clearwater Rivers, respectively. Higher fine material content was found in the confluence zone near to the upstream corner (Braun et al. 2012).

2. METHODOLOGY

2.1 Water velocity and position measurements

A boat-mounted acoustic Doppler current profiler (ADCP) is a versatile tool for riverine studies that can provide measurements of velocity and channel topography. The ADCP measures 3D velocity components along a vertical profile by emitting acoustic pulses, called pings, along four beams. These pings move through the water column and reflect off of scatterers (suspended sediment and organic matter moving with the flow). The frequency shift between the sent and reflected pulses is used to calculate the flow velocity. Velocities from three beams are combined to provide 3D components while the fourth beam gives an estimate of measurement error. As shown in Figure 3, the water column is divided into equally-spaced depth cells, called bins, and the mean velocity from all pings reflected within each cell is placed at the bin center. The raw velocity measured by the ADCP includes contributions from the flowing water and motion of the boat. A measure of the boat velocity is required to isolate the flow velocity. The boat velocity may be determined using either a global positioning system (GPS) or bottom tracking. Bottom tracking measures the movement of the ADCP relative to the channel bed and is accomplished by sending a strong pulse that reflects off of the bed. In addition to providing the velocity of the ADCP, bottom tracking also measures the flow depth at each beam.

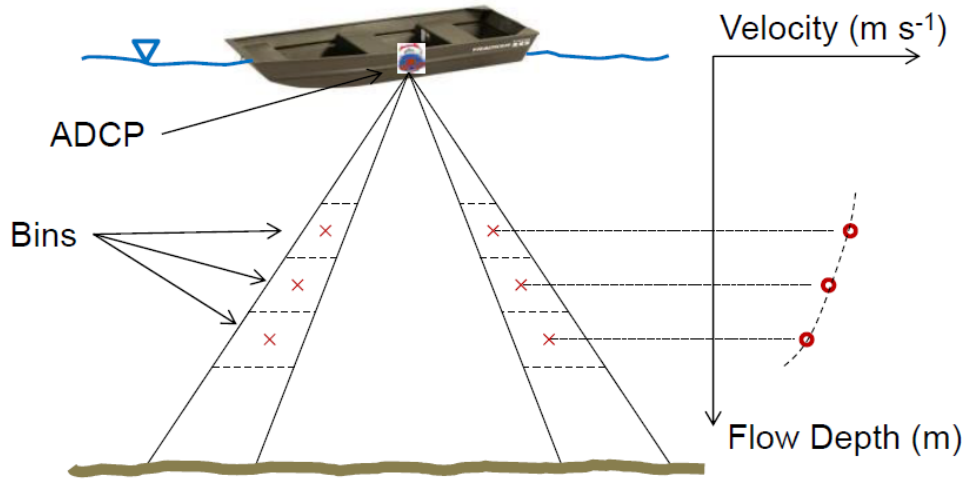


Figure 3: Illustration of a velocity profile measured by a boat-mounted ADCP. In addition to the two beams shown, the ADCP also emits beams into and out of the page.

The spatial and temporal resolution of the velocity measurements is dependent on the type of deployment. During moving-vessel (MV) measurements, the ADCP records continuously while the boat traverses the channel. This is the most common boat-mounted survey procedure and provides accurate measurements of discharge (Oberg & Mueller 2007). Fixed vessel (FV) measurements are performed while the boat is held at a constant position within the channel. The improved temporal resolution can be used to determine mean (e.g., time-averaged) velocity profiles (Petrie et al. 2013) and bed load velocity (Rennie et al. 2002).



Figure 4: equipment used in the field work.

The velocity field in the study area was measured using a Teledyne RDI 1200 kHz RiverPro ADCP installed in a RiverRay float and attached to the boat as shown in Figure 4. Positioning was provided by means of a R6-4 Trimble GPS installed directly above the ADCP and by using bottom tracking. The GPS accuracy was increased by acquiring corrections from Washington State Reference Network (WSRN). The GPS accuracy was tested by using two USGS bench marks, one in Pullman, WA (RZ1887) and the other is in Clarkston, WA near to the Post-confluence stream (RZ1076). The comparison between the GPS data and the USGS database showed that the margin of error is within few centimeters. A TruPulse200x Rangefinder (Figure 4) was used to measure the distances between the starting and ending ADCP positions to the river banks for MV measurement. These distances are essential to estimate discharge passing in the shallow regions near banks, which cannot be measured by the ADCP.

Figure 5 shows the outrigger configuration used to mount the ADCP to the boat. A square tube was placed across the boat width with its extra length extended on one side. The tube was fixed to the boat by elastic straps. The purpose of these square tube was to allow the RiverRay to be attached to the boat side at a distance far enough to prevent the GPS blockage. The RiverRay was connected to both the front and the rear of the boat to limit its movement.



Figure 5: The RiverRay mounted to the boat using an outrigger configuration.

Water velocity profiles were measured along 14 cross sections in the confluence region (Figure 6). These cross sections were selected to cover the entire confluent region including two cross sections up-stream of the confluence in each channel. The density of cross sections was increased in the confluence central zone to better capture the anticipated flow features. A minimum of four moving vessel measurements (transects) were taken at each of the 14 cross sections to enable a proper discharge estimate. A single transect was taken by starting at a location near to one bank and moving along the cross section to the other bank while the ADCP is recording the velocity profile. Also, FV measurements with durations ranging from 15 to 20 minutes were taken at different locations throughout the confluence to investigate the temporal velocity fluctuations.

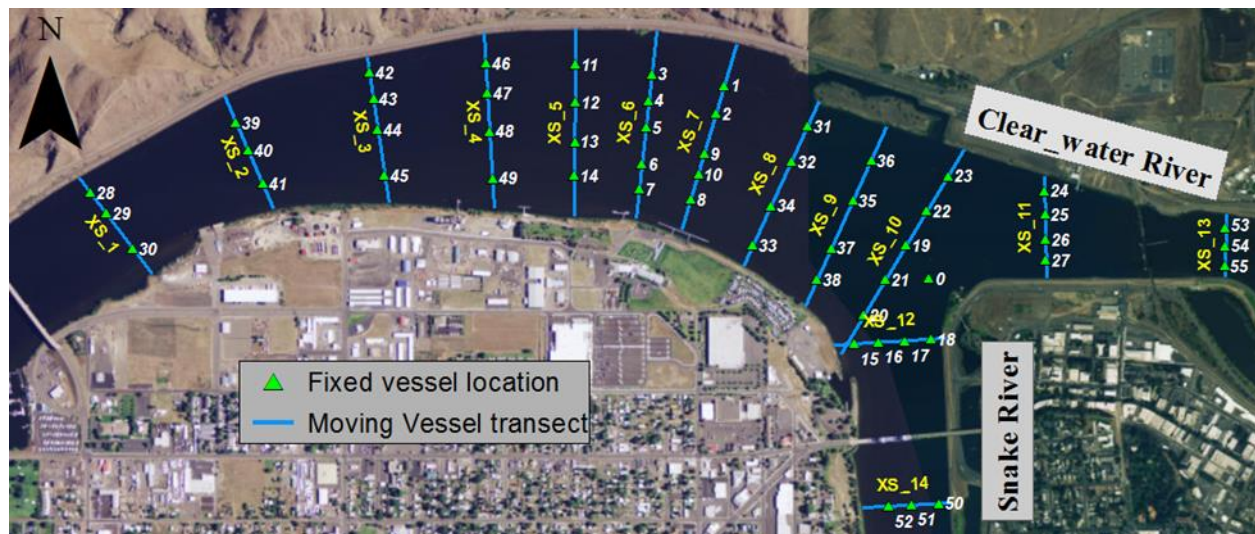


Figure 6: Moving vessel transects and fixed vessel locations

2.2 Sediment samplers

Measurement of bedload in rivers remains challenging due to the significant spatial and temporal variability of the phenomenon (Diplas et al. 2008). For example, laboratory experiments under steady flow required 40 to 50 minutes of sampling to obtain stable mean transport rates (Kuhnle & Southard 1988). Traditionally, bedload is measured by installing a trap-like device on the riverbed to collect the transported material. These intrusive samplers have the disadvantage of disturbing the near-bed flow field and bedload movement. More recently the ADCP, using the bottom tracking feature described previously, has been explored for nonintrusive measurements of bedload transport (Gaeuman & Jacobson 2006; Rennie et al. 2002).

A cable suspended Helley-Smith Sampler (Figure 7) was used to collect bed-load samples in the study area. A Helley-Smith Sampler consists of a metal frame and nozzle holding a mesh bag to collect samples. Helley-Smith samplers are usually deployed in non-wadeable rivers from a boat using a cable and winch. The basic operational procedure is to (1) lower the sampler onto the riverbed, (2) collect a bedload sample for some duration (typically 30 to 120 seconds), (3) raise the sampler off the bed and return it to the boat, and (4) empty the mesh bag. The contents of the mesh bag constitute the bedload sample and the transport rate can be computed from the sample weight and sampling duration while the sample grain size distribution can be determined by sieve

analysis. Due to the spatial and temporal variability of bedload, a large number of samples are typically required to quantify bedload transport rates at a site.

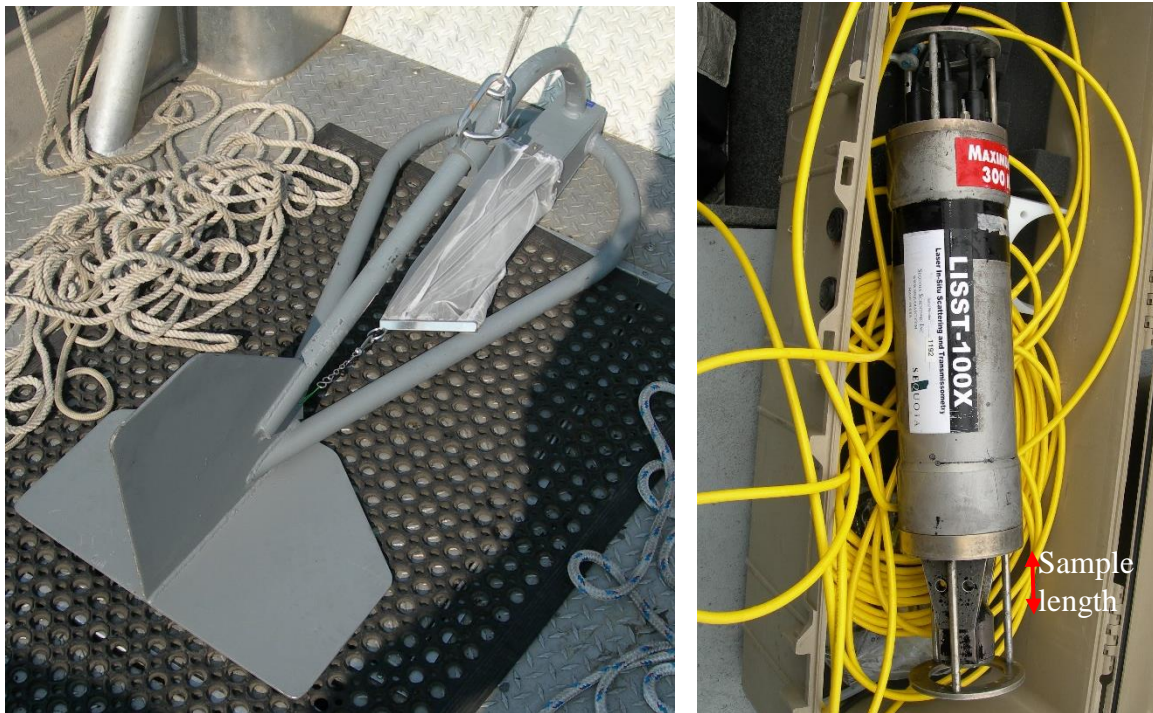


Figure 7: The Helley-Smith bedload sampler (left) and LISST-100X suspended load profiler (right)

Suspended load particle size and volume distributions were measured by a LISST-100X instrument produced by SEQUOIA (Figure 7). The LISST-100X works by sending a laser beam and receiving the reflections off of the suspended sediment particles over a ring of sensors known as a ring detector. The size of the particles is identified by the intensity of the reflected rays and the angle of reflection. The instrument was lowered slowly from the water surface to the river bottom to measure the suspended load distribution over the water column. The device continued measuring while it was lifted back to the boat to obtain another vertical profile (for comparison purposes). A suspended load measurement was taken at each ADCP FV measurement location.

2.3 Bathymetry survey

A 3DSS-DX-450 multi-beam sonar manufactured by Ping DSP (Figure 8) with a frequency of 450 kHz and beam width of 0.4° was used to survey the bathymetry and identify the existent bed morphological elements throughout the confluence. This device is capable of creating high resolution bathymetry maps that resolve bed forms on the river bed even in shallow waters with depths less than 1.0 m. The 3DSS was mounted on a vertical rod to the side of the boat, so that the device is submerged at a known depth below water surface. The river bathymetry survey was performed in the form of overlapped lines, in which the boat was driven in straight paths maintaining an overlap between paths. The width of the line depends mainly on the water depth. The deeper the water column, the wider the area covered on one line.



Figure 8: The 3DSS-DX-450 multi-beam sonar

3 PRINCIPLE FINDINGS AND SIGNIFICANCE

3.1 Flow conditions during the field observations

The total discharge passing through the confluence during the study period ranged between 765 and 903 m³/s as shown in Figure 9 **Error! Reference source not found.**. Discharge is measured at USGS stations 13342500 and 13334300. These two gaging stations are located at distances of 19 km and 46 km upstream from the confluence center in the Snake and the Clearwater Rivers, respectively. The corresponding discharge ratio in the confluence, $Q_r = Q_{\text{Clearwater}} / Q_{\text{Snake}}$, fluctuated between 0.56 and 1.0 during the same period. Low flow conditions were present during the study period, the aforementioned flow rates are low compared to the historic average daily flow during the same period, which was > 1260 m³/s based on data from 2000 to 2014 (<http://waterdata.usgs.gov>). This low flow is likely due to the significantly low snow pack and the relatively high temperatures in this year.

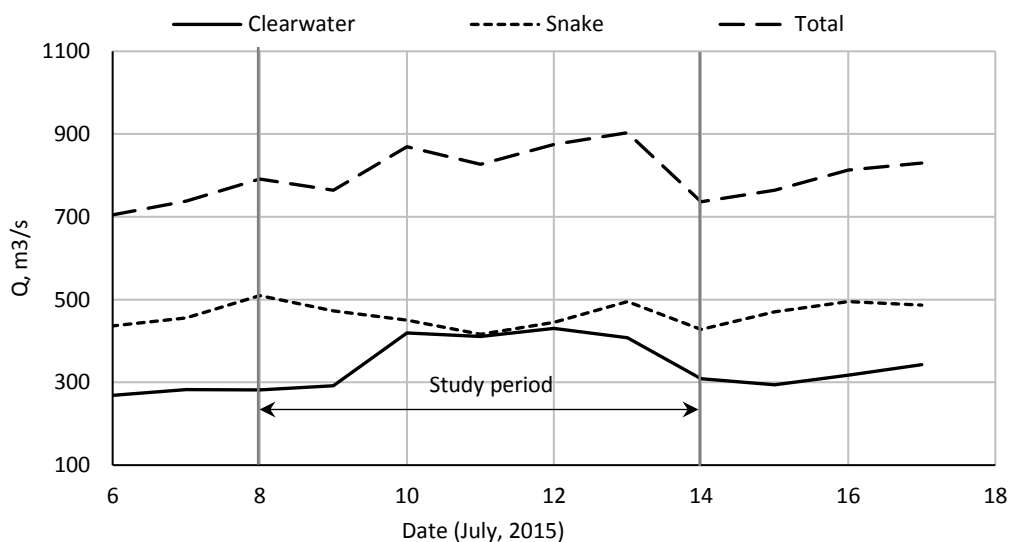


Figure 9: Discharge in the confluence during field measurements.

3.2 Confluence Bathymetry

The results of the bathymetry survey (**Error! Reference source not found.**) show that the maximum depths upstream of the confluence in the Snake and Clearwater Rivers were about 12 m and 7.5 m, respectively. Regions with higher depths (> 16 m) were observed in the vicinity of the upstream bridges, which can be attributed to scour around the bridge piers. The two river beds merge smoothly after entering the confluence creating little to no bed discordance. This observation is consistent with the results obtained in large braid-bar confluences (Szupiany et al. 2009).

Large areas with relatively shallow depths (< 6 m) were observed around the confluence upstream corner, and for a long distance next to the post-confluence left bank starting from the downstream corner and continuing beyond XS_3. This finding could indicate the formation of sediment bars. The confluence thalweg and the surrounding deep region (> 11 m) began as a wide region in the Snake River and then reduced in size and depth at the center of the confluence. Further downstream in the vicinity of XS_5, the thalweg increases in size and depth as it extends through the confluence moving towards the outer bank (right bank facing downstream). Large bed forms develop at the edge of the deep region starting from within the Snake River to the downstream end of the study area. Smaller separated patches with depths > 11 m were also observed in the confluence central zone near the outer bank.

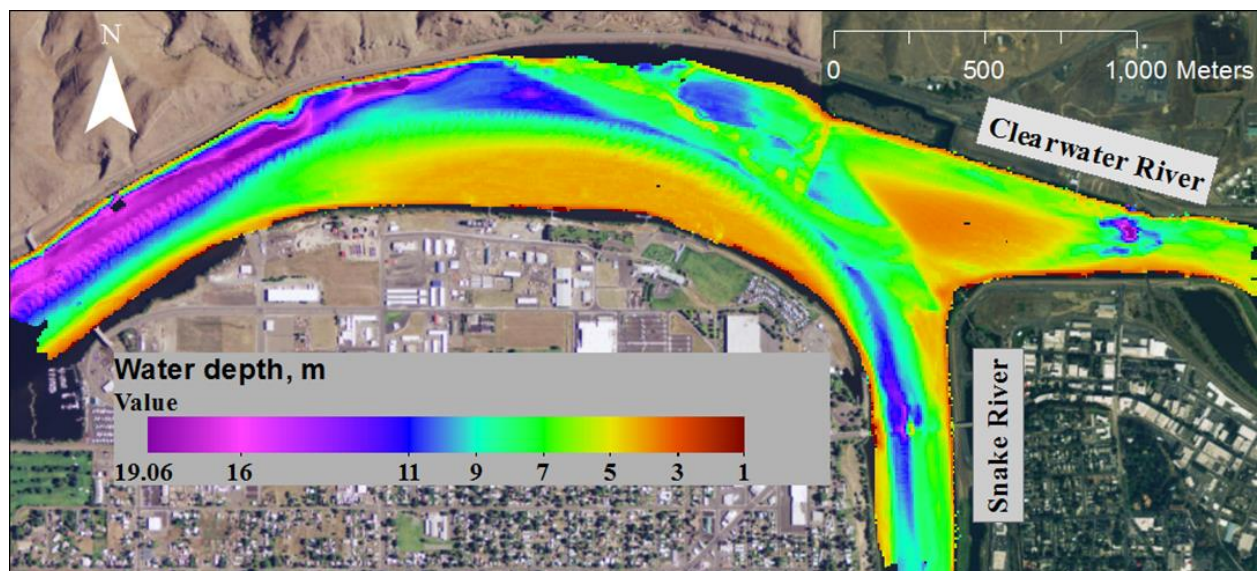


Figure 10: Confluence morphology measured on July, 9th 2015 (vertical datum is the water surface).

3.3 Sediment measurements

The Helley-Smith sampler was used to obtain bedload samples from the confluence region. Two sampling durations of 5 and 60 minutes were tested in locations near to the confluence center (locations expected to have the most bed load transport). No significant bedload was detected in either sample. Additionally, the ADCP bottom track data indicated that the bed was not moving. These observations demonstrate that little to no bedload was present in the test region. This finding is attributed to the significantly low snow pack and resulting low flow conditions through the confluence in the spring of 2015. The processing of the suspended load measurements is in

progress to establish the role of hydrodynamics on mixing of suspended sediment within the confluence.

3.4 Depth-averaged velocity

The moving vessel transects were analyzed using the Velocity Mapping Toolbox (VMT) software (Parsons et al. 2013). The average of all transects taken at each cross section was used to compute the depth-averaged velocity distribution presented in Figure 11 for the 14 cross sections. The cross section average flow velocity in the Clearwater River was ~ 0.4 m/s at XS_13 and reduced to ~ 0.25 m/s at XS_11 before entering the confluence due to the increase in the river cross section. The cross section averaged velocity in the Snake River was about 0.25 m/s at XS_14. At the entrance to the confluence, the velocity increases in the region near to the right bank to ~ 0.35 m/s (see XS_12 in Figure 11). A region of higher velocity starts to develop initially in the confluence central zone near to the shear layer. Further downstream, the maximum velocity region shifts towards the right bank and increases in magnitude, reaching a peak at XS_8 with average velocities > 0.45 m/s. The velocity decreases downstream of XS_8 to a more homogenous average velocity distribution as the mixing interface between the two flows diminishes.

Low velocities with magnitudes < 0.1 m/s were observed along the left bank starting from the confluence downstream corner. In this region, depth-averaged velocities moving upstream were also seen near the left bank in some transects at XS_4 and XS_5. These features may be due to flow deflection around the relatively sharp change in the bank alignment occurring near XS_6. This result indicates the formation of a separation zone in the vicinity of the confluence downstream corner and after the change in bank alignment. The aforementioned flow characteristics and patterns agree with the general hydrodynamics model proposed by Best (1987).

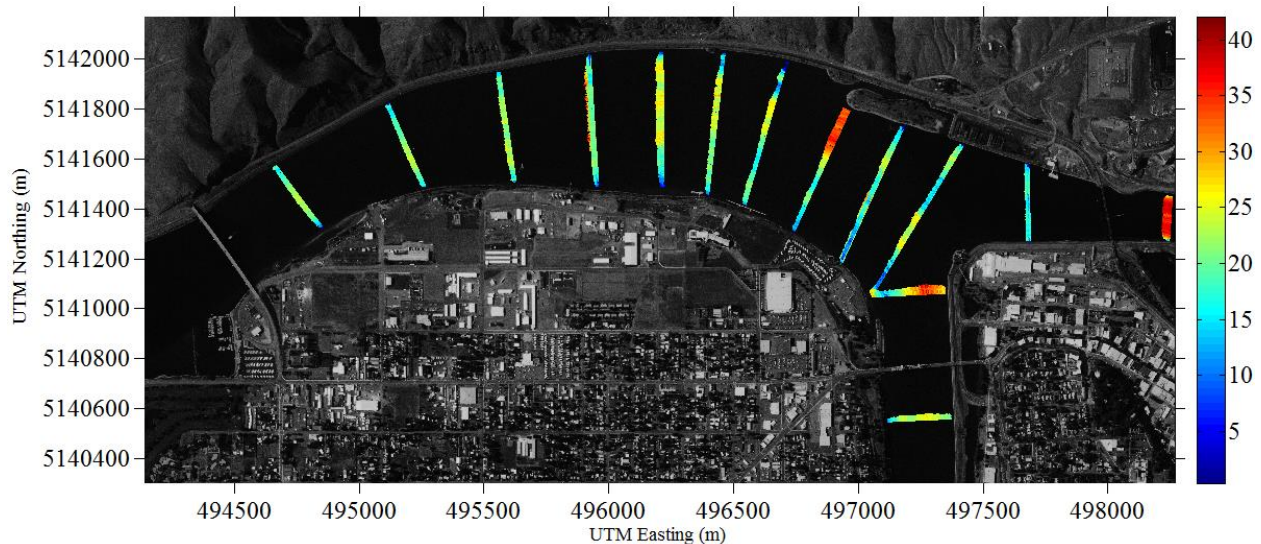


Figure 11: Depth-averaged velocity (cm/s) measured at cross sections in the vicinity of the confluence.

3.5 Secondary circulation

Analysis of the cross stream velocity components was performed using the zero net cross-stream discharge technique. This technique defines the direction of primary flow to minimize secondary

discharge over the whole cross section (Paice 1990). The results demonstrate the development of a clockwise circulation cell (looking downstream) in the Snake River side starting from XS_10 with cross-stream velocity magnitudes comparable to the streamwise velocities that reach magnitudes > 0.35 m/s in some regions (Figure 12a). No significant circulation cells were observed on the Clearwater side at that cross section. This finding may be due to the relatively low velocity field in the Clearwater River entering the confluence compared to the Snake River. As the flow moves further downstream, the circulation cell expands towards the right bank until it includes the majority of the cross section at XS_8 (Figure 12b). The cross stream velocity magnitudes decrease to < 0.22 m/s at XS_8. Further downstream, the circulation cell dissipates as the flow recovers (Figure 12c). The secondary circulation in the vicinity of XS_8 is similar to that observed in meander bends.

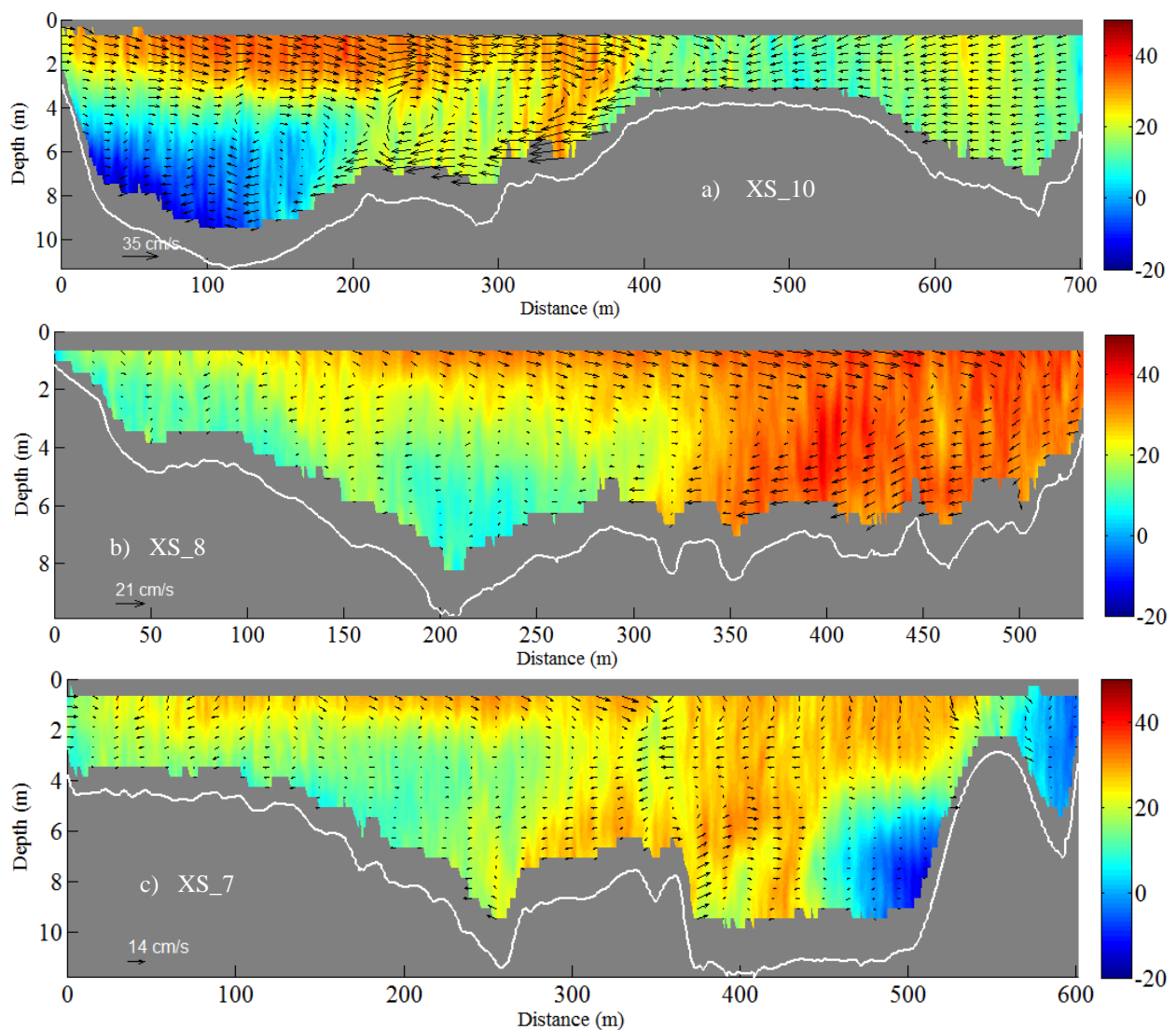


Figure 12: Cross-stream velocity vectors (cm/s) and contours of stream wise velocity (cm/s) at different cross sections in the post-confluence region (facing downstream).

The low flow occurring during measurements is not expected to be significantly responsible for the confluence morphology. Also, the confluence morphology is systemically influenced by dredging operations. However, the measured flow patterns generally agree with the bed bathymetry. Low velocity regions at both the confluence upstream and downstream corners existed in the shallowest flow depths. The maximum velocities were observed in the regions characterized with high flow depths. The secondary circulation pattern is also consistent with the meander planform morphology in the Snake River.

4 LIST OF STUDENTS SUPPORTED

- Mahmoud Shehata, a Washington State University PhD student. Mahmoud participated in collecting and taking the field measurements. He processed the measurement data and prepared the publications under guidance of the PI.
- Gregory Moore, a Washington State University undergraduate student. Gregory participated in setting up and testing the equipment used in the field work.

5 REFERENCES

Benda, L., Poff, N.L., Miller, D., Dunne, T., Reeves, G., Pess, G., & Pollock, M. (2004). The network dynamics hypothesis: how channel networks structure riverine habitats. *BioScience* 54, 413–427.

Best, J.L. (1986). The morphology of river channel confluences. *Prog. Phys. Geogr.* 10, 157–174.

Best, J.L. (1987). Flow Dynamics at River Channel Confluences: Implications for Sediment Transport and Bed Morphology. *Recent Dev. Fluv. Sedimentol.* 39, 27–35.

Best, J.L. (1988). Sediment transport and bed morphology at river channel confluences. *Sedimentology* 35, 481–498.

Best, J.L., & Rhoads, B.L. (2008). Sediment transport, bed morphology and the sedimentology of river channel confluences. *River Conflu. Tribut. Fluv. Netw.* 45–72.

Biron, P., Roy, A., Best, J.L., & Boyer, C.J. (1993). Bed morphology and sedimentology at the confluence of unequal depth channels. *Geomorphology* 8, 115–129.

Biron, P.M., Richer, A., Kirkbride, A.D., Roy, A.G., & Han, S. (2002). Spatial patterns of water surface topography at a river confluence. *Earth Surf. Process. Landf.* 27, 913–928.

Boll, J., Brooks, E., McAtty, J., Barber, M., Ullman, J., McCool, D., Lu, X., Lawler, A., & Ryan, J. (2010). Evaluation of sediment yield reduction potential in agricultural and mixed-use watersheds of the Lower Snake River basin (Pullman, WA: submitted to US Army Corps of Engineers by State of Washington Water Research Center).

Boyer, C., Roy, A.G., & Best, J.L. (2006). Dynamics of a river channel confluence with discordant beds: Flow turbulence, bed load sediment transport, and bed morphology. *J. Geophys. Res. Earth Surf.* 111, F04007.

- Bradbrook, K.F., Lane, S.N., & Richards, K.S. (2000). Numerical simulation of three-dimensional, time-averaged flow structure at river channel confluences. *Water Resour. Res.* *36*, 2731–2746.
- Braun, C.L., Wilson, J.T., Van Metre, P.C., Weakland, R.J., Fosness, R.L., & Williams, M.L. (2012). Grain-size distribution and selected major and trace element concentrations in bed-sediment cores from the Lower Granite Reservoir and Snake and Clearwater Rivers, eastern Washington and northern Idaho, 2010 (US Department of the Interior, US Geological Survey).
- Clark, G.M., Fosness, R.L., & Wood, M.S. (2013). Sediment Transport in the Lower Snake and Clearwater River Basins, Idaho and Washington, 2008-11 (US Geological Survey).
- Constantinescu, G., Miyawaki, S., Rhoads, B., Sukhodolov, A., & Kirkil, G. (2011). Structure of turbulent flow at a river confluence with momentum and velocity ratios close to 1: Insight provided by an eddy-resolving numerical simulation. *Water Resour. Res.* *47*, W05507.
- Constantinescu, G., Miyawaki, S., Rhoads, B., & Sukhodolov, A. (2012). Numerical analysis of the effect of momentum ratio on the dynamics and sediment-entrainment capacity of coherent flow structures at a stream confluence. *J. Geophys. Res. Earth Surf.* *117*, F04028.
- Diplas, P., Kuhnle, R., Gray, J., Glysson, D., & Edwards, T. (2008). Sediment Transport Measurements. In *Sedimentation Engineering*, (American Society of Civil Engineers), pp. 307–353.
- Gaeuman, D., & Jacobson, R.B. (2006). Acoustic bed velocity and bed load dynamics in a large sand bed river. *J. Geophys. Res. Earth Surf.* *111*, F02005.
- Kuhnle, R.A., & Southard, J.B. (1988). Bed load transport fluctuations in a gravel bed laboratory channel. *Water Resour. Res.* *24*, 247–260.
- Lane, S.N., Parsons, D.R., Best, J.L., Orfeo, O., Kostaschuk, R.A., & Hardy, R.J. (2008). Causes of rapid mixing at a junction of two large rivers: Río Paraná and Río Paraguay, Argentina. *J. Geophys. Res. Earth Surf.* *113*, F02024.
- Leite Ribeiro, M., Blanckaert, K., Roy, A.G., & Schleiss, A.J. (2012). Flow and sediment dynamics in channel confluences. *J. Geophys. Res. Earth Surf.* *117*, F01035.
- Mosley, M.P. (1976). An Experimental Study of Channel Confluences. *J. Geol.* *84*, 535–562.
- Oberg, K., & Mueller, D.S. (2007). Validation of streamflow measurements made with acoustic Doppler current profilers. *J. Hydraul. Eng.* *133*, 1421–1432.
- Paice, C. (1990). Hydraulic control of river bank erosion: an environmental approach. University of East Anglia.
- Parsons, D.R., Best, J.L., Lane, S.N., Kostaschuk, R.A., Hardy, R.J., Orfeo, O., Amsler, M.L., & Szupiany, R.N. (2008). Large river channel confluences. In *River Confluences, Tributaries and the Fluvial Network*, pp. 17–32.

- Parsons, D.R., Jackson, P.R., Czuba, J.A., Engel, F.L., Rhoads, B.L., Oberg, K.A., Best, J.L., Mueller, D.S., Johnson, K.K., & Riley, J.D. (2013). Velocity Mapping Toolbox (VMT): a processing and visualization suite for moving-vessel ADCP measurements. *Earth Surf. Process. Landf.* 38, 1244–1260.
- Petrie, J., Diplas, P., Gutierrez, M., & Nam, S. (2013). Data evaluation for acoustic Doppler current profiler measurements obtained at fixed locations in a natural river. *Water Resour. Res.* 49, 1003–1016.
- Rennie, C.D., Millar, R.G., & Church, M.A. (2002). Measurement of Bed Load Velocity using an Acoustic Doppler Current Profiler. *J. Hydraul. Eng.* 128, 473–483.
- Rhoads, B.L. (1996). Mean structure of transport-effective flows at an asymmetrical confluence when the main stream is dominant. *Coherent Flow Struct. Open Channels* 491–517.
- Rhoads, B.L., & Kenworthy, S.T. (1998). Time-averaged flow structure in the central region of a stream confluence. *Earth Surf. Process. Landf.* 23, 171–191.
- Rhoads, B.L., & Sukhodolov, A.N. (2001). Field investigation of three-dimensional flow structure at stream confluences: 1. Thermal mixing and time-averaged velocities. *Water Resour. Res.* 37, 2393–2410.
- Rice, S., Roy, A., & Rhoads, B. (2008). *River confluences, tributaries and the Fluvial Network* (John Wiley & Sons).
- Sukhodolov, A.N., & Rhoads, B.L. (2001). Field investigation of three-dimensional flow structure at stream confluences: 2. Turbulence. *Water Resour. Res.* 37, 2411–2424.
- Szupiany, R.N., Amsler, M.L., Parsons, D.R., & Best, J.L. (2009). Morphology, flow structure, and suspended bed sediment transport at two large braid-bar confluences. *Water Resour. Res.* 45, W05415.
- USACE (2014). *Executive Summary Lower Snake River Draft Programmatic Sediment Management Plan – Final EIS*.

Information Transfer Program Introduction

The WRC staff has been active in outreach with water research and management professionals through presentations and event participation, development of educational programs, service to various professional associations, conference hosting and sponsorship, and through its website and social media presence. Among other activities listed below, the WRC staff gave almost 20 presentations over the year, participated on numerous association and editorial boards, and hosted one workshop and sponsored one.

WRC Information Transfer Program

Basic Information

Title:	WRC Information Transfer Program
Project Number:	2015WA406B
Start Date:	3/1/2015
End Date:	2/28/2016
Funding Source:	104B
Congressional District:	WA 5th
Research Category:	Not Applicable
Focus Category:	Drought, Law, Institutions, and Policy, Water Supply
Descriptors:	None
Principal Investigators:	Jonathan Yoder, Jennifer Adam

Publications

1. Yoder, Jonathan, Michael Brady, & Joseph Cook. Online 2016. Water markets and storage: Substitutes or complements for drought risk mitigation? Water Economics and Policy. <http://www.worldscientific.com/doi/abs/10.1142/S2382624X16500053?src=recsys>
2. Michael Brady, Tongzhe Li, & Jonathan Yoder. 2015. The Columbia River Treaty Renegotiation from the Perspective of Contract Theory. Journal of Contemporary Water Research and Education 150:53-62.
3. Yoder, Jonathan. 2015. Yakima Basin Integrated Plan Benefit-Cost Analysis: An appeal for evidence-based discourse about the State of Washington Water Research Center study of the Yakima Basin Integrated Plan. The Water Report 135(May): 9-17, 20. Response to Malloch and Garrity (Same issue).
4. Yoder, Jonathan November 17, 2015 Integrated Water Resource Management and Benefit Cost Analysis. Panel presentation at the American Water Resources Association. Denver, CO.
5. Yoder, Jonathan October 7-9, 2015. Social Welfare Gain of Water Trade with Population Growth and the Curtailments. Presented at the WaterSmart Innovations 2015 Conference, Las Vegas.
6. Yoder, Jonathan July 2015. Water storage and water markets as substitutes for drought risk mitigation. Presented at the AAEA-WAEA annual meetings, San Francisco CA.
7. Yoder, Jonathan June 16-18, 2016. Water storage and water markets as substitutes for drought risk mitigation. Presented at the Universities Council on Water Resources Conference. Las Vegas, NV
8. Yoder, Jonathan June 16-18. Benefit-Cost analysis of individual IWRM projects. Presented at the Universities Council on Water Resources Conference. Las Vegas, NV
9. Yoder, Jonathan, April 24-25, 2016. Benefit-Cost Analysis of Yakima Basin Integrated Plan Projects: An Interdisciplinary Analysis of an Integrated Water Resource Management Tool. Pacific Northwest Regional Economic Conference, Bellingham, Washington.
10. Yoder, Jonathan, April 1-4, 2016. Benefit-Cost Analysis of Yakima Basin Integrated Plan Projects: An Interdisciplinary Analysis of an Integrated Water Resource Management Tool. 86th Ann. Meeting Northwest Scientific Assoc. Pasco, WA.

Outreach and presentations

Presentations and other in-person information transfer activities are an important part of the information transfer program for the WRC, and represent an important role in the visibility of the Center across the state and in the larger discipline. Below are presentations that are not listed in the NIWR database because they do not satisfy the criteria of “other publications” as defined for the reporting system. The listed items are presentations given by the administrative staff of the WRC during this fiscal year.

Yoder, Jonathan Dec 19, 2015. Benefit-Cost Analyses of the Yakima River Basin Integrated Plan Projects. Requested testimony at the Washington House of Representatives Task Force on Washington Waters. Olympia, WA.

Yoder, Jonathan Dec 19, 2015. Economic fundamentals for water markets. Requested testimony at the Washington House of Representatives Task Force on Washington Waters. Olympia, WA.

Yoder, Jonathan. 2015. Integrated Water Resource Management and Benefit Cost Analysis. Panel presentation at the American Water Resources Association. Denver, CO, November 17, 2015.

Yang, Qingqing, Michael Brady, and Jonathan Yoder. 2015. Social Welfare Gain of Water Trade with Population Growth and the Curtailments. Presented at the WaterSmart Innovations 2015 Conference, Las Vegas, October 7-9.

Yoder, Jonathan. 2015. Water storage and water markets as substitutes for drought risk mitigation. Presented at the AAEE-WAEA annual meetings, San Francisco, July.

Yoder, Jonathan. 2015. Water storage and water markets as substitutes for drought risk mitigation. Presented at the Universities Council on Water Resources Conference. Las Vegas, NV June 16-18.

Yoder, Jonathan. 2015. Benefit-Cost analysis of individual IWRM projects. Presented at the Universities Council on Water Resources Conference. Las Vegas, NV June 16-18.

Yoder, Jonathan. 2015. Benefit-Cost Analysis of Yakima Basin Integrated Plan Projects: An Interdisciplinary Analysis of an Integrated Water Resource Management Tool. Pacific Northwest Regional Economic Conference, Bellingham, Washington, April 24-25.

Yoder, Jonathan. 2015. Benefit-Cost Analysis of Yakima Basin Integrated Plan Projects: An Interdisciplinary Analysis of an Integrated Water Resource Management Tool. 86th Annual Meeting Northwest Scientific Association. Pasco, Washington, April 1-4.

Yoder, Jonathan. 2016. Economics of Externalities: The public costs and benefits of water and water management. Invited panel participant and presentation to the Center for Sustaining

Agriculture and Natural Resources Advisory Committee Meeting. Ellensburg, Washington. March 2.

Yoder, Jonathan. 2015. Integrated Water Resource Management and Benefit Cost Analysis. Panel presentation at the American Water Resources Association. Denver, CO, November 17, 2015.

Yoder, Jonathan. 2015. Water Economics: Making the most of a valuable resource. Invited lecture, Leadership Tri-Cities. Richland, WA. September 16

Adam, J.C., R.E. Hull, C.L. Tague, J. Reyes, and M.L. Liu, 2015. Where should fine-resolution spatial heterogeneity be captured within Earth System Models, American Geophysical Union Fall Meeting, San Francisco, CA, Dec. 14-18.

Adam, J.C., 2015. Impacts of a changing climate on water resources availability and cropping systems. Washington State Tree Fruit Association (WSTFA) Annual Meeting. Yakima, WA, Dec. 7.

Adam, J.C., and K. Rajagopalan, 2015. Direct and Indirect effects of climate change on cereal productivity in the Pacific Northwest region of the U.S., REACCH International Meeting, Minneapolis, MN, Nov. 13-14.

Adam, J.C., 2015. The Columbia River basin long-term water supply and demand forecast. American Water Resources Association-WA 2015 State Conference, Oct. 22.

Adam, J.C., 2015. Scientific inputs to managing natural and agricultural resources in a changing climate. WSU Extension Agricultural and Natural Resources Unit Summer Meeting, Spokane, WA, Jul 22.

Padowski, J., Carrera, L., and Jawitz, J. (2015). Integrating Infrastructure and Institutions to Assess Water Security in Large Urban Areas. American Geophysical Union, San Francisco, CA.

Conference hosting and sponsorships

Spokane River Forum, March 23-24, 2016. Coeur d'Alene, ID.

Padowski, Julie, Jonathan Yoder, Jennifer Adam, Stephanie Hampton, and Chad Kruger. August 2015. Addressing the Food-Energy-Water System Trilemma: Balancing Reliance on Technological and Institutional Solutions. National Science Foundation SEES workshop proposal: Interactions of Food Systems with Water and Energy Systems. \$44,953. Funded/completed.

Seminar partial sponsor for Bart Nijssen (from the regional artc modeling project) and Ian Kraucunas (from the PNNL earth system modeling project).

Shared sponsorship for visit of Nicholas Brozovic, Director of Policy at the Robert B. Daugherty Water for Food Institute and Richael Young, Mammoth Consulting for a seminar to WSU faculty, a workshop with the Washington State Department of Ecology Water Resources Program, and Roza Irrigation district, to discuss innovations in water markets.

Education program

The WRC is actively engaged in the process of developing a Certificate in Water Sciences and Management for undergraduate and graduate students at WSU. In an effort to be sensitive to other department's course development and to most effectively use the existing water-related curriculum, we are identifying a core curriculum of existing WSU water-related courses. These courses will be grouped into several major themes a student can pursue, for example Riparian/aquatic ecology, Water management and policy, Water Quality, Groundwater, and Surface Water. Certificate requirements will be consistent with WSU guidelines. In addition to a Certificate, the WRC is also reviewing different strategies for implementing a "floating" interdisciplinary graduate program. Several universities have successful examples of these types of programs.

Professional service

Adam, Jennifer and Jonathan Yoder. Universities Council on Water Resources (UCOWR) Yoder, Lead Delegate for WSU, Adam, Delegate. Yoder is on the UCOWR Board of Directors.

Padowski, J.C.; Adam, J.C.; Yoder, J., McCabe J. 2015. NSF FEW Workshop White Paper- Addressing the Food-Energy-Water System Trilemma: Balancing Reliance on Technological and Institutional Solutions. Submitted to the National Science Foundation in partial satisfaction of an NSF workshop grant focusing on the Food-Energy-Water Nexus.

Reyes, J.J., J. Schellberg, S. Siebert, M. Elsaesser, J.C. Adam, and F. Ewert, 2015. Refining estimates of nitrogen uptake in grasslands: Application of the nitrogen dilution curve, *Agronomy for Sustainable Development*, doi 10.1007/s13593-015-0321-2.

Yoder, Jonathan 2016-2017. Editorial board member, Journal of Water Economics and Policy.

Yoder, Jonathan 2015-2017. Universities Council on Water Resources (UCOWR) Board of Directors.

Yoder, Jonathan 2016. WA State Department of Natural Resources Expert Council on Climate and Environmental Change.

Yoder, Jonathan. 2015. Reviewer for UCOWR Dissertation awards.

Padowski, Julie 2016. Scientific Advisor for the 2016 Columbia River Basin Forecast Project.

Padowski, Julie 2015-2016. Ad hoc reviewer for the following peer-reviewed journals: Water Resources Research, Forests, Environmental Research Letters, and Ecological Economics.

Padoski, Julie 2015-2016. Faculty rep on Executive Committee for Sustainability and Environmental Committee at WSU

Adam, Jennifer 2015-2016. Sat on PhD and MS committees outside of Civil and Environmental Engineering (e.g., Keyvan Malek in Biological Systems Engineering who I co-advise with Claudio Stockle, Muhammad Azeem Khan in Biological Systems Engineering, Justin Poinsatte and Sarah Anderson in Biology, Cody Miller in the School of the Environment, and Tristan Mullis in computer sciences)

Adam Jennifer 2015-2016. Participated in water-related meetings and conferences, including the American Geophysical Union (AGU) which is the largest hydrologic science meeting of the year, the annual Pacific Northwest Climate Science Conference, the Washington State Tree Fruit Association (WSTFA) annual meeting, the American Water Resources Association (AWRA) Washington State annual meeting. Dr. Adam had invited talks related to WRC research at most of these meetings.

Adam, Jennifer 2015-2016. Acted as water lead for the moving of water faculty from three colleges (VCEA, CAS, CAHNRS) into the new PACCAR Environmental Technology Building, where the WRC administration is now co-located with CEREO. Dr. Adam continues to act as water lead for all PACCAR-related activities.

Adam, Jennifer 2015-2016. WSU President Search: Advisory Committee Member.

Adam, Jennifer provided services for AGU Hydrology Section: Horton Research Student Grant Program Reviewer and Panelist.

Adam, Jennifer provided services for American Meteorological Society (AMS): Hydrology Committee member.

Adam, Jennifer provided services for CUAHSI hydrologic model benchmarking working group member. Dr. Adam was invited to a related workshop in Boulder, CO to share her ideas about the importance of hydrologic connectivity in hydrologic models.

Internet, print media, and social media

The WRC Website is accessible at swwrc.wsu.edu. It includes summaries of recent and current 104b seed grant projects, recent and current extramural research projects managed through the WRC, a news page, and information about affiliated agencies, institutes, and researchers. We also maintain a twitter account: @WA_WRC with which we post WRC and Washington State water related news.

USGS Summer Intern Program

None.

Student Support					
Category	Section 104 Base Grant	Section 104 NCGP Award	NIWR-USGS Internship	Supplemental Awards	Total
Undergraduate	5	0	0	0	5
Masters	1	0	0	0	1
Ph.D.	2	0	0	0	2
Post-Doc.	0	0	0	0	0
Total	8	0	0	0	8

Notable Awards and Achievements

Yoder, Jonathan, Jennifer Adam, Michael Brady, Joseph Cook, Stephen Katz, Daniel Brent, Shane Johnston, Keyvan Malek, John McMillan, nad Qingqing Yang. 2015: Yakima Basin Integrated Plan Benefit-Cost analysis. Yoder, Project Lead (PI). Winner of the College of Agricultural and Natural Resource Sciences Interdisciplinary Team Research Award for 2015.

Yoder, Jonathan. 2015: Winner of the Western Agricultural Economics Association Outstanding Published Research Award for 2014 for the publication: Yoder, Jonathan, Adrienne Ohler, & Hayley Chouinard. 2014. What floats your boat? Preference revelation from lotteries over complex goods. Journal of Environmental Economics and Management 67:412-430. Related to valuation methods for water-based recreation.

Adam, Jennifer 2015: Outstanding Research Faculty Award, Department of Civil & Environmental Engineering, WSU.

Adam, Jennifer 2015: Editors' Citation for Excellence in Referring for Earth's Future

Adam, Jennifer 2015: INSIGHT Into Diversity Magazine's Top 100 Inspiring Women in STEM Award

Publications from Prior Years

1. 2010WA305B ("Developing a Novel, Interdisciplinary Approach to Understand Hot Moments in Reservoir Nutrient Transformation") - Articles in Refereed Scientific Journals - Deemer, B.R., J.A. Harrison, and E.W. Whitling (2011) Microbial nitrogen removal and nitrous oxide production in a small eutrophic reservoir: an in situ approach to quantifying hypolimnetic process rates. *Limnology and Oceanography*, 56(4) 1189-1199, doi:10.4319/lo.2011.56.4.1189. Henderson, S.M., and B.R. Deemer. 2012. Vertical propagation of lakewide internal waves. *Geophysical Research Letters* 39, doi:10.1029/2011GL050534.
2. 2010WA305B ("Developing a Novel, Interdisciplinary Approach to Understand Hot Moments in Reservoir Nutrient Transformation") - Dissertations - Deemer, Bridget, 2016, Patterns and controls on nitrogen removal and greenhouse gas production in reservoirs ,Ph.D. Dissertation, School of the Environment, Washington State University, Vancouver, Washington.
3. 2012WA344B ("Response of River Runoff to Black Carbon in Snow and Ice in Washington State") - Other Publications - Kaspari, Delaney, Ian, Weyand, Skiles 2015 "Firefighters Prepare for War as Wildfire Season Approaches" - NBC News feature
4. 2010WA317B ("Understanding the Vulnerability of Columbia Basin Irrigated Agriculture to Predicted Climate Changes using a Coupled Hydrological-crop Model") - Articles in Refereed Scientific Journals - Clark, M.P., Y. Fan, D.M. Lawrence, J.C. Adam, D. Bolster, M. Kumar, L.R. Leung, D. Scott Mackay, C. Shen, S.C. Swenson, X. Seng, et al, 2015. Improving the representation of hydrologic processes in Earth System Models, *Water Resources Research*, doi: 10.1002/2015WR017096.
5. 2009WA255B ("Adaptive Management of Mountain Forests to Prevent Mass Wasting under Climate Change") - Articles in Refereed Scientific Journals - Barik, M.G., J.C. Adam, M.E. Barber, B. Muhunthan, 2016. Improved landslide susceptibility prediction to inform sustainable forest management activities in an Altered Climate (submitted).